



Westinghouse  
Electric Corporation

Energy Systems

Box 355  
Pittsburgh Pennsylvania 15230-0355

AW-95-903

November 17, 1995

Document Control Desk  
U.S. Nuclear Regulatory Commission  
Washington, D.C. 20555

ATTENTION: MR. T. R. QUAY

APPLICATION FOR WITHHOLDING PROPRIETARY  
INFORMATION FROM PUBLIC DISCLOSURE

SUBJECT: WESTINGHOUSE RESPONSES TO NRC REQUESTS FOR ADDITIONAL  
INFORMATION ON THE AP600

Dear Mr. Quay:

The application for withholding is submitted by Westinghouse Electric Corporation ("Westinghouse") pursuant to the provisions of paragraph (b)(1) of Section 2.790 of the Commission's regulations. It contains commercial strategic information proprietary to Westinghouse and customarily held in confidence.

The proprietary material for which withholding is being requested is identified in the proprietary version of the subject report. In conformance with 10CFR Section 2.790, Affidavit AW-95-903 accompanies this application for withholding setting forth the basis on which the identified proprietary information may be withheld from public disclosure.

Accordingly, it is respectfully requested that the subject information which is proprietary to Westinghouse be withheld from public disclosure in accordance with 10CFR Section 2.790 of the Commission's regulations.

Correspondence with respect to this application for withholding or the accompanying affidavit should reference AW-95-903 and should be addressed to the undersigned.

Very truly yours,

Brian A. McIntyre, Manager  
Advanced Plant Safety and Licensing

/nja

cc: Kevin Bohrer NRC 12H5

2625A

9511270454 951117  
PDR ADOCK 05200003  
A PDR

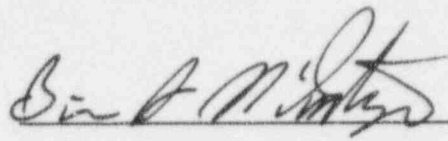
AFFIDAVIT

COMMONWEALTH OF PENNSYLVANIA:

ss

COUNTY OF ALLEGHENY:

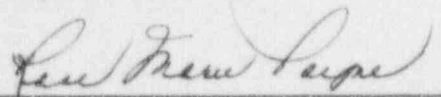
Before me, the undersigned authority, personally appeared Brian A. McIntyre, who, being by me duly sworn according to law, deposes and says that he is authorized to execute this Affidavit on behalf of Westinghouse Electric Corporation ("Westinghouse") and that the averments of fact set forth in this Affidavit are true and correct to the best of his knowledge, information, and belief:



---

Brian A. McIntyre, Manager  
Advanced Plant Safety and Licensing

Sworn to and subscribed  
before me this 17 day  
of November, 1995



---

Notary Public

Notarial Seal  
Rose Marie Payne, Notary Public  
Monroeville Boro, Allegheny County  
My Commission Expires Nov. 4, 1996

Member, Pennsylvania Association of Notaries

- (1) I am Manager, Advanced Plant Safety And Licensing, in the Advanced Technology Business Area, of the Westinghouse Electric Corporation and as such, I have been specifically delegated the function of reviewing the proprietary information sought to be withheld from public disclosure in connection with nuclear power plant licensing and rulemaking proceedings, and am authorized to apply for its withholding on behalf of the Westinghouse Energy Systems Business Unit.
- (2) I am making this Affidavit in conformance with the provisions of 10CFR Section 2.790 of the Commission's regulations and in conjunction with the Westinghouse application for withholding accompanying this Affidavit.
- (3) I have personal knowledge of the criteria and procedures utilized by the Westinghouse Energy Systems Business Unit in designating information as a trade secret, privileged or as confidential commercial or financial information.
- (4) Pursuant to the provisions of paragraph (b)(4) of Section 2.790 of the Commission's regulations, the following is furnished for consideration by the Commission in determining whether the information sought to be withheld from public disclosure should be withheld.
  - (i) The information sought to be withheld from public disclosure is owned and has been held in confidence by Westinghouse.
  - (ii) The information is of a type customarily held in confidence by Westinghouse and not customarily disclosed to the public. Westinghouse has a rational basis for determining the types of information customarily held in confidence by it and, in that connection, utilizes a system to determine when and whether to hold certain types of information in confidence. The application of that system and the substance of that system constitutes Westinghouse policy and provides the rational basis required.

Under that system, information is held in confidence if it falls in one or more of several types, the release of which might result in the loss of an existing or potential competitive advantage, as follows:

- (a) The information reveals the distinguishing aspects of a process (or component, structure, tool, method, etc.) where prevention of its use by any of Westinghouse's competitors without license from Westinghouse constitutes a competitive economic advantage over other companies.
- (b) It consists of supporting data, including test data, relative to a process (or component, structure, tool, method, etc.), the application of which data secures a competitive economic advantage, e.g., by optimization or improved marketability.
- (c) Its use by a competitor would reduce his expenditure of resources or improve his competitive position in the design, manufacture, shipment, installation, assurance of quality, or licensing a similar product.
- (d) It reveals cost or price information, production capacities, budget levels, or commercial strategies of Westinghouse, its customers or suppliers.
- (e) It reveals aspects of past, present, or future Westinghouse or customer funded development plans and programs of potential commercial value to Westinghouse.
- (f) It contains patentable ideas, for which patent protection may be desirable.

There are sound policy reasons behind the Westinghouse system which include the following:

- (a) The use of such information by Westinghouse gives Westinghouse a competitive advantage over its competitors. It is, therefore, withheld from disclosure to protect the Westinghouse competitive position.
- (b) It is information which is marketable in many ways. The extent to which such information is available to competitors diminishes the Westinghouse ability to

sell products and services involving the use of the information.

- (c) Use by our competitor would put Westinghouse at a competitive disadvantage by reducing his expenditure of resources at our expense.
  - (d) Each component of proprietary information pertinent to a particular competitive advantage is potentially as valuable as the total competitive advantage. If competitors acquire components of proprietary information, any one component may be the key to the entire puzzle, thereby depriving Westinghouse of a competitive advantage.
  - (e) Unrestricted disclosure would jeopardize the position of prominence of Westinghouse in the world market, and thereby give a market advantage to the competition of those countries.
  - (f) The Westinghouse capacity to invest corporate assets in research and development depends upon the success in obtaining and maintaining a competitive advantage.
- (iii) The information is being transmitted to the Commission in confidence and, under the provisions of 10CFR Section 2.790, it is to be received in confidence by the Commission.
- (iv) The information sought to be protected is not available in public sources or available information has not been previously employed in the same original manner or method to the best of our knowledge and belief.
- (v) Enclosed is Letter NTD-NRC-95-4598, November 17, 1995 being transmitted by Westinghouse Electric Corporation (W) letter and Application for Withholding Proprietary Information from Public Disclosure, Brian A. McIntyre (W), to Mr. T. R. Quay, Office of NRR. The proprietary information as submitted for use by Westinghouse Electric Corporation is in response to questions concerning the AP600 plant and the associated design certification application and is expected to be

applicable in other licensee submittals in response to certain NRC requirements for justification of licensing advanced nuclear power plant designs.

This information is part of that which will enable Westinghouse to:

- (a) Demonstrate the design and safety of the AP600 Passive Safety Systems.
- (b) Establish applicable verification testing methods.
- (c) Design Advanced Nuclear Power Plants that meet NRC requirements.
- (d) Establish technical and licensing approaches for the AP600 that will ultimately result in a certified design.
- (e) Assist customers in obtaining NRC approval for future plants.

Further this information has substantial commercial value as follows:

- (a) Westinghouse plans to sell the use of similar information to its customers for purposes of meeting NRC requirements for advanced plant licenses.
- (b) Westinghouse can sell support and defense of the technology to its customers in the licensing process.

Public disclosure of this proprietary information is likely to cause substantial harm to the competitive position of Westinghouse because it would enhance the ability of competitors to provide similar advanced nuclear power designs and licensing defense services for commercial power reactors without commensurate expenses. Also, public disclosure of the information would enable others to use the information to meet NRC requirements for licensing documentation without purchasing the right to use the information.

The development of the technology described in part by the information is the result of applying the results of many years of experience in an intensive Westinghouse effort and the expenditure of a considerable sum of money.

In order for competitors of Westinghouse to duplicate this information, similar technical programs would have to be performed and a significant manpower effort, having the requisite talent and experience, would have to be expended for developing analytical methods and receiving NRC approval for those methods.

Further the deponent sayeth not.

Attachment A to NTD-NRC-95-4598

Enclosed Responses to NRC Requests for Additional Information

<b>Re: LOFTRAN Computer Code</b>	<b>Re: NOTRUMP Computer Code</b>
440.281	440.436
440.283	440.471
440.292	440.474 **
440.293	440.476
440.294	440.481
440.295	440.486 **
440.296	440.491
440.297	440.512 **
440.298	440.514
440.303	
440.304	<b>Re: AP600 OSU Test Facility</b>
440.313	480.223
440.317	480.243
440.318	480.246
440.319	480.247
	480.249
<b>Re: WCOBRA/TRAC Computer Code</b>	480.250
440.343 **	480.251
440.344 **	480.260
440.346	480.261
440.347	480.262
440.348 **	480.267
440.349	480.268
440.350	480.269
440.351 **	480.270
440.352 **	480.272

\*\* Contains Westinghouse proprietary information



**Enclosure 2 to NTD-NRC-95-4598**

**Non-proprietary copy of Enclosure 1**

## NRC REQUEST FOR ADDITIONAL INFORMATION



Question 440.281

Re: WCAP-14234 (LOFTRAN CAD)

Page 2-5. How many tubes will be modelled in a tube rupture event using LOFTRAN? Please provide the information that substantiates that "The ADS is not required for mitigation of design-basis non-LOCA and steam generator tube rupture events", such as tube ruptures and steam line breaks.

Response:

The design basis SGTR event modeled with the LOFTRAN based LOFTTR2AP code is a double-ended rupture of a single steam generator tube. The analyses presented in Chapter 15 of the draft SSAR markup (Reference 440.281-1) demonstrate that all applicable limits are met for SGTR and non-LOCA (including steamline break) events without requiring that the ADS be actuated.

Reference

440.281-1 Westinghouse Letter NTD-NRC-95-4480, "Preliminary Markups of AP600 SSAR Chapter 15 (Accident Analyses)", June 2, 1995

SSAR Revision: NONE

## NRC REQUEST FOR ADDITIONAL INFORMATION



Question 440.283

Re: WCAP-14234 (LOFTRAN CAD)

Page 2-4. How can it be assumed that "The CMT model of the LOFTRAN-AP code version simulates the dynamics of a single CMT and assumes the performance of both CMTs is identical" when the length of the two CMT cold leg pressure balance lines may be different? Please provide the calculations that demonstrate that these differences are negligible for the emptying, refill, and recirculation of the CMTs during a long term transient.

Response:

LOFTRAN simulates only the dynamics of a single CMT and assumes that the performance of both CMTs is identical. There are no design basis events analyzed with LOFTRAN which use the CMT for mitigation where asymmetric conditions occur in the cold legs affecting the CMT performance.

In AP600, each CMT is connected to the RCS with a cold leg balance line and a direct vessel injection line. The two cold leg balance lines (one per CMT) are connected on two cold legs of the same RCS loop. LOFTRAN simulates separately the two AP600 loops, lumping together the two cold legs of the same loop.

There are a limited number of design basis transients analyzed with LOFTRAN where asymmetric flow could occur in the cold legs on a given loop. None of these events rely upon the CMT's for mitigation. These events are:

- Partial loss of forced reactor coolant flow events
- Locked or broken RCP shaft events
- Startup of an inactive RCP

During events where the CMTs are used for mitigation, a CMT actuation signal is accompanied by a single failure proof reactor coolant pump trip signal. As a result of tripping all four RCPs, there are no non-LOCA transient analyzed with LOFTRAN where non symmetric behavior of the two cold legs of the same loop occurs.

In AP600, the line layout of the two CMTs may be different. However the CMT discharge lines contain orifices which are used to equalize the overall line resistances of both CMTs such that they both are within a design tolerance. Included in the ITACCs are CMT tests to demonstrate that the line resistances are within a certain tolerance of one another.

Variations in the two CMT layouts is handled by using the more limiting of the two layout characteristics to give conservative bounding performance. Selection of the limiting characteristics is performed on an event by event basis. For example, the analysis of a steam line break would use the higher of the two CMT line resistances to minimize CMT flow and boration capability. The analysis for inadvertent actuation of the CMT would use the minimum of the two CMT line resistances to maximize the CMT injection flow.

This philosophy is also extended to the initial condition variations and any other hardware uncertainties associated with the CMT design. Minimum and maximum bounding performance data are used for the safeguards systems such



---

as the CMT in the analyses. Table 2-5 of WCAP 14234 highlights other bounding CMT characteristics used in the safety analyses.

Emptying or refill of the CMTs does not occur during non-LOCA transients analyzed with LOFTRAN. The CMTs operate in the single phase water recirculation mode only.

SSAR Revision: NONE

NRC REQUEST FOR ADDITIONAL INFORMATION



Question 440.292

Re: WCAP-14234 (LOFTRAN CAD)

Section 3.2.1, page 3-5. Please provide a technical description of the IRWST model in terms of the equations that are used and the method of solution.

Response: [Note: This response also addresses RAIs 440.304 and 440.318]

It is assumed that the heat transferred to the IRWST through the PRHR heat exchanger will be rapidly distributed through the IRWST fluid. Therefore, the IRWST is modeled as a single node containing a homogeneous mixture (i.e. perfect mixing is assumed in the IRWST). The IRWST model is designed to provide a secondary side temperature and pressure for use in the PRHR heat exchanger heat transfer calculations. The heat transferred to the IRWST from each PRHR heat exchanger tube node is a function of the fluid conditions on the secondary side of the tubes, i.e. in the IRWST (among other factors as described in Section 3.2.3 and Appendix A of the CAD).

The initial IRWST temperature is input by the user and is updated by the code at the end of every timestep to reflect the heat added. The local secondary pressure for each primary side tube node is calculated at the start of the timestep using the pressure at the top of the tank (containment pressure), with a pressure increase to account for the depth of the node in the tank. The containment pressure can be input by the user as a function of time, although a constant value is typically used. The density of water at the containment pressure and IRWST temperature is used together with the depth of the individual heat exchanger node and the containment pressure to compute the local secondary pressure.

At the end of each timestep, the IRWST temperature is updated to reflect the heat added to the fluid. The energy transferred to the IRWST in the timestep is used to calculate the increase in IRWST temperature using Equation 440.292-1 below. The IRWST temperature is limited to the saturation temperature corresponding to the user input containment pressure. If the calculated temperature is less than the saturation temperature at the user input containment pressure no adjustment to the IRWST mass is required. Heat transferred once saturation is reached in the IRWST is dissipated by steaming off some of the fluid. If Equation 440.292-1 would result in the IRWST temperature exceeding the saturation temperature then Equation 440.292-2 is used to dissipate the energy through steaming and the IRWST mass is reduced accordingly and the IRWST temperature is reset to the saturation temperature.

$$T_{\text{pool}_{t+\Delta t}} = T_{\text{pool}_t} + \frac{Q_{\text{total}_{\Delta t}} \cdot dT}{M_{\text{pool}_t} \cdot C_P} \quad (440.292-1)$$

$$M_{\text{pool}_{t+\Delta t}} = M_{\text{pool}_t} - \frac{(T_{\text{pool}_t} - T_{\text{sat}_t}) \cdot M_{\text{pool}_t} \cdot C_P}{h_{fg}} \quad (440.292-2)$$



Where:

$T_{pool}$	= Average pool temperature in the IRWST (°F)
$Q_{total}$	= Total energy transferred by PRHR heat exchanger in the timestep (Btu/sec)
$dT$	= Length of timestep (sec)
$C_p$	= Heat capacity of IRWST fluid (Btu/lbm-°F)
$M_{pool}$	= Mass of fluid in the IRWST at the start of a timestep (lb)
$T_{sat}$	= Saturation temperature at containment pressure (°F)
$h_{fg}$	= Heat of vaporization of IRWST fluid (Btu/lbm)

subscripts

$i$	= value at start of timestep
$dt$	= value at the end of timestep

The adjusted IRWST temperature and fluid mass are used in the next timestep's heat transfer and secondary pressure calculations. The fluid mass in the IRWST is used only to determine the depth of the heat exchanger nodes in calculating the secondary side local pressure. The code always assumes that the heat exchanger is completely submerged, so the IRWST level has no other effect on the calculations. [The containment pressure is user input and is not adjusted to account for the effects of steaming from the IRWST.]

The IRWST temperature changes very slowly (on the order of 1/100 °F per second) therefore the preceding equations are solved directly without iteration or stability difficulties.

SSAR Revision: NONE



**NRC REQUEST FOR ADDITIONAL INFORMATION**



---

Question 440.293

Re: WCAP-14234 (LOFTRAN CAD)

Section 3.2.1, page 3-5. Please show how the stability of the IRWST model is affected by any explicit connection to the RCS.

Response:

Please see the Westinghouse response to RAI 440.295.

SSAR Revision: NONE

**NRC REQUEST FOR ADDITIONAL INFORMATION**



---

Question 440.294

Re: WCAP-14234 (LOFTRAN CAD)

(440.294)32. Section 3.2.1, page 3-5. Please substantiate that lagging to past time values is not performed for the IRWST to RCS connections in order to smooth the response.

Response:

Please see the Westinghouse response to RAI 440.295.

SSAR Revision: NONE



## NRC REQUEST FOR ADDITIONAL INFORMATION



Question 440.295

Re: WCAP-14234 (LOFTRAN CAD)

Section 3.2.1, page 3-5. Since the IRWST is a new model for LOFTRAN, please demonstrate that mass, momentum, and energy are conserved in the IRWST and at the connections between the IRWST and the RCS.

Response:

The IRWST serves two safety functions which are:

- to supply a heat sink for the PRHR heat exchanger
- to provide an inventory source for the injection of fluid to the RCS following ADS actuation.

Injection from the IRWST to the RCS is not used for mitigation of design basis non-LOCA events. During non-LOCA events the IRWST is used as a heat sink for the PRHR heat exchanger. The IRWST model in LOFTRAN only simulates the heat sink function. There is no mass transfer between the IRWST and the RCS in the LOFTRAN model. Further details of the energy and mass solution for the IRWST can be found in the response to RAI 440.292.

SSAR Revision: NONE



Westinghouse

440.295-1

**NRC REQUEST FOR ADDITIONAL INFORMATION**



---

Question 440.296

Re: WCAP-14234 (LOFTRAN CAD)

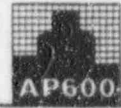
Section 3.2.1, page 3-5. Please demonstrate that the volume and mass error in the IRWST and at the interface between the RCS and IRWST does not increase and accumulate beyond acceptable ranges for the transients simulated.

Response:

Please see the Westinghouse response to RAI 440.295.

SSAR Revision: NONE

**NRC REQUEST FOR ADDITIONAL INFORMATION**



---

Question 440.297

Re: WCAP-14234 (LOFTRAN CAD)

Please explain how time step control is accomplished between the IRWST and the RCS. Do the results remain stable for continually decreasing the time step? Please provide substantiation.

Response:

Please see the Westinghouse response to RAI 440.295.

SSAR Revision: NONE

NRC REQUEST FOR ADDITIONAL INFORMATION



---

Question 440.298

Re: WCAP-14234 (LOFTRAN CAD)

Please provide any details on whether the IRWST and the RCS execute at different time steps. If this is the case, please provide the logic that insures both modules reach the same point in time.

Response:

Please see the Westinghouse response to RAI 440.295.

SSAR Revision: NONE

## NRC REQUEST FOR ADDITIONAL INFORMATION



Question 440.303

Re: WCAP-14234 (LOFTRAN CAD)

How will the effects of noncondensables be modelled in the system after accumulator injection? No mention of noncondensable effects is made in the report.

Response:

The noncondensable gas of the accumulators can be injected into the RCS only if the accumulators empty completely. During events simulated with LOFTRAN, such as a large design basis steam line break, the accumulators may be actuated but are not emptied. The situation where significant noncondensable gases exist in the RCS does not occur during the non-LOCA design basis events analyzed with LOFTRAN.

SSAR Revision: NONE

**NRC REQUEST FOR ADDITIONAL INFORMATION**



---

Question 440.304

Re: WCAP-14234 (LOFTRAN CAD)

Pages 3-5.3-6. Please explain how the PRHR heat transfer is incorporated in the energy solution of the IRWST. Please provide justification of the stability limits.

Response:

Please see the Westinghouse response to RAI 440.292.

SSAR Revision: NONE

## NRC REQUEST FOR ADDITIONAL INFORMATION



Question 440.313

Re: WCAP-14234 (LOFTRAN CAD)

Page 2-16. It is stated that "Method 'a' is the same as is used on current PWRs for determining RCCA position versus time analysis input." Do current PWRs have their cold legs lumped together in LOFTRAN as is done for the AP-600 PWRs for option a of the RCCA position versus time? How is the asymmetry of an RCP in the cold leg of an AP-600 model used in the context of option a for the RCCAs? Is the same procedure used for current PWRs? Please explain.

Response:

LOFTRAN uses a point neutron core kinetics model and simulates reactor trip with a table of negative reactivity added as a function of time following reactor trip. The RCCA position as a function of time used to develop the reactivity versus time table is a function of the net core flow.

For non-LOCA events sensitive to RCCA insertion time, a longer RCCA insertion time will result in more severe results. The time required for the RCCAs to drop into the core following a reactor trip signal is a function of the net core flow. The higher the core flow, the longer it will take for the RCCAs to be inserted. Conversely if partial RCP operation (symmetric or asymmetric) is occurring or if all RCPs are not operating, the net core flow and the time for the RCCAs to fall into the core will be reduced. It is clearly conservative to use a high flow when calculating the RCCA insertion time.

In current PWRs the RCCA insertion versus time characteristics used in all non-LOCA design basis events is calculated conservatively assuming all RCPs are operating. This calculational method is referred to as "Method a" in WCAP 14234. On current PWRs this method is used for all non-LOCA events even during complete and partial loss of forced RCS flow events where less than full flow would in reality result in faster RCCA insertion times.

In the past, lumping of loops together in conjunction with "Method a" was used in models for the licensing of operating Westinghouse PWRs. Most of these analyses have been replaced with updated analyses which do not use lumped loops. However, a few operating plants continue to use some analyses with loops lumped together for their current licensing basis analyses.

For selected AP600 analyses, an alternate method referred to as "Method b" in WCAP 14234 was developed which credited the effect of the transient reduction in core flow on the RCCA insertion time following reactor trip. In "Method b" the RCCA position versus time characteristics were calculated assuming a coincident coastdown of all four RCPs. Thus if the all RCPs are coasting down simultaneously with reactor trip or are coasting down prior to reactor trip then "Method b" is applicable and conservative. Of the non-LOCA analyses presented in the AP600 SSAR, "Method b" is only used in the complete loss of forced RCS flow analyses presented in SSAR Section 15.3.2. In SSAR Section 15.3.2 the initiating event is the coasting down of all four RCPs. A reactor trip is then generated when low RCP speed is detected.

## NRC REQUEST FOR ADDITIONAL INFORMATION



All other AP600 non-LOCA analyses including the asymmetric pump coastdown events of SSAR Section 15.3.1 and the faulted RCP shaft events of SSAR Sections 15.3.3 & 4 conservatively assume that full RCS flow exists (i.e., "Method a") for the calculation of RCCA insertion versus time characteristics. This procedure ("Method a") is the same as is used on current PWRs.

SSAR Revision: NONE





NRC REQUEST FOR ADDITIONAL INFORMATION



Question 440.317

Re: WCAP-14234 (LOFTRAN CAD)

Page 3-6. Why is volumetric flow used in the K loss term of the momentum equation for the PRHR and not in the CMT momentum equations? Why not be consistent?

Response:

The same formulation is used for the CMT and the PRHR momentum equations, with some minor modification of the presentation. The momentum equation of the PRHR (see page 3-6 of WCAP-14234) is:

$$\frac{dw}{dt} = \frac{g_c}{V/A^2} [(P_{IN} - P_{OUT}) - \Delta P_f + \Delta P_{BH}] \quad (440.317-1)$$

where:

$dw/dt$	=	rate of change of the PRHR flow, lbm/sec <sup>2</sup>
$P_{IN}$ & $P_{OUT}$	=	inlet & outlet pressure to PRHR system, psia
$\Delta P_{BH}$	=	net buoyancy head in the PRHR loop
$[(P_{IN} - P_{OUT}) + \Delta P_{BH}]$	=	$\Delta P_{Driving}$ , this term represents the PRHR loop driving head.
$V/A^2$	=	inertial length (L/A) of the PRHR loop
$\Delta P_f$	=	friction and form pressure loss through the PRHR loop.
$g_c$	=	conversion factor, lbm ft/lbf sec <sup>2</sup>

$\Delta P_f$  is calculated using:

$$\Delta P_f = \sum_{i=1}^n k_i W Q$$

where:

- n = the number of nodes in the PRHR loop
- $k_i$  = the pressure loss coefficient (psf/[gpm lbm/sec] ) for node i
- W = PRHR loop mass flow

Q = PRHR loop volumetric flow. Volumetric flow is equal to mass flow divided by fluid density (Q = W/ $\rho$ )

Rearranging terms and substituting, Equation 440.317-1 becomes:



$$\frac{dw}{dt} = \frac{g_c}{L/A} \left[ \Delta P_{Driving} - \sum_{i=1}^n k_i \frac{W^2}{\rho} \right] \quad (440.317-2)$$

This form of the momentum equation is the same form as that used for the CMT on page 3-2 of WCAP-14234.

SSAR Revision: NONE

NRC REQUEST FOR ADDITIONAL INFORMATION



---

Question 440.318

Re: WCAP-14234 (LOFTRAN CAD)

How was the nodalization for the IRWST arrived at? Is the IRWST a two-region node with mixture level tracking?  
How is the mixture level used with PRHR heat transfer?

Response:

Please see the Westinghouse response to RAI 440.292.

SSAR Revision: NONE

**NRC REQUEST FOR ADDITIONAL INFORMATION**



---

Question 440.319

Re: WCAP-14234 (LOFTRAN CAD)

How can natural circulation in the RCS and the CMTs proceed correctly with a symmetric (one CMT versus two) CMT model and the cold legs lumped together ? Please explain.

Response:

Please see the Westinghouse response to RAI 440.283.

SSAR Revision: NONE



Question 440.343

Re: WCAP-14171 (WCOBRA/TRAC CAD)

The following questions relate to the WCOBRA/TRAC simulation of Cylindrical Core Test Facility (CCTF) Run 58.

- a) On page 3-9, Westinghouse stated the broken loop hot leg steam flow was overpredicted due to less condensation and the underprediction of liquid flow into the hot leg. Clarify this statement as Westinghouse also noted the subcooling at the quench front goes to zero in the calculation. Would this not imply that any liquid entrained into the hot legs is at saturation and not capable of condensing steam (see Eqn. 5-174)? Would less evaporation better describe the broken loop hot leg phenomena occurring in the calculation?
- b) For the hot leg liquid flow differences noted by Westinghouse, could this be due to a density difference because the calculated subcooling at the quench front went to zero? Also, Westinghouse never stated whether a similar loss of subcooling at the quench front was noted in the experimental data. If possible, clarify the amount of subcooling at the quench front in the experiment.
- c) Westinghouse also compared the measured and calculated fluid temperatures in the broken loop pump suction. Clarify how the fluid temperature comparison in the broken loop pump suction (Figure 3.1-50) shows there is less liquid flow in the calculation. Is the implication that the higher WCOBRA/TRAC calculated fluid temperature is due to more steam superheating because of lower liquid flow? Would not the temperature of the fluid in the pump suction reflect the temperature of the steam generator secondary? If yes, does the difference between the calculated and measured temperatures indicate a possible steam generator secondary problem? If no, provide additional information to clarify the reasons for the differences between the two fluid temperatures in Figure 3.1-50.
- d) Clarify the reasons for overpredicting the intact loop cold leg steam flow (see Figure 3.1-41).
- e) Westinghouse also stated on page 3-9 that, because the differential pressure across the intact loop pump simulator was in closer agreement with the test data, this indicated the experimental water mass flow may be greater than the calculated flow. Clarify the basis for this statement.

Response:

- a) The statement that the broken loop hot leg steam flow was overpredicted due to less condensation is incorrect since condensation cannot occur on saturated liquid. A sensitivity calculation presented under RAI 440.348(c) has shown that the relative flow rates in intact and broken loops are sensitive to the hydraulic loss coefficients assigned to the loops. The relative values of these loss coefficients also affect both the core inlet flow rate and the subsequent steam production rate. It is judged that ] a, c  
] a, c  
 improved modeling presented in the response to RAI 440.348(c) based on the improved agreement obtained from Evaporation plays no significant role in broken loop hot leg behavior.



- b) The available experimental data does not show conclusively whether loss of subcooling occurred at the quench front. It is believed that, with the exception of the lower elevations of the core where the power density is lower, loss of subcooling at the quench front occurred in the test. Density differences between the calculation and test at and below the quench front are not significant. The hot leg liquid flow differences have been explained in the response to part (a) above.
- c) The fluid temperature in the broken loop pump suction pipe is calculated to be higher than that measured, but both are showing considerable superheat, which indicates that there is no liquid in the pump suction. The superheating is the result of a combination of the superheated steam entering the broken loop hot leg from the core, together with the heat added from the secondary side of the SG simulator. The higher broken loop loop seal superheat in the calculation reflects less liquid entrained into the hot leg. The broken loop SG simulator secondary temperature is higher in the calculation than in the test because less heat is transferred in the calculation to the primary, due to the low entrained liquid flow into the SG simulator tubes.
- d) The intact loop 1 cold leg steam flow (Fig. 3.1-41) is overpredicted because WCOBRA/TRAC has underpredicted the condensation rate of steam on the colder Low Pressure Coolant Injection (LPCI) water in the intact cold leg. The calculated intact loop 1 cold leg steam flow is approximately equal to the sum of the intact loop 1 hot leg steam flow and liquid flow (the latter being vaporized in the tubes of the steam generator simulator). This indicates that very little condensation is calculated to occur. In the experiment, however, the intact loop 1 cold leg steam flow is less than the sum of the loop 1 hot leg steam and liquid flows, indicating that some of the steam was condensed by the LPCI water injected into the cold leg. This, however, is not reflected in the measured water mass flowrate in loop 1 (Figure E-173 of Reference 440.343-1) which shows zero flow. It is believed that this is because the measuring instrument used to measure the high accumulator injection water flowrate was not sensitive enough to pick up the relatively low flowrate of the LPCI injection.
- e) The statement on page 3-9 that "the differential pressure across the pump simulator in loop 1 is however in closer agreement indicating that the experimental flow may be greater than the calculated flow" is not correct. The flows referred to are those in the intact cold legs. A comparison of these flows between the calculation and the experiment is addressed by answer (d) above. A corrected statement in WCAP-14171 would be that "the differential pressure across the pump simulator in loop 1 shows good agreement between calculation and test early in the transient because the total flow through the pump simulator is superheated steam and is the sum of the vapor and liquid flows through the loop 1 hot leg, which are predicted well (WCAP-14171, Figures 3.1-44 and 3.1-45)."

#### Reference

- 440.343-1 Sugimoto, J., et. al., "Data Report on Large Scale Reflood Test 78 - CCTF Core - II Test C2-AA2 (Run 058)," JAERI - memo 59-446, February 1985

SSAR Revision: NONE

## NRC REQUEST FOR ADDITIONAL INFORMATION



Question 440.344

Re: WCAP-14171 (WCOBRA/TRAC CAD)

The following questions relate to the WCOBRA/TRAC simulation of Upper Plenum Test Facility (UPTF) Test 21.

- a) For Test 21, all phases of the test show that the cold leg filling behavior (Figures 3.2-23, 3.2-31, and 3.2-39) was not calculated well. Clarify why and discuss any implications for AP600 best estimate large break loss-of-coolant accidents (BE LBLOCA).
- b) For Test 21, Phase B I, clarify the reasons for the different lower plenum filling behavior (see Figure 3.2-24) between the test results and the WCOBRA/TRAC results. Provide a similar discussion for the differences in the downcomer pressure in Figure 3.2-28.
- c) Clarify the statement on page 3-71 that Phase B I overpredicted the bypass by a smaller amount than Phase A. Comparison of Figures 3.2-19 (Phase A) and 3.2-27 (Phase B I) shows a larger difference between the calculated and measured integrated break flows in Phase B I relative to the difference in Phase A.
- d) For Phase B II, clarify why the broken loop cold leg steam flow is underpredicted (see Figure 3.2-33) while the integrated break flow is calculated well (see Figure 3.2-35). Provide similar information clarifying why the lower plenum mass is underpredicted in Phase B II (see Figure 3.2-32) even though the integrated break flow is calculated well (Figure 3.2-35).

Response:

- a) Inspection of the UPTF 21 test results shows that the mechanism for the cold legs filling with water is as follows. The upflow of steam in the downcomer supports water injected through the ECCS nozzles. The ECCS nozzle 1 is adjacent to the broken cold leg, and this water exits the downcomer quickly. ECCS nozzle 2 water must traverse the downcomer before it can reach the broken cold leg. This water passes over cold leg 3 nozzle and consequently, this cold leg has the largest amount of water. Cold leg 2 is adjacent to ECCS nozzle 2 on the other side, and this cold leg has the second largest amount of water. Cold leg 1 is not on the path from either ECCS nozzle to the broken cold leg and consequently, this cold leg contains the least amount of water. In the UPTF test facility, the ECCS nozzles are slightly above the level of the hot and cold legs, whereas, in the AP600 the DVI nozzle centerlines are about 3 feet below the level of the cold leg centerlines. In this test the pump simulators are closed, i.e., there is no steam flow through the cold legs. The cold legs fill because initially they are full of steam and as subcooled liquid from the ECC flows across the cold leg nozzle in the downcomer, condensation occurs, reducing the pressure in the cold leg and drawing liquid in. The flow of steam up through the downcomer in the test is sufficient to hold the water in the cold legs.

In run 272 phase A there is reasonable prediction of the water in cold leg 3, but there is no predicted penetration of cold legs 1 and 2. In run 274 phase B I predicted penetration into cold leg 3 is slower than the measured rate, but the cold leg fills by the end of the test phase. Loops 1 and 2 do not significantly fill in this test phase. In run 274 phase B2 some penetration is measured into cold leg 3, which is not predicted. There is no measured penetration in cold legs 1 and 2 in this phase. In run 274 phase B3 the penetration into cold leg 3 is predicted



too slowly, but the leg fills up before the end of the test phase. Penetration into cold legs 1 and 2 is underpredicted in this phase.

To predict the build up of water in the cold legs accurately, it is necessary to predict both the correct quantity of water in the downcomer and also its location within the downcomer. It can be seen from figures 3.2.19, 3.2.27 and 3.2.35 that break flow is overpredicted in run 272 phase A and run 274 phases B1 and B3. Break flow is well predicted in run 274 phase B2. These differences lead to the discrepancy in downcomer inventory prediction. Also, the grid employed to model the downcomer is not sufficiently fine to model this phenomenon because of its sensitivity to the exact position of the water in the downcomer.

The ability to predict water build up in the cold legs in this test is not important to AP600 safety analysis for the following reasons:

In the AP600 the DVI nozzle centerline is about 3 feet below the cold leg centerline and so it is more likely that the water will exit the broken cold leg than flow into the cold legs.

In the AP600 there will be a flow path from the upper plenum to the intact cold legs through the loops and so the condensation depressurization mechanism which fills the intact cold legs in this test will not apply.

Also, since the break flow is overpredicted and the water build up in the cold legs is underpredicted, these calculations show that the code is conservative in this respect.

In summary, WCOBRA/TRAC is conservative in its calculation of the amount of ECC bypass and rate of vessel lower plenum refill, as seen in UPTF test 21. However, this conservatism is accentuated by the non-prototypic features of the test and would be reduced for the bypass flow conditions expected during a postulated large break LOCA in AP600.

- b) In Phase B1 of UPTF test 21, the measured lower plenum filling rate is fairly steady from the start of ECC injection at 46 seconds (Figure 3.2-24, WCAP-14171) with a slightly higher rate at about 50 seconds resulting from water entering the vessel from the loop 2 cold leg (Figure 3.2-31). The WCOBRA/TRAC calculation shows ECC injection water initially filling the lower plenum quite rapidly as slugs of water penetrate down the downcomer (Figure 3.2-30) between 50 seconds and 70 seconds. From 70 seconds to 110 seconds WCOBRA/TRAC calculates the ECC injection to be predominantly bypassed to the break. A gradual buildup of liquid occurs in the downcomer (Fig. 3.2-29) which by about 110 seconds has sufficient head to overcome the upward flow of steam; at that time a plug of ECC injection fluid is calculated to penetrate into the lower plenum. The downcomer pressure decreases, the break discharge decreases, and the downcomer inventory falls when the predicted ECC penetration occurs.

It is believed that the more rapid downcomer pressurization calculated by WCOBRA/TRAC was caused by the

[ ] a, c





[ with an appropriate ]<sup>a,c</sup>  
 loss coefficient and used the boundary condition of the pressure at the pipe flow meter location. As shown in the response to 440.348 (c), this simpler model provided an improved prediction of downcomer pressure and higher mass flows out of the break. The simple break separator model predicts a lower rate of penetration than was seen in WCAP-14171, with more water carried out through the break.

- c) The magnitude of the overprediction is comparable for Phases A and BI. Note also that the overprediction of Phase BI has increased somewhat in the computations performed with revised modeling of the UPTF test facility as reported in the response to RAI 440.348 part (c). The predicted Phase BI bypass is now approximately equal to the total mass of steam and water injected.
- d) During phase B2 the broken cold leg steam flow (Figure 3.2-33) is under-predicted, whereas, the broken cold leg integrated mixture flowrate (Figure 3.2-35) is well predicted. This indicates that the liquid exit flow is correspondingly slightly over-predicted by an equal amount. The percentage error for the vapor flow will be much larger than for the liquid flow because of the relative sizes of the vapor and liquid mass flows. Since the steam flow is underpredicted, the rate of condensation in the downcomer must be over-predicted. This does not result in an under-prediction of pressure, because of the problems of modelling the break separator as discussed in the response to part (b).

If the measured exit steam mass flow rate were regarded as accurate, it would indicate that the rate of condensation in the downcomer is overpredicted. However, good agreement is obtained between the WCOBRA/TRAC calculated and the measured liquid temperature at the bottom of the downcomer in UPTF Test 6, indicating that downcomer condensation is well predicted by WCOBRA/TRAC. Consequently, it is judged that it is the steam mass flow measurements which are inaccurate and the underprediction of exit steam mass flow is less than is indicated by Figure 3.2-33. An analysis in Reference 440.344-1 also indicates that the measured exit steam flow is too high in the UPTF facility. Furthermore, there is a relatively large uncertainty in the mass balance for the tests. In the sensitivity calculation reported as the response to question 440.348 (c), the break modelling is improved. This causes the predicted steam flow rate for phase B2 to increase, i.e., it is underpredicted by less. The mixture mass flow rate is unchanged in the sensitivity calculations. No build up of liquid in the lower plenum during test phase B2 is predicted (Figure 3.2-32). However, the measured build up is approximately 5000 lb (i.e., 2.5 seconds of injected flow), which is short compared to the total duration of the test phase B2. The effect of the lower plenum mass discrepancy on the overall mass balance cannot be assessed because the mass of liquid suspended in the downcomer was not available from the test measurements.

#### Reference

- 440.344-1 "Summary of Results from the UPTF Downcomer Separate Effects Tests, Comparison to Previous Scaled Tests and Application to U. S. Pressurized Water Reactors," MPR-1163, July 1990

SSAR Revision: NONE

## NRC REQUEST FOR ADDITIONAL INFORMATION



Question 440.346

Re: WCAP-14171 (WCOBRA/TRAC CAD)

The AP600 has a 2 x 4 configuration. This means the broken cold leg is in a loop with one hot leg and another, intact, cold leg. How has WCOBRA/TRAC modeling of this break configuration been assessed? If it has not been assessed, justify the uncertainty applied to the AP600 WCOBRA/TRAC calculated results and the applicability of WCOBRA/TRAC to this break configuration.

Response:

The AP600 2X4 configuration is the same as a Combustion Engineering or Babcock & Wilcox PWR. There is no specific loop configuration data supporting the licensed LOCA models for these plants. WCOBRA/TRAC modeling of the AP600 2 x 4 loop configuration does not require further assessment. The AP600 is equipped with a safety grade RCP trip feature, which is activated after receipt of an "S" signal once a timer delay has elapsed. Since the delay associated with the timer is 15 seconds, the RCPs continue to operate during the majority of the blowdown phase of a large break LOCA event. Offsite power is considered to remain available both because the probability is high that it will and because assuming its loss would accentuate the core cooling obtained from reverse flow downward through the core to feed the break for the limiting cold leg breaks. After trip occurs, the RCP in the intact leg of the broken loop coasts down in almost the same fashion as the intact loop RCPs (Figure 440.346-1) in the Reference 440.346-1 CD=0.8 DECLG break case. Prediction of RCP powered operation and subsequent coastdown after trip is well within the capability of WCOBRA/TRAC as documented in the CQD and requires no further assessment.

The Reference 440.346-1 SSAR large break LOCA analysis indicates that forward flow through the intact cold leg and RCP of the broken loop is maintained for the first seven seconds of blowdown, as shown for the CD=0.8 DECLG break analyzed with WCOBRA/TRAC (Figure 440.346-2). At that time voiding in the RCS degrades the performance of all RCPs (Figure 440.346-3). Flow reverses through the RCP in the intact cold leg of the broken loop to feed the break. Since the broken cold leg itself in the broken loop is no different from the broken cold leg in the more common 4 X 4 loop configuration, it is modeled in the same way as the standard Westinghouse plants. The Reference 440.346-1 analysis is therefore using a fully assessed broken loop cold leg model methodology from the CQD, and existing WCOBRA/TRAC assessments are sufficient to conclude that the code is applicable to modeling the AP600 cold leg break configuration.

Referring to the PIRT provided in WCAP-14171, the number of cold legs could influence the ECC bypass phenomena. The AP600 has 4 cold legs, which is what was tested in UPTF with direct vessel injection. Therefore, this aspect of the AP600 geometry is addressed. Again referring to the PIRT, the number of hot legs is somewhat important during blowdown reverse flow and during reflood for entrainment. WCOBRA/TRAC has been validated against the LOFT tests, which have two hot legs (Reference 440.346-2). Therefore, while no single test has the AP600 2 x 4 geometry, the most important PIRT phenomena are already separately addressed by other tests. Furthermore, in terms of the uncertainty to be applied to the AP600 WCOBRA/TRAC analysis, there is no need to add anything to the standard uncertainty computation to account for the 2 X 4 loop configuration because of this evaluation and because both the break flow modeling and RCP two-phase performance prediction remain the same.



Reference:

- 440.346-1 Letter NTD-NRC-95-4503, "Preliminary Marked Up Sections of SSAR Chapter 15, Revision 5", July 10, 1995
- 440.346-2 Bajorek, S. M., et. al., "Code Qualification Document for Best Estimate Analysis," WCAP-12945-P, Revision 1 (Proprietary), Volume 3, Chapter 14.

SSAR Revision: NONE



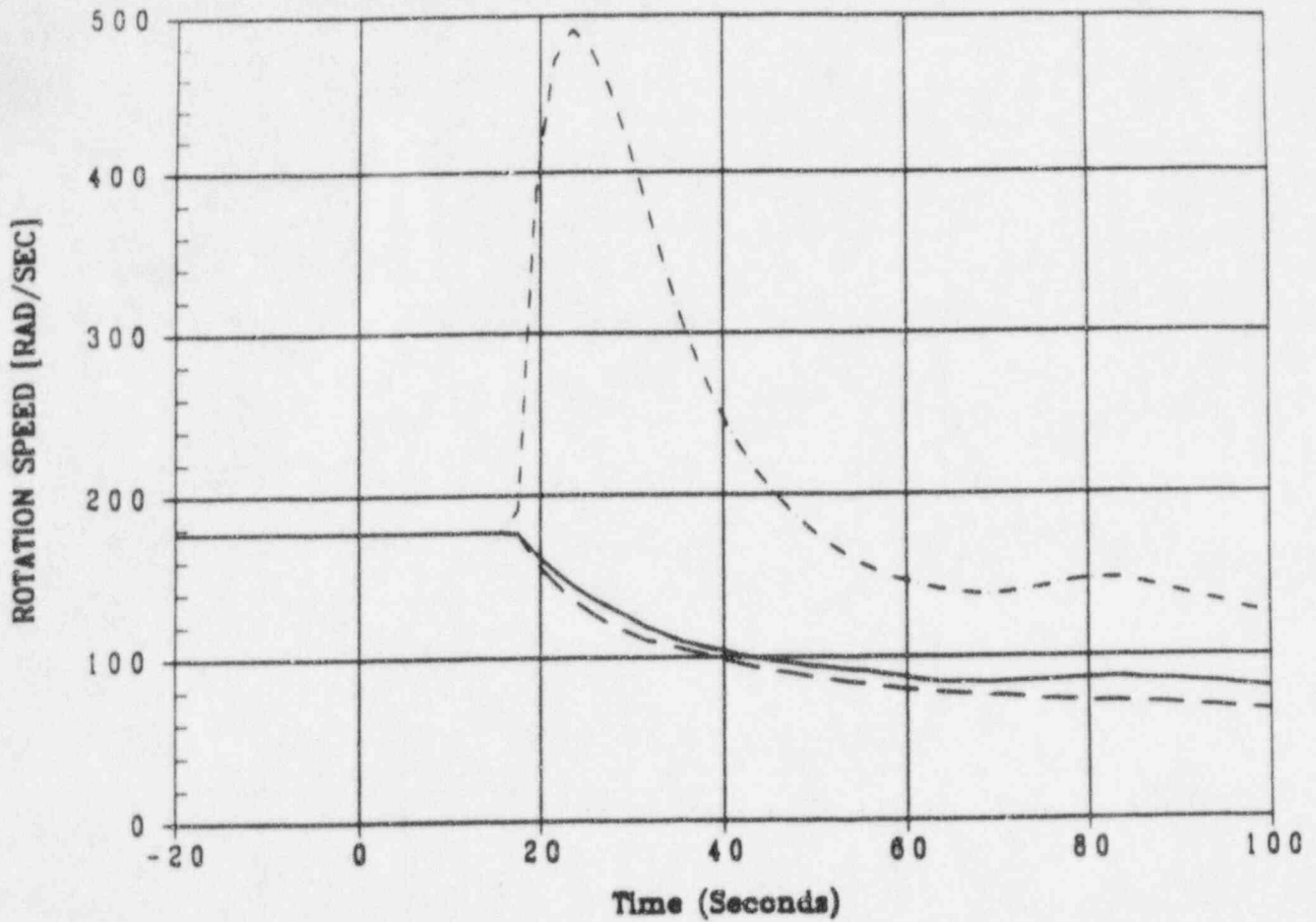
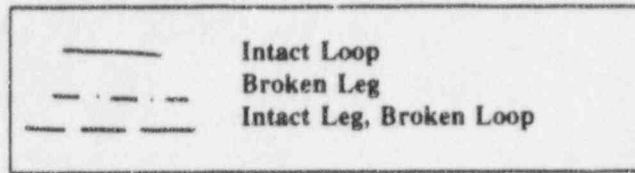


Figure 440.346-1 CD=0.8 DECLA Break Transient - AP600, Pump Speeds

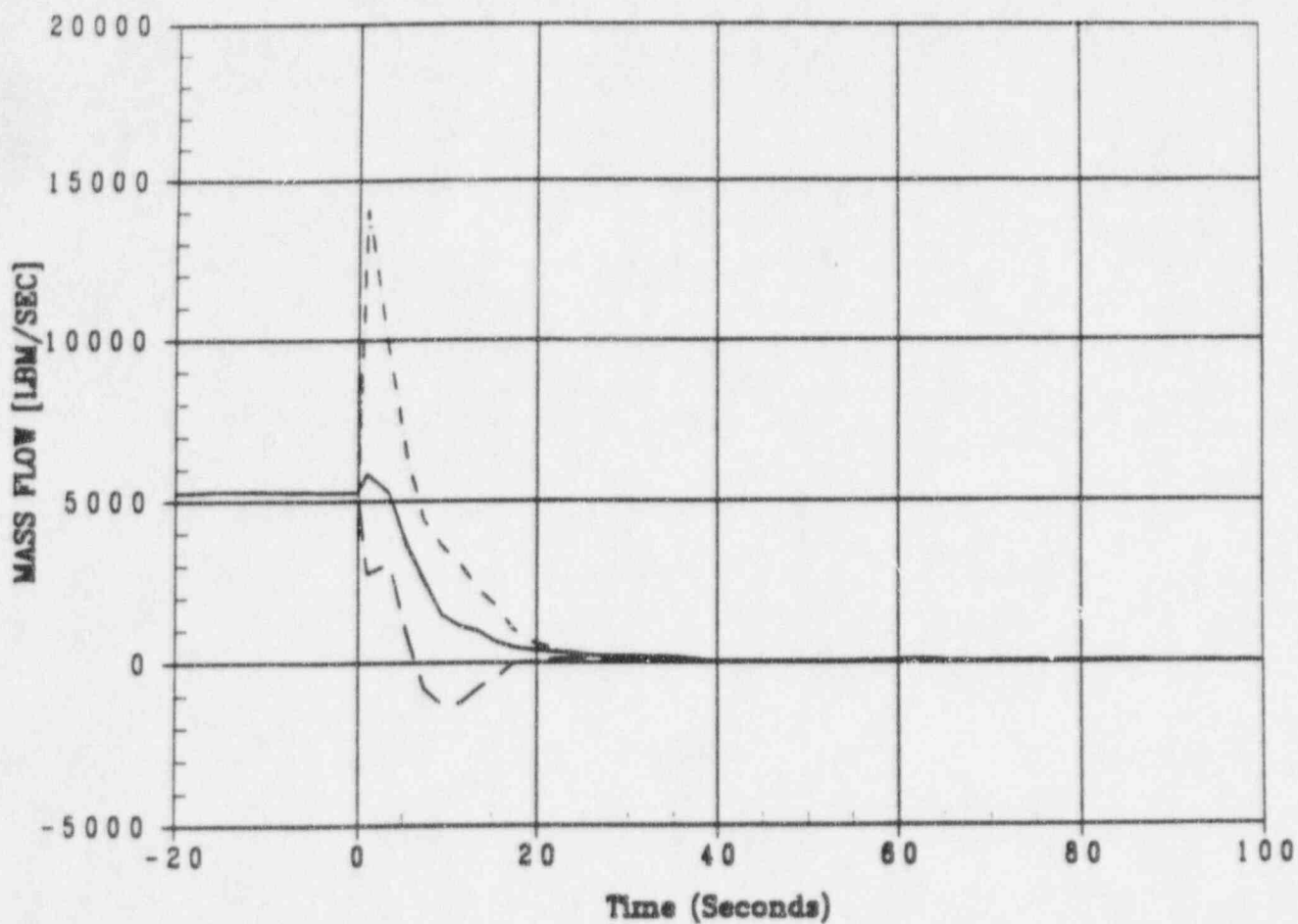
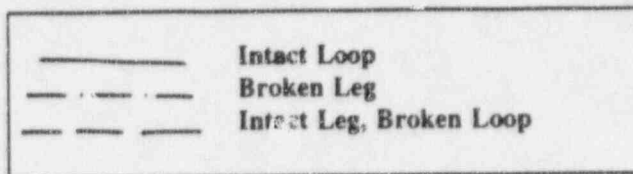


Figure 440.346-2 CD=0.8 DECLG Break Transient - AP600, Pump Mass Flows

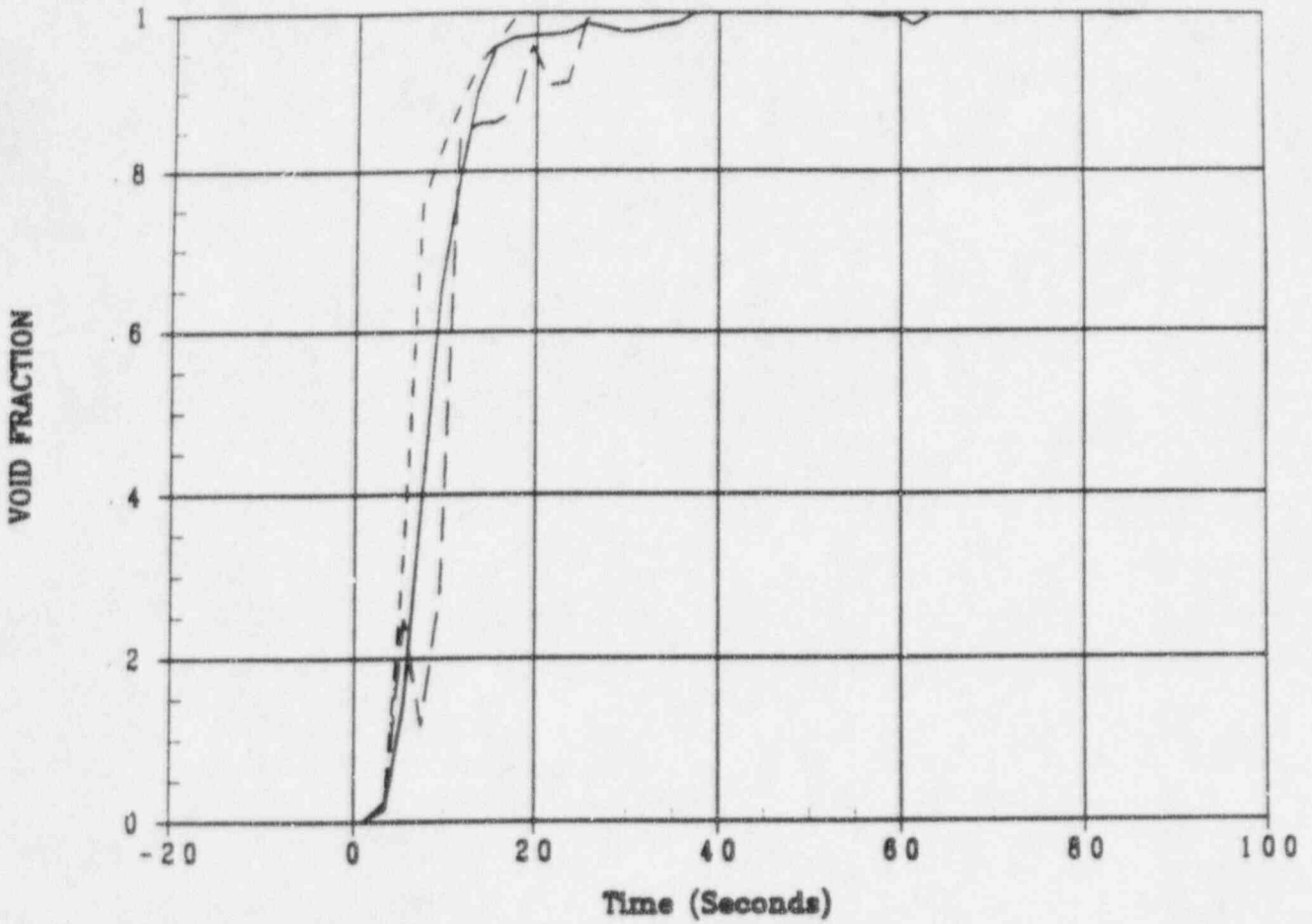
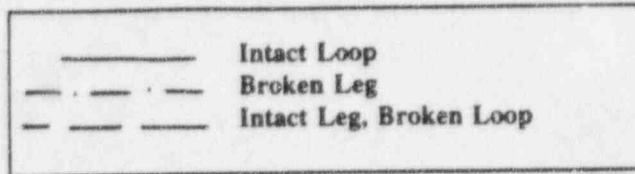


Figure 440.346-3 CD=0.8 DECLG Break Transient - AP600, Pump Void Fractions

## NRC REQUEST FOR ADDITIONAL INFORMATION



Question 440.347

Re: WCAP-14171 (WCOBRA/TRAC CAD)

The WCOBRA/TRAC calculated results for AP600 show significant blowdown cooling due to flow from the upper head. Westinghouse indicated that in some WCOBRA/TRAC calculations, this blowdown cooling results in the quenching of the entire core (all rods at all elevations). Because of the impact of this quenching on the stored energy in the rods at the beginning of reflood, clarify what WCOBRA/TRAC assessments demonstrate the accuracy of WCOBRA/TRAC's calculation of this behavior. Justify that the assessed conditions cover the range of conditions expected in AP600 analyses. If no assessment was done, provide WCOBRA/TRAC comparisons to test data that cover the required range of conditions.

Response:

WCOBRA/TRAC calculations of the G1 and G2 top down flow blowdown tests (Reference 440.347-1) have shown that WCOBRA/TRAC provides a good prediction of the thermal hydraulic behavior associated with these flow conditions. The results show that there was a tendency for WCOBRA/TRAC to underpredict film boiling heat transfer and rewetting at the center of the bundle and, in the case of the G1 comparison, to overpredict the extent of rewetting at both ends of the bundle. It should be noted, however, that the rod thermocouple data averaging procedure eliminated readings which were greater than 3 standard deviations from the mean. Therefore, heater rod readings which indicated early rewet were procedurally removed along with bad thermocouple readings, resulting in a calculated average which was higher than the true average temperature, especially at the ends of the bundle, where rewetting was more predominant.

An assessment of the WCOBRA/TRAC calculated blowdown flow conditions for a reference AP600 DECLG ( $C_D=0.8$ ) break transient shows that the calculated mass fluxes through the core are very similar to the range of conditions modeled in the G1 and G2 tests. The liquid flux down into the top of each fuel assembly is calculated to exceed 100 lbm/sec.-sq.ft. for about four seconds in the reference case. Furthermore, several significant differences between the conditions in the AP600 transient and the G1 and G2 tests simulated indicate cooling and the initiation of fuel rod quenching in AP600 are more easily achieved. These differences are discussed below.

First, the hot rod and hot assembly rod fuel rod temperatures of AP600 agree well with the G1 and G2 tests, while the rest of the core has significantly lower initial rod temperatures than in the G1 and G2 tests (by 400 to 500°F). Also, the average linear rating for each of the AP600 rods is lower than those of the G1 and G2 tests simulated. The AP600 hot assembly linear power equals 0.396 KW/ft at the time of peak downflow into the core, compared to 0.669 KW/ft and 0.642 KW/ft for G1 and G2, respectively; the other AP600 fuel rods modeled exhibit even lower powers. Significant top down flow is calculated in the AP600 transient by 6.0 seconds in the core channel connected directly to the upper head via the guide tubes, and even earlier in the low power core periphery channel. At this time, the system pressure is 350 psi higher than that modeled in the G1 and G2 tests, and the higher pressure promotes better steam cooling of the AP600 fuel due to the higher density of the steam. In addition, the AP600 fuel design has more grids in the upper half of the core (8 compared to 3 in the G1 and G2 test facilities). The added grids promote additional cooling via increased turbulence and droplet breakup, and they also provide additional sites which will quench prior to the fuel rods themselves. AP600 fuel rods differ from the test heater rod fuel simulators in that a gap exists between the fuel pellets and the clad. This gap retards heat transfer to the clad from the heat



generated in the fuel pellets, allowing the clad to quench more rapidly than the clad of the test heater rods, which is thermally more closely connected to the heater element by filler material. WCOBRA/TRAC underpredicts the film boiling heat transfer and rewetting at the center of the core in the G1 and G2 simulations. All the differences noted above improve the rod to fluid heat transfer and/or promote quenching of rods in AP600 relative to those in the G1 and G2 tests. Basing the prediction of fuel rod quench in the AP600 transient on the models as benchmarked in Reference 440.347-1 is appropriate and conservative.

Reference

440.347-1 Bajorek, S. M., et. al., "Code Qualification Document for Best Estimate Analysis," WCAP-12945-P, Revision 1 (Proprietary), Volume 2, Chapter 11, Sections 11-3 and 11-4.

SSAR Revision: NONE





## NRC REQUEST FOR ADDITIONAL INFORMATION



Question 440.348

Re: WCAP-14171 (WCOBRA/TRAC CAD)

To clarify WCOBRA/TRAC's ability to calculate downcomer injection:

- a) Compare the WCOBRA/TRAC flooding curves for the CCTF and UPTF calculations to the those based on the test data. Include comparisons to the Wallis and Kutateladze flooding curves as appropriate. Clarify the reasons for any differences between the WCOBRA/TRAC curves and the test data or the WCOBRA/TRAC curves and the Wallis and Kutateladze curves.
- b) Compare the WCOBRA/TRAC calculated and the experimentally measured vessel refill rates for the CCTF and UPTF tests.
- c) Analyze the baseline tests for CCTF Run 58 and UPTF Test 21 with WCOBRA/TRAC. Compare the calculated and measured results for all the tests and clarify if the trends observed in the experiments from the baseline case to the test case were properly calculated by WCOBRA/TRAC. If not, clarify why and discuss any implications for AP600 BE LBLOCA analyses.
- d) Because only one PCT comparison was available from the downcomer injection tests presented in WCAP- 141 71, provide the results of other CCTF tests with downcomer injection if possible. Alternately, downcomer injection tests from other test facilities could be used to provide additional, quantitative PCT data on WCOBRA/TRAC's ability to accurately calculate downcomer injection. If additional downcomer injection tests with PCT are not available, provide additional comparisons to downcomer injection tests without PCT data if available.
- e) Compare the conditions in CCTF Run 58 and UPTF Test 21 to those expected in AP600. For those conditions in AP600 not covered by the CCTF or UPTF tests, justify the use of WCOBRA/TRAC to calculate the AP600 response under those conditions, or provide additional assessments to cover the required range of conditions.

Response:

- a) The CCTF test 58 does not simulate the ECC water bypass period of a LBLOCA transient, so it is not considered in this response.

The direct comparison between the calculation and the experiment of the lower plenum liquid penetration rates is consistent with WCOBRA/TRAC providing a good prediction of "flooding", with a tendency to underpredict the liquid penetration rate. This conclusion is further substantiated by UPTF test 21 sensitivity calculations which investigated the effects of increasing the broken loop pressure loss coefficients (Refer to RAi response part (c)).

The Wallis and Kutateladze correlations are not appropriate to the UPTF facility because it is full scale, and the correlations are based on data from reduced scale facilities. It was found in Reference 440.348-1 that it is not possible to fit this type of correlation to UPTF total downcomer penetration because of the effect of location



of ECC injection. Also it was noted in Reference 440.348-1 that during a test, penetration far away from the broken loop can be injection limited, while there is no penetration from injection points close to the broken leg.

The UPTF test 21 data for downcomer liquid penetration has been compared with the correlation presented in Reference 440.348-2. This correlation is based on the approaches of Wallis and Kutateladze, but it has been extended to account for the scale dependent effects that are observed in the full scale UPTF facility. The main difference between Kutateladze scaling and the correlation of Reference 440.348-2 is that the correlation accounts for the azimuthal distribution of the sources of injected water to the downcomer, whereas the Kutateladze approach assumes homogenous flow. It is observed in the tests that penetration occurs around the injection sources far from the broken cold leg, but much less penetration occurs near the broken cold leg.

The correlation predicts for phases A and B1 that there is no penetration from the downcomer nozzle close to the broken cold leg and complete penetration from the downcomer nozzle far from the broken cold leg, (i.e., the rate of lower plenum water build-up for phases A and B1 are 2006 lb/sec and 1884 lb/sec respectively). The measured rate of lower plenum liquid buildup in phase A (Figure 3.2-16) is of the order of 1000 lb/sec during 50-80 seconds and no penetration at other times. The measured rate of liquid build-up in the lower plenum in phase B1 (Figure 3.2-24) is approximately 250 lb/sec over the full duration of the phase. The correlation predicts that for phase B2 there is no penetration from either downcomer nozzle. The measured rate of liquid build-up in the lower plenum during phase B2 (Figure 3.2-32) is approximately 75 lb/sec. The correlation predicts that for phase B3 there is complete penetration of the liquid from both downcomer nozzles, i.e., a combined flow rate of 3791 lb/sec. The measured rate of liquid buildup in the lower plenum during phase B3 (Figure 3.2-32) is approximately 1300 lb/sec for 20 seconds and then no further liquid penetration.

Thus, it can be seen that the correlation overpredicts the rate of liquid penetration in phases A, B1, and B3. This overprediction is attributed to the downcomer water injection velocity. In UPTF test 6, water is injected from the intact cold legs with a typical average velocity of 3 feet/second, whereas in UPTF test 21, the water is injected from the downcomer nozzles with a typical average velocity of 80 feet/second. The higher injection velocity in UPTF test 21 causes more effective break-up of the water jet, which decreases the amount of penetration to the lower plenum and increases the amount of carryover to the broken cold leg.

Thus, the correlation of Reference 440.348-1 is not applicable to UPTF test 21. However, as has been stated in the report, WCOBRA/TRAC has provided good modelling of the phenomena occurring during the test and the WCOBRA/TRAC calculations are in reasonable agreement with the test results.

- (b) CCTF Run 58 simulates the reflood phase of a LBLOCA. It was initiated with the lower plenum filled to a level of 2.82 ft. The downcomer quickly fills with water after initiation of accumulator injection and the downcomer remains full up to the cold leg elevation (Figure 3.1-35, WCAP-14171). As shown, the WCOBRA/TRAC calculation accurately predicts this refill sequence, as well as the filling of the vessel during the subsequent core reflood.

UPTF Test 21 simulates the end of the blowdown phase of a large break LOCA. The integrated mixture discharge rates can be seen in Figures 3.2-19, 3.2-27 and 3.2-34 and the lower plenum refill rates can be inferred from Figures 3.2-16, 3.2-24 and 3.2-32. The mixture discharge rate is over-predicted in test phases A, B1 and





B3. The discharge is well predicted in test phase B2. In phase A the lower plenum penetration is not predicted. In phase B1 the rate of penetration is over-predicted initially, then penetration is predicted to cease until the end of the test phase. In phase B2 the penetration is not predicted. In phase B3 the measured penetration is at a uniform rate, then the penetration ceases. In the calculation of phase B3, the initial rate is correct and the penetration is then predicted to cease. Only the duration of the penetration is underpredicted. Hence the general tendency for the predictions is to overpredict discharge at the break and underpredict penetration to the lower plenum.

- (c) In response to this question, the direct vessel injection calculations which are discussed below were performed in a manner consistent with WCOBRA/TRAC CQD RAI responses using the latest modeling criteria. Changes to the CCTF model include the losses in the broken cold leg leading to the containment simulator tanks, heater rod material properties, and minor adjustments to flow areas and wetted perimeters in the vessel. Results obtained for Run 62 are provided in Reference 440.348-3. The UPTF model was similarly changed to improve the broken cold leg pressure loss calculation. The cold leg break modeling was [

[

] a, c  
] a, c

The baseline test for CCTF is C2-4 (Run 62). This test simulated cold leg injection and can be compared directly to the downcomer injection test C2-AA2 (Run 58), which is similar in all respects except for the ECC injection location. The major differences in the experimental data of the two tests are as follows. Run 58 experienced significant downcomer/core flow oscillations throughout the test which were not evident in Run 62. The explanation for these oscillations put forward by the experimentalists states that they are perpetuated by the following sequence of events. When the downcomer collapsed liquid level rises, the downcomer injection nozzles became submerged and the condensation of steam is reduced, resulting in an increase in the downcomer pressure. At the same time, the core level falls, causing a reduction in the steam production rate in the core. The increased  $\Delta P$  between the downcomer and the core forces the liquid back into the core, which uncovers the downcomer injection nozzles. The consequences of the core recovering and the associated decrease in downcomer level are increased steam production in the core, uncovering of the downcomer nozzles that results in an increased condensation rate at the ECC injection point, resulting in a reduced downcomer pressure which causes the cycle to repeat.

Another difference between the two tests is that the downcomer liquid in Run 58 is more subcooled because the ECC liquid is injected directly into the downcomer without mixing with the intact loop steam. The injected ECC liquid in the base case test, however, is significantly heated by its nearly complete mixing with intact loop steam in the cold legs before it enters the downcomer.

The final difference is the effect of the oscillatory downcomer/core flow on the quench front progression in Run 58. The quench front progression is retarded in Run 58 compared to the base case because the transfer of heat from the rods is reduced during the period of decreased liquid level in the core, which corresponds to the flow reversal period of the oscillation cycle.



A brief summary description of the WCOBRA/TRAC calculated results is now provided. The times discussed refer to the start of the transient in the experiment, i.e. time zero is the start of accumulator injection to the lower plenum.

#### CCTF Calculation Run 62 (Reference 440.348-3)

The calculated system pressure shows good agreement with the data throughout the transient. A good prediction of the steam flow in the two hot legs is achieved except for a slight overprediction in the broken loop (~ 0.5 lb/sec) after 200 seconds. Again, a good prediction of the liquid flows in the hot legs is achieved except for an overprediction (~ 0.5 lb/sec) in both the intact and broken loops between 60 and 200 seconds. The total core differential pressure is underpredicted after 300 seconds, and a stable oscillatory flow behavior is indicated during the period from 200 to 500 seconds. The pressure oscillations are fairly significant (~ 0.5 psi) and are not observed in the experiment. The pressure fluctuation is, as expected, reflected in the calculated total downcomer differential pressure. The downcomer differential pressure falls below the data after 200 seconds. The calculated overall core thermal response is good. There is a tendency to overpredict the clad temperatures above mid-elevation due to an underprediction of the quench front progression, which is approximately 50 seconds delayed compared to experiment. The calculated peak clad temperatures in the lower half of the core are well predicted.

#### CCTF Calculation Run 58

Figures 440.348-1 through 440.348-35 are attached to compare the newly calculated system parameters for CCTF Test 58 with the experimental data. The system pressure is slightly overpredicted for the majority of the transient. This corresponds to the overprediction of steam production in the core due to predicting an early advancement of the quench front. The hot leg steam flow is slightly overpredicted in the intact loops (~ 0.3 lb/s) and is a bit more overpredicted in the broken loop (0.6 to 1.0 lb/s). Liquid flow in the intact loop hot legs is generally well predicted by WCOBRA/TRAC until more than 500 seconds have elapsed and is overpredicted from 150-300 seconds. After this time hot leg liquid flows are significantly overpredicted, probably due to the advanced quench front. The calculated total core differential pressure agrees well with the test data, while the downcomer differential pressure is slightly lower than the data, indicating that the collapsed liquid level is lower in the calculation. In terms of the calculated core thermal response, the peak clad temperatures at all elevations are well predicted with a tendency for overprediction at very high elevations (10 ft). The greatest discrepancy is the quench front progression, which is calculated to be in advance of the data by approximately 80 seconds.

#### Comparison between WCOBRA/TRAC test predictions of the data

The calculations are very similar in most respects except for the effects of the different rates of quench front progression. The rates of quench front progression seen in the calculations are retarded and advanced relative to those observed in the experiments for CCTF Test 62 and Test 58, respectively. The cause of each difference appears to be the same: the core oscillatory flow behavior corresponds to a lower quench front progression rate than does a more stable core flow. In Run 58 the calculated collapsed downcomer liquid level stabilizes below the downcomer injection point, so the rapid oscillating flow cycle observed in the test is not calculated in either magnitude or time interval. In Run 62 an oscillatory flow between the downcomer and the core is predicted by





WCOBRA/TRAC, contrary to what is seen in the test, and quench front advancement is underpredicted. The code prediction may be explained by the following argument. Liquid slugs falling into the downcomer from the cold legs force an increased amount of liquid into the core. The resulting increase in core steam production in turn forces the downcomer liquid level to rise, and the liquid is ejected into the broken cold leg. This causes a local pressurization as the steam from the intact loops flows out the broken cold leg with an increased liquid content and therefore at an increased pressure drop. The downcomer liquid level then decreases, and the flow cycle continues. This flow behavior cause the calculated collapsed liquid level to fall below the data. This is indicated by the downcomer differential pressure comparison. By 400 seconds, the WCOBRA/TRAC downcomer differential pressure is more than one psi below the data of Run 62 (Reference 440.348-3). The downcomer fluid subcooling difference observed between the experimental tests is also seen in the calculations.

The WCOBRA/TRAC simulation of Run 58 overpredicts the upper plenum pressure (Figure 440.348-19) because the code is removing energy at a faster rate than the test, as shown in quench front plots 440.348-16, 17 and 18. The code predicts a faster reflood than occurred in the test, but the high powered rod PCT prediction are conservatively high.

#### UPTF WCOBRA/TRAC Predictions

The baseline test for the UPTF series of tests is test 6. These are five different phases (131, 132, 133, 135, and 136) associated with this test. All simulate cold leg injection with no direct downcomer injection and model the bypass flow period of an LBLOCA. The total ECC injection flow was ~ 3,200 lb/sec for each phase, and the combined steam generator and core simulator- injected steam flow varied from 230 lb/sec to 960 lb/sec over the range of phases. The ECC liquid subcooling varied from 50° F to 110° F. In comparison, the equivalent downcomer ECC injection test, Test 21 phases A, BI, BII and BIII, simulated an ECC injection rate of ~ 4160 lb/sec (885 lb/sec for BII) with a corresponding range of steam flows, from 500 to 1515 lb/sec. The liquid subcooling varied from 85°F to 380°F. Unlike the CCTF test 62 and 58, the UPTF tests are not directly comparable, so only general trends will be described.

The experimental test results for each phase of test 6 show that water penetration to the lower plenum was mainly controlled by the cold leg arrangement with respect to the break and steam injection rate. There is complete bypass from the cold leg adjacent to the break with partial delivery to the lower plenum from the two opposite cold legs for steam flows greater than 600 lb/sec. There is complete bypass from the adjacent cold leg and nearly complete delivery from the opposite cold legs for steam flows between 220 to 600 lb/sec. There is partial delivery from the adjacent cold leg and complete delivery from the opposite cold legs for steam flows less than 220 lb/sec. The delivery of flow to the lower plenum was in the form of plugs of liquid which first accumulated in the cold legs. The measurement of subcooling in the downcomer indicated that the water present in the downcomer was localized around the cold leg nozzles, leading to a heterogeneous flow.

The downcomer flow regime for the UPTF test 21 was different and relates to the method of ECC liquid injection. The flow from the injection nozzles deflected off the core barrel and dispersed around the downcomer. The upward flow of steam from the core carried a significant proportion of the liquid out of the break. Some penetration occurred and the rest was deposited in the intact loops where it accumulated. The



process of dispersing liquid around the downcomer causes the ECC liquid delivery rate to the lower plenum to be significantly less for the downcomer injection test, UPTF 21, compared to cold leg injection UPTF test 6.

The calculated results for the different phases of UPTF test 6 are similar in terms of their comparison with the data (Reference 440.348-3). The system pressure for each of the phases is in general slightly underpredicted. The delivery into the downcomer and lower plenum is by slugs of liquid from the intact legs, as observed in the experiment. The rate of delivery was accurately calculated; however, the timing in all cases was delayed. As a consequence of the delay the degree of bypass was overpredicted.

Inspection of the predictions for UPTF test 21 shows that there is a tendency to underpredict the discharge of steam from the break and to over-predict the pressure in the system. This is attributed to the modelling of the break separator. In the calculations reported in WCAP-14171, the break separator has been modelled <sup>a, c</sup> <sub>a, c</sub>

results of these calculations are attached as Figures 440.348-36 through 440.348-59, and they correspond to Figures 3.2-16 to 3.2-39 in WCAP-14171. The downcomer injection UPTF test 21 simulations exhibited a tendency to underpredict the downcomer pressure. The different flow behavior as a result of the ECC water break up on the core barrel was predicted by the calculations. For the low steam flow test phases, B2 and B3, the calculation predicted a high rate of penetration into the lower plenum at the start of phase B3, but the duration of the penetration was less, resulting in a smaller quantity of water reaching the lower plenum. The lower rate of penetration observed in the test during phase B2 was not predicted. For the higher steam flow phases, A and B1, no significant liquid penetration into the lower plenum was predicted.

The UPTF test comparisons presented in Reference 440.348-3, in WCAP-14171 and herein show that the WCOBRA/TRAC computer code is capable of predicting the different ECC flow behaviors associated with either cold leg or downcomer injection. The rate of liquid delivery into the lower plenum is for the majority of cases well predicted, while the timing and duration of this delivery is not. This results in the overprediction of the ECC bypass flow for all tests considered, which is conservative.

Regarding the AP600 ECCS performance analysis, the oscillations which were observed in the CCTF Test 58 are judged to be less likely to occur during the reflooding of the AP600 core. At CCTF the downcomer injection nozzle was located at almost the same elevation as the cold legs, so the covering and uncovering of the ECC injection stream and the subsequent condensation effects are pronounced. The AP600 reactor vessel design, on the other hand, locates the DVI nozzle at an elevation two feet below the bottom of the cold leg. Once the nozzles recover, ECC injection flow is likely to remain submerged throughout the core reflood phase of a postulated large break LOCA event in AP600. Downcomer condensation and the associated oscillations will therefore be minimized.

- (d) Test C2 - AA2 (Run 58) is the only CCTF test which simulated long term downcomer injection with the vent valves (which allow a flow path between the upper plenum and the downcomer) in the closed position. Tests which simulated downcomer injection with the vent valves open exhibit different flow behavior which is not prototypic of the AP600 plant design, so these tests are not appropriate as validation data for WCOBRA/TRAC.

**NRC REQUEST FOR ADDITIONAL INFORMATION**



Overall, the test comparisons provide the necessary assurance that WCOBRA/TRAC can properly predict the large break LOCA thermal-hydraulic performance of the AP600. Within the core itself, the reflood heat transfer behavior of the fuel rods is independent of whether the ECC injection locations are in the downcomer or the cold legs. Also, the PCT behavior of CCTF Test C2-AA2 is not significantly different from the CCTF tests with which WCOBRA/TRAC was compared in the CQD.

- (e) The design of the UPTF test facility was based on a 3900 MWt German PWR. Runs 272 and 274, selected for analysis from the series of five quasi-steady state runs which form UPTF Test 21, simulate the end of blowdown and beginning of refill phases of a LBLOCA. The two runs were performed to investigate the possible bypass of the ECC water to the broken loop. The test conditions were as tabulated below:

UPTF Cases

Run/Phase	Total ECC Injection To Downcomer (lb/sec)	Steam Flowrate From Core To Downcomer (lb/sec)	Subcooling Of ECC Water (°F)
272/A	4017	692	211
274/BI	3750	657	101
274/BII	1951	227	56
274/BIII	3791	225	47

An assessment of the WCOBRA/TRAC calculation for a typical AP600 DECLGB ( $C_D = 0.8$ ) transient shows that during the period of bypass of ECC water to the broken loop, the corresponding calculated conditions vary as shown below:

WCOBRA/TRAC  $C_D = 0.8$ , DECLG Break

Total ECC Injection To Downcomer (lb/sec)	Steam Flowrate From Core To Downcomer (lb/sec)	Subcooling Of ECC Water (°F)
1860 to 1940	550 to 250	280 to 167



The major parameters affecting bypass are the steam velocity up the downcomer to the break, the ECC injection locations and rate of injection and the subcooling of the ECC water. Both UPTF and AP600 have four cold legs and two downcomer injection nozzles. The height and cross-sectional flow areas of the downcomers are similar and therefore the steam flowrates up the downcomer should be approximately the same, in order for the steam velocities and bypass phenomena to be similar. The above tables show that the AP600 steam flowrates are within the range covered by the UPTF tests. The ECC injection rates in AP600 correspond to the lowest of those used in the UPTF tests. The higher pressures associated with the early phase of the bypass period in the AP600 transient produce ECC subcoolings which are greater than those simulated in the UPTF test phases, however during the later phase of bypass when complete bypass is no longer calculated the ECC subcooling is comparable with the UPTF test conditions.

Given the conservative calculations of the amount of ECC liquid bypassed to the break by WCOBRA/TRAC, we believe that the overall good correspondence between the UPTF and AP600 conditions gives confidence that this phase of a LBLOCA is well validated by the UPTF calculations. Furthermore, the AP600 reactor vessel is equipped with flow diverters opposite the direct vessel injection line penetrations to direct flow downward.

CCTF Run 58 simulates the end of refill and reflood phases of a LBLOCA typical of Appendix K conditions for a "standard" 4-loop plant. One of the main objectives of the experiment was the assessment of the PCT during the transient. This is dictated, to a large extent, by the stored energy in the fuel rods at the beginning of reflood. In CCTF Run 58, the PCT at the beginning of reflood was 1466°F, which is representative of an unquenched core following blowdown.

The WCOBRA/TRAC calculations for a typical AP600 DECLGB ( $C_D = 0.8$ ) transient shows that the PCT at the beginning of reflood is only 670°F. This relatively low value is the result of the core-wide quench produced by the flow from the upper head during blowdown.

We believe that the good WCOBRA/TRAC calculation of the reflood behavior and clad temperatures of CCTF Run 58 gives added confidence to the existing reflood validation evidence. We therefore are confident that WCOBRA/TRAC adequately calculates reflood behavior for the less onerous conditions associated with AP600.

Also, the WCOBRA/TRAC simulations of other CCTF tests, tests which responded similarly to Run 58, comprise a large data base assessing WCOBRA/TRAC for large break LOCA reflood.

#### References:

- 440.348-1 "Summary of Results from the UPTF Downcomer Separate Effects Tests - Comparison to Previous Scaled Tests and Application to U. S. PWRs", MPR-1163, July 1990
- 440.348-2 H. Glaeser, "Downcomer and Tie Plate Counter-current Flow in the Upper Plenum Test Facility (UPTF)," Nuclear Eng. and Des., 133, (1992), pp 259-283.





**NRC REQUEST FOR ADDITIONAL INFORMATION**



---

440.348-3 Letter, N. J. Liparulo to USNRC, "Preliminary Responses to Requests for Additional Information Regarding WCAP-12945-P," NTD-NRC-95-4399, Attachment U, February 9, 1995

SSAR Revision: NONE



## List of Figures

Figure	Title
1	CCTF Run 58, Low Powered Rod, Clad Temperature at 1.25 ft
2	CCTF Run 58, Low Powered Rod, Clad Temperature at 3.33 ft
3	CCTF Run 58, Low Powered Rod, Clad Temperature at 6 ft
4	CCTF Run 58, Low Powered Rod, Clad Temperature at 8 ft
5	CCTF Run 58, Low Powered Rod, Clad Temperature at 10 ft
6	CCTF Run 58, Medium Powered Rod, Clad Temperature at 1.25 ft
7	CCTF Run 58, Medium Powered Rod, Clad Temperature at 3.33 ft
8	CCTF Run 58, Medium Powered Rod, Clad Temperature at 6 ft
9	CCTF Run 58, Medium Powered Rod, Clad Temperature at 8 ft
10	CCTF Run 58, Medium Powered Rod, Clad Temperature at 10 ft
11	CCTF Run 58, High Powered Rod, Clad Temperature at 1.25 ft
12	CCTF Run 58, High Powered Rod, Clad Temperature at 3.33 ft
13	CCTF Run 58, High Powered Rod, Clad Temperature at 6 ft
14	CCTF Run 58, High Powered Rod, Clad Temperature at 8 ft
15	CCTF Run 58, High Powered Rod, Clad Temperature at 10 ft
16	CCTF Run 58, Quench Envelope - Low Powered Rod
17	CCTF Run 58, Quench Envelope - Medium Powered Rod
18	CCTF Run 58, Quench Envelope - High Powered Rod
19	CCTF Run 58, Upper Plenum Pressure
20	CCTF Run 58, Downcomer Differential Pressure
21	CCTF Run 58, Core Differential Pressure
22	CCTF Run 58, Upper Plenum to Containment Differential Pressure
23	CCTF Run 58, Loop 1 Pump Simulator Differential Pressure
24	CCTF Run 58, Loop 4 Pump Simulator Differential Pressure
25	CCTF Run 58, Loop 1 Cold Leg Water Mass Flow
26	CCTF Run 58, Loop 1 Cold Leg Steam Mass Flow
27	CCTF Run 58, Loop 4 Cold Leg Water Mass Flow
28	CCTF Run 58, Loop 4 Cold Leg Steam Mass Flow
29	CCTF Run 58, Loop 1 Hot Leg Water Mass Flow
30	CCTF Run 58, Loop 1 Hot Leg Steam Mass Flow
31	CCTF Run 58, Loop 4 Hot Leg Water Mass Flow
32	CCTF Run 58, Loop 4 Hot Leg Steam Mass Flow
33	CCTF Run 58, Vessel Side Cold Leg Integrated Liquid Break Flow
34	CCTF Run 58, Vessel Side, Loop 4, Cold Leg Fluid Temperature
35	CCTF Run 58, Loop 4, Loop Seal Fluid Temperature



List of Figures (cont.)

Figure	Title
36	UPTF Test 21, Phase A, Lower Plenum Mass Inventory
37	UPTF Test 21, Phase A, Broken Cold Leg Steam Mass Flow
38	UPTF Test 21, Phase A, Broken Cold Leg Mixture Mass Flow
39	UPTF Test 21, Phase A, Broken Cold Leg Integrated Mixture Mass Flow
40	UPTF Test 21, Phase A, Downcomer Pressure
41	UPTF Test 21, Phase A, Downcomer Collapsed Liquid Level
42	UPTF Test 21, Phase A, Downcomer Mass Flow Above Bottom of Core Barrel
43	UPTF Test 21, Phase A, Intact Cold Leg Mass Inventories
44	UPTF Test 21, Phase B I, Lower Plenum Mass Inventory
45	UPTF Test 21, Phase B I, Broken Cold Leg Steam Mass Flow
46	UPTF Test 21, Phase B I, Broken Cold Leg Mixture Mass Flow
47	UPTF Test 21, Phase B I, Broken Cold Leg Integrated Mixture Mass Flow
48	UPTF Test 21, Phase B I, Downcomer Pressure
49	UPTF Test 21, Phase B I, Downcomer Collapsed Liquid Level
50	UPTF Test 21, Phase B I, Downcomer Mass Flow Above Bottom of Core Barrel
51	UPTF Test 21, Phase B I, Intact Cold Leg Mass Inventories
52	UPTF Test 21, Phase B II&III, Lower Plenum Mass Inventory
53	UPTF Test 21, Phase B II&III, Broken Cold Leg Steam Mass Flow
54	UPTF Test 21, Phase B II&III, Broken Cold Leg Mixture Mass Flow
55	UPTF Test 21, Phase B II&III, Broken Cold Leg Integrated Mixture Mass Flow
56	UPTF Test 21, Phase B II&III, Downcomer Pressure
57	UPTF Test 21, Phase B II&III, Downcomer Collapsed Liquid Level
58	UPTF Test 21, Phase B II&III, DC Mass Flow Above Bottom of Core Barrel
59	UPTF Test 21, Phase B II&III, Intact Cold Leg Mass Inventories



LOW POWERED ROD - CLAD TEMPERATURE AT 1.25 ft (DEG F)

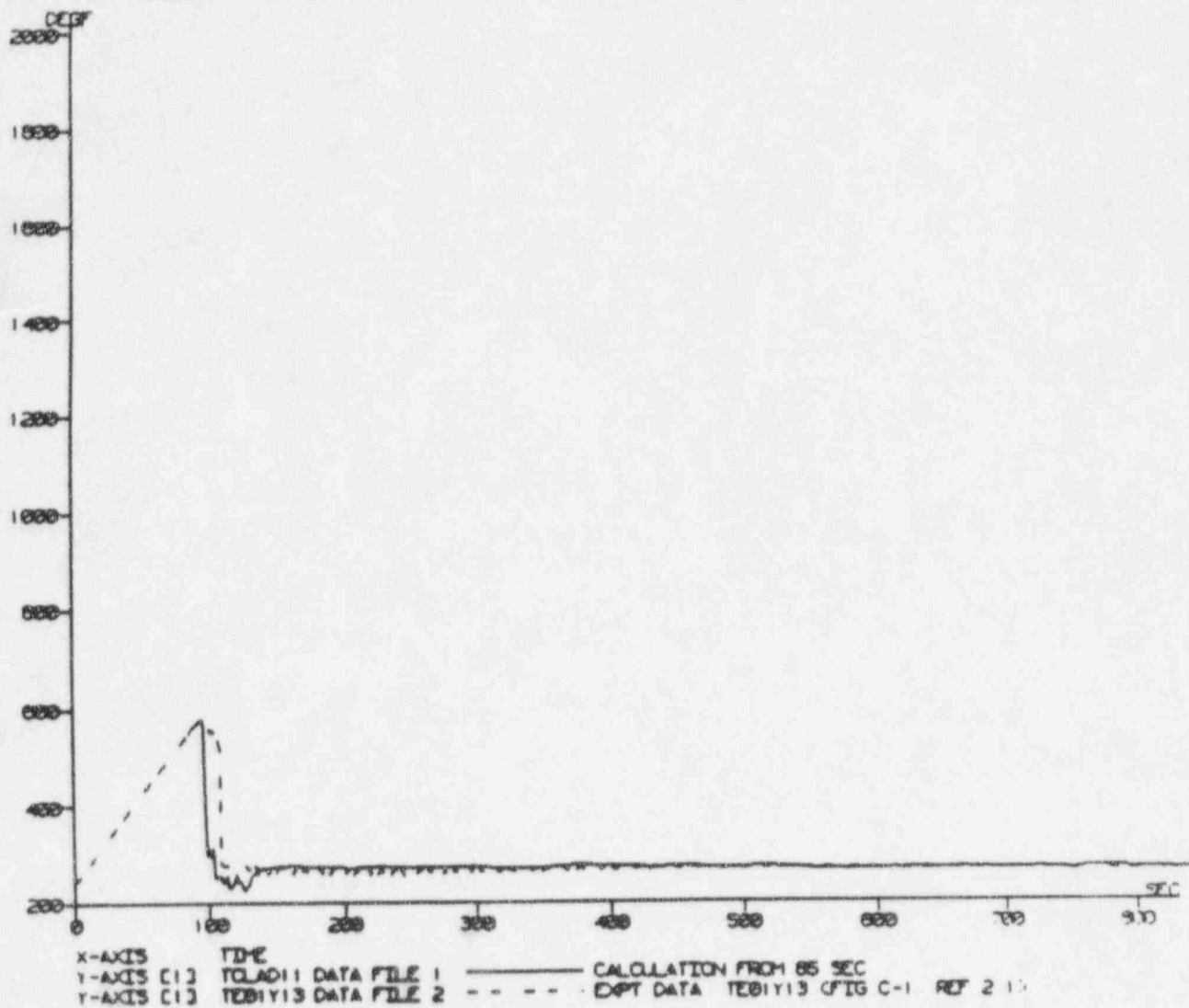


Figure 440.348-1 CCTF Run 58, Low Powered Rod, Clad Temperature at 1.25 ft



LOW POWERED ROD - CLAD TEMPERATURE AT 3.33 ft (DEG F)

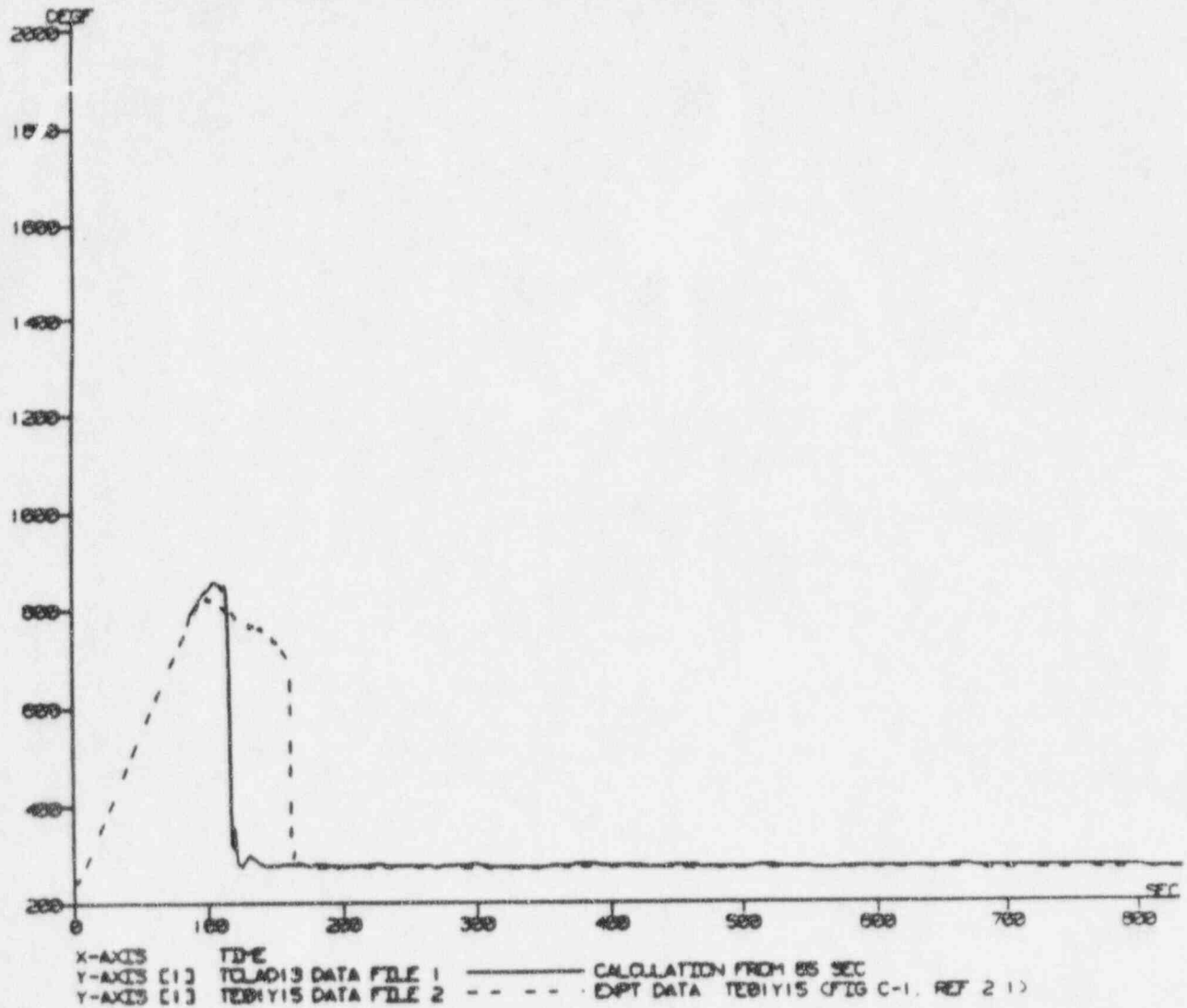


Figure 440.348-2 CCTF Run 58, Low Powered Rod, Clad Temperature at 3.33 ft



LOW POWERED ROD - CLAD TEMPERATURE AT 6 ft (DEG F)

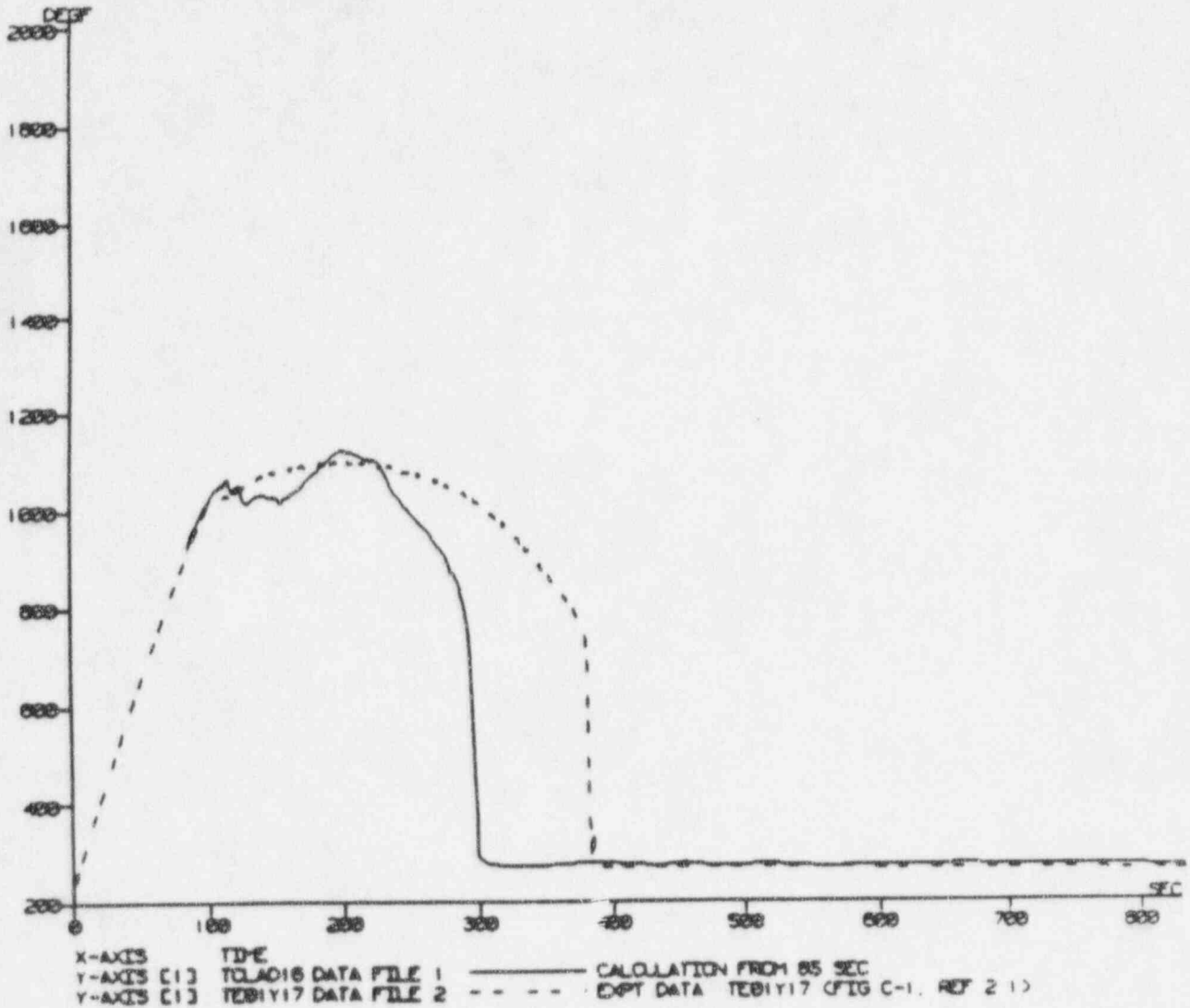


Figure 440.348-3 CCTF Run 56, Low Powered Rod, Clad Temperature at 6 ft



LOW POWERED ROD - CLAD TEMPERATURE AT 8 ft (DEG F)

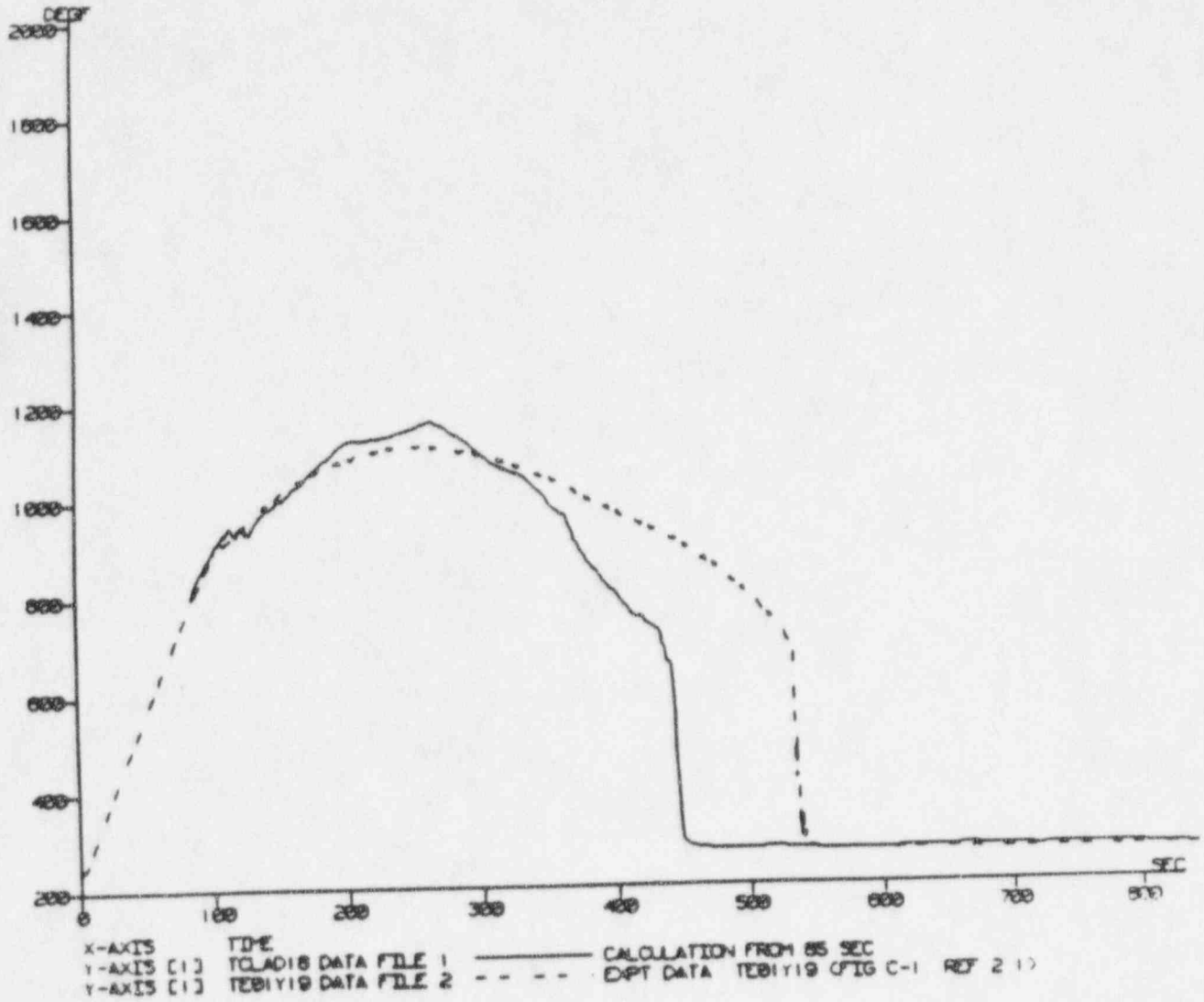


Figure 440.348-4 CCTF Run 58, Low Powered Rod, Clad Temperature at 8 ft



LOW POWERED ROD - CLAD TEMPERATURE AT 10 ft (DEG F)

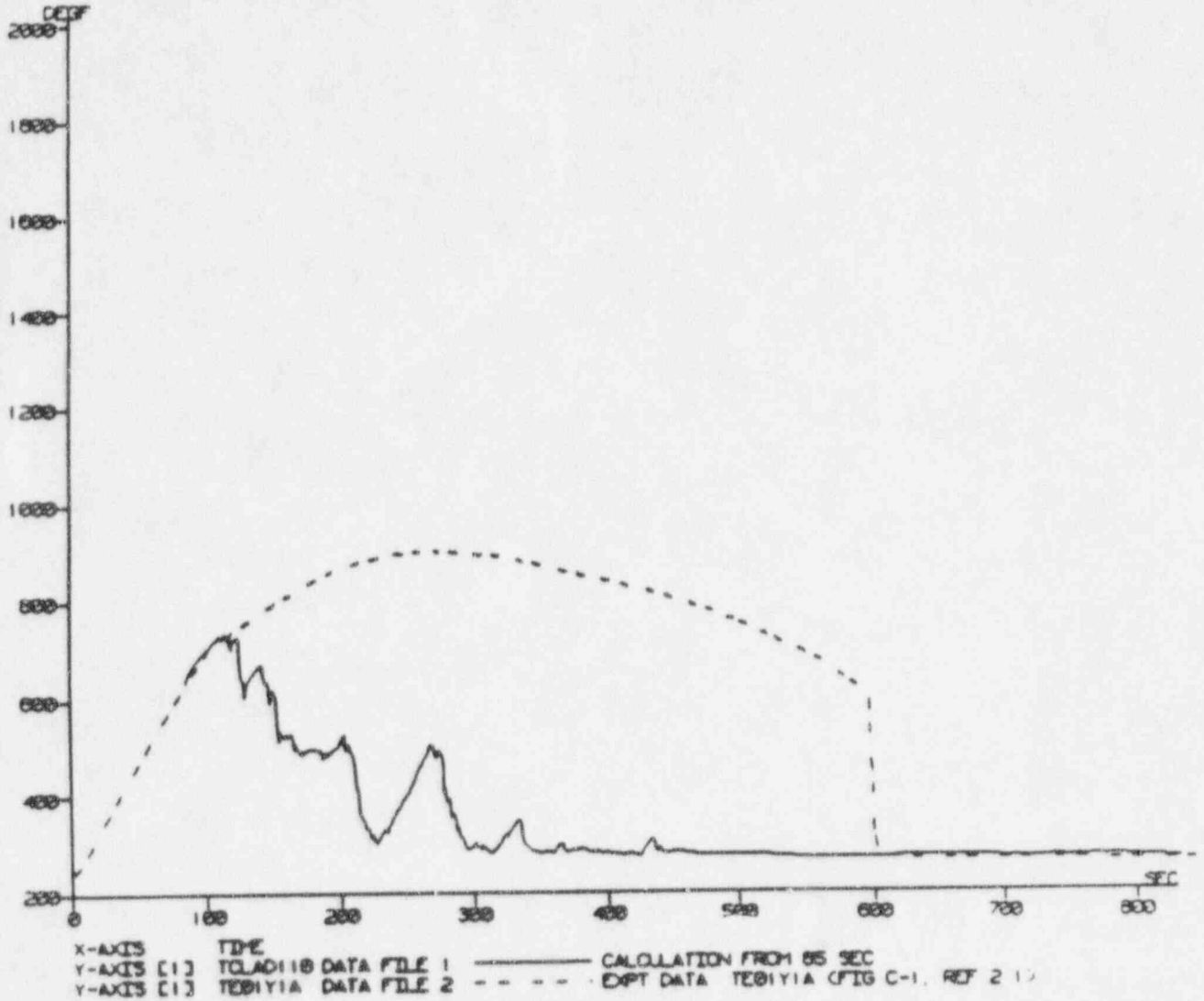


Figure 440.348-5 CCTF Run 58, Low Powered Rod, Clad Temperature at 10 ft





MEDIUM POWERED ROD - CLAD TEMPERATURE AT 1.25 ft (DEG F)

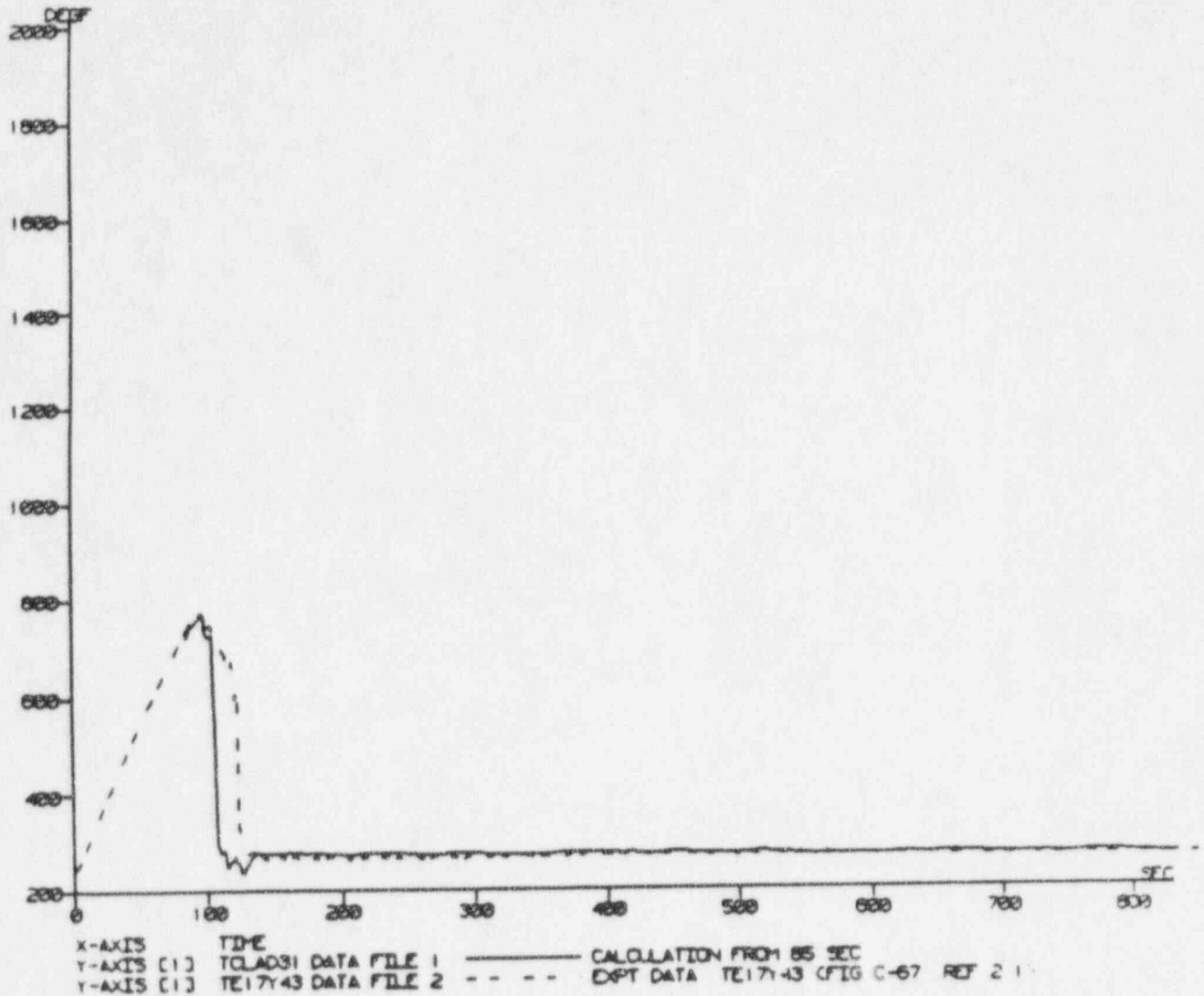


Figure 440.348-6 CCTF Run 58, Medium Powered Rod, Clad Temperature at 1.25 ft

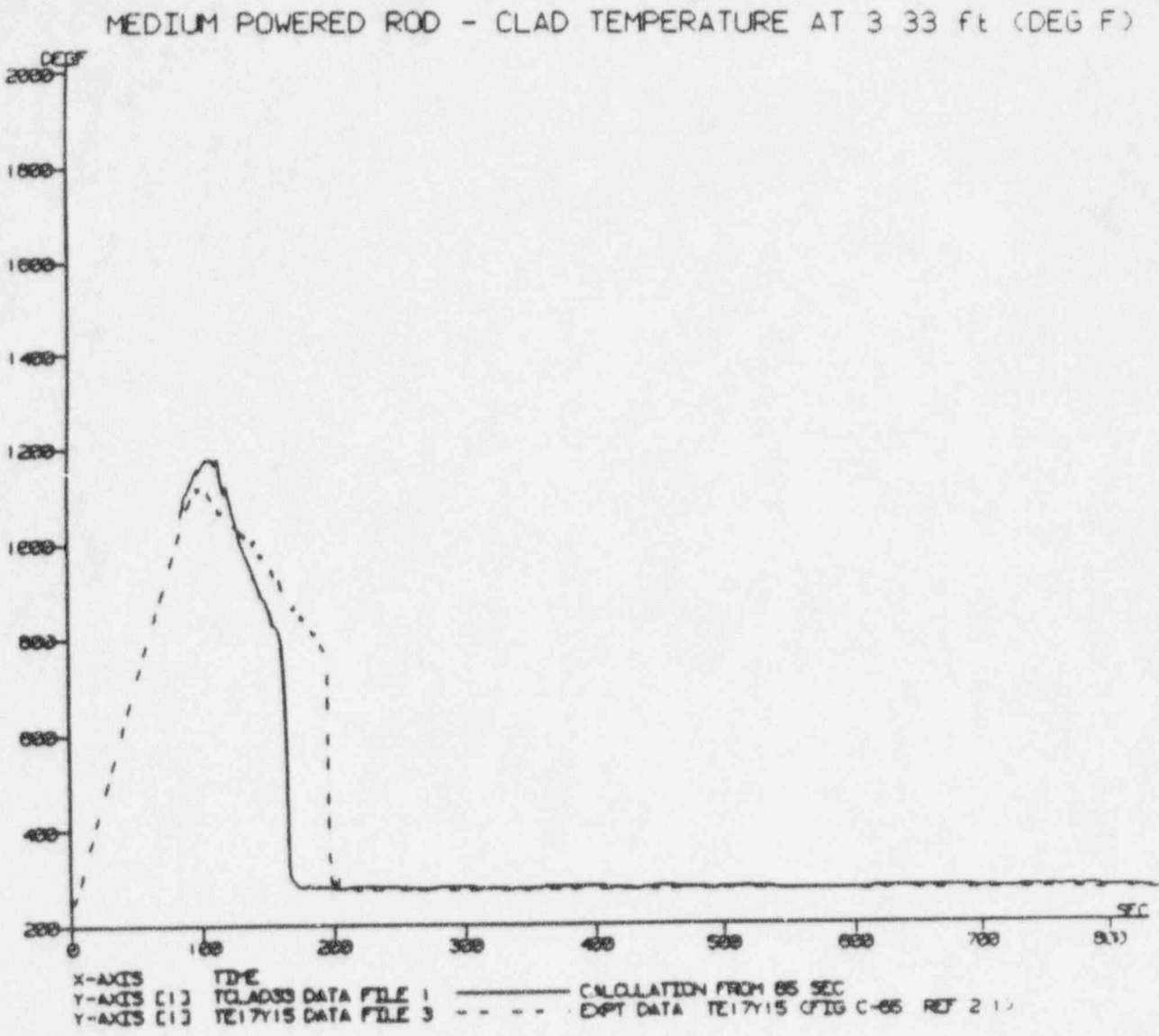
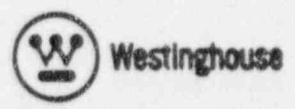


Figure 440.348-7 CCTF Run 58, Medium Powered Rod, Clad Temperature at 3.33 ft





MEDIUM POWERED ROD - CLAD TEMPERATURE AT 6 ft (DEG F)

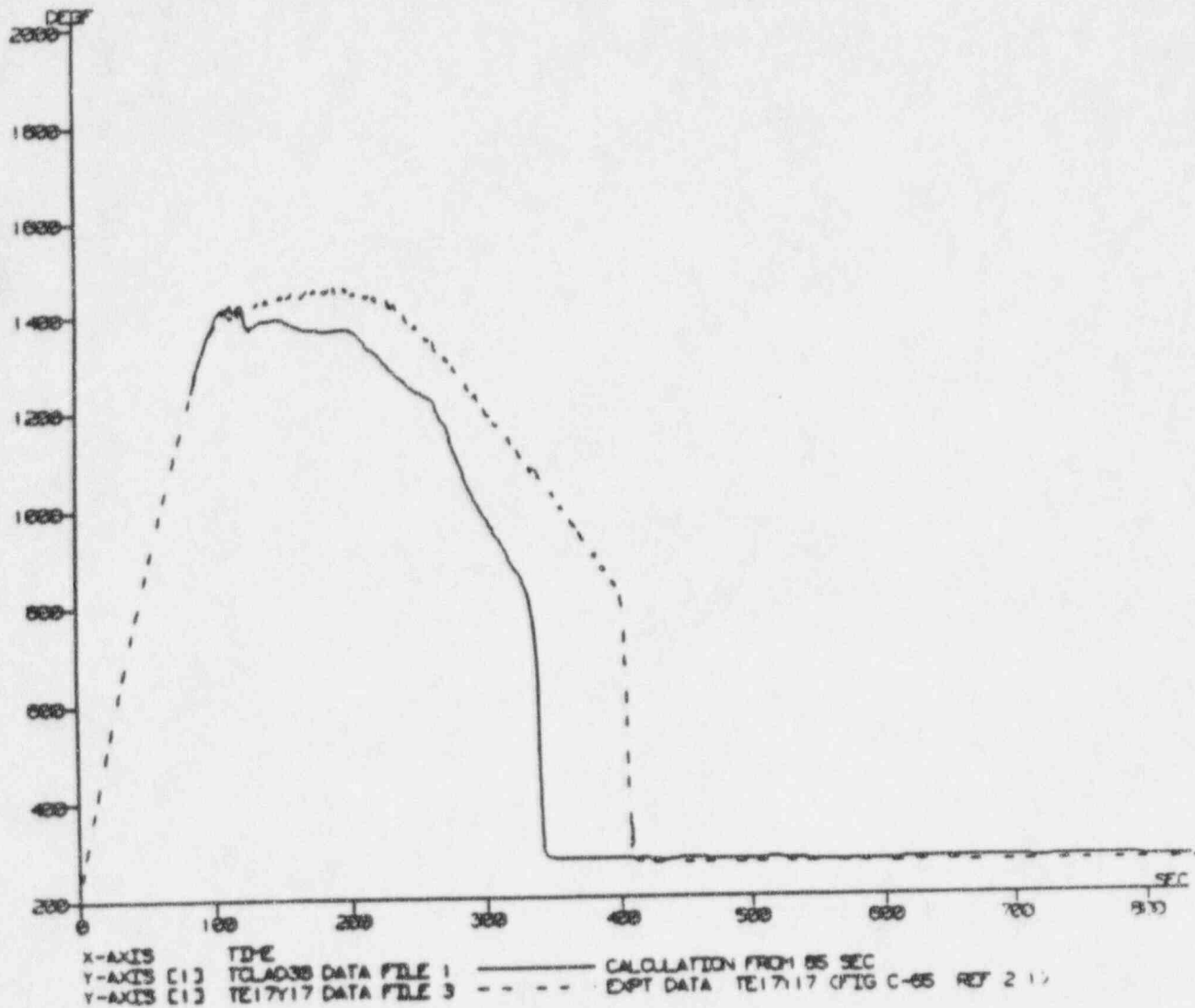


Figure 440.348-8 CCTF Run 58, Medium Powered Rod, Clad Temperature at 6 ft



MEDIUM POWERED ROD - CLAD TEMPERATURE AT 8 ft (DEG F)

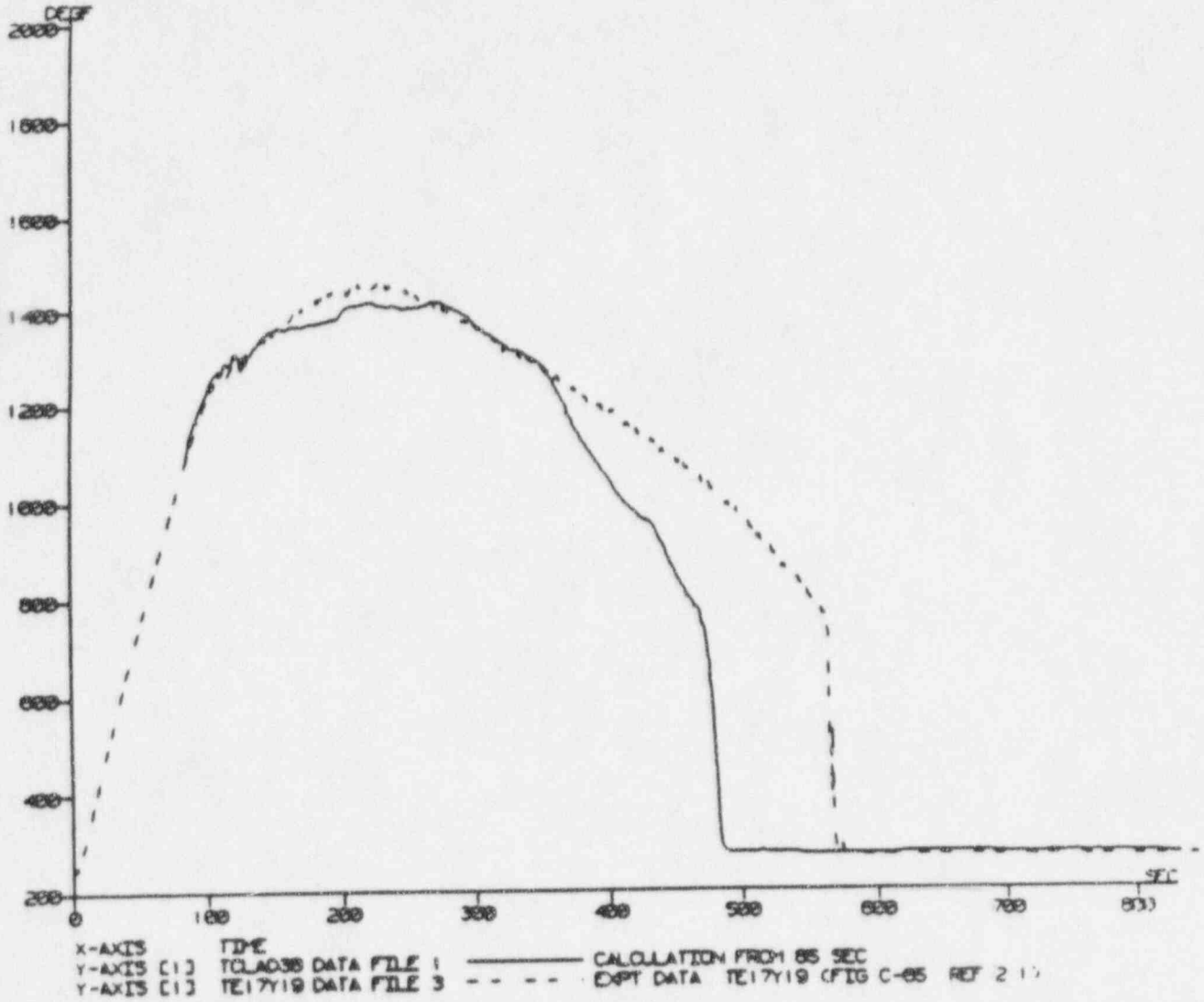


Figure 440.348-9 CCTF Run 58, Medium Powered Rod, Clad Temperature at 8 ft

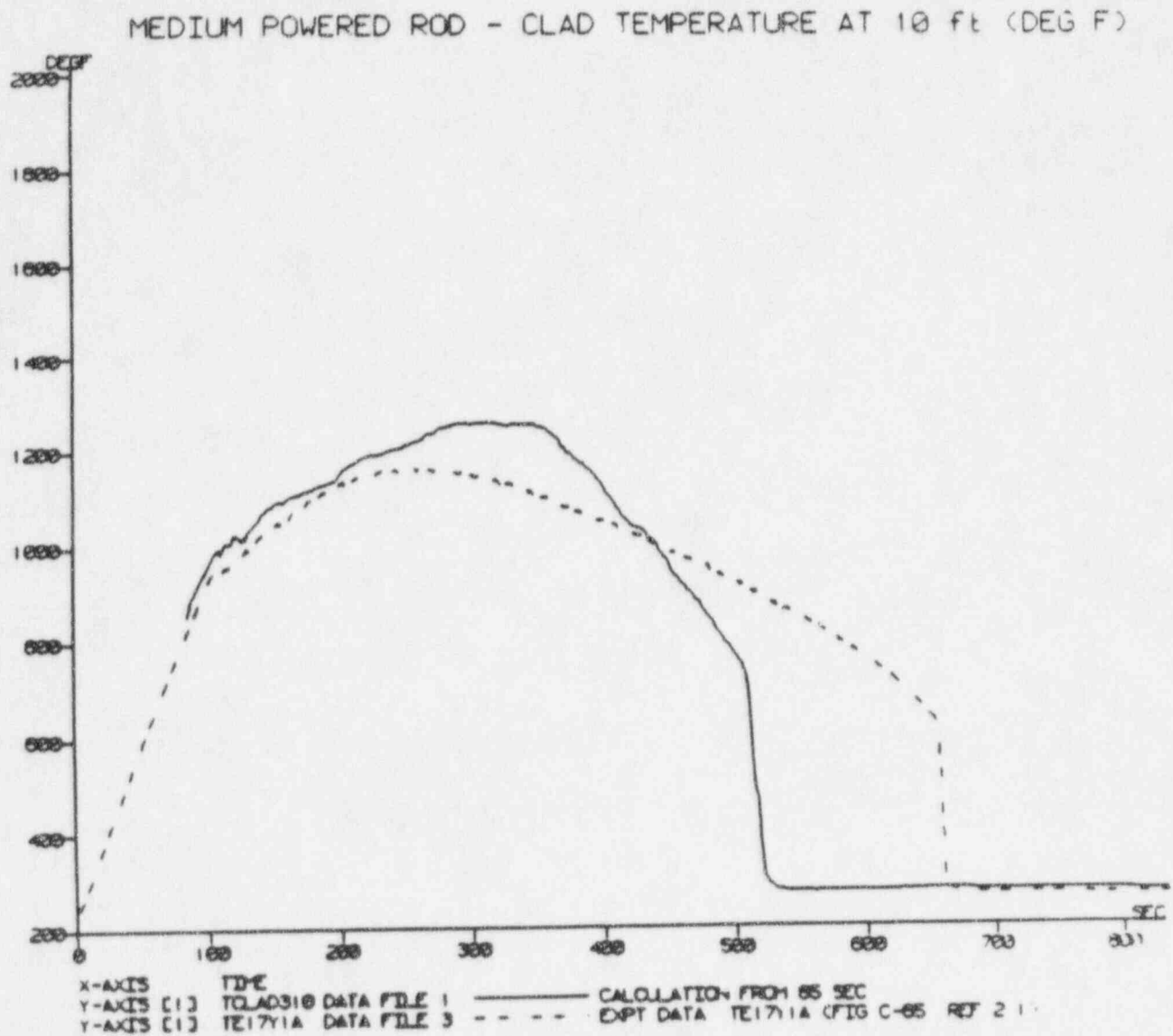


Figure 440.348-10 CCTF Run 58, Medium Powered Rod, Clad Temperature at 10 ft



MEDIUM POWERED ROD - CLAD TEMPERATURE AT 10 ft (DEG F)

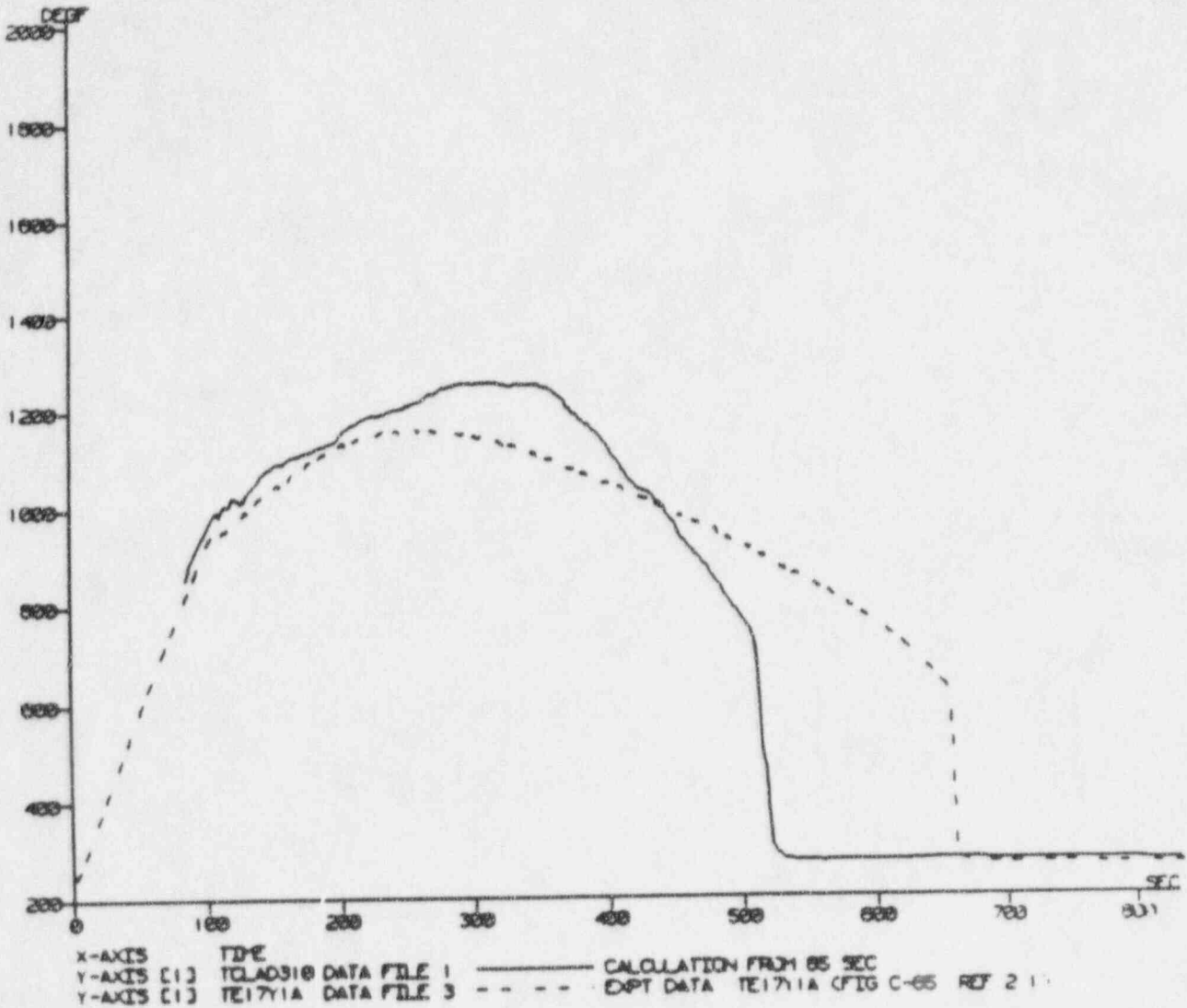


Figure 440.348-10 CCTF Run 58, Medium Powered Rod, Clad Temperature at 10 ft



HIGH POWERED ROD - CLAD TEMPERATURE AT 1.25 FT (DEG F)

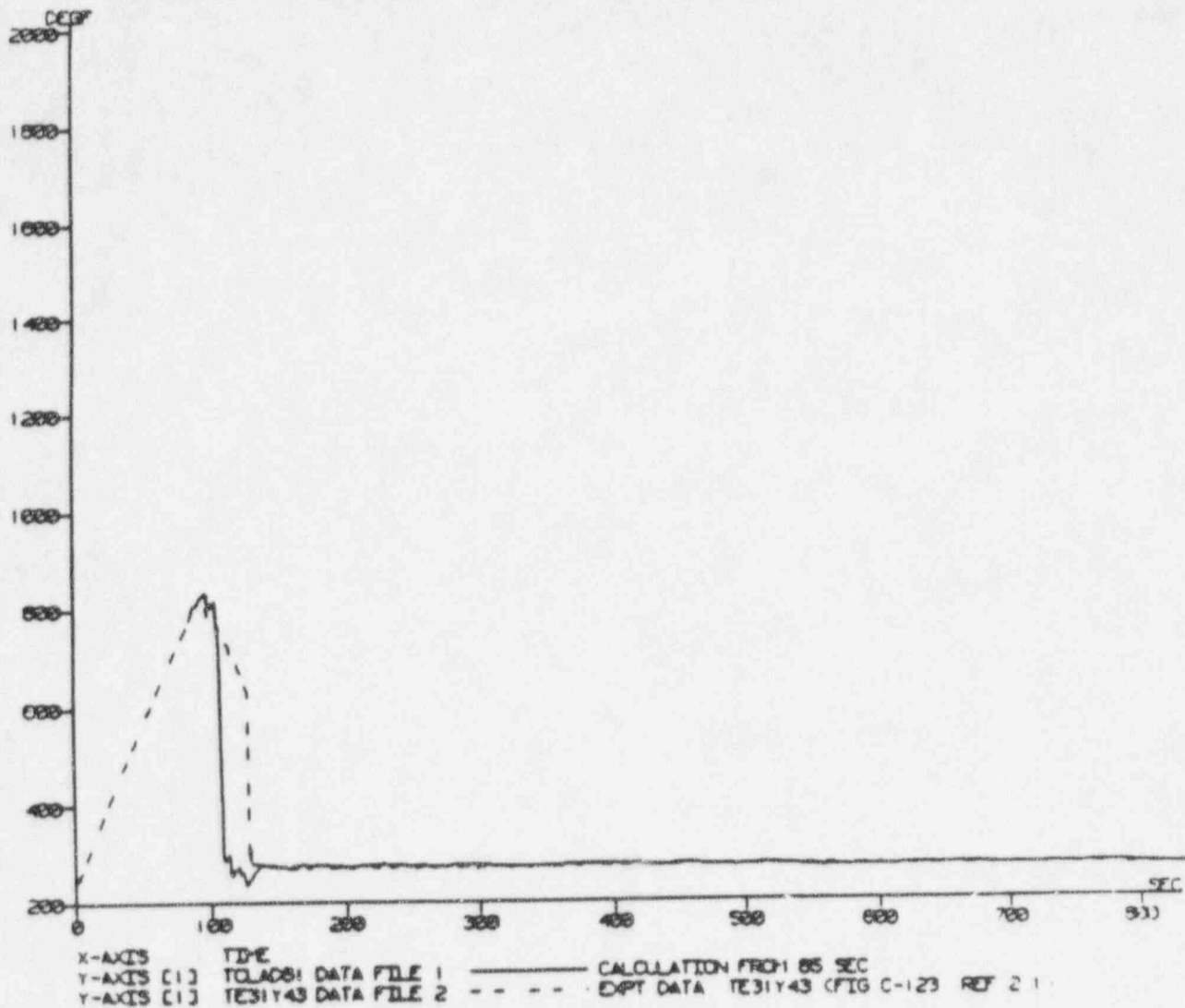


Figure 440.348-11 CCTF Run 58, High Powered Rod, Clad Temperature at 1.25 ft

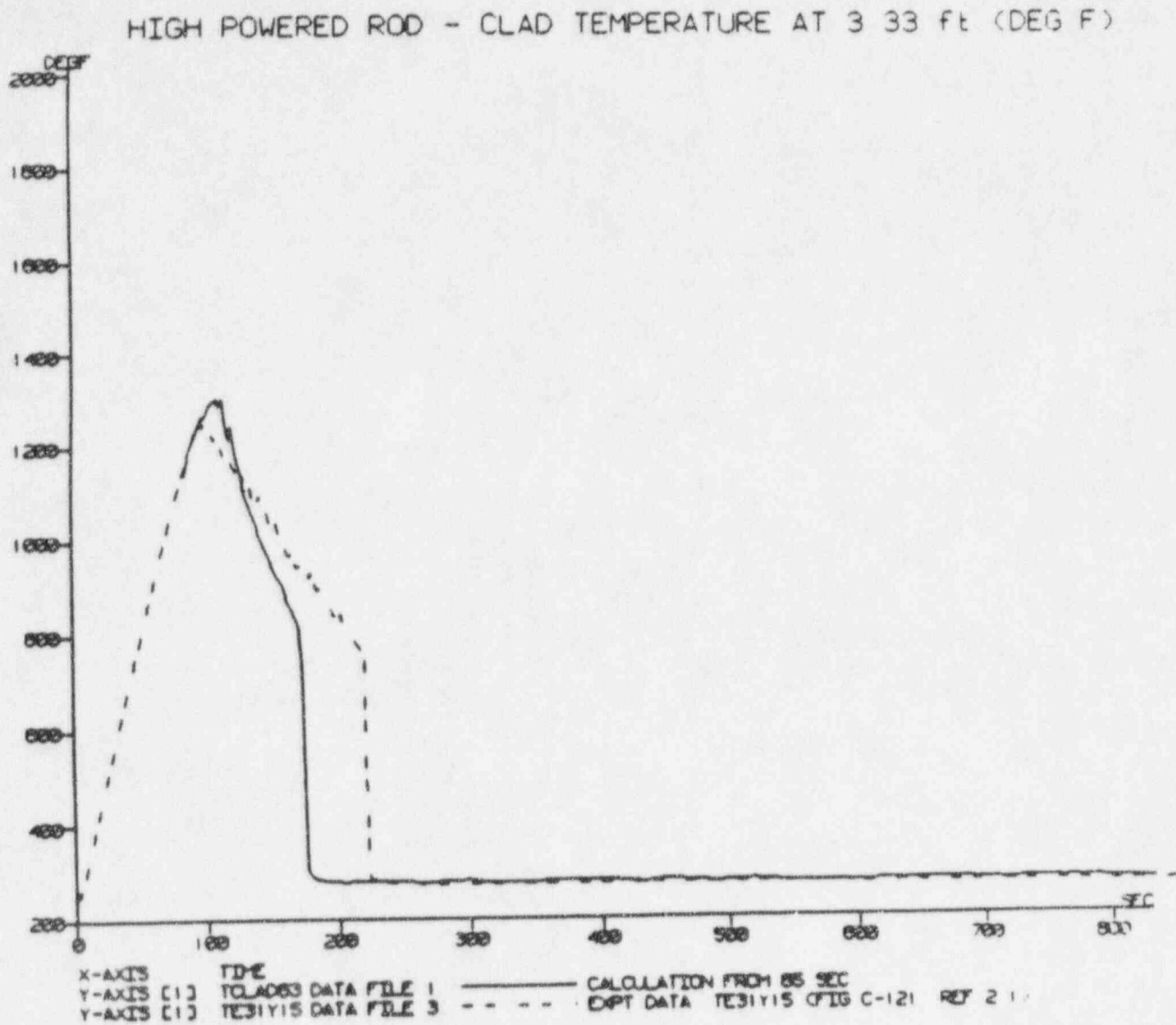


Figure 440.348-12 CCTF Run 58, High Powered Rod, Clad Temperature at 3.33 ft





HIGH POWERED ROD - CLAD TEMPERATURE AT 6 ft (DEG F)

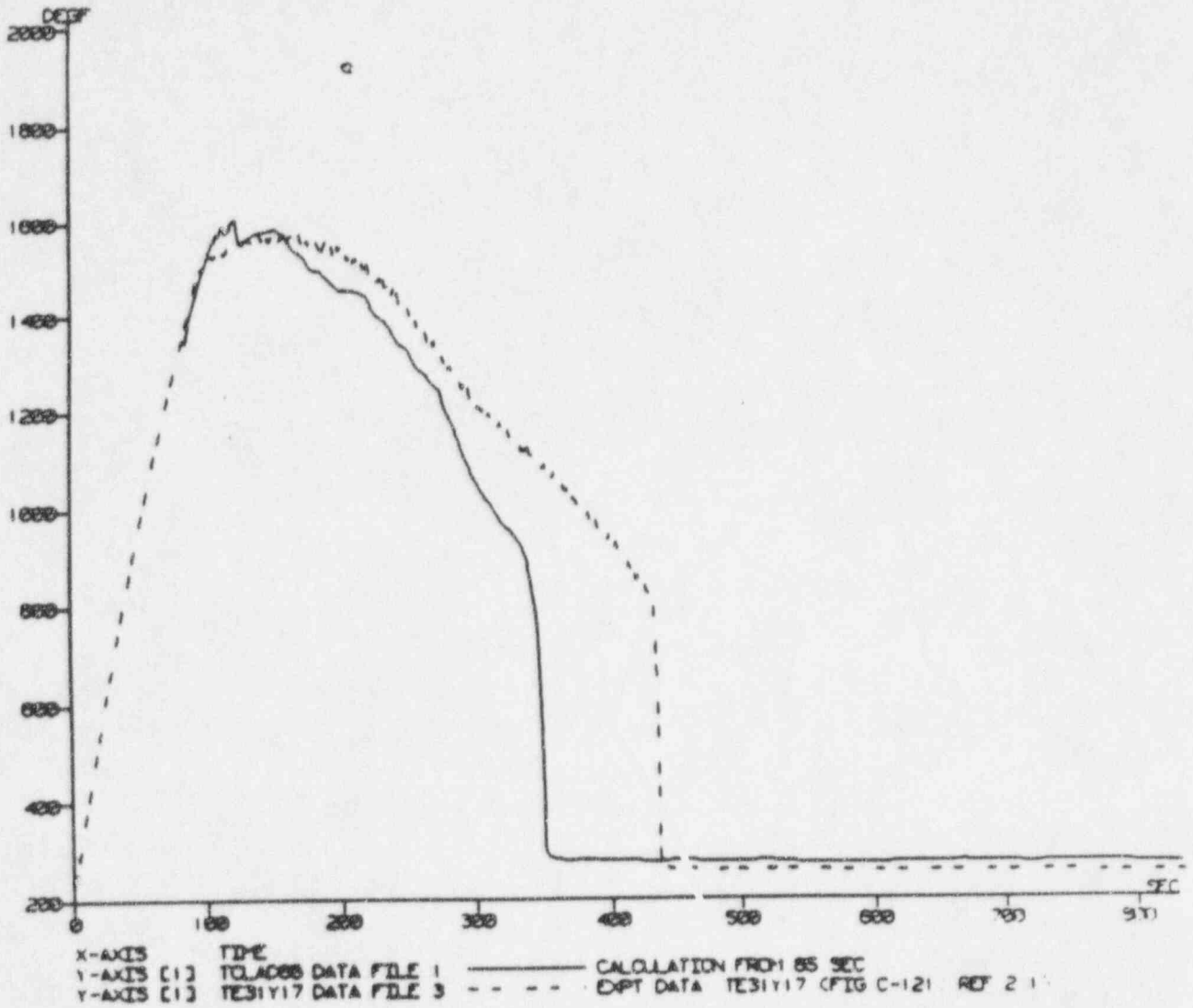


Figure 440.348-13 CCTF Run 58, High Powered Rod, Clad Temperature at 6 ft



HIGH POWERED ROD - CLAD TEMPERATURE AT 8 ft (DEG F)

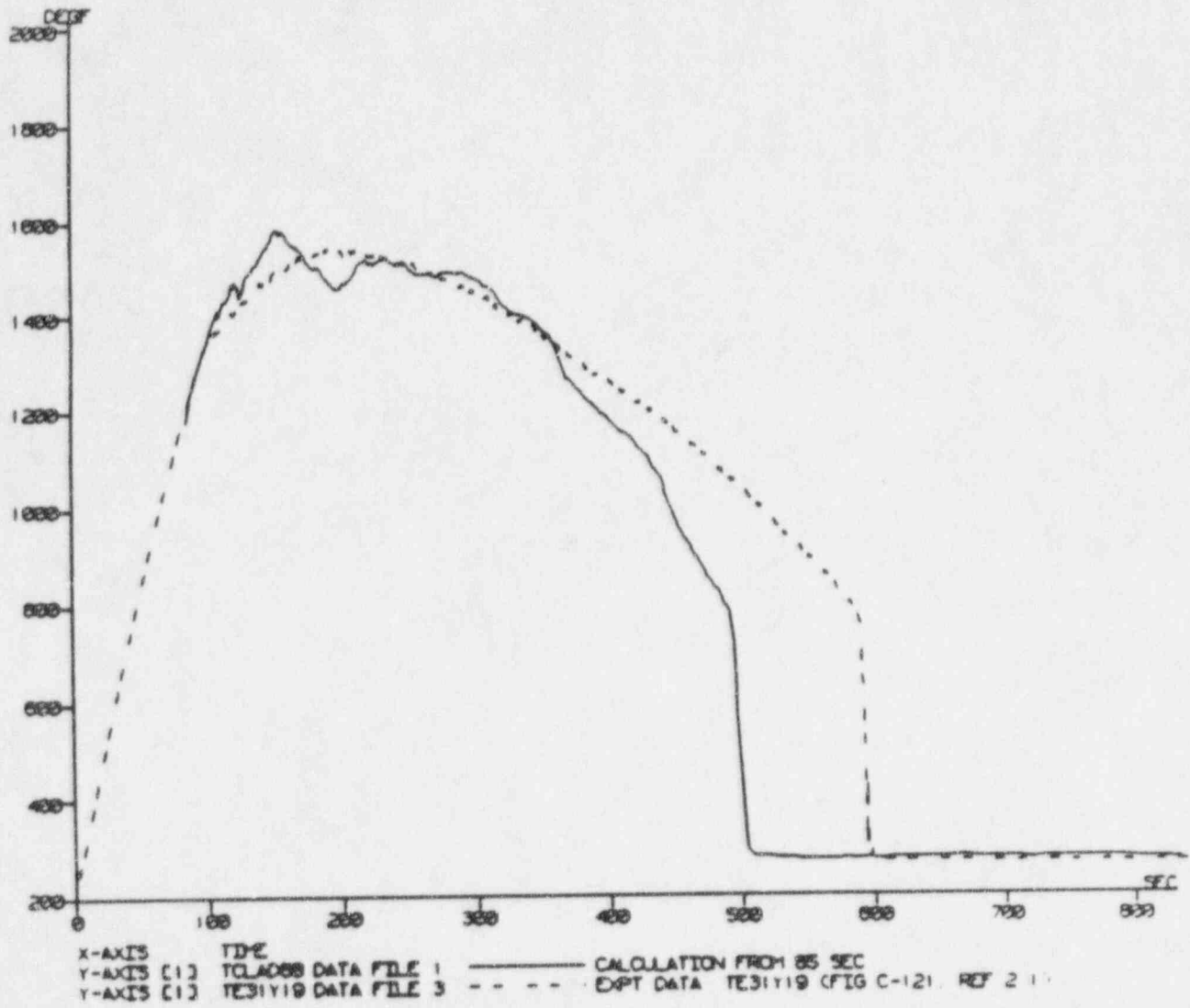


Figure 440.348-14 CCTF Run 58, High Powered Rod, Clad Temperature at 8 ft



HIGH POWERED ROD - CLAD TEMPERATURE AT 10 ft (DEG F)

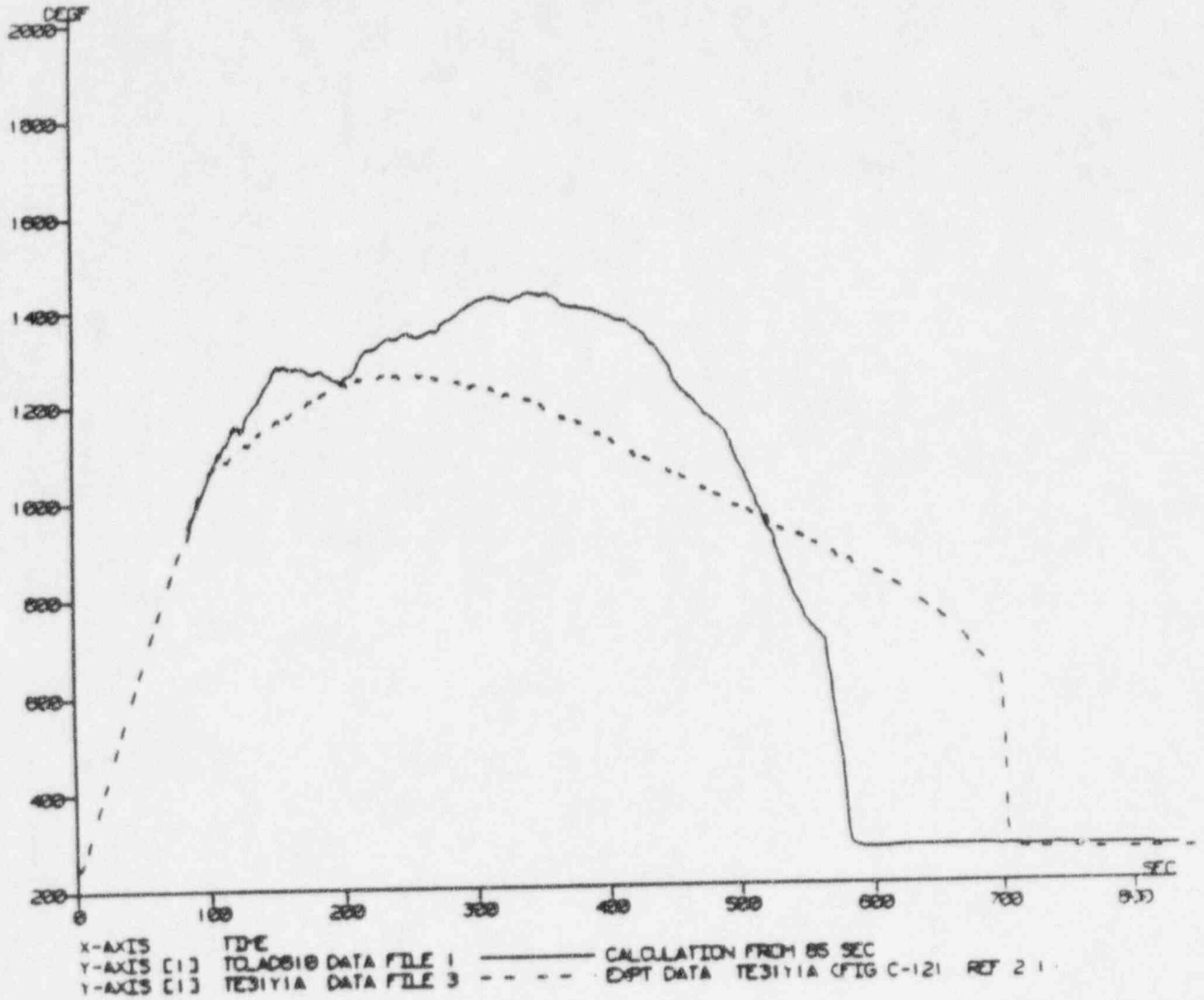


Figure 440.348-15 CCTF Run 58, High Powered Rod, Clad Temperature at 10 ft



LOW POWERED ROD QUENCH ENVELOPE (ft) - Ref BOCREC at 93s

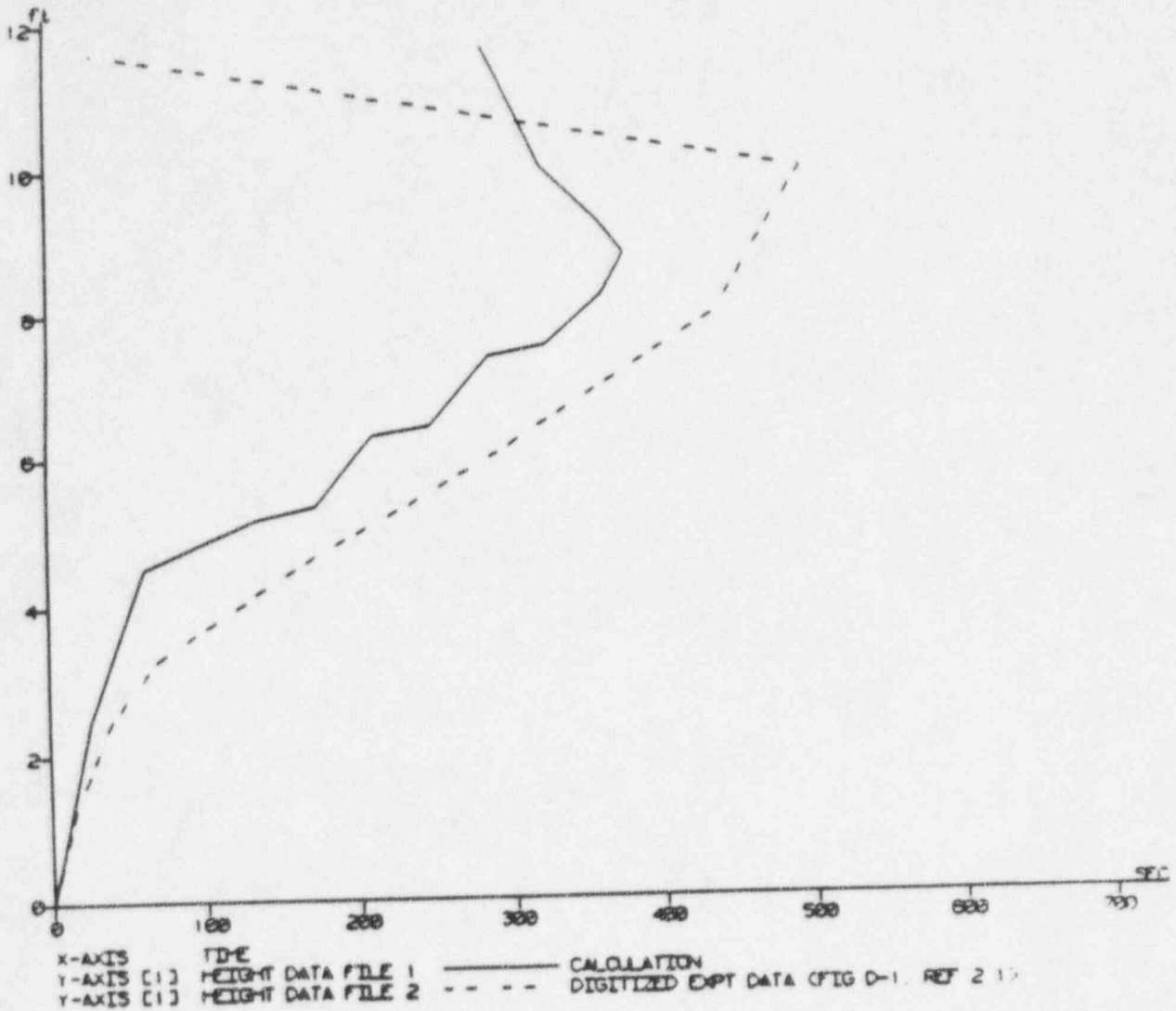


Figure 440.348-16 CCTF Run 58, Quench Envelope - Low Powered Rod



MEDIUM POWERED ROD QUENCH ENVELOPE (ft) - Ref BOCREC at 93s



Figure 440.3-17 CCTF Run 58, Quench Envelope - Medium Powered Rod



HIGH POWERED ROD QUENCH ENVELOPE (ft) - Ref BOCREC at 93 s

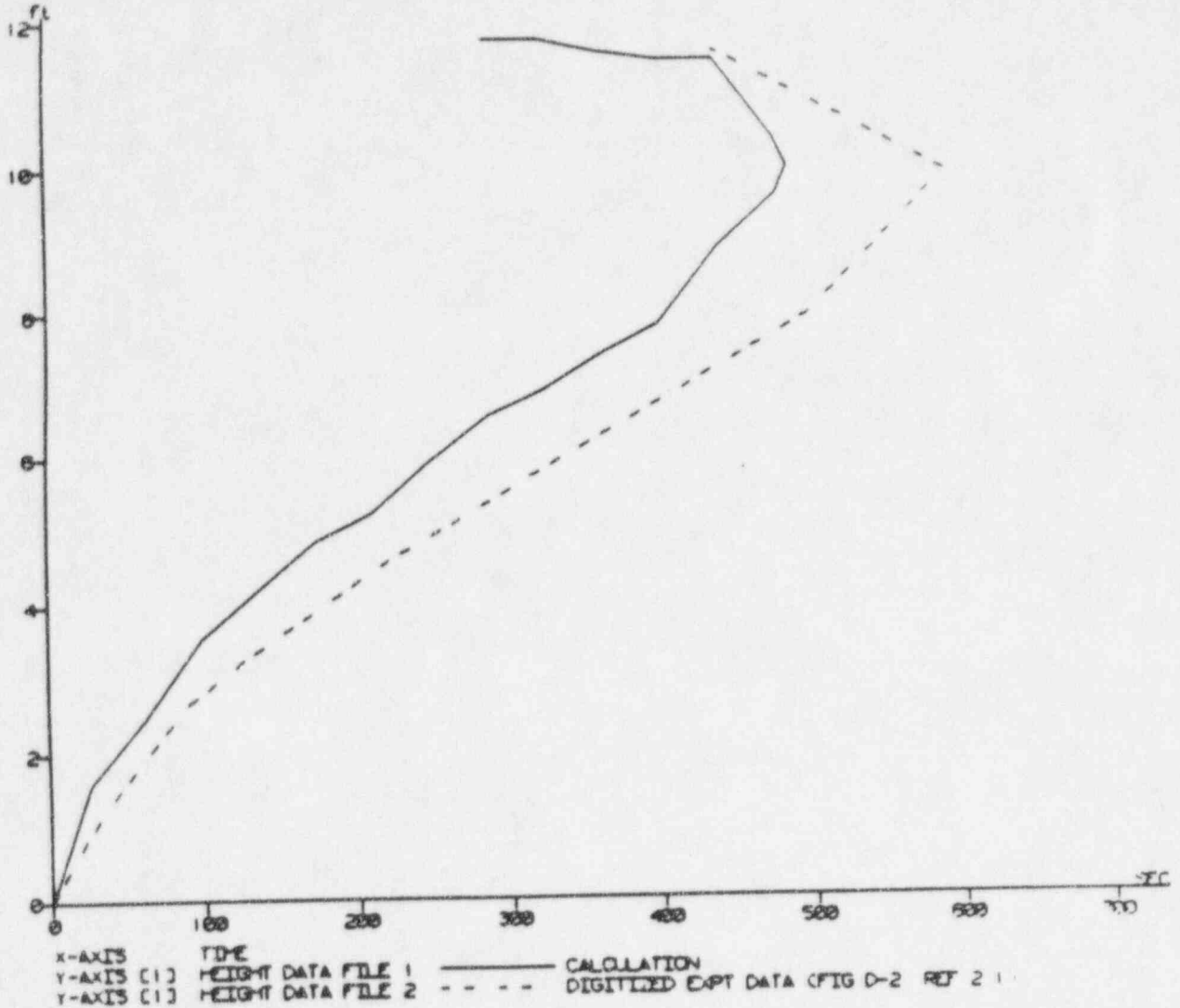


Figure 440.348-18 CCTF Run 58, Quench Envelope - High Powered Rod



UPPER PLENUM PRESSURE (psi)

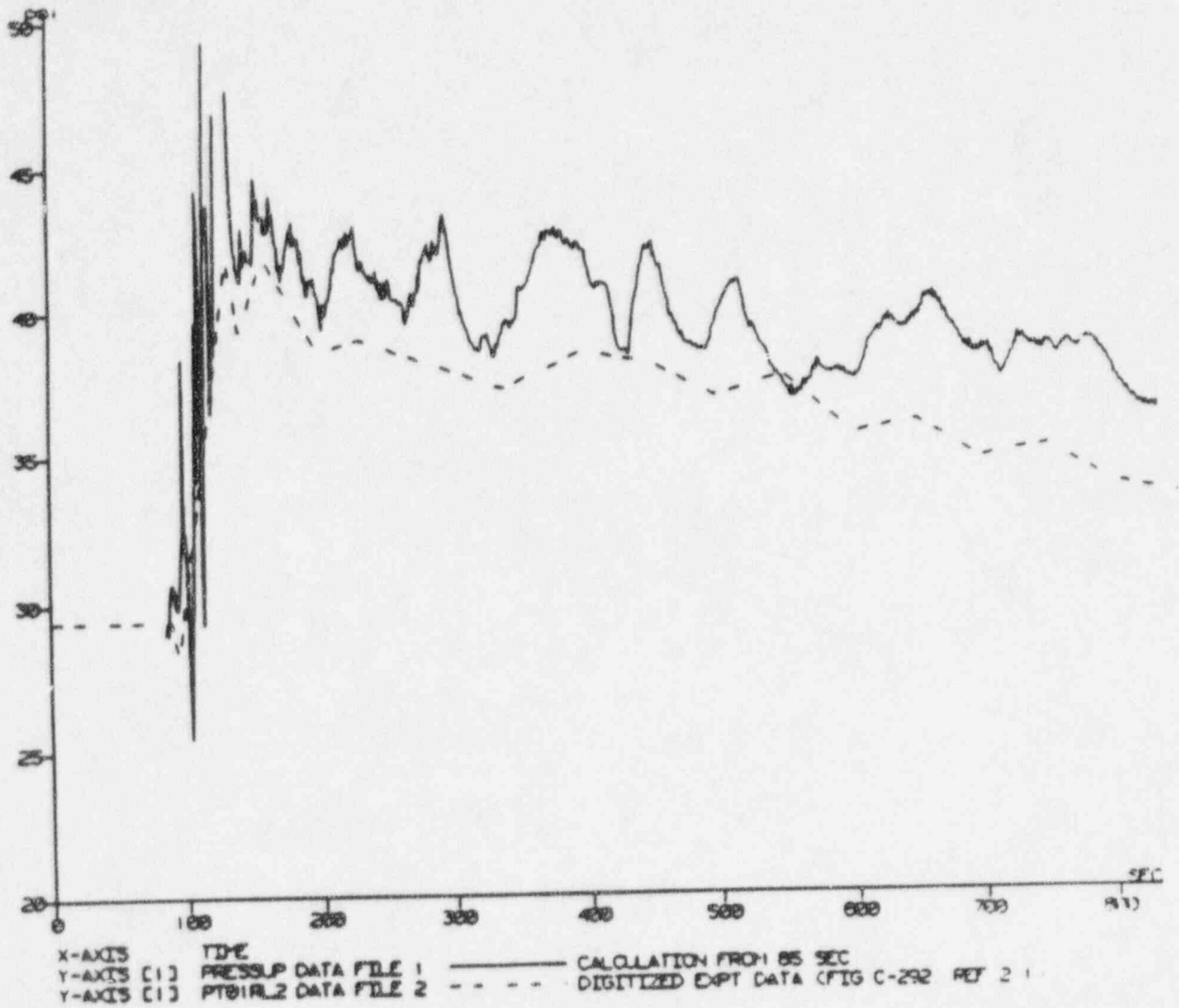


Figure 440.348-19 CCTF Run 58, Upper Plenum Pressure



DOWNCOMER DIFFERENTIAL PRESSURE (psi)

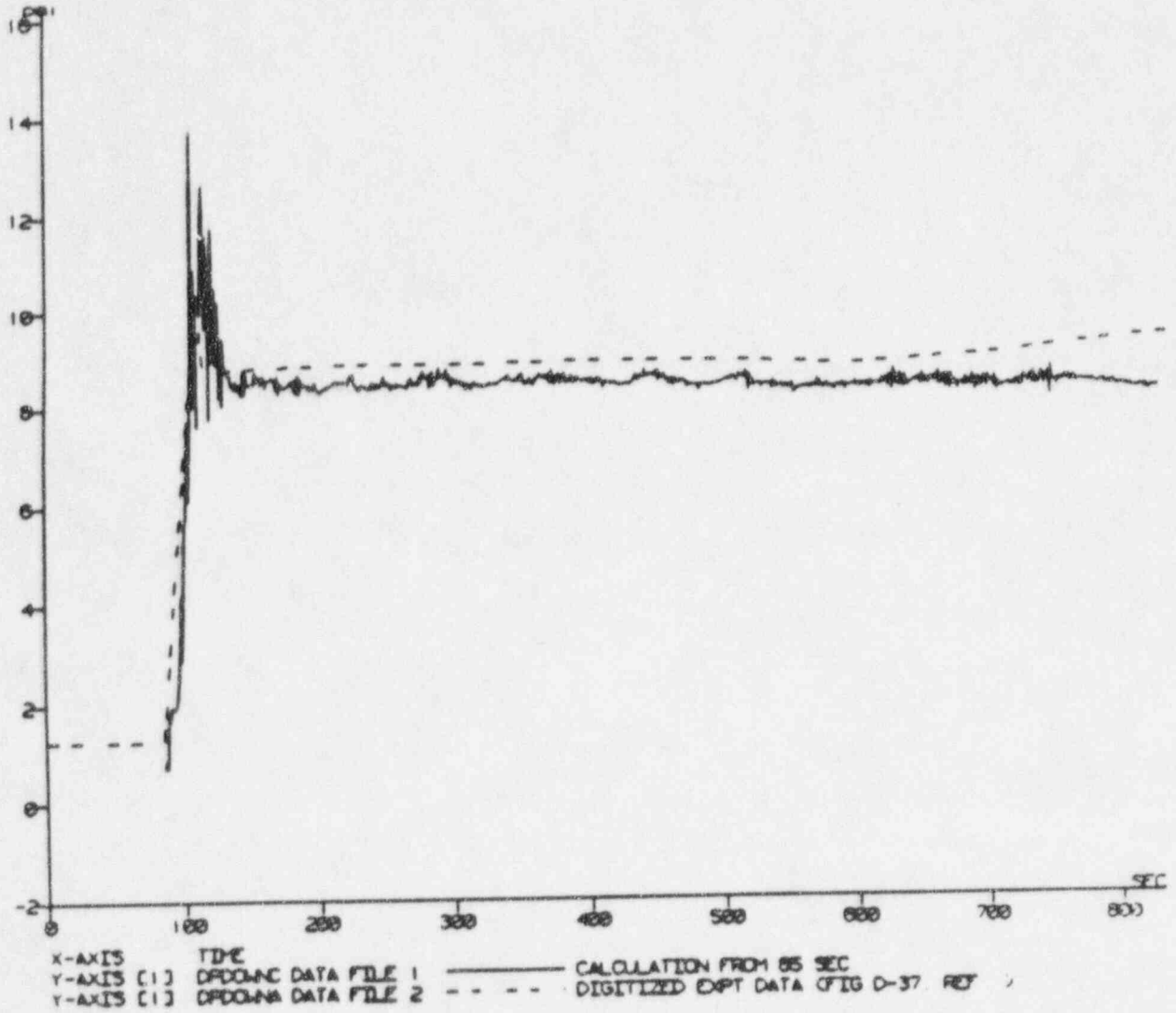


Figure 440.348-20 CCTF Run 58, Downcomer Differential Pressure





CORE DIFFERENTIAL PRESSURE (psi)

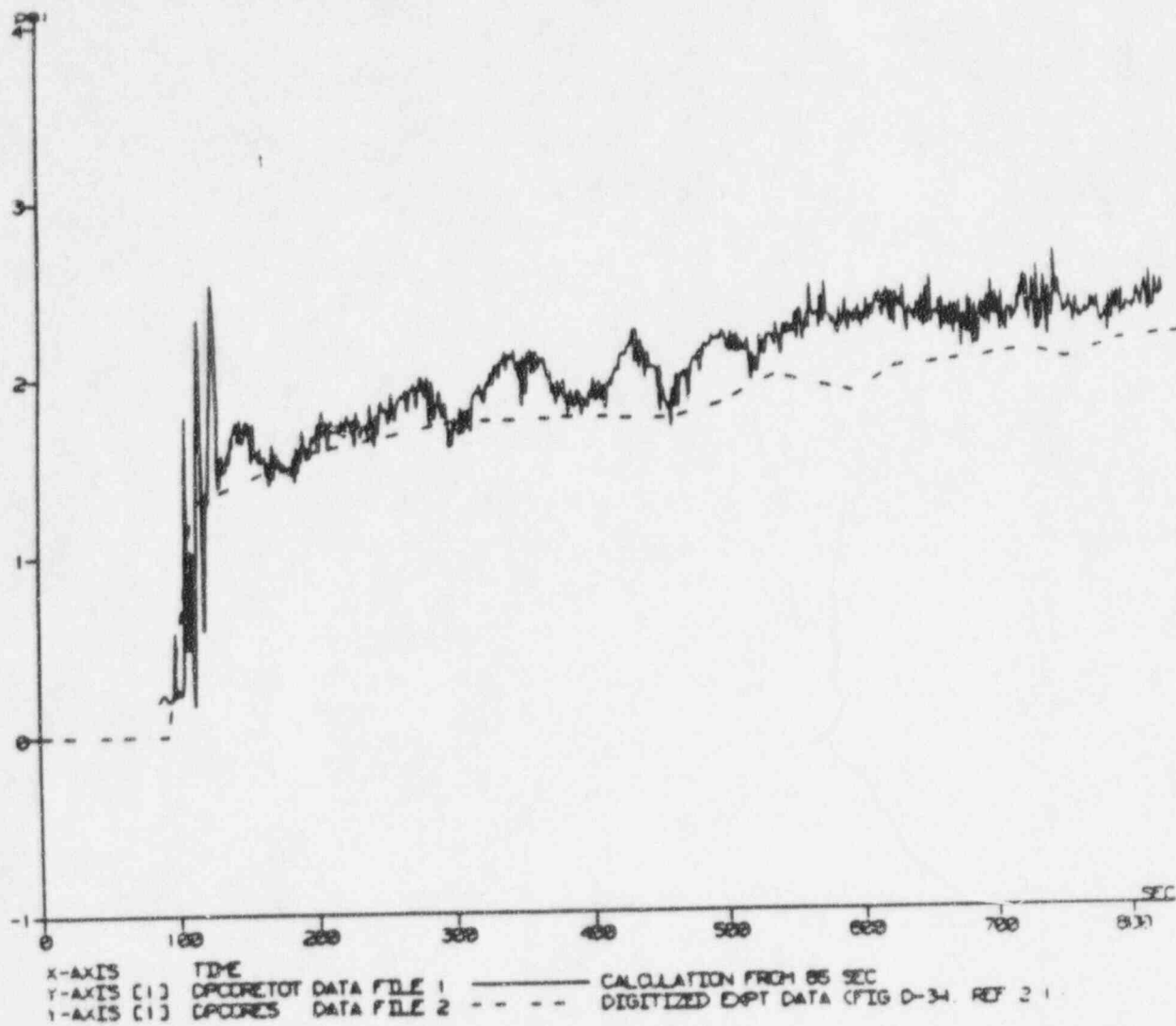


Figure 440.348-21 CCTF Run 58, Core Differential Pressure



UPPER PLENUM TO CONTAINMENT DIFFERENTIAL PRESSURE (psi)

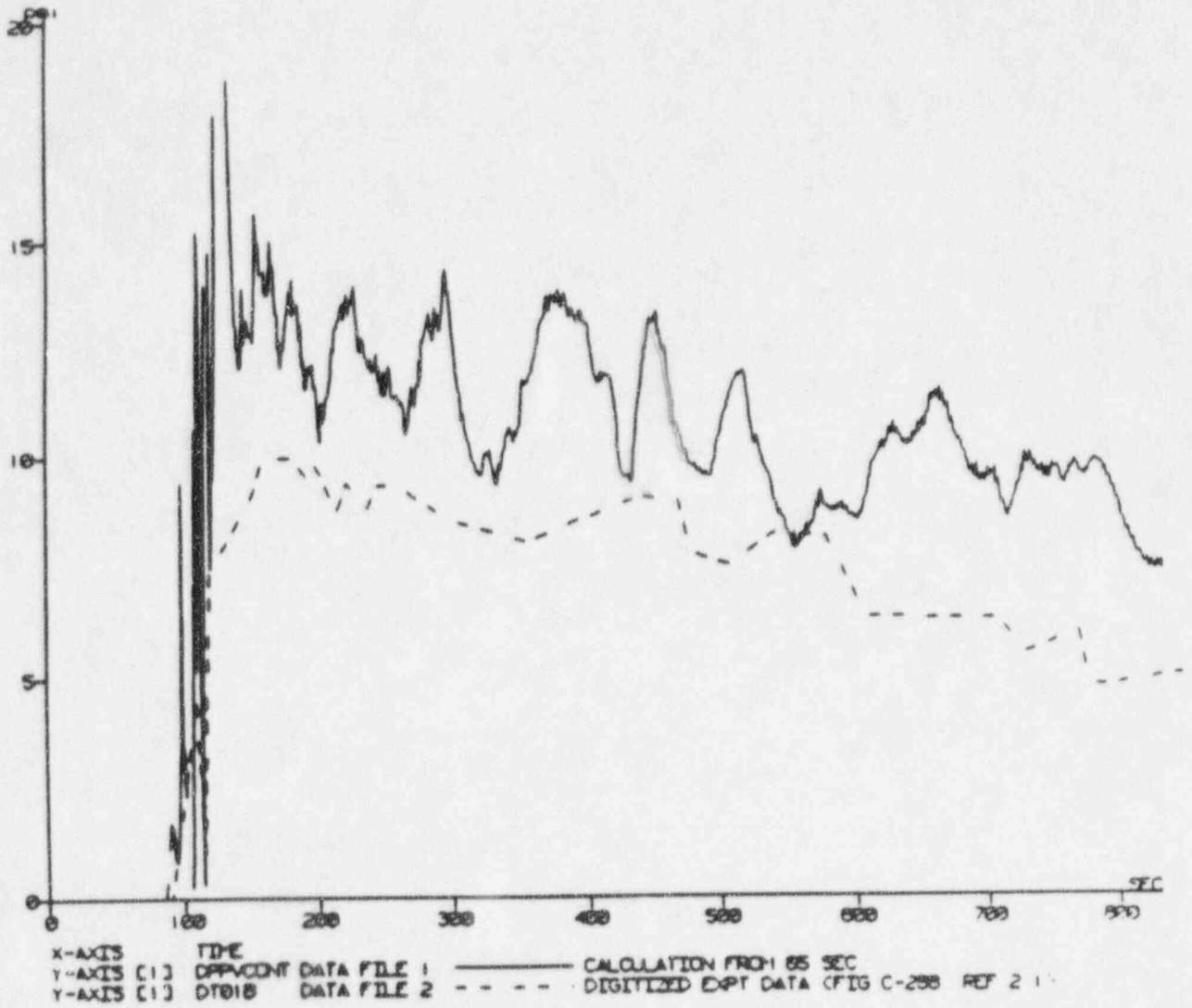


Figure 440.348-22 CCTF Run 58, Upper Plenum to Containment Differential Pressure



LOOP 1 - PUMP DIFFERENTIAL PRESSURE (psi)

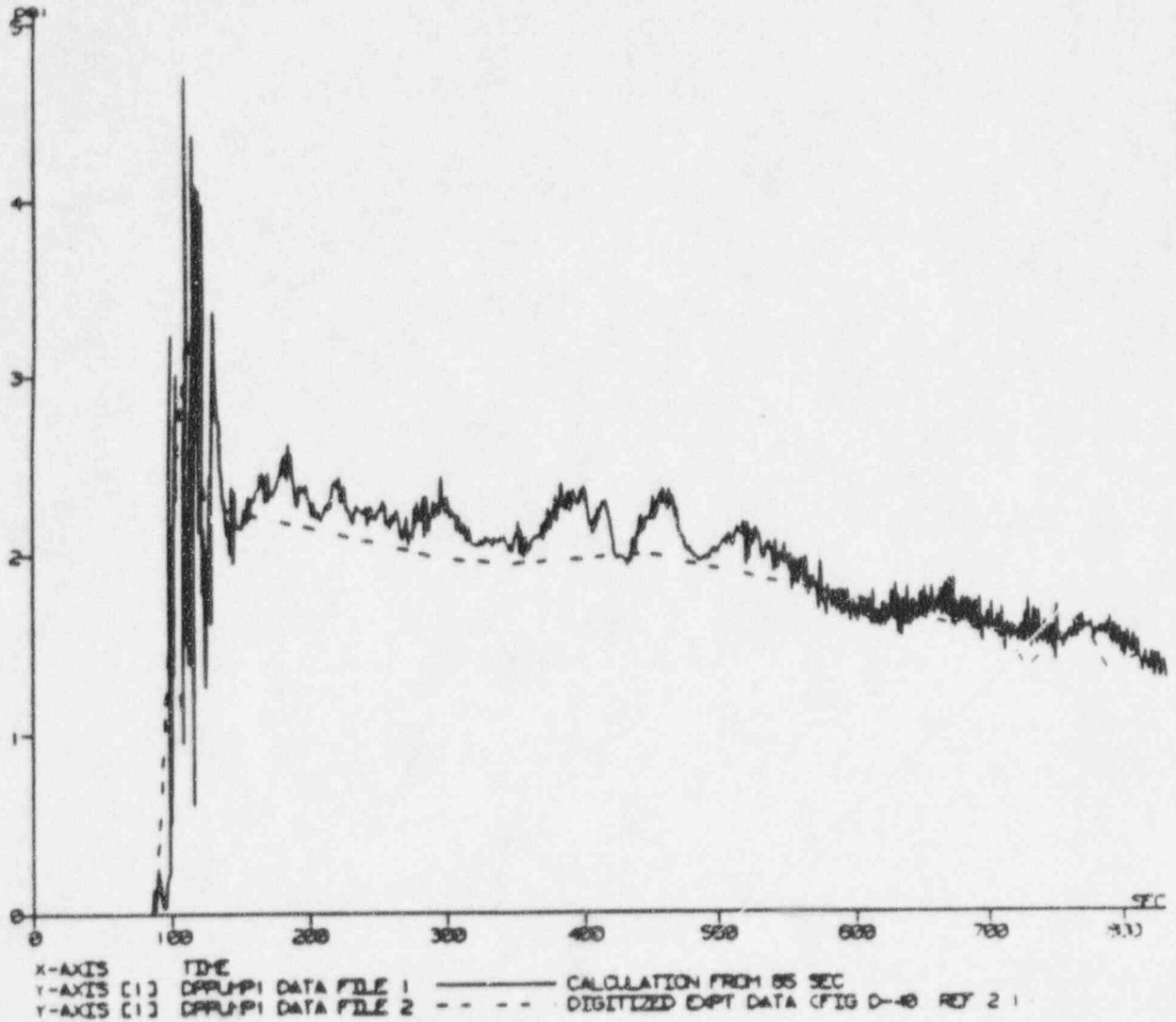


Figure 440.348-23 CCTF Run 58, Loop 1 Pump Simulator Differential Pressure



LOOP 4 (BROKEN) - PUMP DIFFERENTIAL PRESSURE (psi)

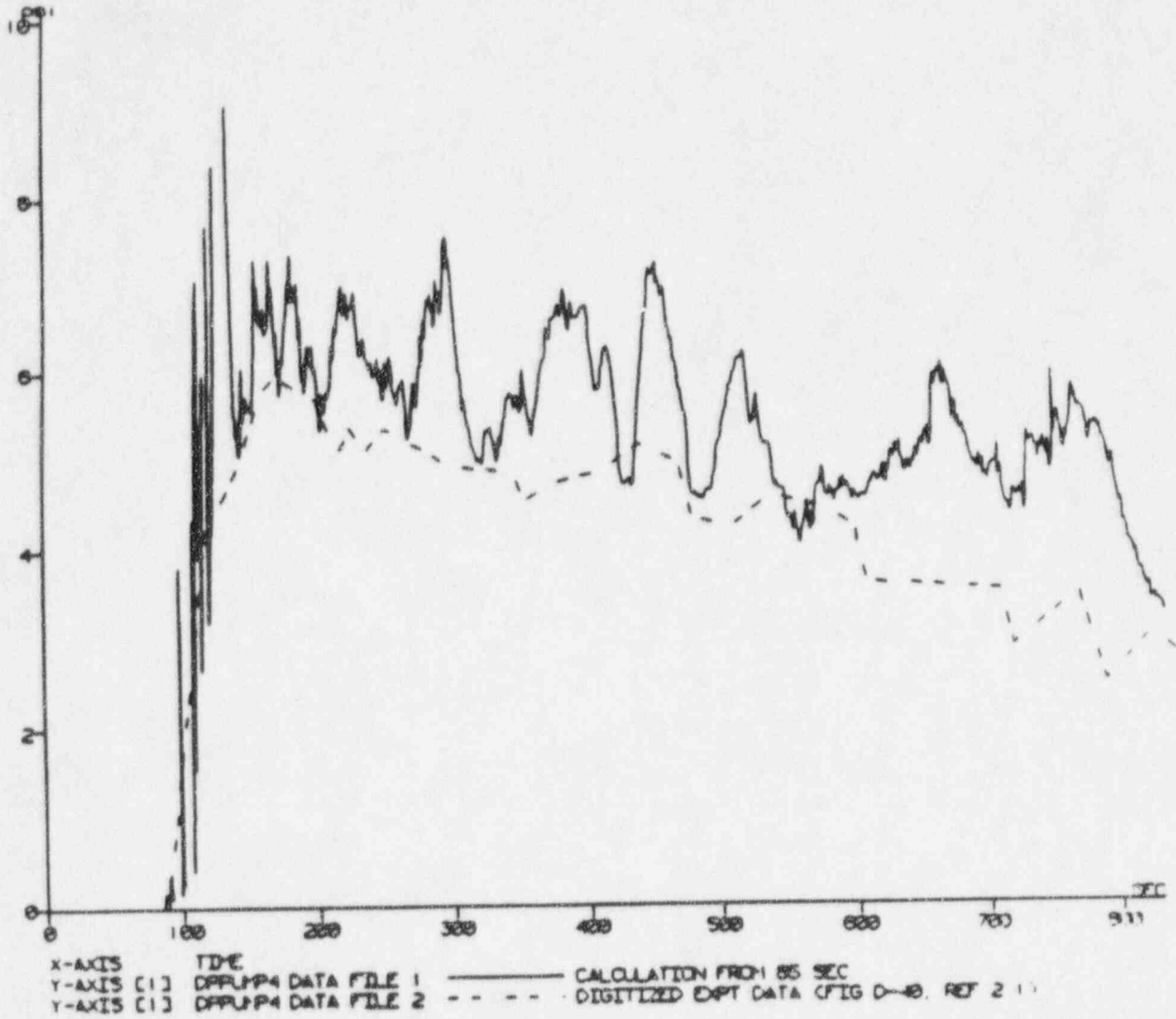


Figure 440.348-24 CCTF Run 58, Loop 4 Pump Simulator Differential Pressure



LOOP 1 - COLD LEG WATER MASS FLOW (lb/s)

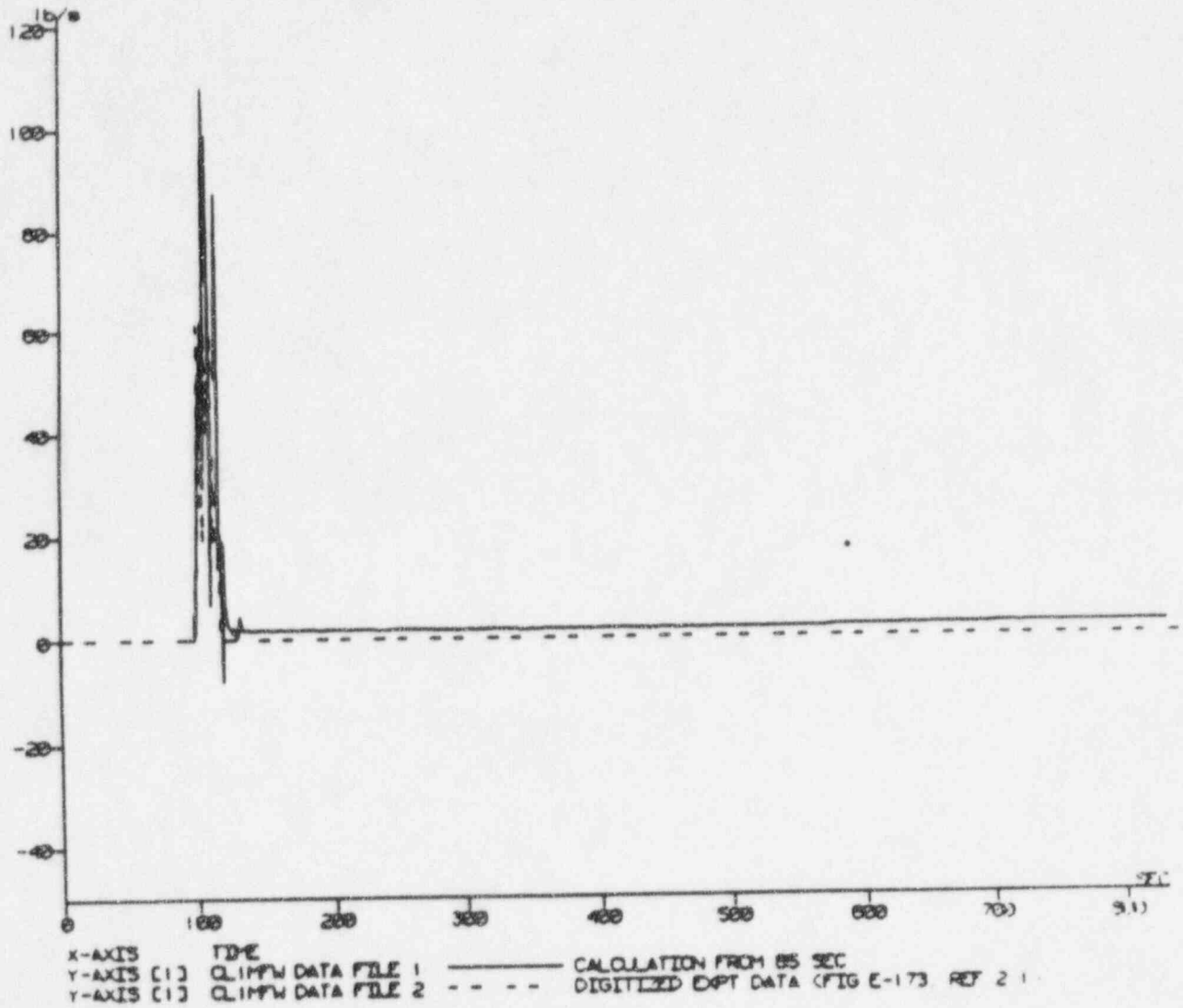


Figure 440.348-25 CCTF Run 58, Loop 1 Cold Leg Water Mass Flow

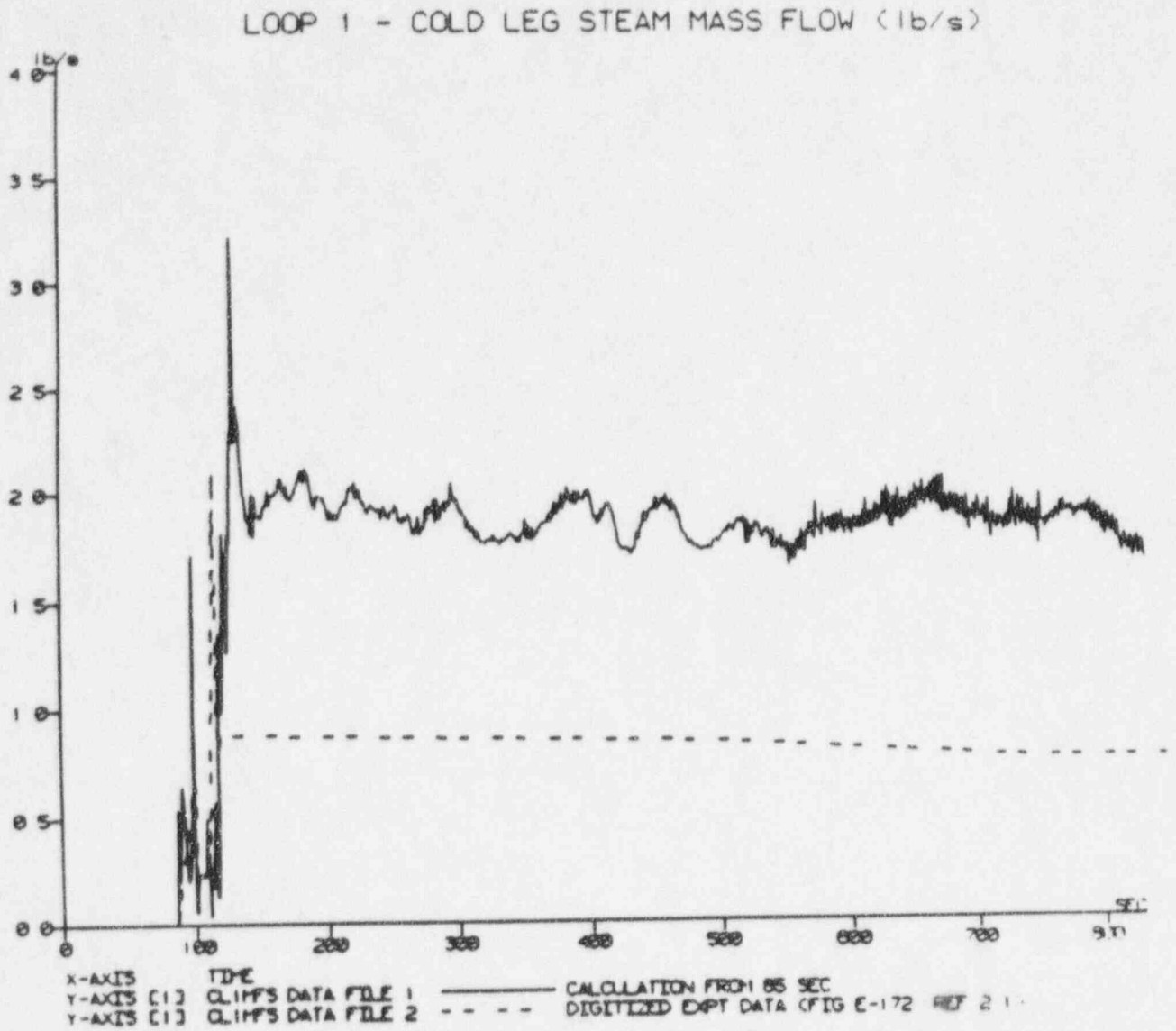


Figure 440.348-26 CCTF Run 58, Loop 1 Cold Leg Steam Mass Flow



LOOP 4 - COLD LEG WATER MASS FLOW (lb/s)

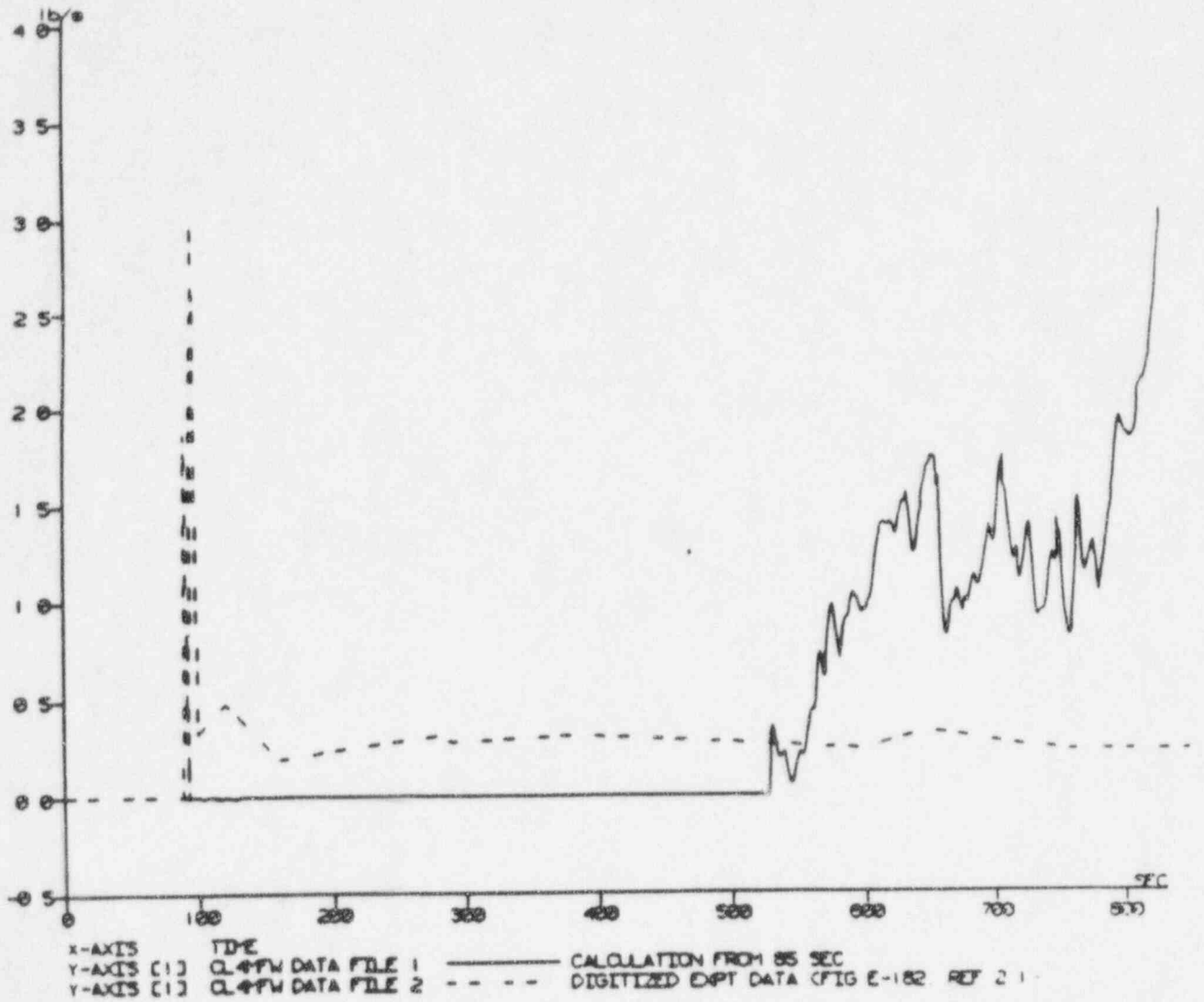


Figure 440.348-27 CCTF Run 58, Loop 4 Cold Leg Water Mass Flow



LOOP 4 - COLD LEG STEAM MASS FLOW (lb/s)

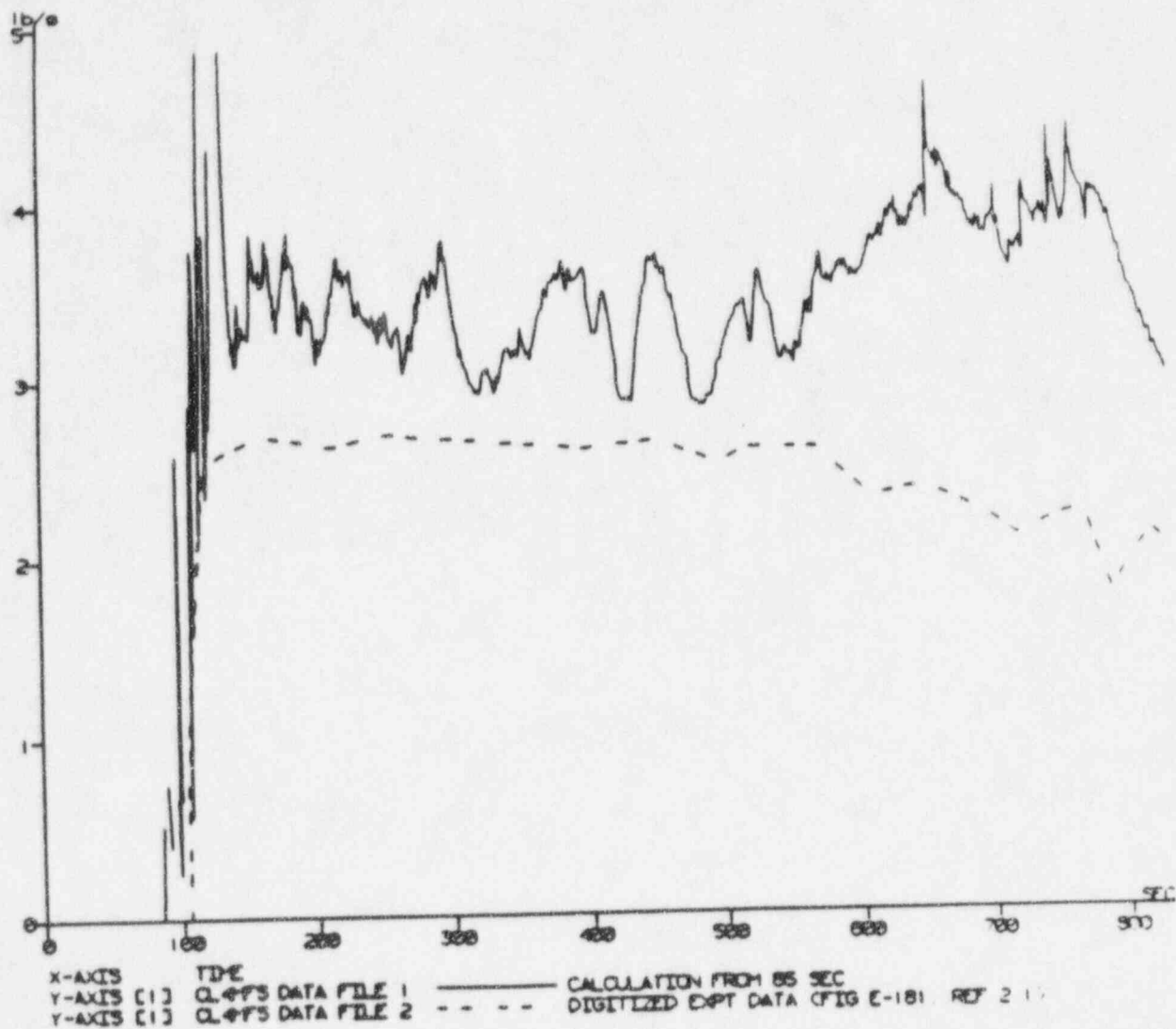


Figure 440.348-28 CCTF Run 58, Loop 4 Cold Leg Steam Mass Flow





LOOP 1 - HOT LEG WATER MASS FLOW (lb/s)

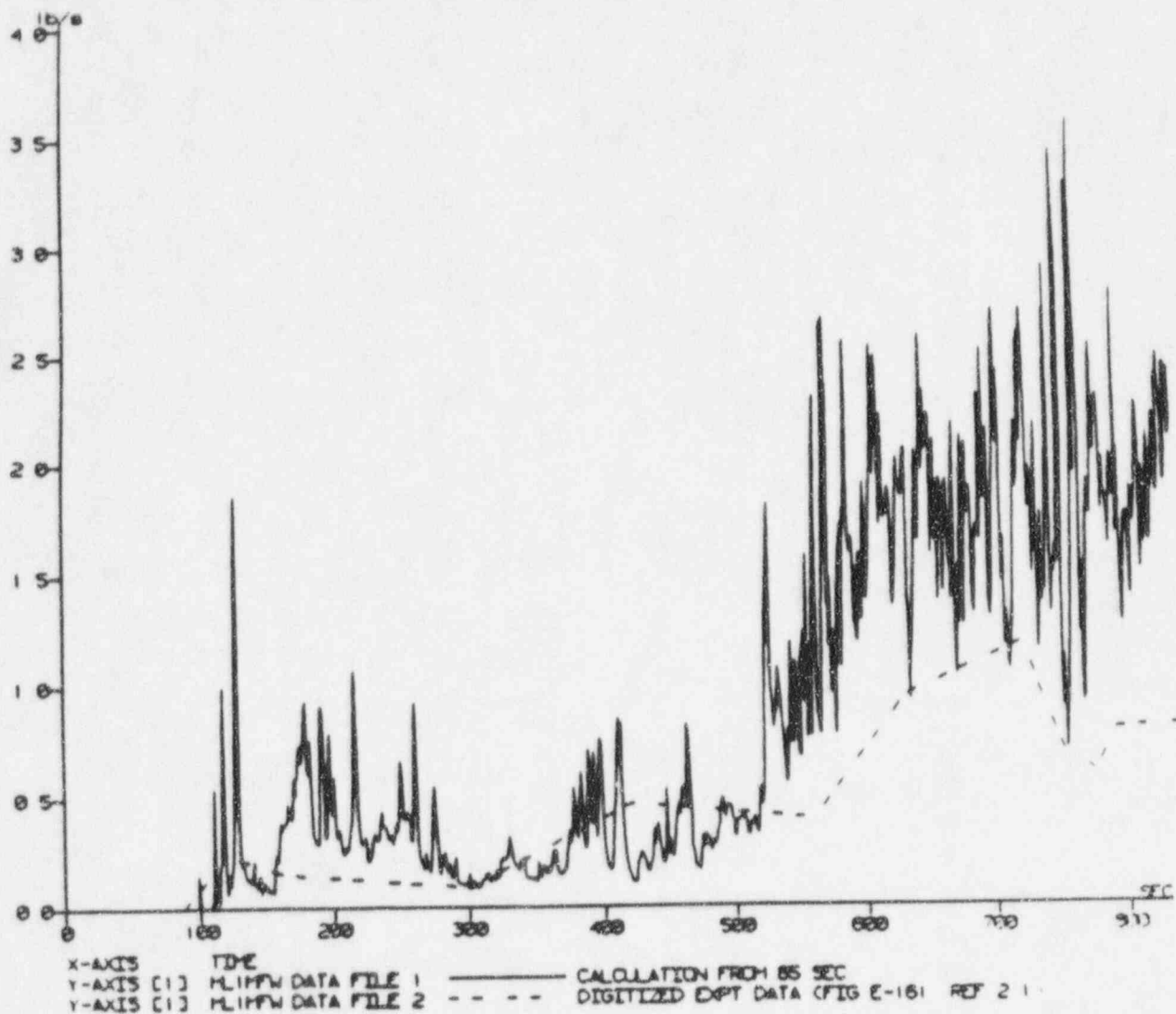


Figure 440.348-29 CCTF Run 58, Loop 1 Hot Leg Water Mass Flow



LOOP 1 - HOT LEG STEAM MASS FLOW (lb/s)

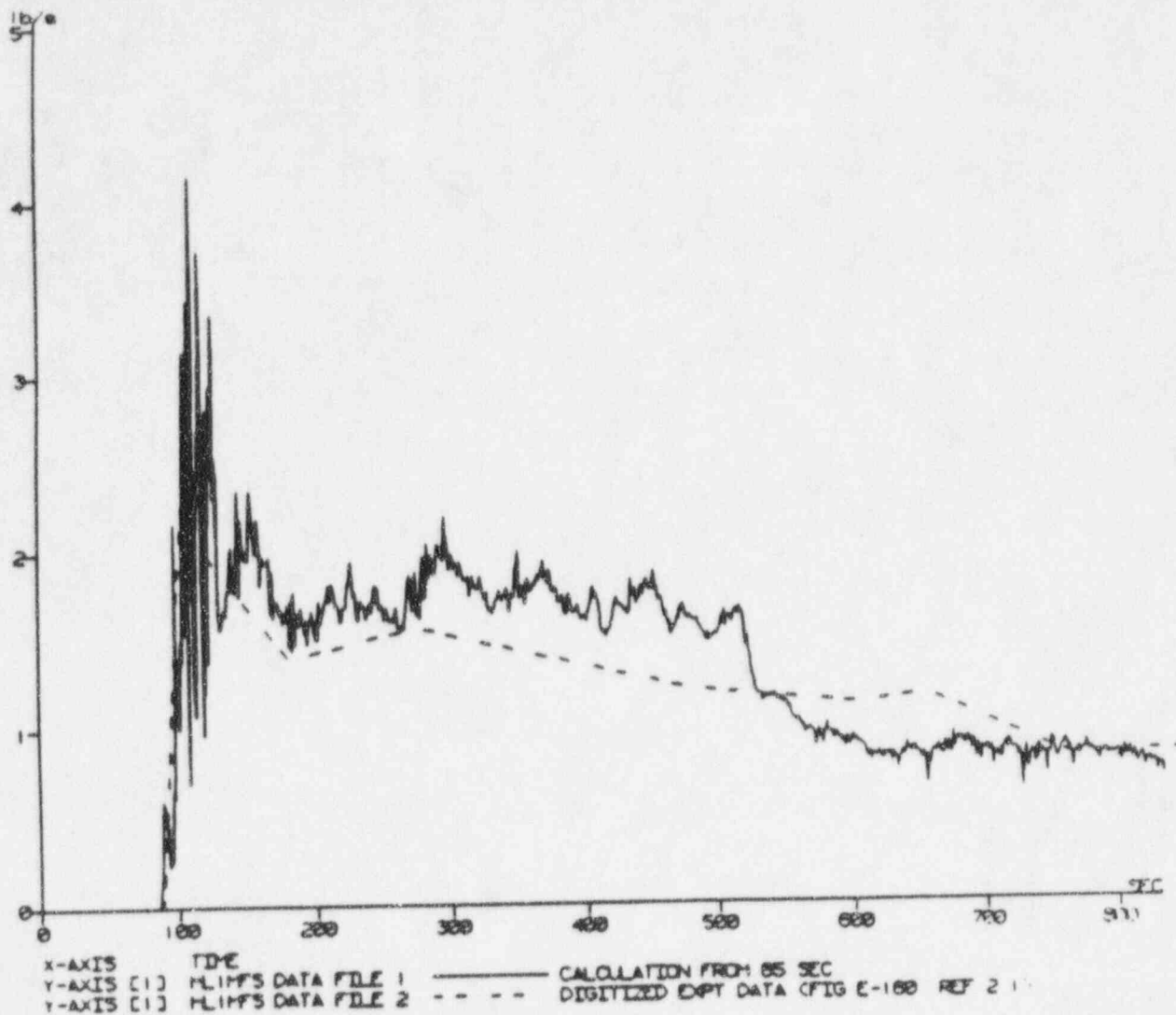


Figure 440.348-30 CCTF Run 58, Loop 1 Hot Leg Steam Mass Flow



LOOP 4 - HOT LEG WATER MASS FLOW (lb/s)

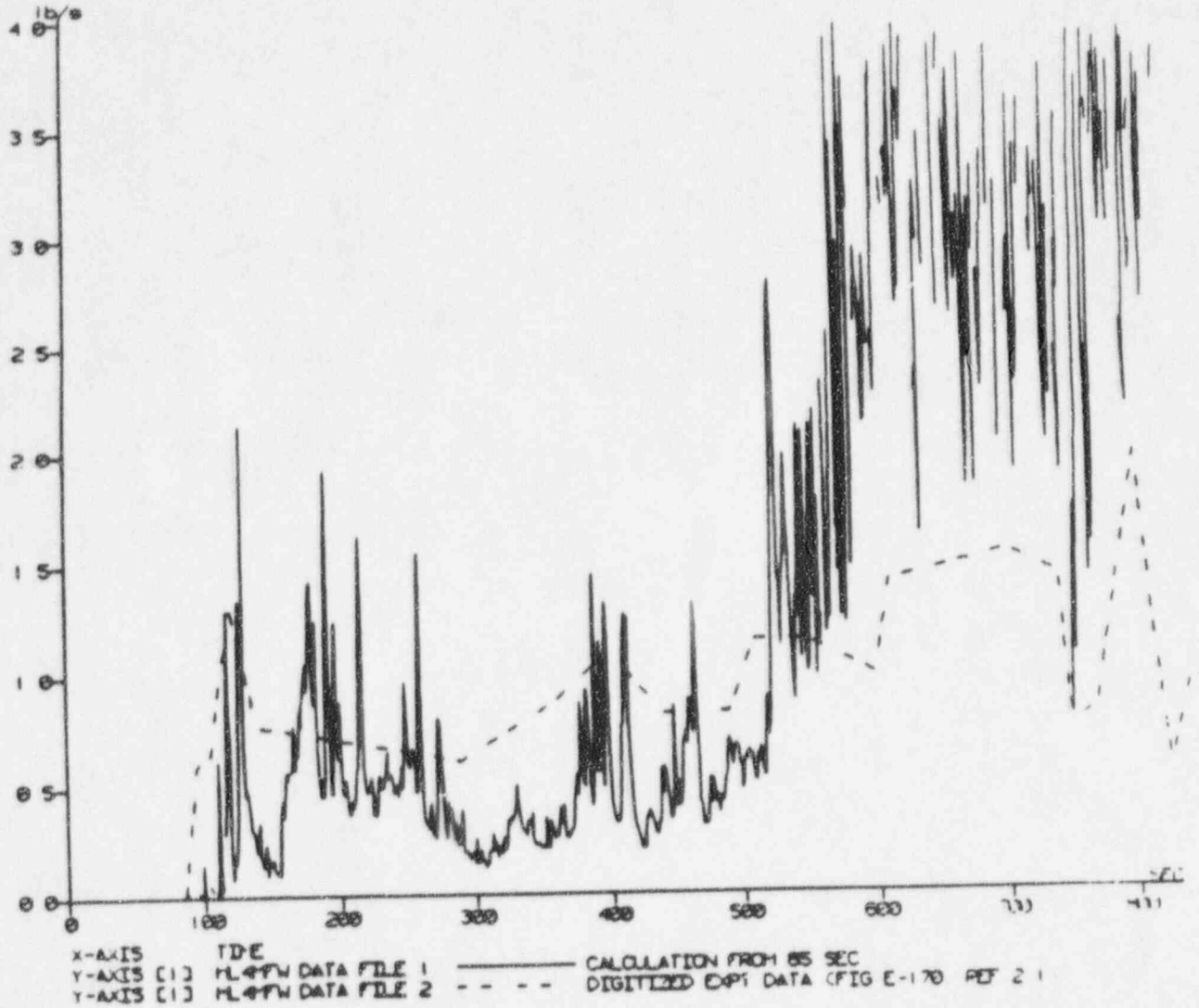


Figure 440.348-31 CCTF Run 58, Loop 4 Hot Leg Water Mass Flow



LOOP 4 - HOT LEG STEAM MASS FLOW (lb/s)

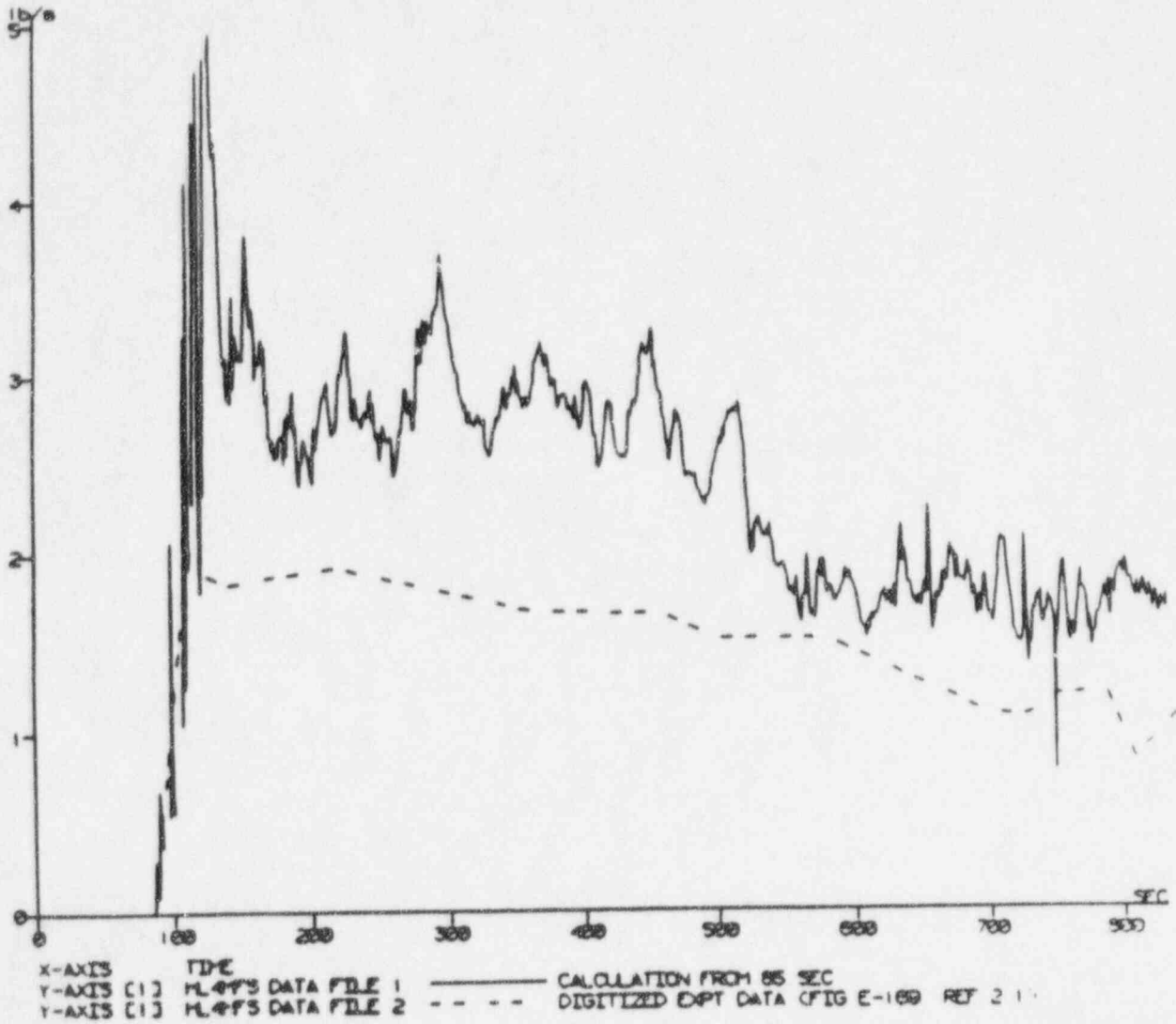


Figure 440.348-32 CCTF Run 58, Loop 4 Hot Leg Steam Mass Flow



VESSEL SIDE COLD LEG INTEGRATED LIQUID BREAK FLOW (LB)

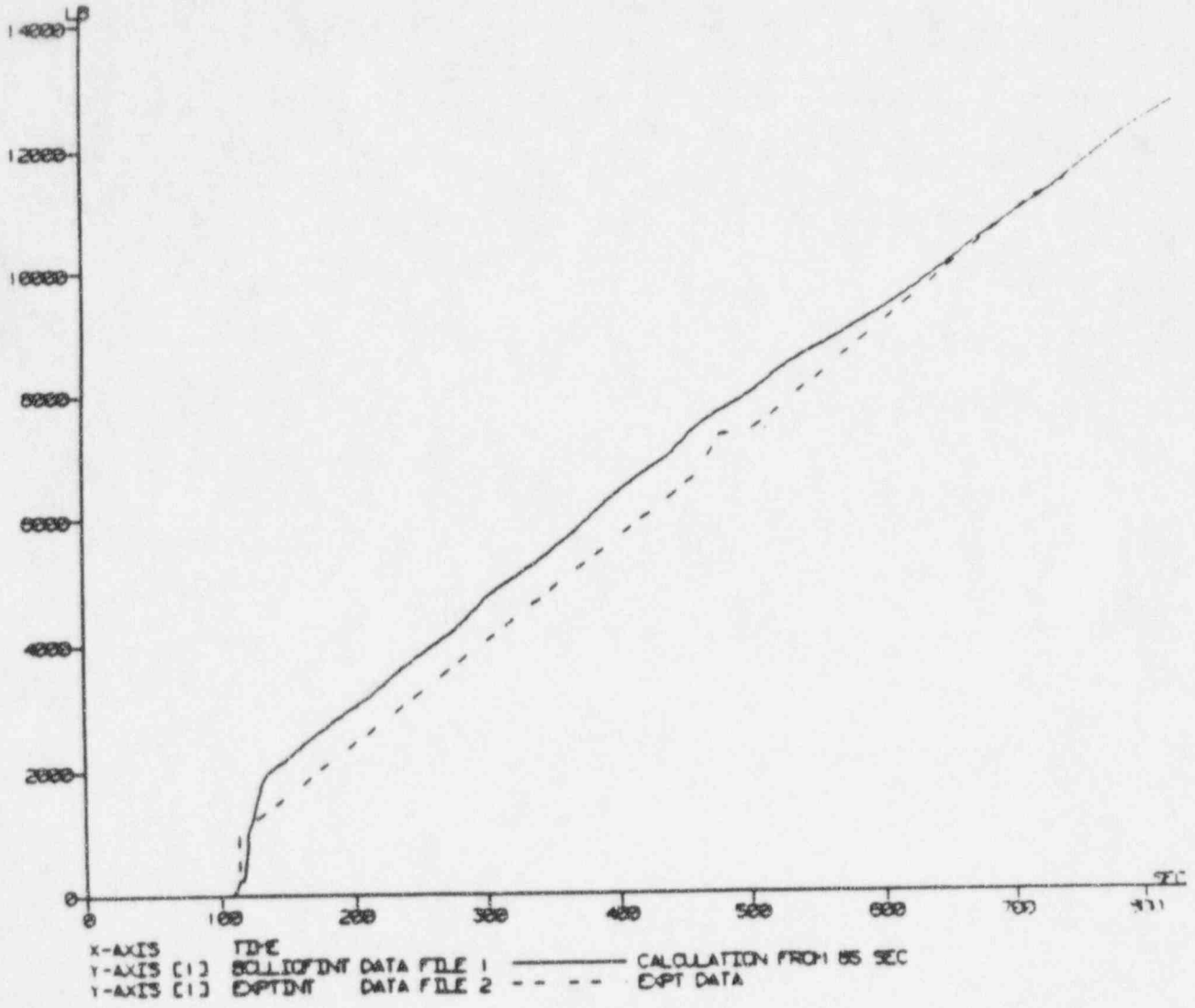


Figure 440.348-33 CCTF Run 58, Vessel Side Cold Leg Integrated Liquid Break Flow

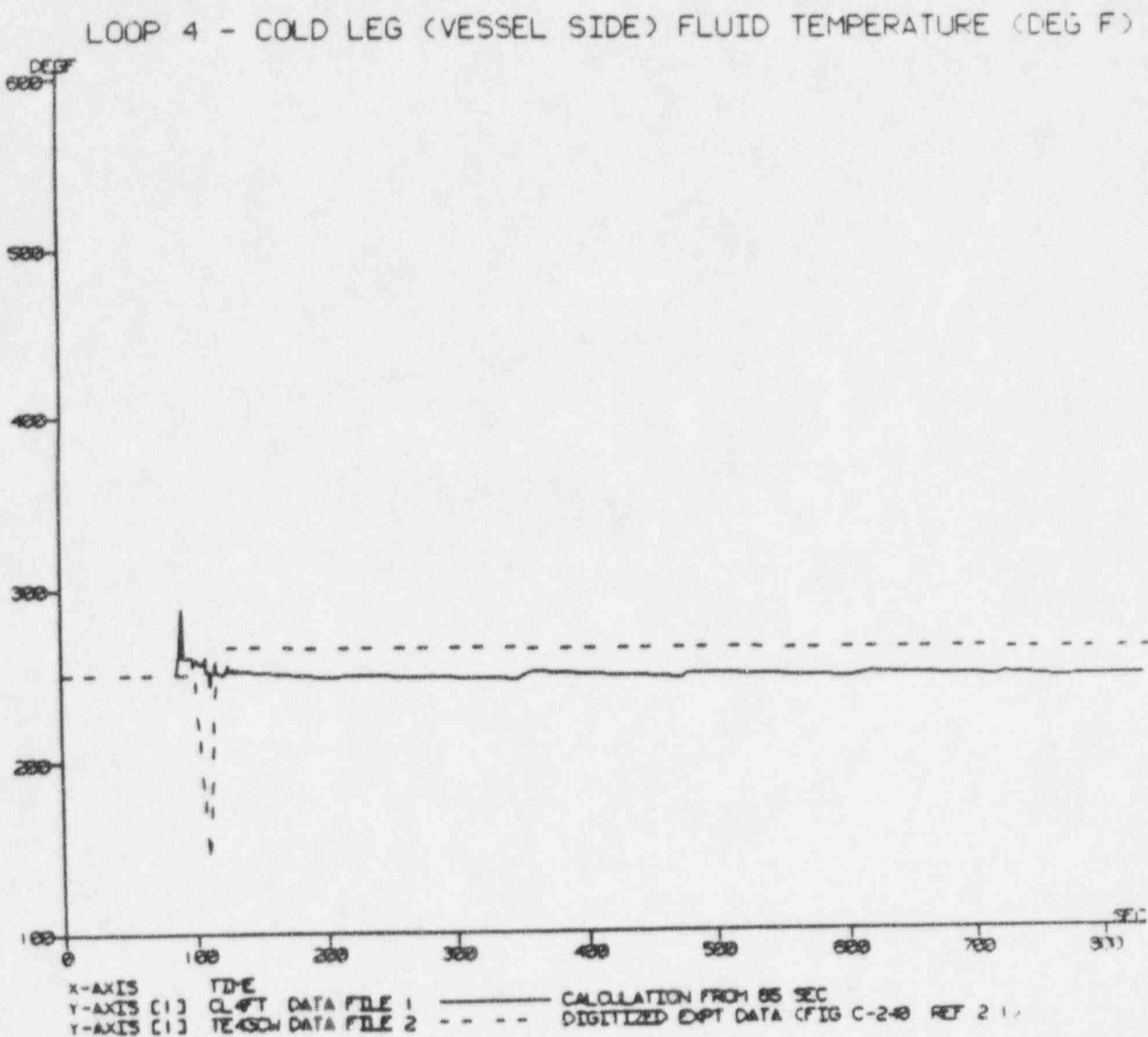


Figure 440.348-34 CCTF Run 58, Vessel Side, Loop 4, Cold Leg Fluid Temperature



LOOP 4 - LOOP SEAL FLUID TEMPERATURE (DEG F)

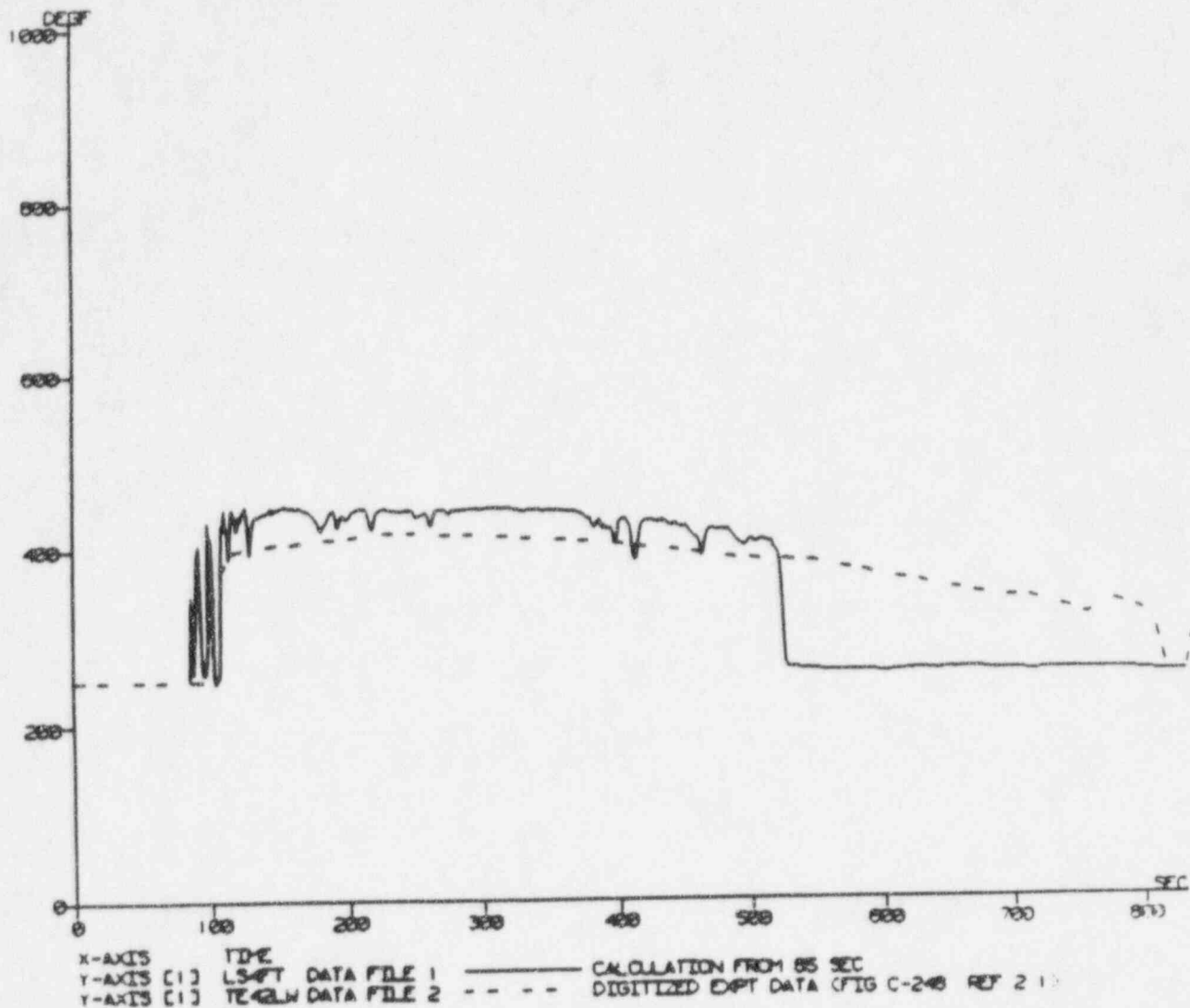
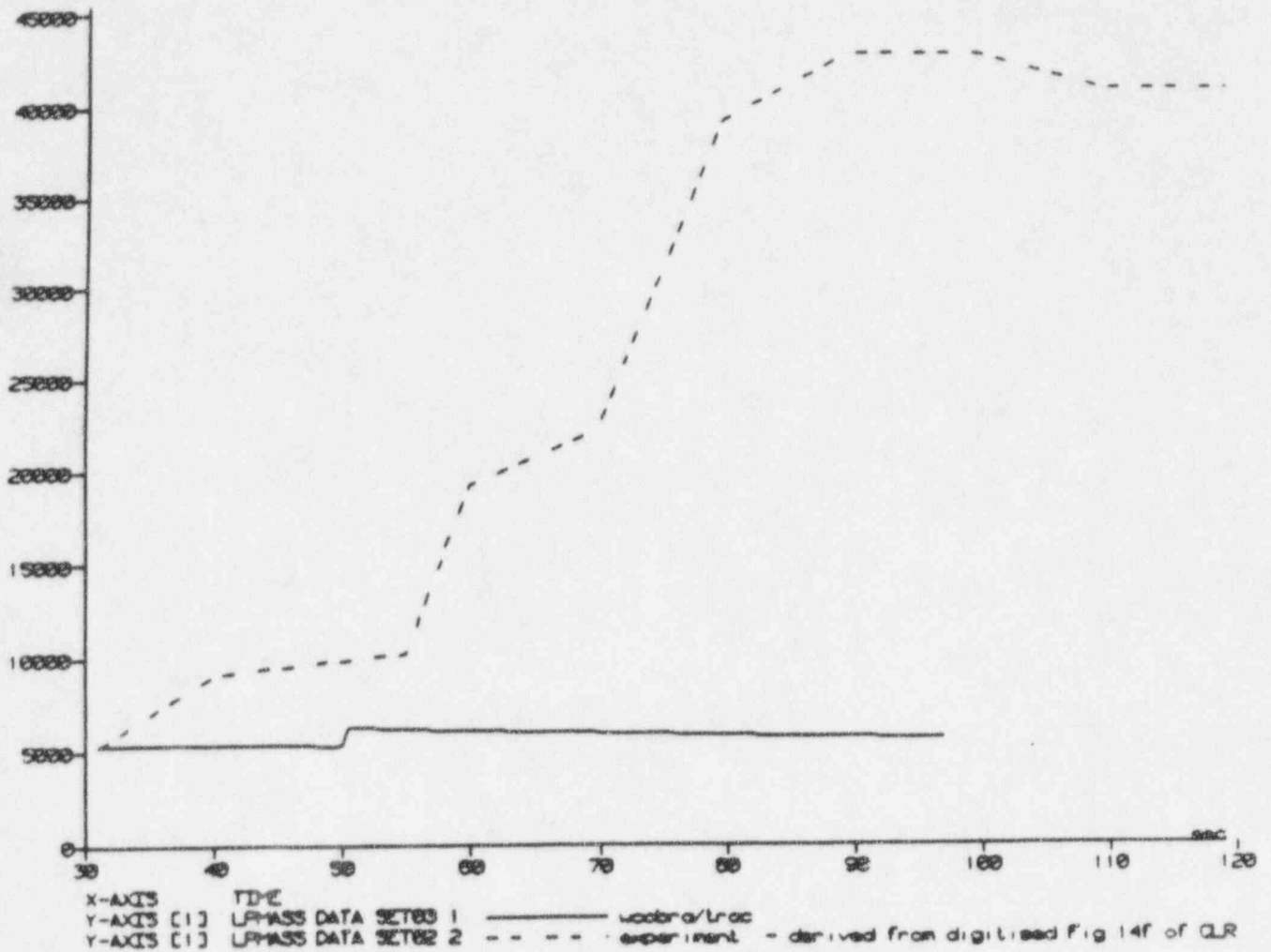


Figure 440.348-35 CCTF Run 58, Loop 4, Loop Seal Fluid Temperature



LOWER PLENUM MASS INVENTORY (lb)



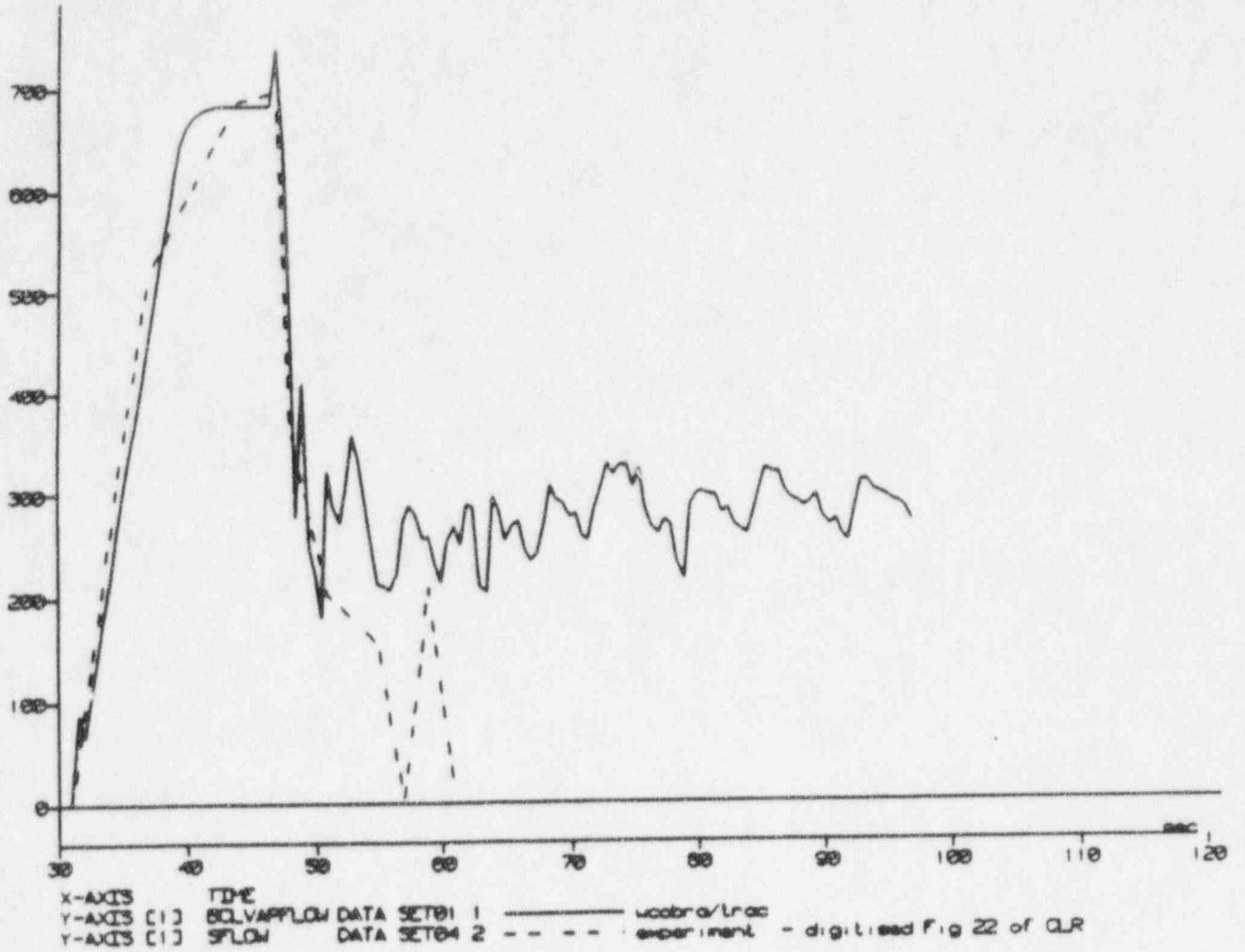
UPTF Test 21 Run 272 Phase A

Figure 440.348-36 UPTF Test 21, Phase A, Lower Plenum Mass Inventory





BROKEN COLD LEG VAPOUR FLOWRATE (lb/s)

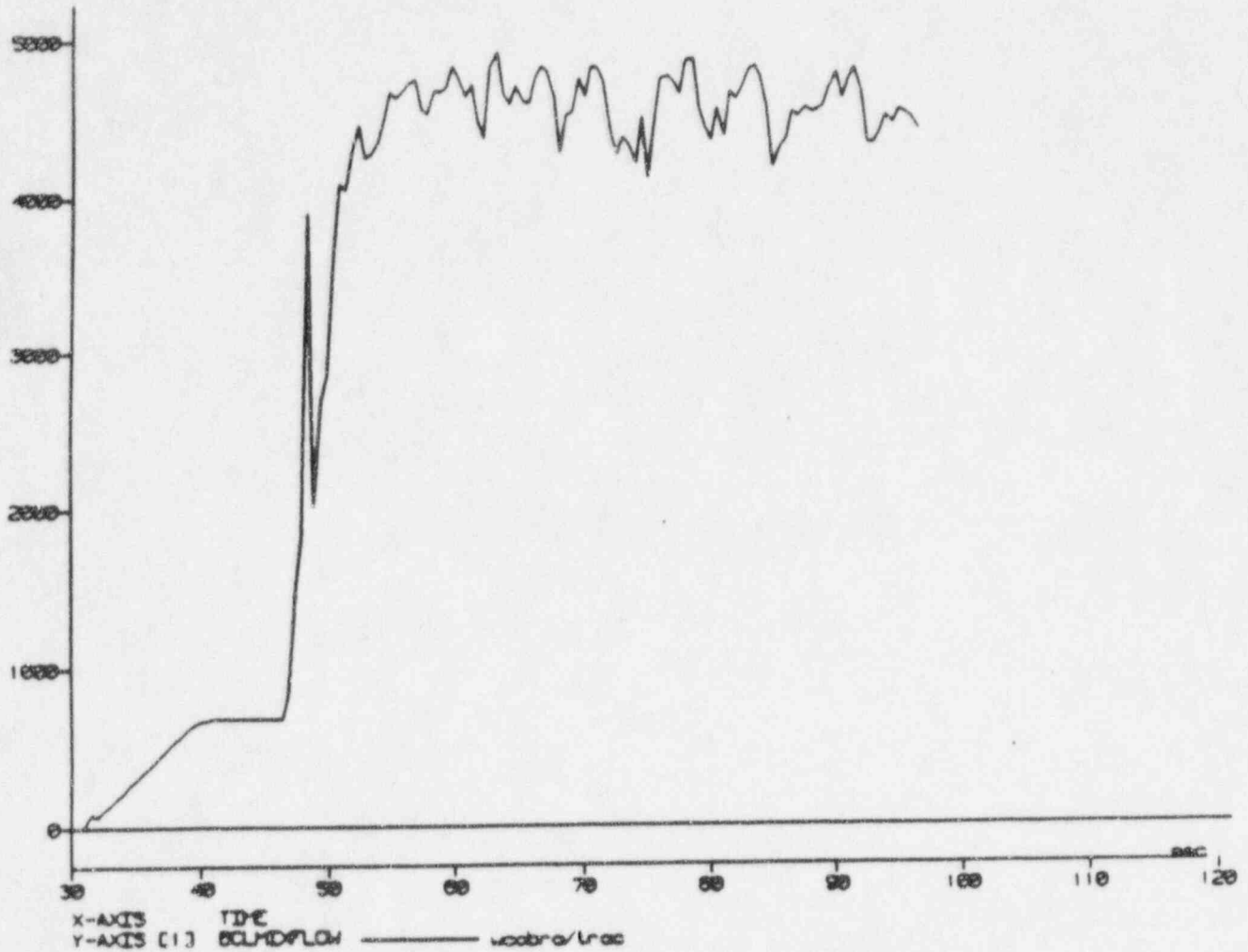


UPTF Test 21 Run 272 Phase A

Figure 440.348-37 UPTF Test 21, Phase A, Broken Cold Leg Steam Mass Flow



BROKEN COLD LEG MIXTURE FLOWRATE (lb/s)

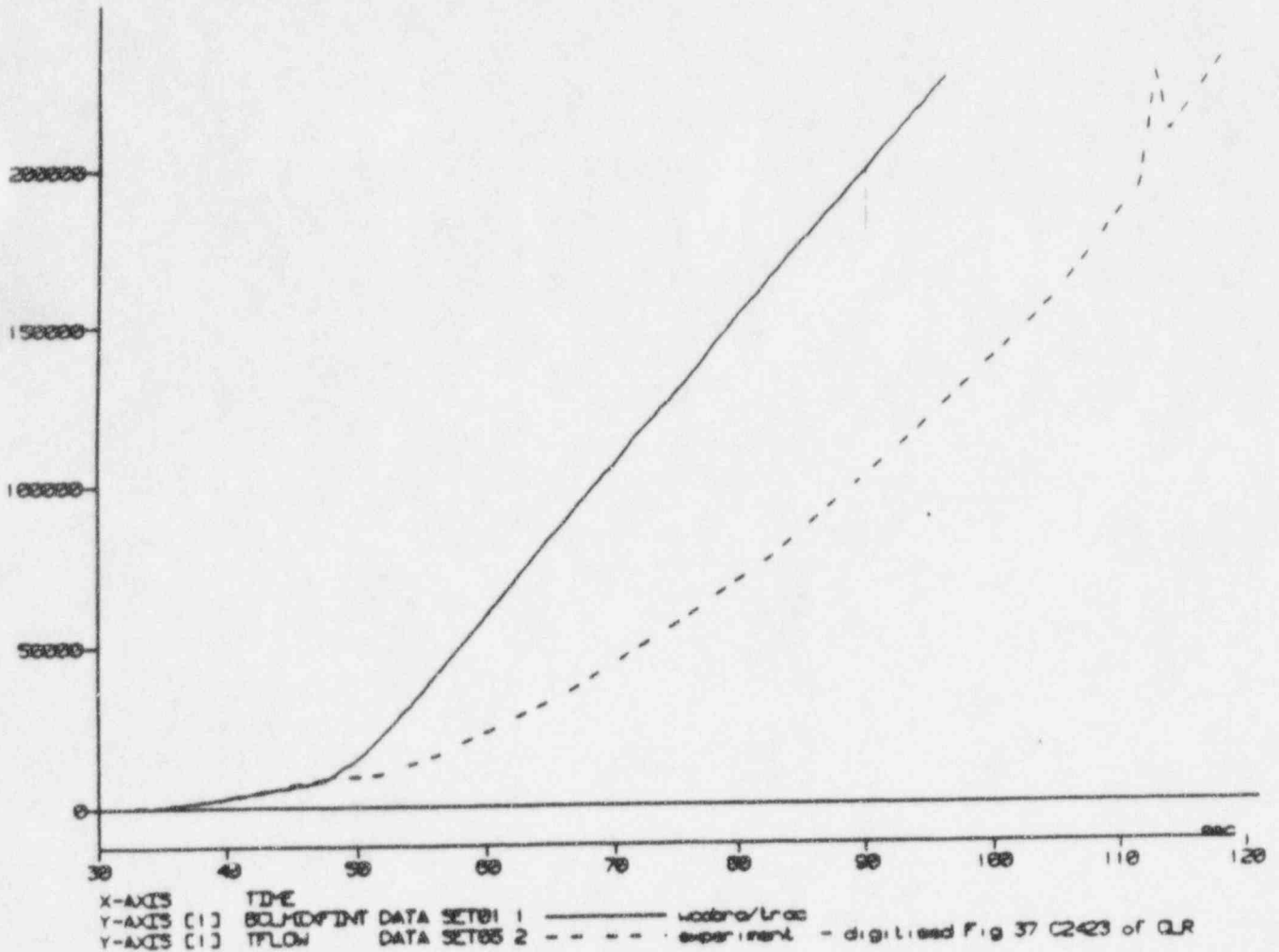


UPTF Test 21 Run 272 Phase A

Figure 440.348-38 UPTF Test 21, Phase A, Broken Cold Leg Mixture Mass Flow



BROKEN COLD LEG INTEGRATED MIXTURE FLOWRATE (1b)



UPTF Test 21 Run 272 Phase A

Figure 440.348-39 UPTF Test 21, Phase A, Broken Cold Leg Integrated Mixture Mass Flow

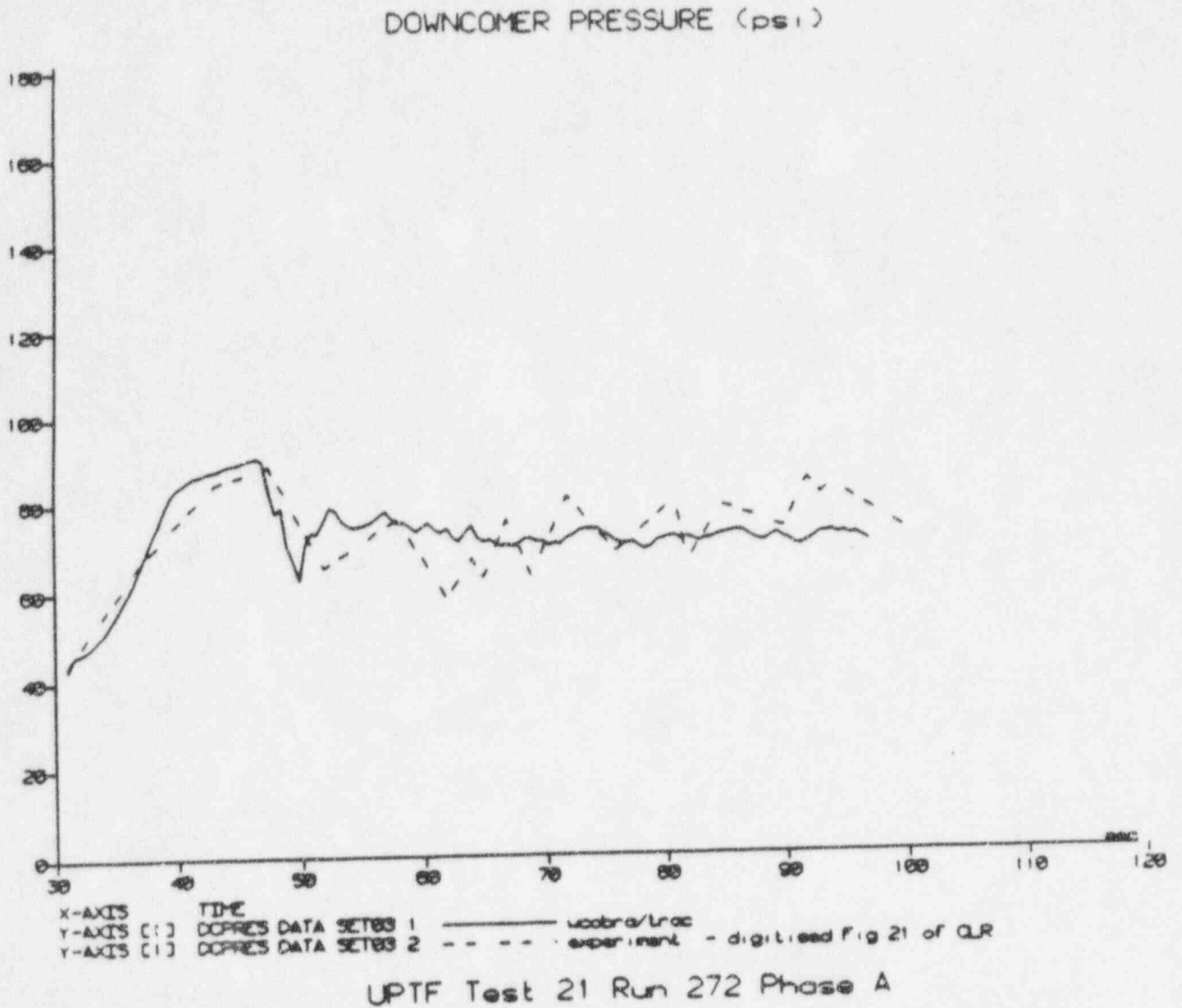
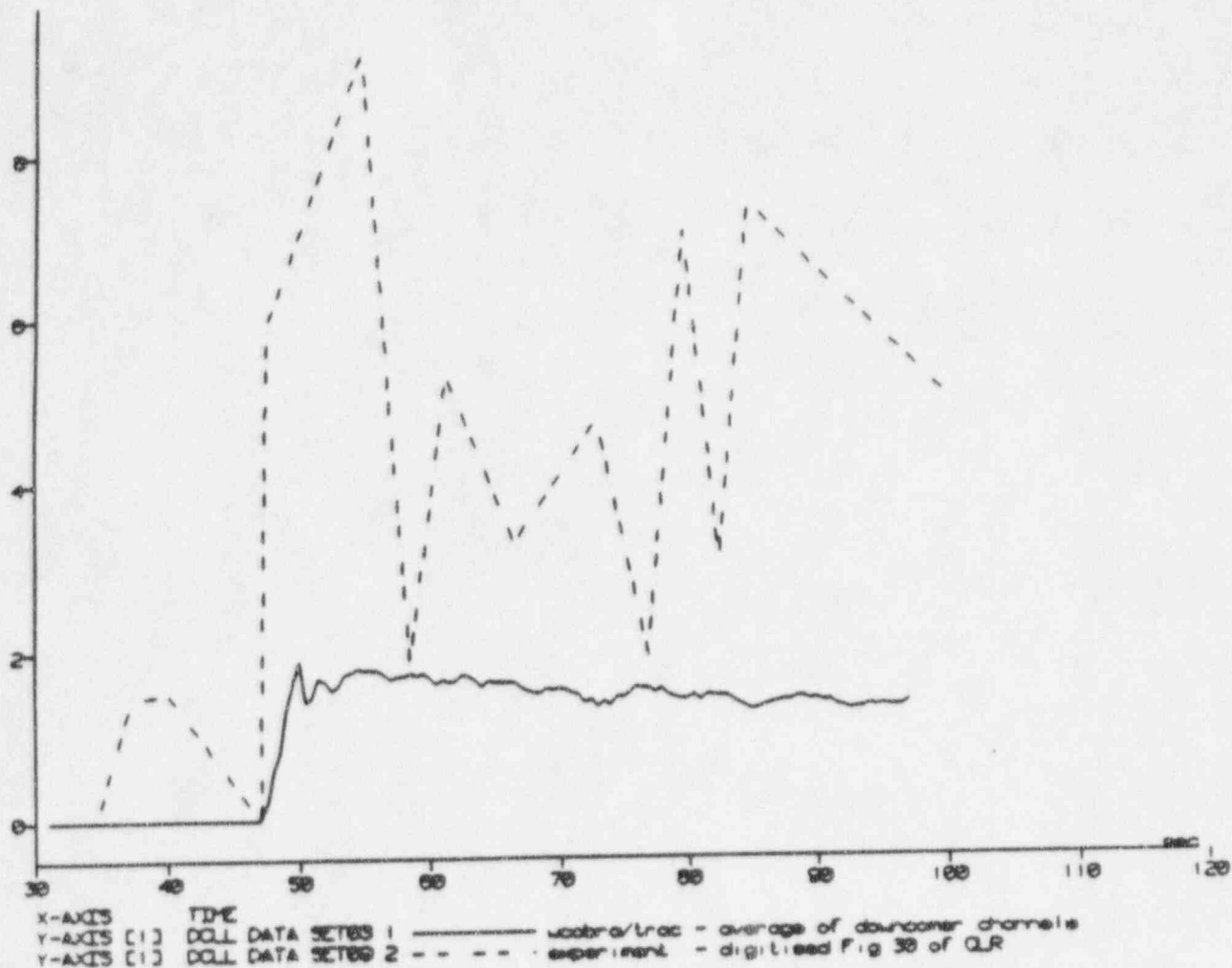


Figure 440.348-40 UPTF Test 21, Phase A, Downcomer Pressure



AVERAGE DOWNCOMER LIQUID LEVEL (ft)

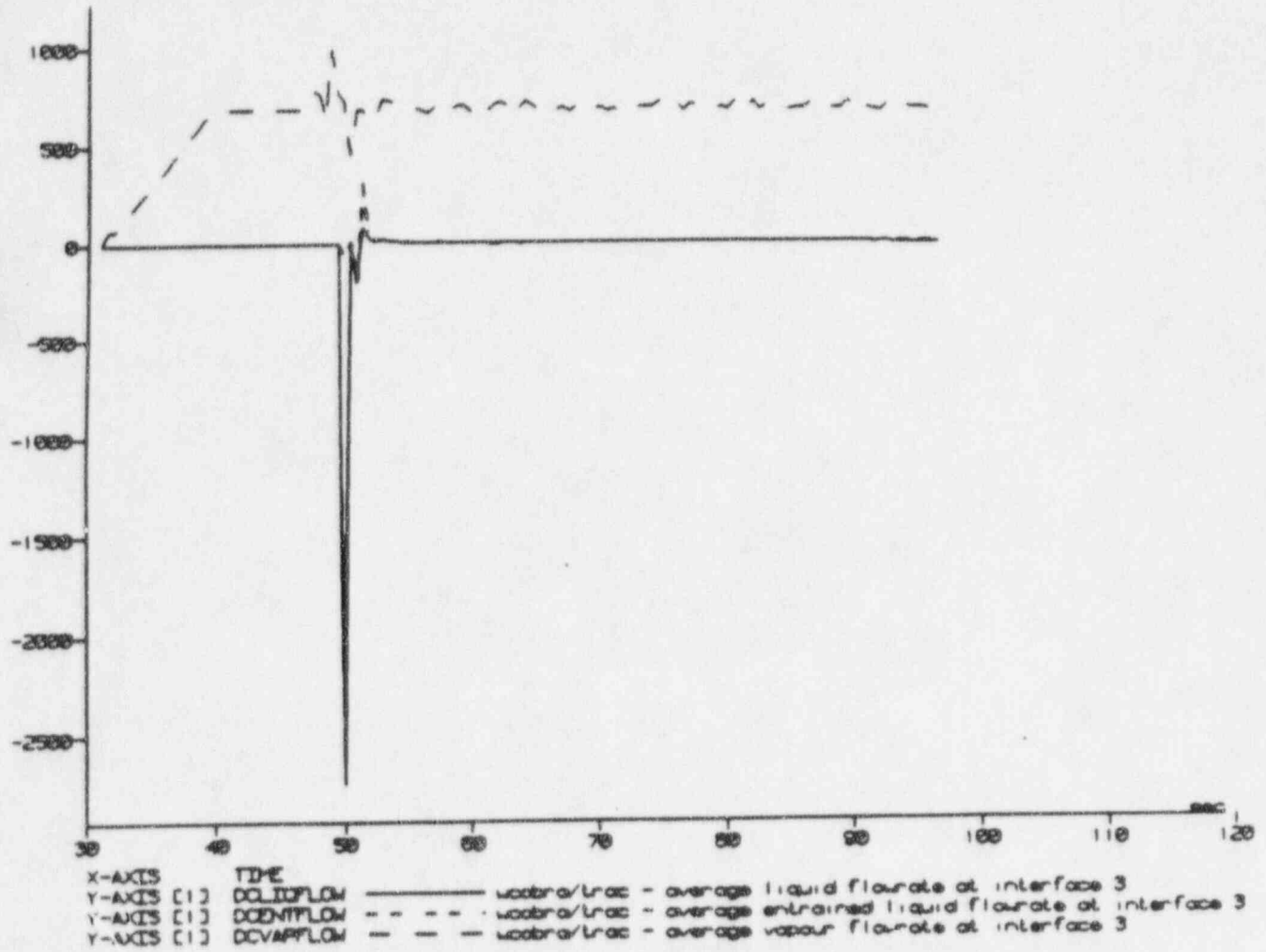


UPTF Test 21 Run 272 Phase A

Figure 440.348-41 UPTF Test 21, Phase A, Downcomer Collapsed Liquid Level



DOWNCOMER FLOWRATES JUST ABOVE BOTTOM OF CORE BARREL (lb/s)

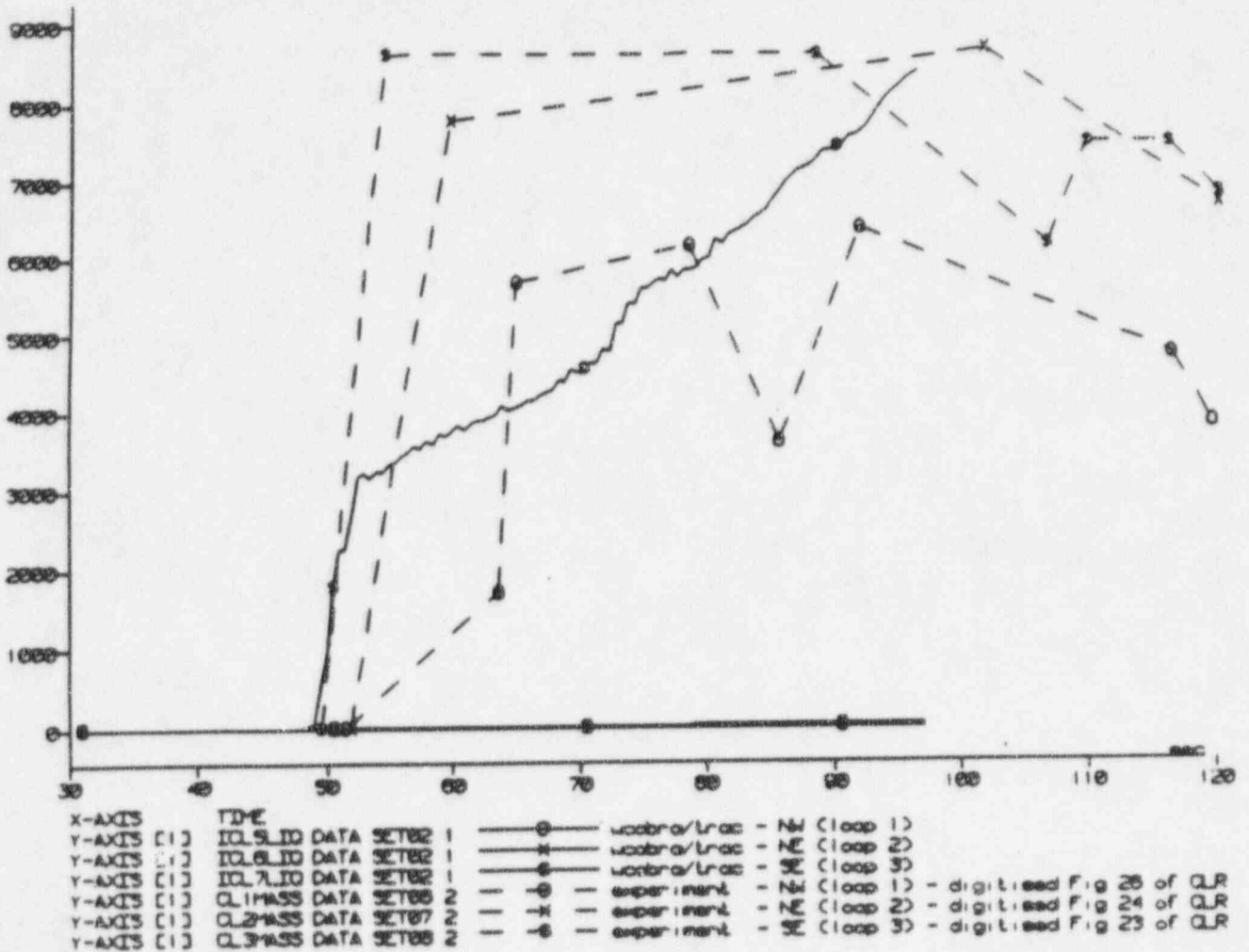


UPTF Test 21 Run 272 Phase A

Figure 440.348-42 UPTF Test 21, Phase A, Downcomer Mass Flow Above Bottom of Core Barrel



INTACT COLD LEG LIQUID MASSES (lb)

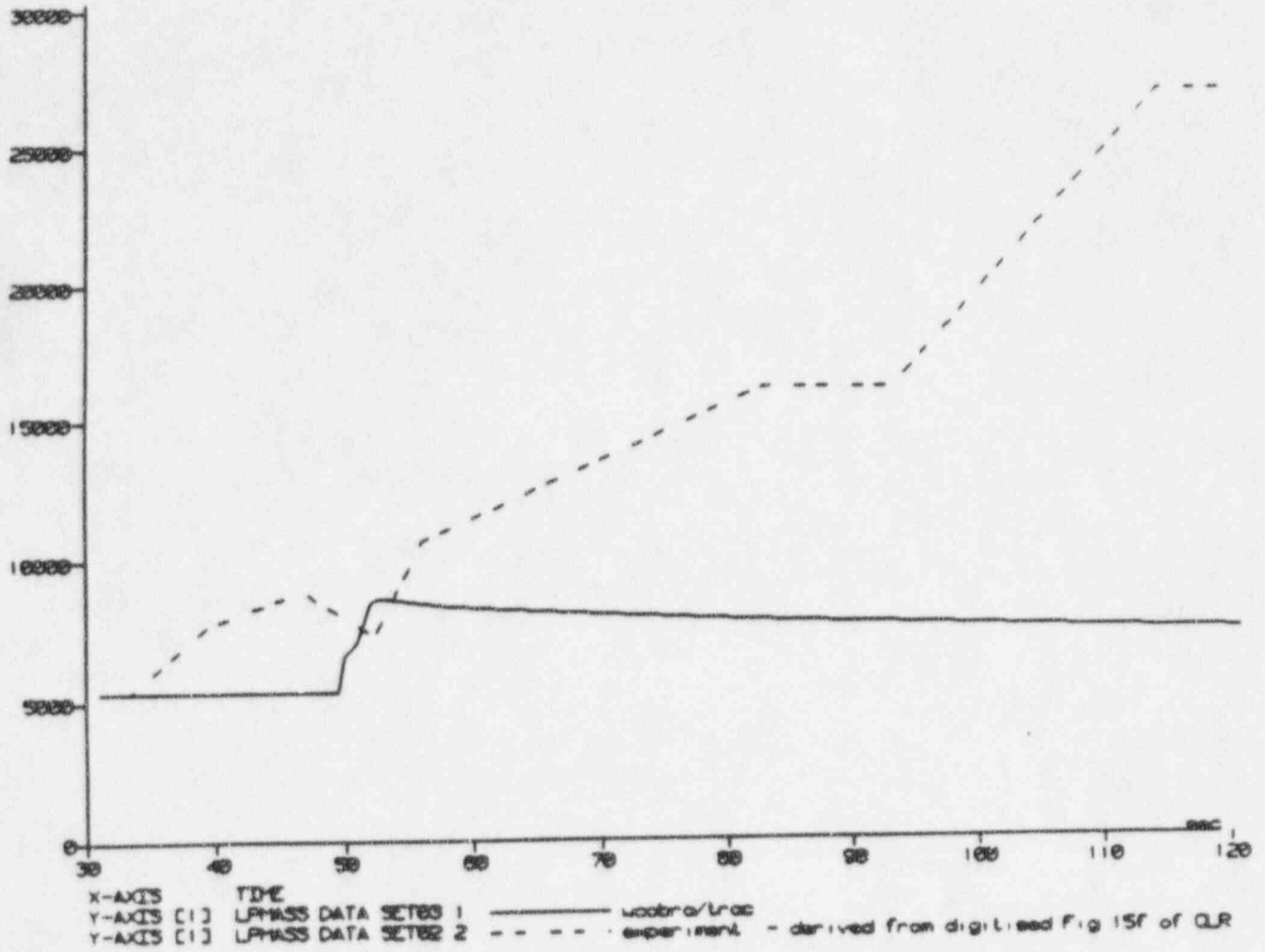


UPTF Test 21 Run 272 Phase A

Figure 440.348-43 UPTF Test 21, Phase A, Intact Cold Leg Mass Inventories



LOWER PLENUM MASS INVENTORY (1b)



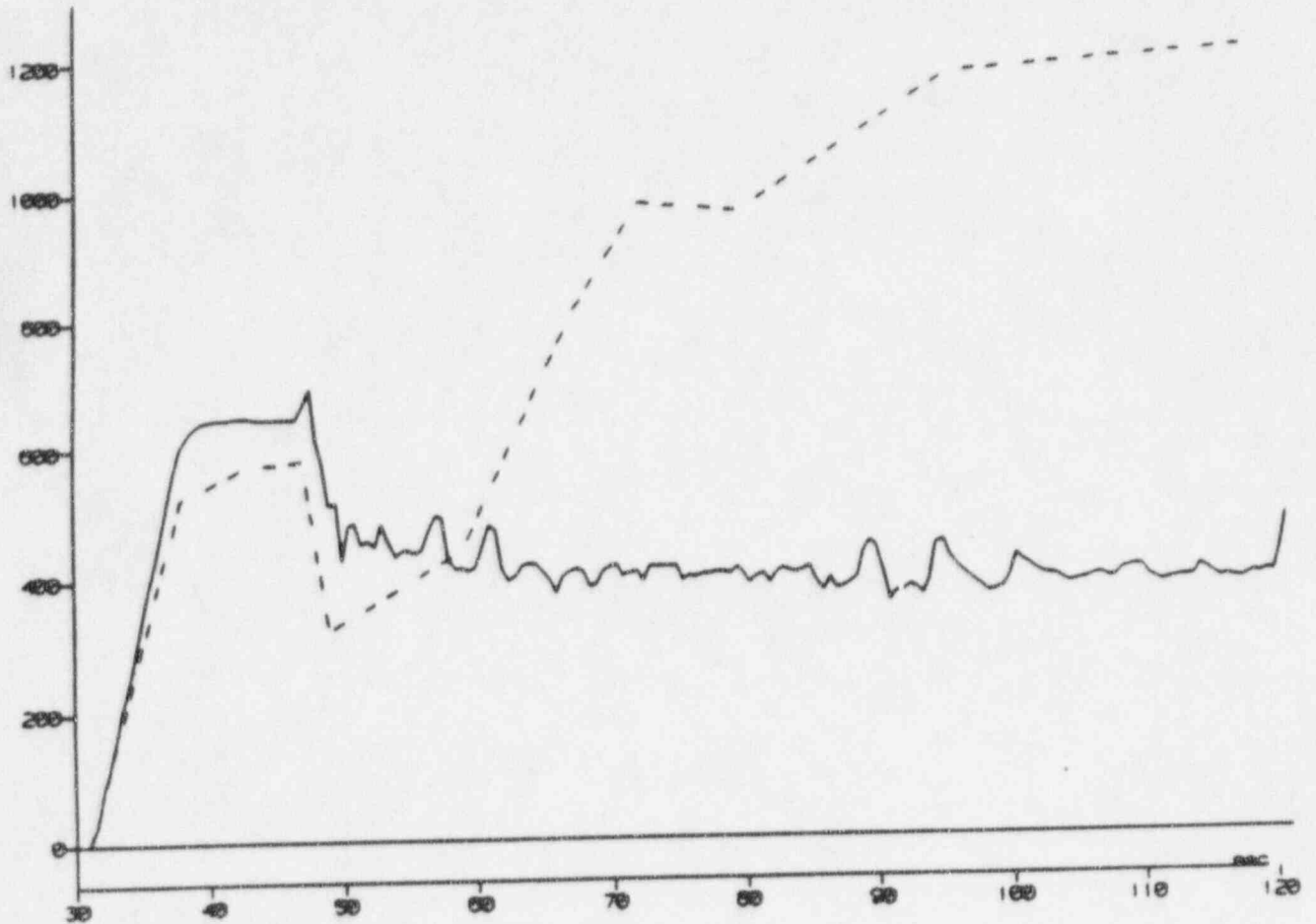
UPTF Test 21 Run 274 Phase B I

Figure 440.348-44 UPTF Test 21, Phase B I, Lower Plenum Mass Inventory





BROKEN COLD LEG VAPOUR FLOWRATE (lb/s)



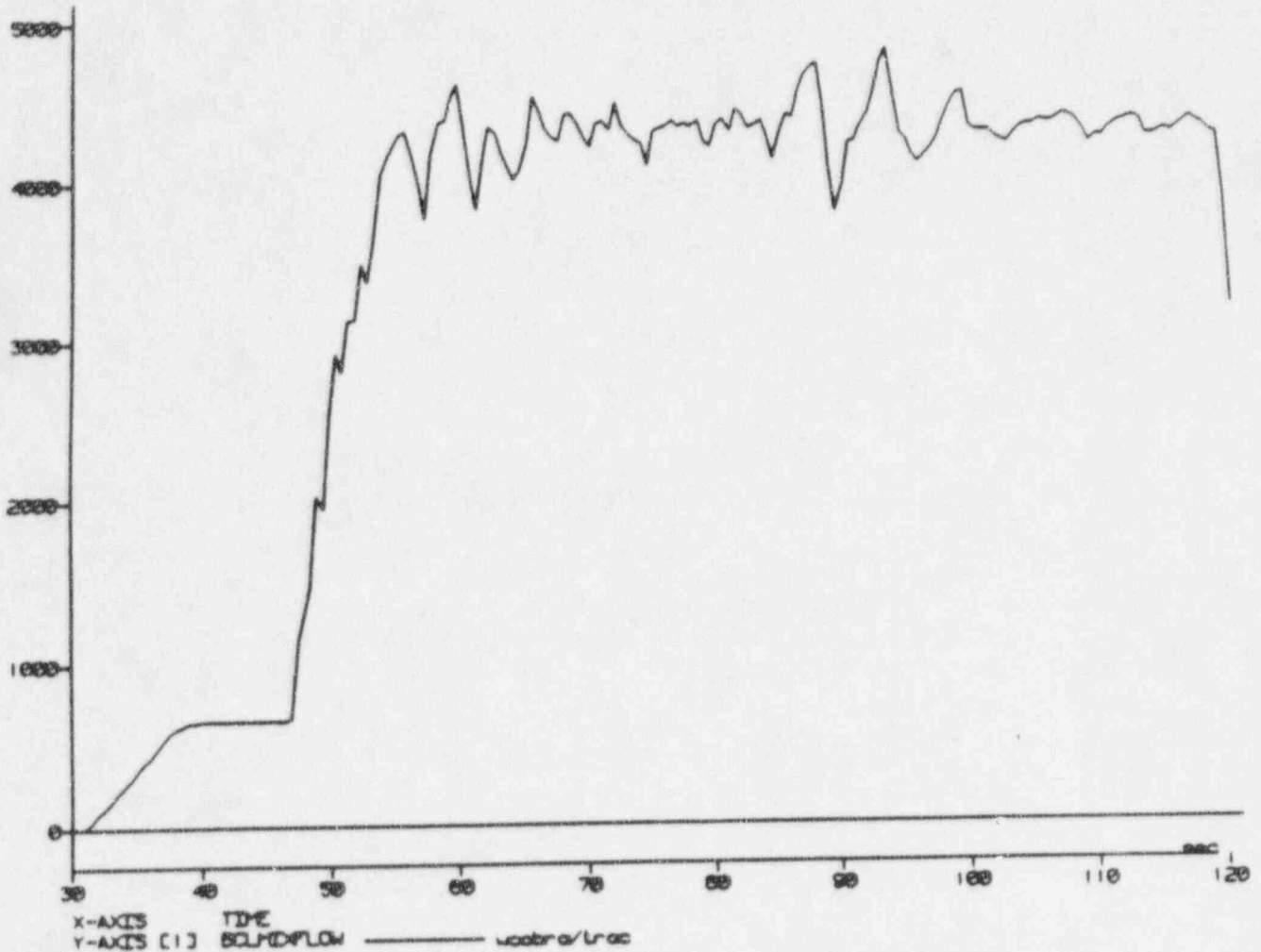
X-AXIS TIME  
Y-AXIS [1] BCLVAFFLOW DATA SET#1 1 ———— wabro/braz  
Y-AXIS [2] SFLOW DATA SET#4 2 - - - - experiment - digitized Fig 33 of CLR

UPTF Test 21 Run 274 Phase B I

Figure 440.348-45 UPTF Test 21, Phase B I, Broken Cold Leg Steam Mass Flow



BROKEN COLD LEG MIXTURE FLOWRATE (lb/s)

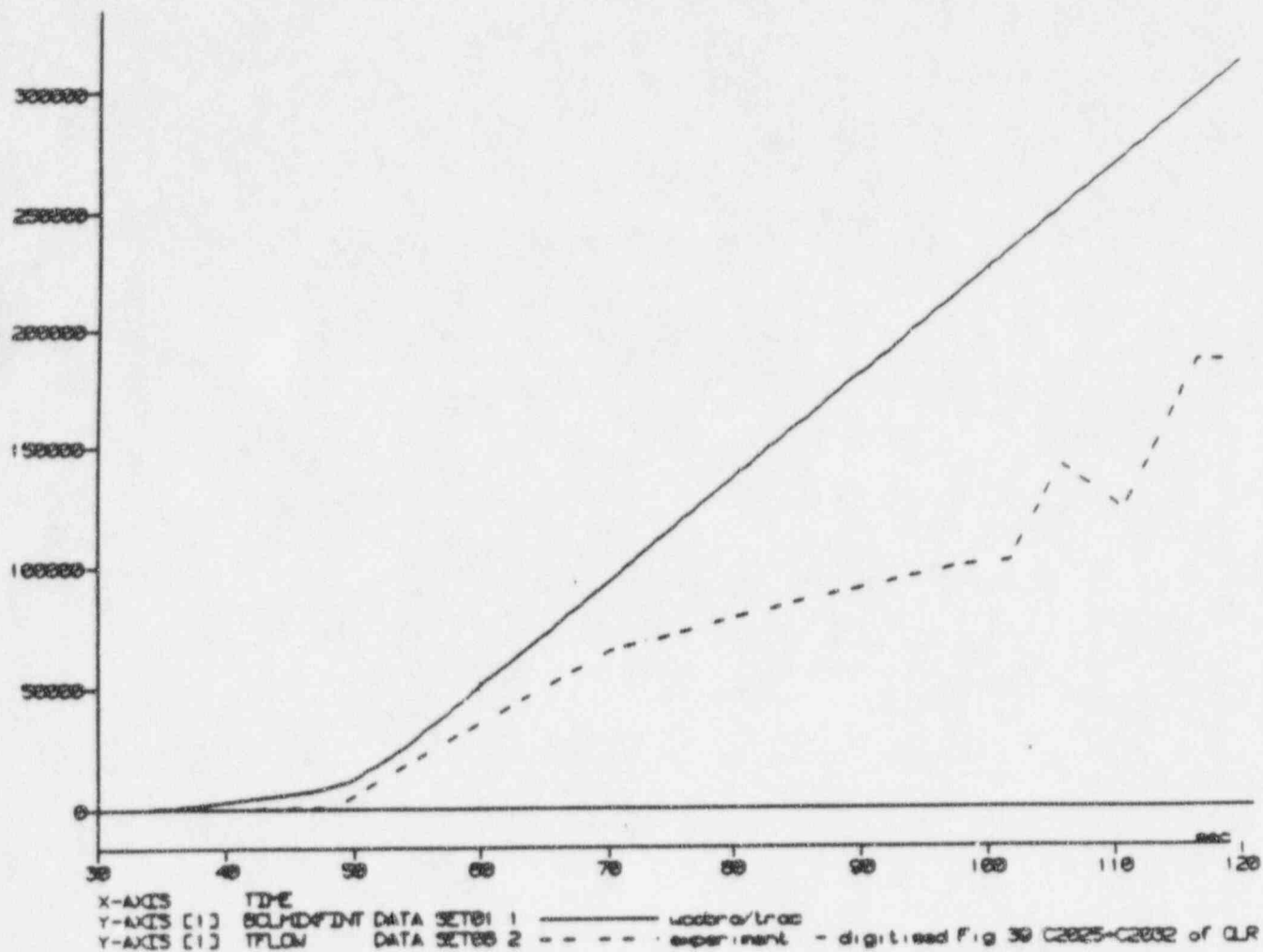


UPTF Test 21 Run 274 Phase B I

Figure 440.348-46 UPTF Test 21, Phase B I, Broken Cold Leg Mixture Mass Flow



BROKEN COLD LEG INTEGRATED MIXTURE FLOWRATE (lb)

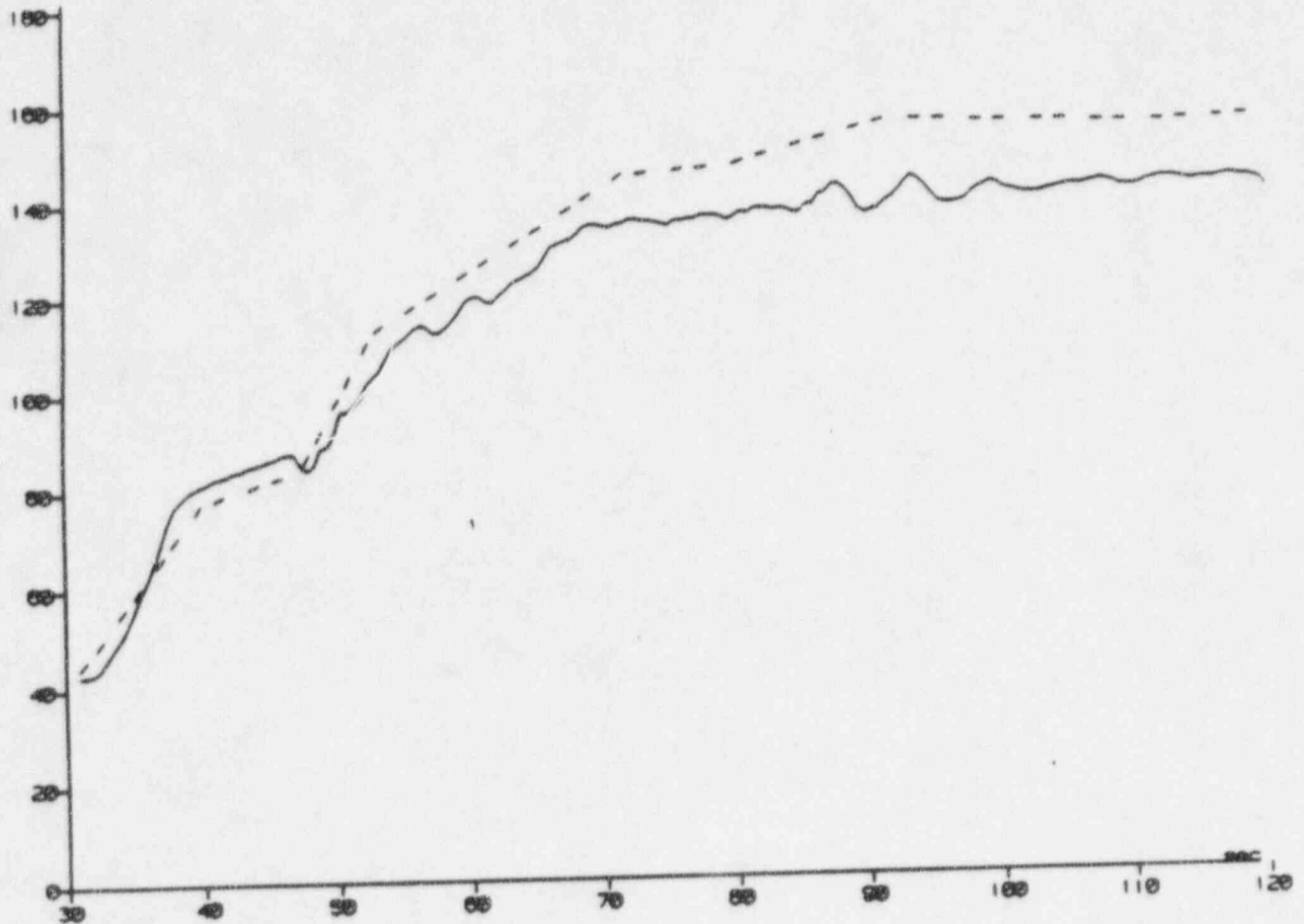


UPTF Test 21 Run 274 Phase B I

Figure 440.348-47 UPTF Test 21, Phase B I, Broken Cold Leg Integrated Mixture Mass Flow



DOWNCOMER PRESSURE (psi)



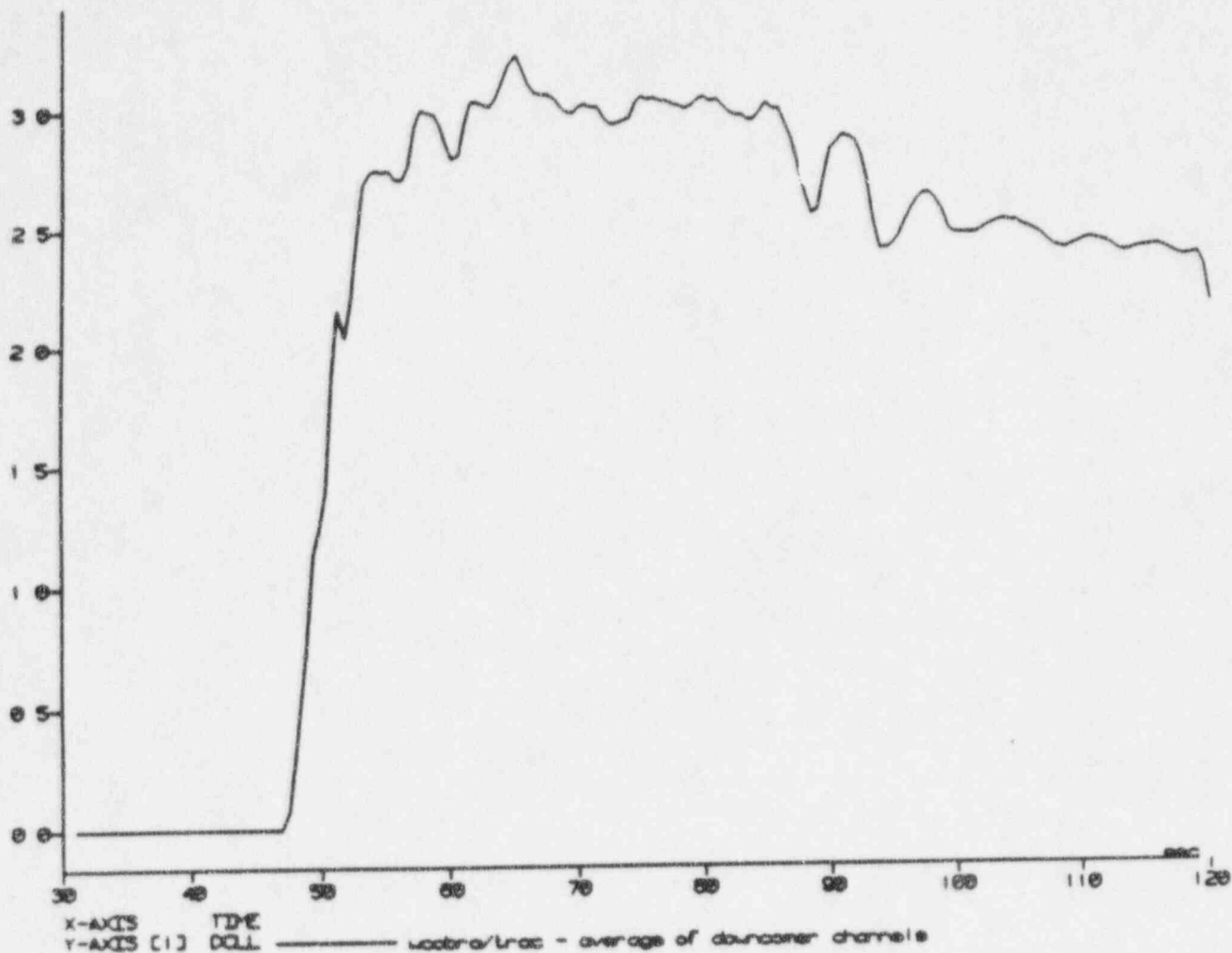
X-AXIS TIME  
Y-AXIS (1) DOPRES DATA SET00 1 ———— water/trac  
Y-AXIS (2) DOPRES DATA SET00 2 - - - - experiment - digitized Fig 32 of QLR

UPTF Test 21 Run 274 Phase B I

Figure 440.348-48 UPTF Test 21, Phase B I, Downcomer Pressure



AVERAGE DOWNCOMER LIQUID LEVEL (ft)

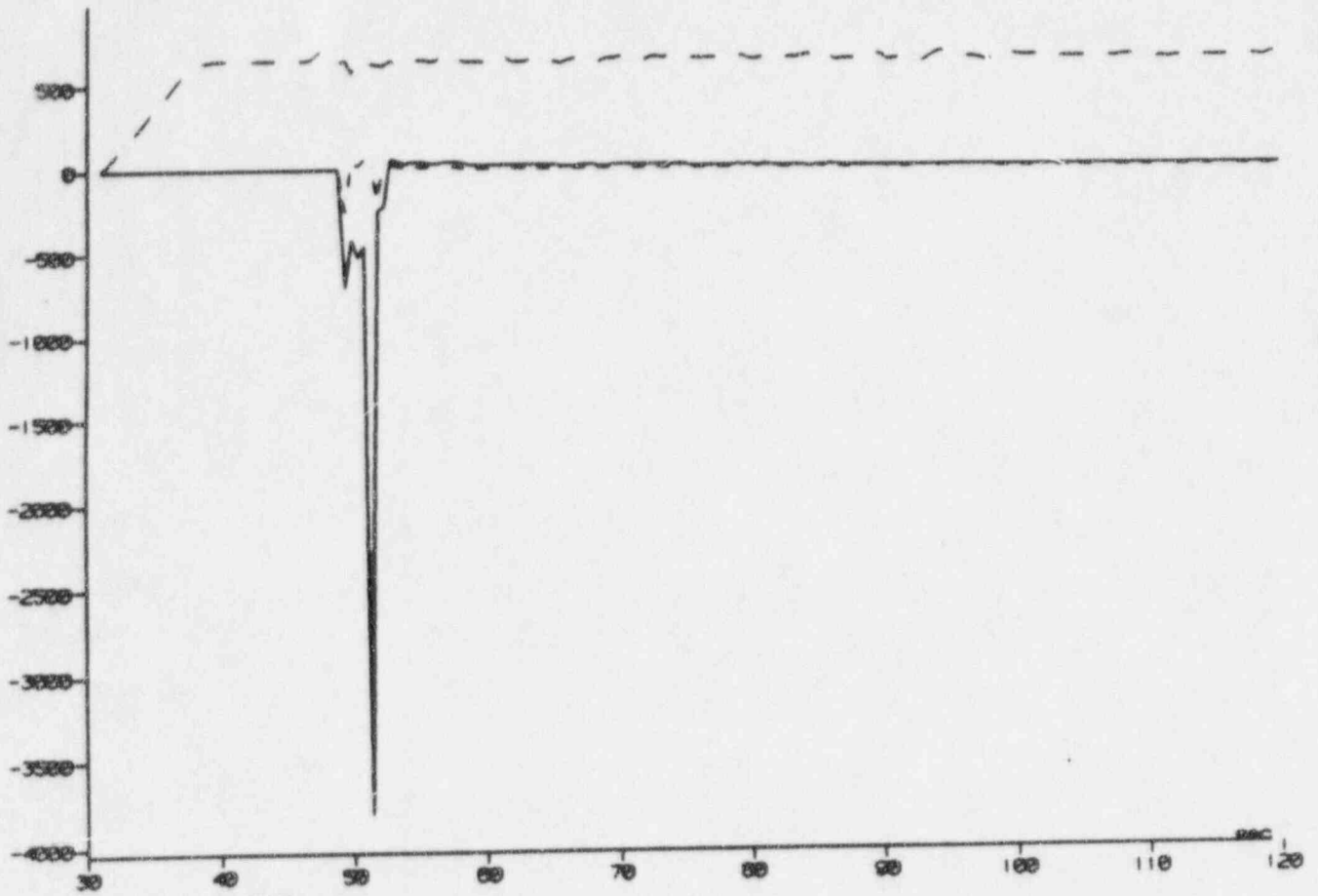


UPTF Test 21 Run 274 Phase B I

Figure 440.348-49 UPTF Test 21, Phase B I, Downcomer Collapsed Liquid Level



DOWNCOMER FLOWRATES JUST ABOVE BOTTOM OF CORE BARREL (lb/s)



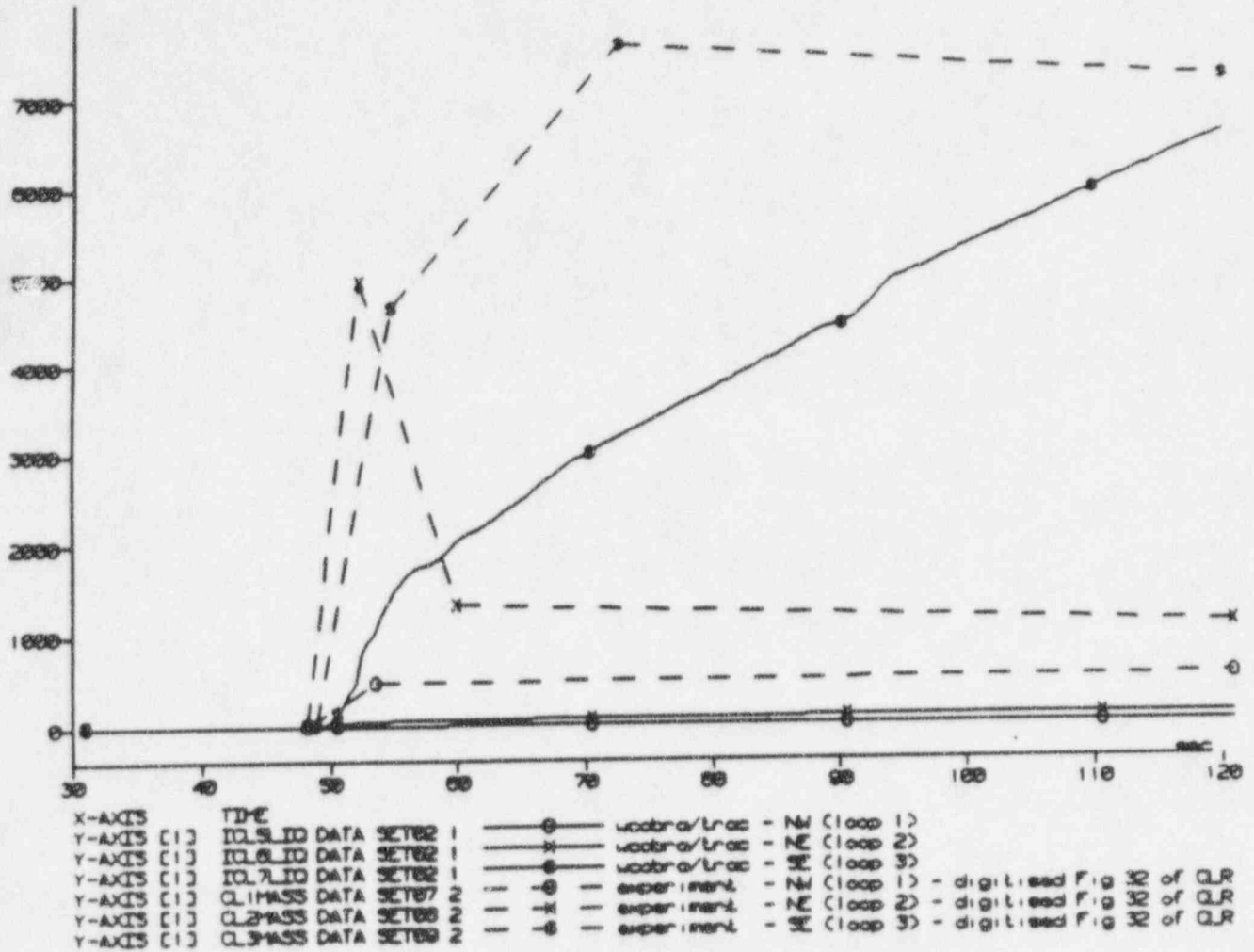
X-AXIS TIME  
 Y-AXIS [1] DC LIQ FLOW ——— wobra/trac - average liquid flowrate at interface 3  
 Y-AXIS [1] DC ENTR FLOW - - - - wobra/trac - average entrained liquid flowrate at interface 3  
 Y-AXIS [1] DC VAP FLOW - . - . - wobra/trac - average vapour flowrate at interface 3

UPTF Test 21 Run 274 Phase B I

Figure 440.348-50 UPTF Test 21, Phase B I, Downcomer Mass Flow Above Bottom of Core Barrel



INTACT COLD LEG LIQUID MASSES (lb)

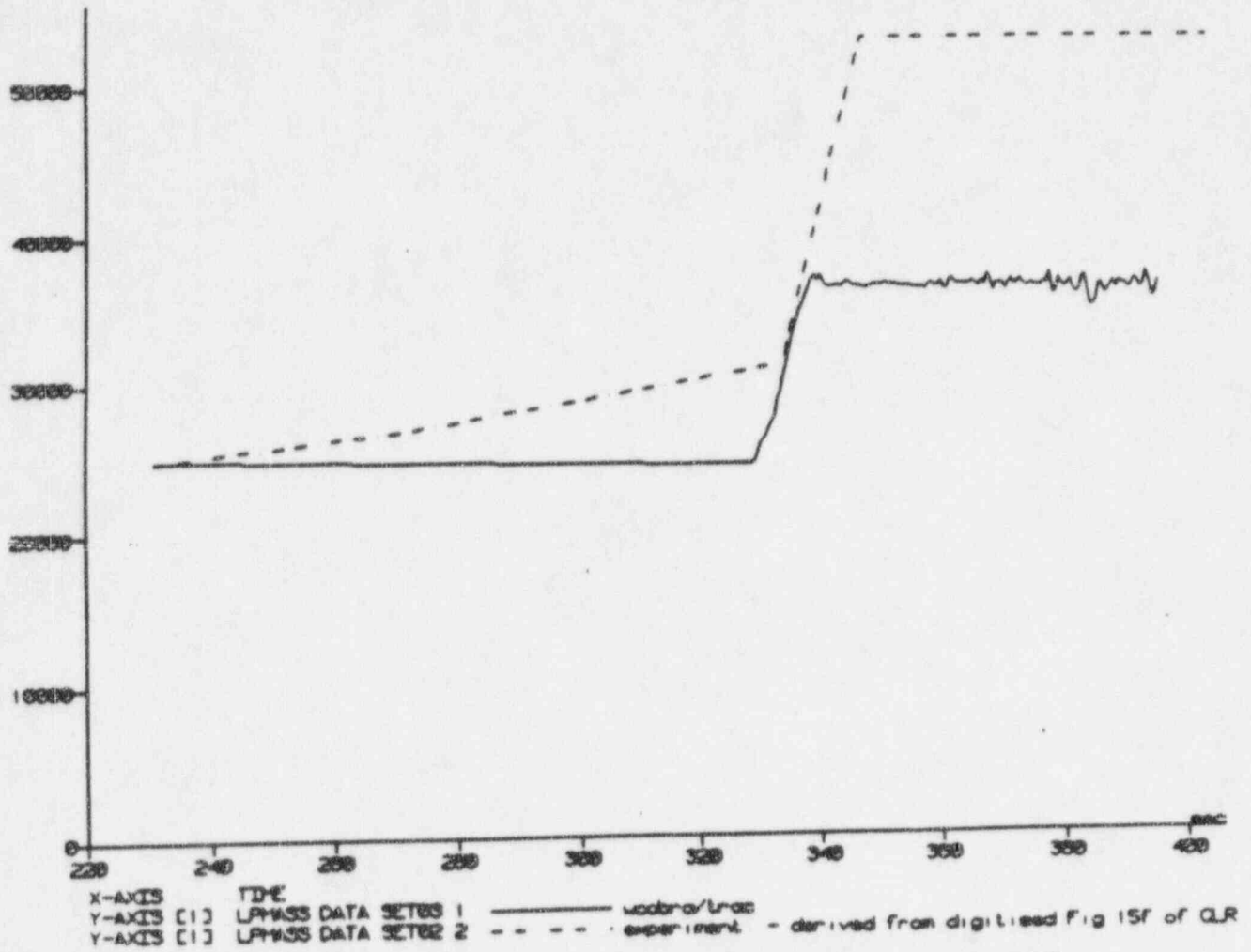


UPTF Test 21 Run 274 Phase B I

Figure 440.348-51 UPTF Test 21, Phase B I, Intact Cold Leg Mass Inventories



LOWER PLENUM MASS INVENTORY (1b)



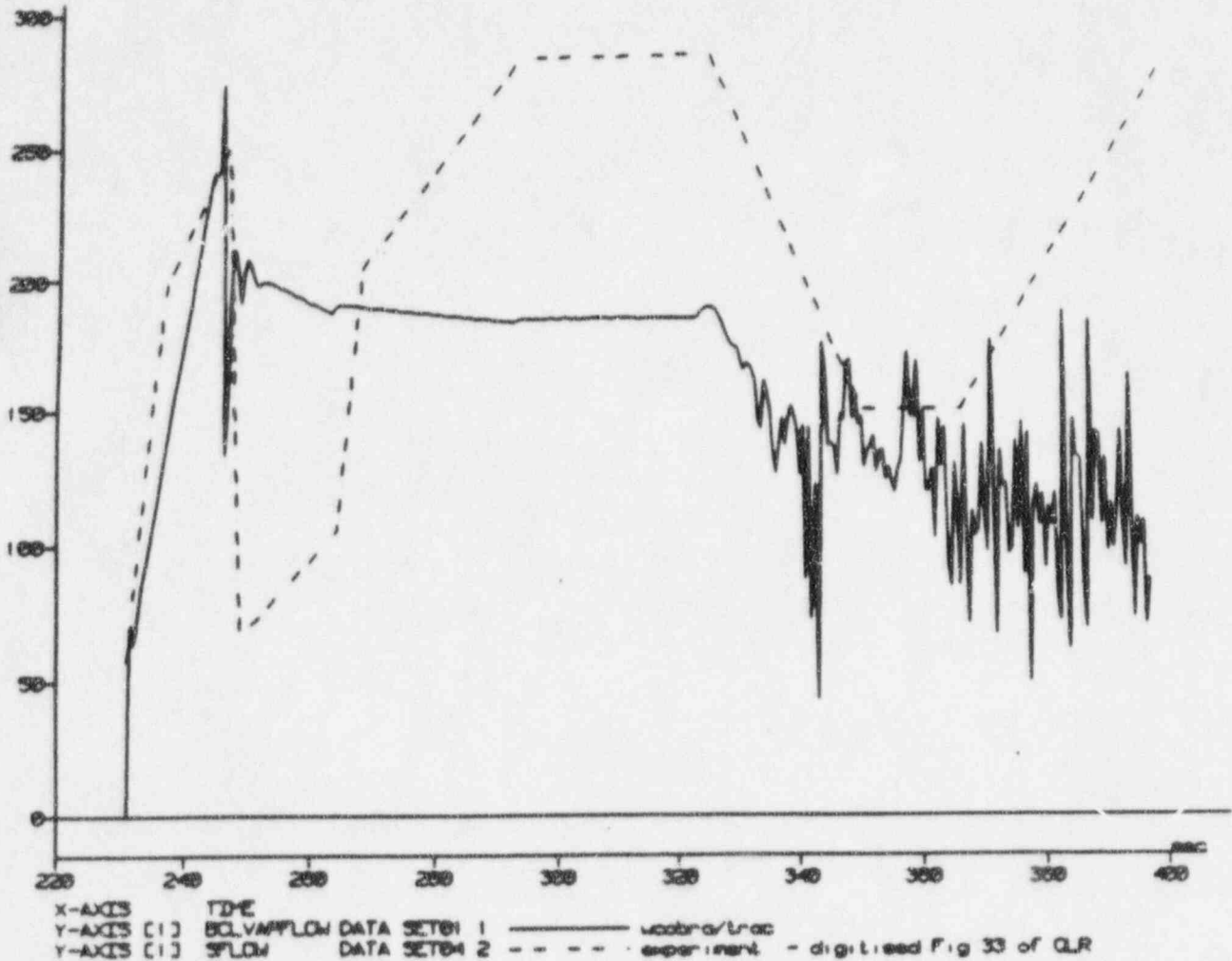
UPTF Test 21 Run 274 Phases B II & III

Figure 440.348-52 UPTF Test 21, Phase B II&III, Lower Plenum Mass Inventory



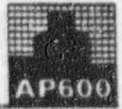


BROKEN COLD LEG VAPOUR FLOWRATE (lb/s)

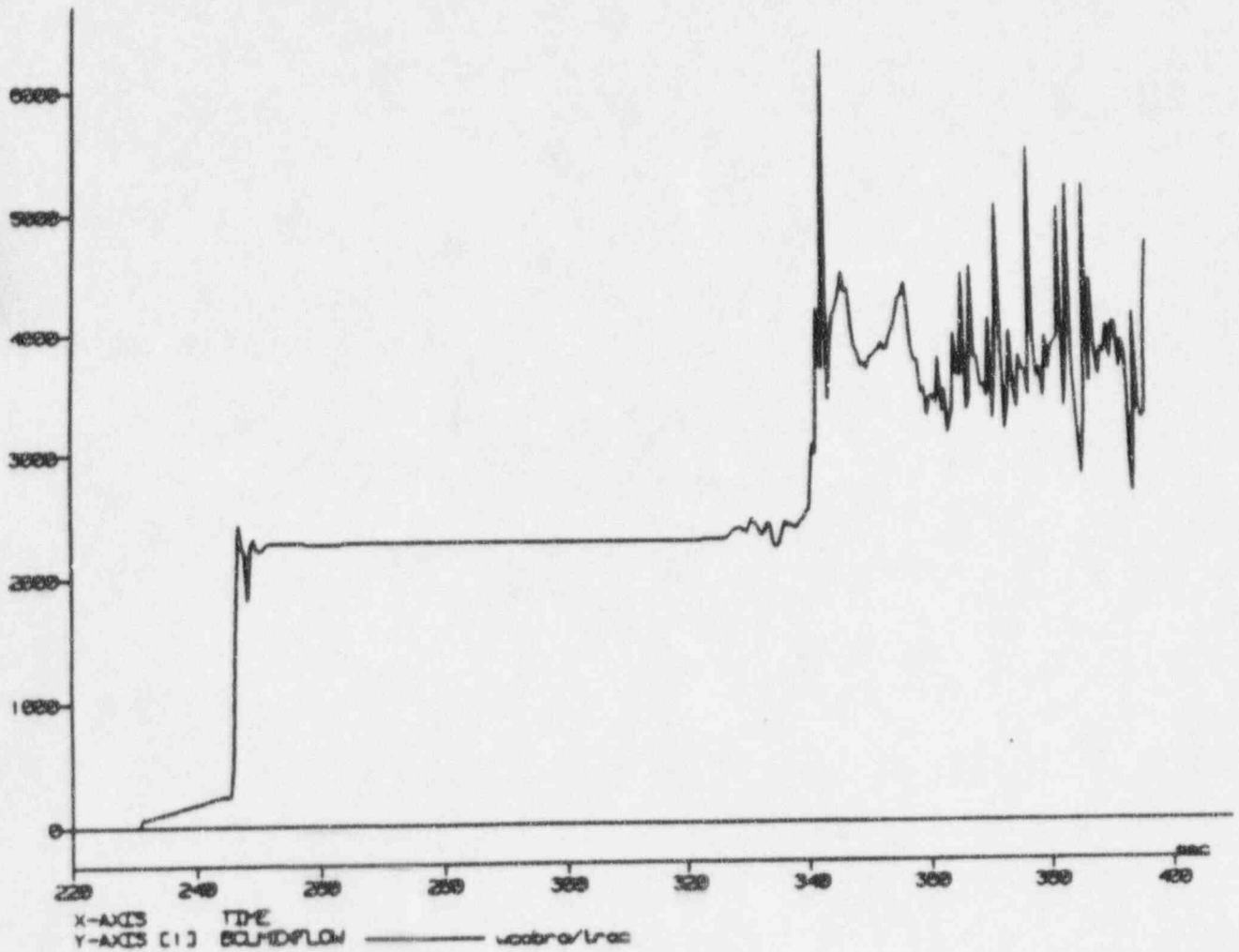


UPTF Test 21 Run 274 Phases B II & III

Figure 440.348-53 UPTF Test 21, Phase B II&III, Broken Cold Leg Steam Mass Flow



BROKEN COLD LEG MIXTURE FLOWRATE (lb/s)

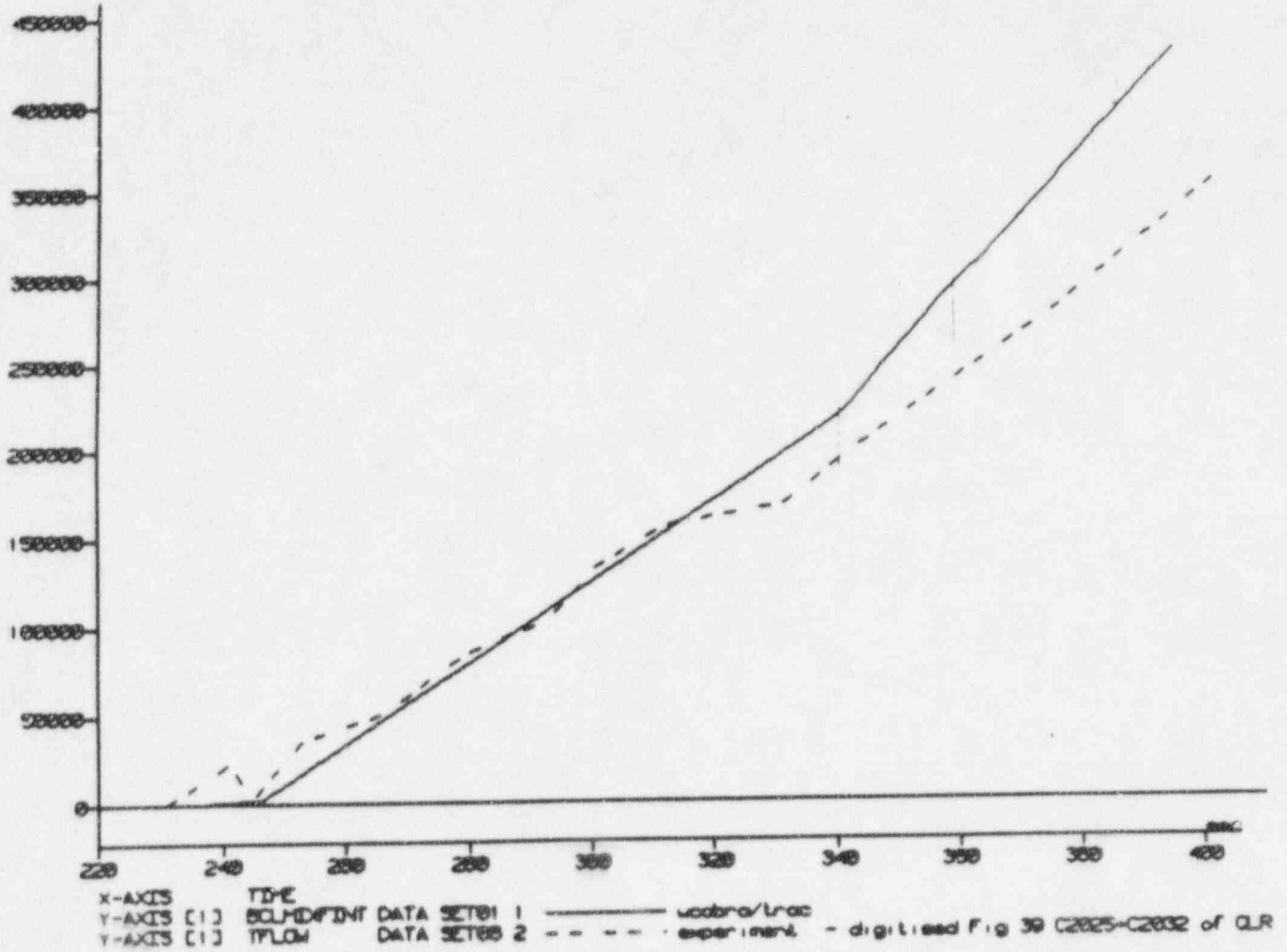


UPTF Test 21 Run 274 Phases B II & III

Figure 440.348-54 UPTF Test 21, Phase B II&III, Broken Cold Leg Mixture Mass Flow



BROKEN COLD LEG INTEGRATED MIXTURE FLOWRATE (lb)

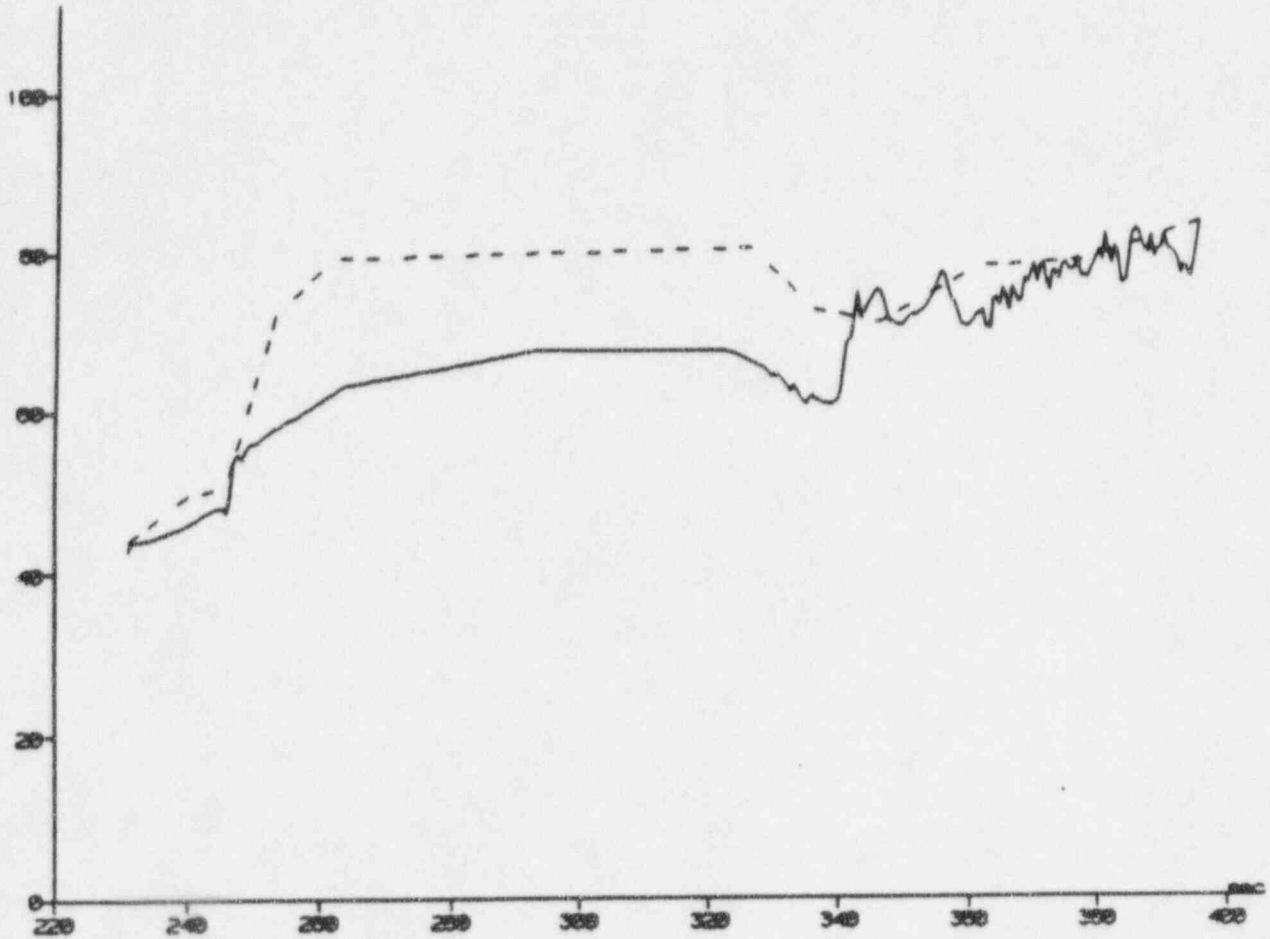


UPTF Test 21 Run 274 Phases B II & III

Figure 440.348-55 UPTF Test 21, Phase B II&III, Broken Cold Leg Integrated Mixture Mass Flow



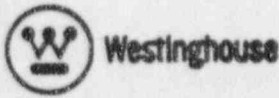
DOWNCOMER PRESSURE (psi)



X-AXIS TIME  
Y-AXIS (1) DOBRES DATA SETS 1 ———— uobra/trac  
Y-AXIS (1) DOBRES DATA SETS 2 - - - - experiment - digitized Fig 32 of QLR

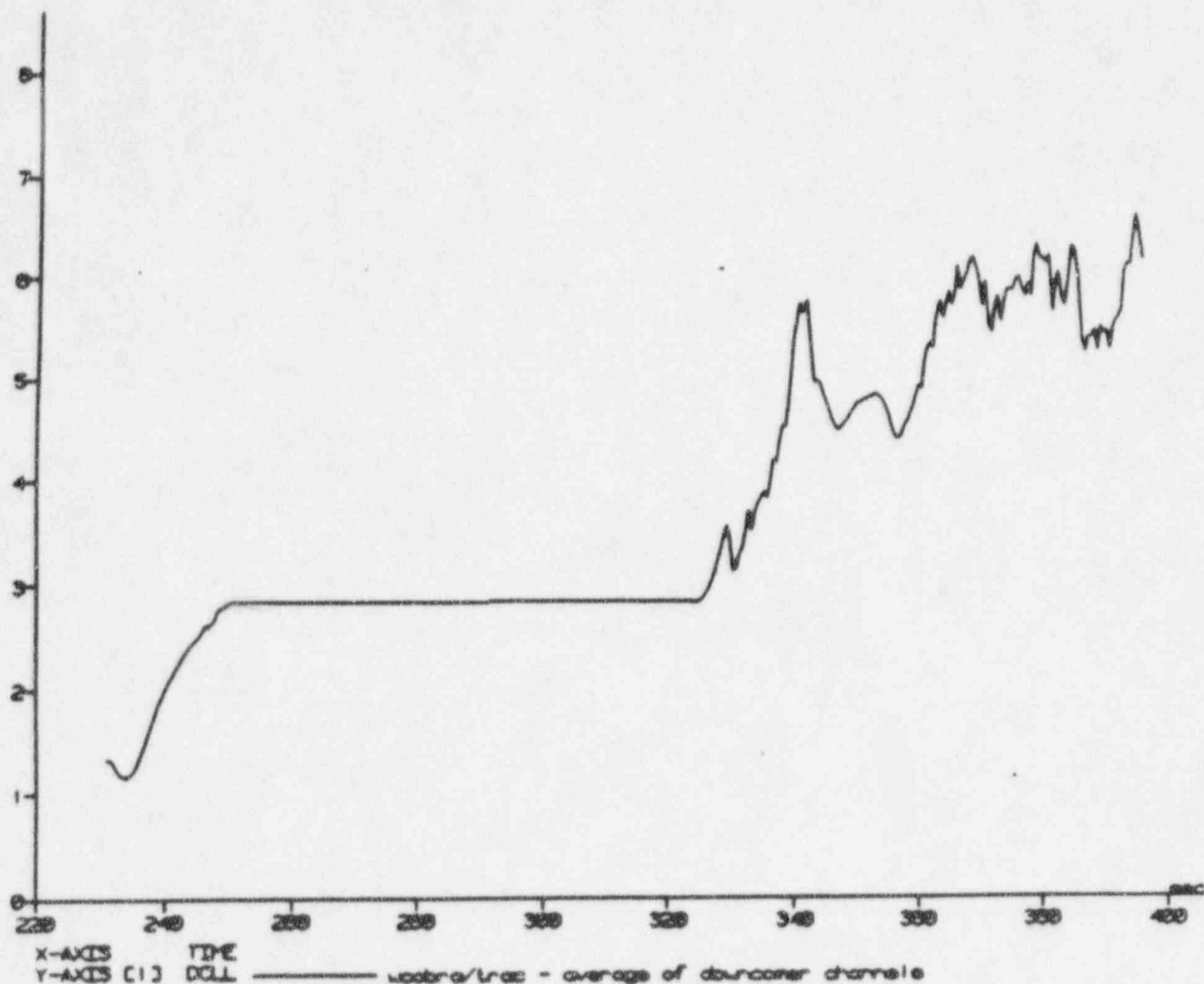
UPTF Test 21 Run 274 Phases B II & III

Figure 440.348-56 UPTF Test 21, Phase B II&III, Downcomer Pressure





AVERAGE DOWNCOMER LIQUID LEVEL (ft)

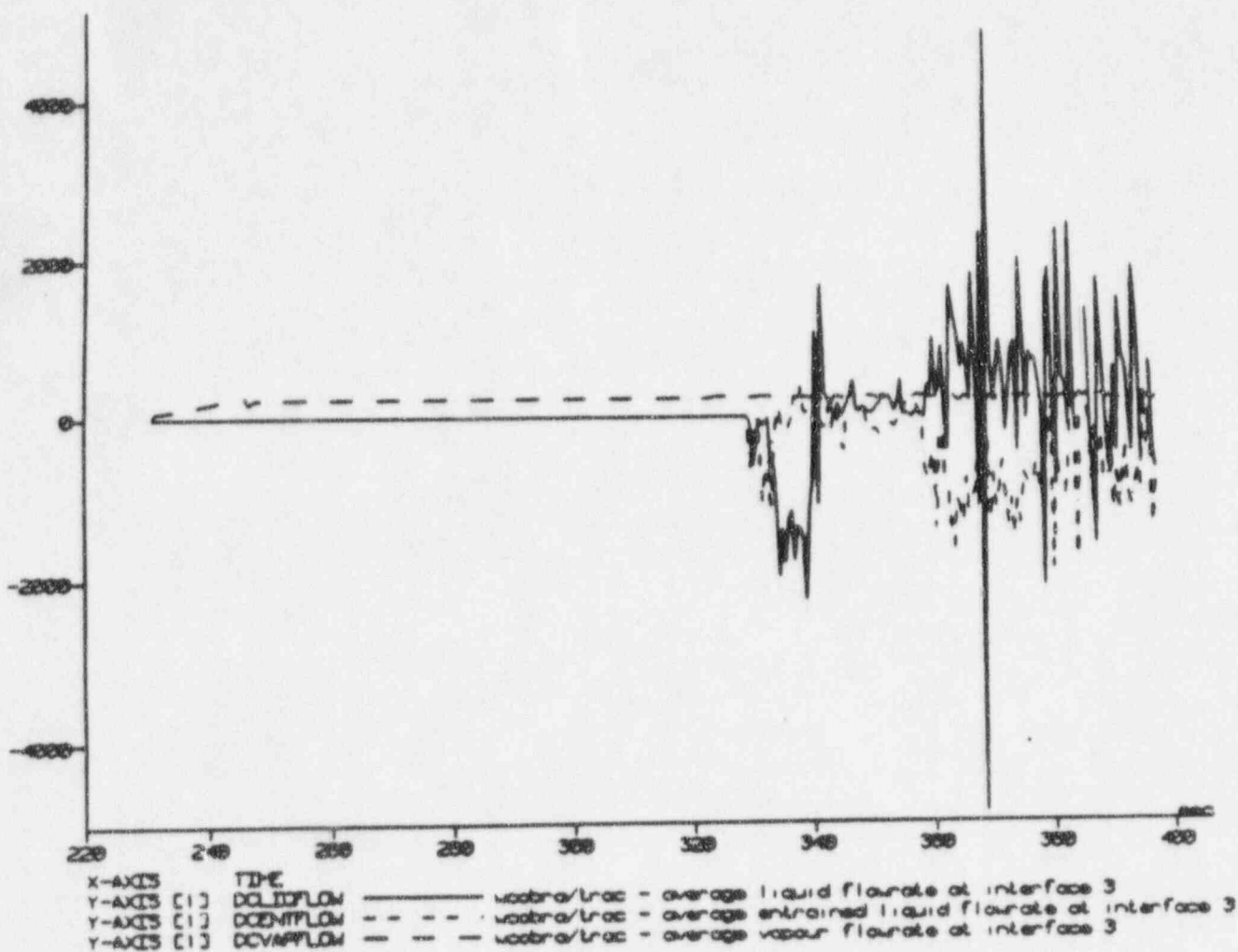


UPTF Test 21 Run 274 Phases B II & III

Figure 440.348-57 UPTF Test 21, Phase B II&III, Downcomer Collapsed Liquid Level



DOWNCOMER FLOWRATES JUST ABOVE BOTTOM OF CORE BARREL (lb/s)



UPTF Test 21 Run 274 Phases B II & III

Figure 440.348-58 UPTF Test 21, Phase BII&III, DC Mass Flow Above Bottom of Core Barrel



'INTACT COLD LEG LIQUID MASSES (1b)

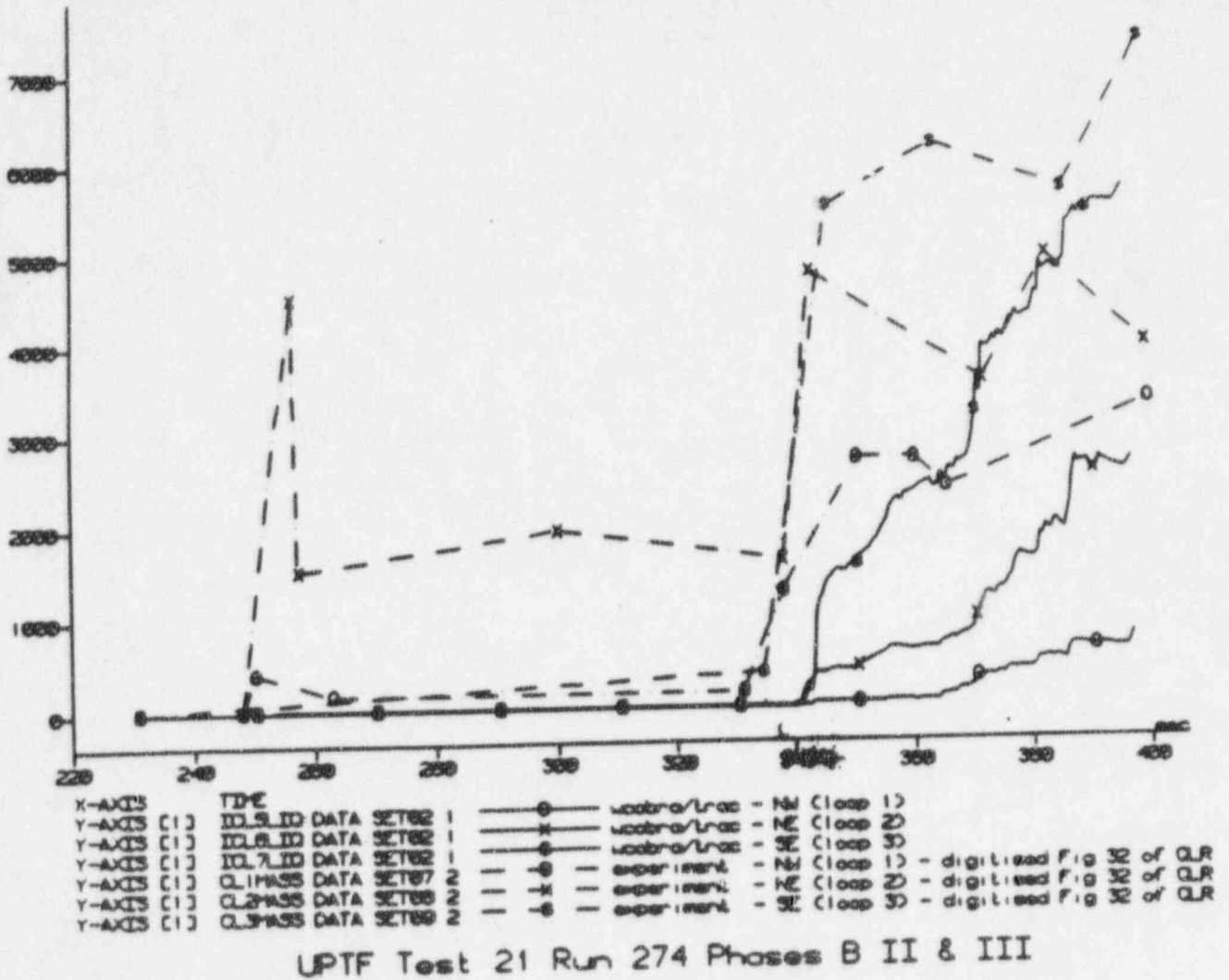


Figure 440.348-59 UPTF Test 21, Phase B II&III, Intact Cold Leg Mass Inventories

## NRC REQUEST FOR ADDITIONAL INFORMATION



Question 440.349

Re: WCAP-14171 (WCOBRA/TRAC CAD)

The WCOBRA/TRAC Code Qualification Document (CQD), Section 28-2, in discussing compliance with Regulatory Guide (RG) 1.157, stated that application of WCOBRA/TRAC to the AP600 design was considered acceptable based on information in the CQD and confirmatory tests and comparisons currently being performed on the unique features of the AP600, the results of which will be provided in other reports. Please describe the specific features of AP600 that will be evaluated with these tests, and show how the results demonstrate WCOBRA/TRAC meets the requirements of RG 1.157, Regulatory Position 1.

Response:

The AP600 contains only three features requiring specific evaluation of impact for the WCOBRA/TRAC analysis of large break LOCA ECCS performance: downcomer injection of safety injection water, core makeup tank delivery and phenomena, and PRHR heat transfer phenomena. The downcomer injection assessment has been addressed as documented in WCAP-14171 and is augmented in responses to a number of RAIs. The core makeup tank modeling used in WCOBRA/TRAC is documented in Reference 440.349-1, which shows that for the pertinent conditions prevalent during a large break LOCA event, namely cold CMT liquid receiving steam flow through a voided balance line from a voided cold leg, WCOBRA/TRAC properly predicts phenomena in and delivery from the core makeup tank. The PRHR heat exchanger, although actuated early in the large break LOCA transient due to an "S" signal, receives little flow from the voided hot leg and does not affect the system behavior or the calculated PCT. This was illustrated by the sensitivity study presented in Reference 440.349-2. All of this AP600-specific assessment extends the extensive assessment of WCOBRA/TRAC provided in the CQD itself. As regards RG 1.157, Regulatory Position 1, the recent (Reference 440.349-3) Westinghouse report addressing WCOBRA/TRAC compliance applies to AP600 as well. In addition, the AP600-specific WCOBRA/TRAC modeling is shown to be in compliance with Regulatory Position 1 as follows: both the downcomer injection and CMT predictions have been shown to be realistic by comparison with applicable experiments; the PRHR heat exchanger is modeled in the large break LOCA analysis with little effect on the result, so any development of a more detailed model is not justified.

References:

- 440.349-1 Haberstroh, R.C., et.al., "MT01-GSR-003: WCOBRA/TRAC Core Makeup Tank Preliminary Validation Report," Westinghouse Electric Corporation, February 1995.
- 440.349-2 Letter NTD-NRC-95-4503, "Preliminary Marked Up Sections of SSAR Chapter 15, Revision 5", July 10, 1995
- 440.349-3 Letter, N.J. Liparulo (Westinghouse) to USNRC, "Revised WCAP-12945-P Methodology: Combination of Uncertainties and Compliance with Regulatory Guide 1.157", NTD-NRC-95-4571, September 29, 1995.

SSAR Revision: NONE



## NRC REQUEST FOR ADDITIONAL INFORMATION



Question 440.350

Re: WCAP-14171 (WCOBRA/TRAC CAD)

The AP600 downcomer is not typical of a current generation PWR. It has a larger annular gap, and there is no thermal shield in the annular region. The design includes a reflector: a large metal mass occupying most of the region between the fuel region and the inside of the core barrel. Also, the lower plenum is significantly more open than a current generation PWR; there are no instrument penetrations and there is a single lower core support which also is used for bundle inlet flow distribution. Based on the above, answer the following questions:

- (a) Explain how the above design differences will affect ECC penetration in AP600.
- (b) Address how thermal contact between the reflector and the core barrel will affect heat transfer to the downcomer fluid (hot wall effects).
- (c) Address the influence of the reduced resistance in lower plenum during blowdown and the effect on lower plenum sweep out. How will the reduced resistance affect the expected duration of reverse steam flow, and what is the impact on the duration of the ECC bypass period?
- (d) What test comparisons demonstrate the capability of WCOBRA/TRAC to correctly calculate ECC penetration and bypass in the AP600 downcomer with the above system design differences? Provide comparisons of WCOBRA/TRAC results and test data to demonstrate the code adequately calculates the effects of the above design differences.

Response:

- a) The AP600 reactor vessel downcomer is typical of current generation PWR designs. The vessel design is similar to current Westinghouse three-loop plants. The downcomer annular gap in AP600 lies between a vessel wall inside diameter of 157 inches and a core barrel outer diameter of 137.75 inches; the corresponding values of the three-loop plants are 157 inches and 137.875 inches. The annular gaps are therefore almost identical. The downcomer annular gap of Westinghouse four-loop plants is of similar size, at 10.2 inches radial length. The gap between core barrel and reactor vessel wall in the UPTF facility is 9.84 inches radially, which is intermediate among the three-loop, AP600 and four-loop plant downcomer gap dimensions. Thus, the most important parameter in the UPTF simulation, downcomer annular gap length, is representative of Westinghouse plant designs, including AP600. Many three-loop and four-loop Westinghouse plants are equipped with neutron pads rather than thermal shields; the neutron pads are only 2.69 inches thick and are located over less than one-half of the total core barrel circumference. Overall, downcomer annulus differences are minimal between the AP600 and many of the current generation Westinghouse plants, so any geometric effects on ECC penetration during a large break LOCA event will also differ minimally.
- b) The contact between the core barrel and the radial reflector in the AP600 is significant only in that the stored energy of the core barrel metal which contacts the downcomer annulus is now equivalent to that of a much thicker metal slab. As described in Reference 440.350-1, the WCOBRA/TRAC modeling of AP600 takes into account the metal in the radial reflector and its associated heat transfer surfaces. The heat transfer through the



relatively low conductivity stainless steel core barrel will heat the fluid in the downcomer during LOCA transients. This is computed in the SSAR WCOBRA/TRAC large break LOCA analyses. The capability of WCOBRA/TRAC to model heat transfer from a thick metal component to the surrounding fluid has been validated by modeling test facilities, in particular LOFT with its reactor vessel fillers which constitute a large metal heat source. (Reference 440.350-2).

- c) In the most recent AP600 SSAR large break LOCA analysis (Reference 440.350-1) lower plenum refill with ECC water begins 28 seconds into the CD=0.8 DECLG break transient. The duration of the calculated bypass period differs among downcomer channels modeled. Liquid fills those downcomer channels which are linked directly to the DVI lines immediately after accumulator injection begins at 13 seconds (Figure 440.350-1). Flow proceeding up the downcomer to the cold leg break location prevents liquid accumulation in the non-DVI downcomer channels until 22 seconds. The three-dimensional modeling capability of WCOBRA/TRAC provides a detailed picture of the downcomer condition during ECC injection. While the lower plenum resistance of the AP600 is smaller than in the Westinghouse three-loop plant, the AP600 lower plenum geometry is a closer fit to the test facility geometries against which WCOBRA/TRAC has been validated. The removal of bottom-mounted instrumentation from the AP600 and the radius of the lower vessel head produce a geometry which is similar to that of the LOFT facility. The documented capability of WCOBRA/TRAC to predict the LOFT lower plenum filling behavior (Reference 440.350-2) provides confidence it can also do well predicting AP600 lower plenum refill phenomena.
- d) As noted above, the AP600 downcomer geometry is very similar to existing Westinghouse plants. Furthermore, the LOFT simulations indicate the capability of WCOBRA/TRAC to predict ECC penetration for downcomer metal heat and lower plenum geometry conditions similar to AP600. The CCTF and UPTF simulations of downcomer injection illustrate that the code capably models the AP600 direct vessel injection geometry. Collectively, these simulations show that WCOBRA/TRAC can predict AP600 large break LOCA analysis vessel downcomer behaviors adequately.

#### References:

- 440.350-1 Letter NTD-NRC-95-4503, "Preliminary Marked Up Sections of SSAR Chapter 15, Revision 5", July 10, 1995
- 440.350-2 Bajorek, S. M., et. al., "Code Qualification Document for Best Estimate Analysis," WCAP-12945-P, Revision 1 (Proprietary), Volume 3, Chapter 14

SSAR Revision: NONE



# NRC REQUEST FOR ADDITIONAL INFORMATION



Question 440.351

Re: WCAP-14171 (WCOBRA/TRAC CAD)

For CCTF Test 75, Westinghouse stated the poor core heat transfer was the result of underpredicting the system pressure (see CQD Section 14-2-6-5).

- a) Provide additional information to support this conclusion.
- b) Provide additional explanation to clarify the reasons for underpredicting the vessel-to-broken cold pressure drop.

Response:

a) Reference 440.351-1 provides a system pressure sensitivity comparison. Three tests were examined: C2 - 8 (Run 67), C2 - 4 (Run 62) and C2 - 1 (Run 55). These tests modeled the following pressures: 0.15 MPa (Run 67, 21.8 psia), 0.2MPa (Run 62, 29 psia) and 0.4 MPa (Run 55, 58 psia). It was concluded that lower system pressure results in a higher temperature rise, longer turnaround time and longer quench time. The poorer rod to fluid heat transfer at lower pressure was attributed to the lower density of the steam during the early part of the transient (0 → 60 sec), and then to local void fraction and distance from the quench front in addition to the lower steam density for the later part of the transient. The experimentalists' assessment of the test data coincides with WCOBRA/TRAC as regards the impact of system pressure on core cooling.

b) The pressure loss coefficient assigned to the VESSEL/broken cold leg junction in the CCTF analysis was the same as that used in the full plant calculations and is based on the UPTF test data. [ ] a, c

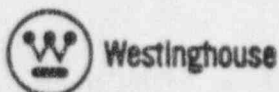
[ ] These calculations, which are discussed in the response to RAI 440.348, showed better agreement with the CCTF data in terms of the system pressure history and the flows in the intact and broken loops. ] a, c

[ ] The sensitivity calculations also showed that the core thermal hydraulics are influenced by the [ ] a, c  
] If the pressure losses in the broken loops are not correctly calculated then the flow through the core will be different from that observed in the experiment, which may have a significant impact on the predicted clad temperatures. Application of the more appropriate hydraulic loss coefficients in the CCTF Test 58 calculation reported in the response to RAI 440.348 part (c) produced better agreement between measured and predicted peak clad temperatures above the core midplane.

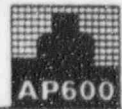
### Reference

440.351-1 Quick Look Report on CCTF Core II Reflood Test C2 - 8 (Run 67)

SSAR Revision: NONE



440.351-1



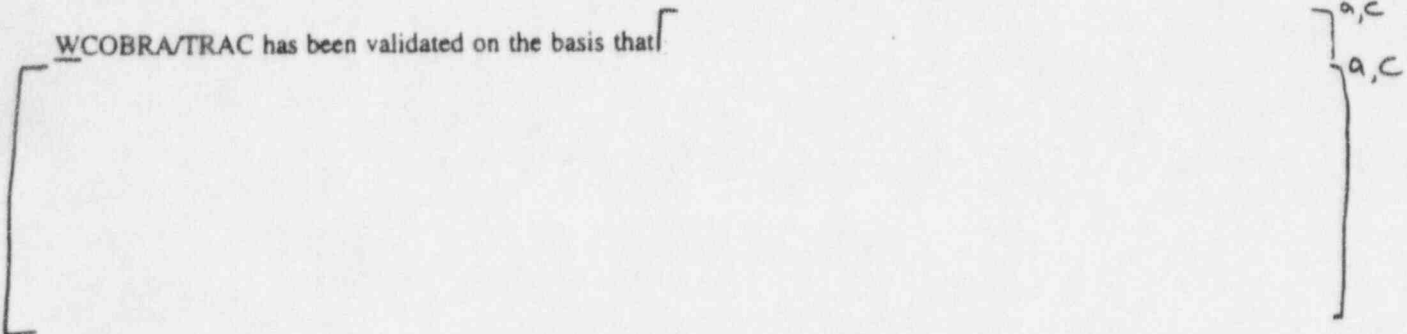
Question 440.352

Re: WCAP-14171 (WCOBRA/TRAC CAD)

In the WCOBRA/TRAC analyses of CCTF (see discussion for Run 63, page 14-2-19) in the CQD, WCOBRA/TRAC was not able to calculate the correct mass in the upper core region. This was attributed to a flow regime transition, possibly from rewetting of structural members that Westinghouse did not simulate. This rewetting in the experiment resulted in the upper core mass retention. Does the structural rewetting need to be accounted for in the WCOBRA/TRAC flow regime transition model? Clarify whether and why the WCOBRA/TRAC models in this area produce an adequate representation of core reflood phenomena.

Response:

WCOBRA/TRAC has been validated on the basis that



Another contributing factor to the core thermal hydraulics is the accuracy with which the pressure losses in the broken and intact loops are calculated. These will be a function of the two-phase flows that are predicted in the loops. Sensitivity calculations have shown that the reflood flow through the core and subsequent steam production and entrainment rates are influenced by the relative values of the loss coefficients. Therefore, the upper core pressure loss will also be affected.

Structural rewetting need not be accounted for in WCOBRA/TRAC flow regime transitions. It is already taken into account via the code/data comparisons. WCOBRA/TRAC flow regimes are defined such that one is either in a hot wall or cold wall condition. It is conservative to ignore the effect of structural rewetting on flow regimes such that the hot rod remains in a hot wall flow regime.

SSAR Revision: NONE

## NRC REQUEST FOR ADDITIONAL INFORMATION



Question 440.436

Re: NOTRUMP ADS PVR (RCS-GSR-003)

Please explain how the NOTRUMP code uses Equation 4-1 in computations of the fluid quality.

Response:

The NOTRUMP code does not use Equation 4-1 of RCS-GSR-003 in computations of the fluid quality. Equation 4-1 was used to calculate the fluid quality from test data. NOTRUMP calculates fluid qualities in fluid nodes as described in Section 3 and Appendix L of Reference 440.436-1. In particular, the fluid quality for a pressure  $P$  and a specific enthalpy  $h$  is calculated from equation (L-33) of Reference 440.436-1, i.e.,

$$X(P, h) = \frac{h - h_l(P)}{h_g(P) - h_l(P)} \quad (440.436-1)$$

if

$$h_l(P) < h < h_g(P). \quad (440.436-2)$$

As discussed in Section 3 and Appendix L of Reference 440.436-1, the state variables for an interior fluid node are the mixture region internal energy  $U_M$ , the mixture region mass  $M_M$ , the vapor region internal energy  $U_V$ , and the vapor region mass  $M_V$ . (An homogeneous node has positive values of  $U_M$  and  $M_M$  and  $U_V = M_V = 0$ .) Appendix L also describes the "pressure search," in which all thermodynamic properties for each region of an interior fluid node, including a pressure common to both regions, are calculated given the internal energies and masses in each region ( $U_M$ ,  $M_M$ ,  $U_V$ , and  $M_V$ ) and the volume  $V$  of the node. Quantities calculated include  $P$ ,  $h_M$ ,  $h_V$ ,  $h_l(P)$ , and  $h_g(P)$ . Once these are calculated, then the region fluid qualities  $X_M$  and  $X_V$  are calculated using equation (440.436-1).

Flow qualities are calculated for NOTRUMP flow links as described in Section 5 of Reference 440.436-1. In particular, equation (5-19) is used for cocurrent flow and equation (5-18) for countercurrent flow.

### Reference

440.436-1 P. E. Meyer, et al., "NOTRUMP - A Nodal Transient Small Break and General Network Code." WCAP-10079-P-A (Proprietary), WCAP-10080-A (Non-proprietary), August 1985.

SSAR Revision: NONE



Question 440.471

Re: NOTRUMP PVR FOR OSU TESTS, LTCT-GSR-001, JULY 1995

In Section 4.6, the contact coefficient changes state that the partitioning model places all of the vapor flowing into a node into the region in physical contact with the recipient end of the flow link. In the event the two-phase level is above a flow link end and the upstream volume contains steam, then the steam would enter the downstream two-phase region. Moreover, if the downstream node is large, artificially mixing the steam throughout the two-phase region could result in the placement of large amounts of steam at elevations well below the elevation of the piping inlet connection. This would result in over-swelling the level and produce errors in the two-phase level predictions. Discuss this result in light of the AP600 NOTRUMP modeling and show that this behavior would not adversely affect the AP600 level swell results.

Response:

Section 4.6 of LTCT-GSR-001 and PXS-GSR-002 discusses several options which override the code's default partitioning of vapor and liquid flows. NOTRUMP's default flow partitioning is described in Section F-5 of Reference 440.471-1. It places the vapor flowing into a node into the (potentially) two regions of the node in proportion to the area of each region subtending the recipient end of the flow link. This is represented by equations (F-41) and (F-43). Vapor leaving a node is removed from the (potentially) two regions of the node in proportion to the area of the vapor phase of each region subtending the donor end of the flow link. This is represented by equations (F-42) and (F-44). The changes described in Section 4.6 relate to the KGFL and KFFL options which allow one to override the code's default flow partitioning when it may not accurately represent the physical problem under consideration.

This RAI is asking about the default flow partitioning model, not the KGFL and KFFL options which override the default model and are described in Section 4.6. The default model is also overridden where NOTRUMP's horizontally stratified flow model is used. This is described in Section 4.5 of LTCT-GSR-001 and PXS-GSR-002. The NOTRUMP Node Stacking and Mixture Level Tracking Model also overrides the default flow partitioning model under certain conditions. It is described in Appendix N of Reference 440.471-1 and in Section 4.18 of LTCT-GSR-001 and PXS-GSR-002. The default flow partitioning is appropriate for flow into or out of homogeneous nodes, i.e., nodes where only a mixture region ever exists.

The scenario hypothesized in the RAI does not occur anywhere that level swell is calculated. The reason for this is the AP600 NOTRUMP modeling with its appropriate use of both the default flow partitioning model and the other models described above which override it.

Consider the AP600 NOTRUMP modeling used for the OSU test facility and depicted by the noding scheme shown in Figure 2-1 of LTCT-GSR-001. In the inner vessel, represented by nodes 2 - 8, two levels are calculated. Nodes 2 - 7 are in a stack (i.e., they use the NOTRUMP Node Stacking and Mixture Level Tracking Model) and therefore calculate a single mixture level for the stack. Links 2-6 are point contact flow links connecting the very top of one node to the very bottom of the node above it. As such, each link is flowing between two mixture regions (if the link is below the stack mixture elevation) or between two vapor regions (if the link is above the stack mixture elevation) unless the stack mixture elevation is at the boundary between two stacked nodes, in which case some



special overrides are calculated as described in Section 4.18. Thus, if steam is flowing in these links, it is appropriately convected between mixture regions if the link is covered and between vapor regions if the link is uncovered. Therefore the scenario described in the RAI does not occur and level swell results are not adversely impacted.

Node 8 is a stratified node with its own calculated mixture level. It represents the upper head. Links 7 and 8, connecting it with the upper plenum and downcomer, respectively, are point contact flow links. Flow link 8 uses  $KGFL = 3$ . Thus mixture level results are not adversely impacted.

Other places where stacked nodes are used are the two steam generators (nodes 11-16 and nodes 21 - 26), the two CMT's (nodes 50, 52, and 54 - 56 and nodes 60, 62, and 64 - 66), the two balance lines (nodes 53 and 153 and nodes 63 and 163), and the IRWST (nodes 67 and 77). Thus mixture level results are not adversely impacted for these components.

Node 74 is a stratified node with its own calculated mixture level. It represents the PRHR inlet line. Links 74 and 57 connecting it with the hot leg and PRHR, respectively, have non-zero values for  $KGFL$  and  $KFFL$ . Thus its mixture level is not adversely impacted.

The hot and cold legs (nodes 10 and 20 and nodes 18, 19, 28, 29, 38, 39, 48, and 49 are stratified nodes. The links connecting them are either horizontally stratified flow links or have  $KGFL=1$ . Thus the hypothesized scenario does not occur and mixture level results are not adversely impacted.

Finally the PRHR (nodes 59, 111-117, 75, and 76) is modeled with homogeneous nodes. Here the default flow partitioning is appropriate as discussed above.

#### Reference:

440.471-1 P.E. Meyer, et. al., "NOTRUMP - A Nodal Transient Small Break and General Network Code", WCAP-10079-P-A (Proprietary), WCAP-10080-A (Non-proprietary), August 1985

SSAR Revision: NONE





Question 440.474

Re: NOTRUMP PVR FOR OSU TESTS, LTCT-GSR-001, JULY 1995

Provide the derivations and the expressions for the partial derivatives comprising the implicit bubble rise model formulation of Eq. 4.9-1. Also, show the finite difference form of Eq. 4.9-1 and the terms accompanying the independent variables that would appear on the left hand side of the solution matrix. Please provide a stability and consistency analysis that show both time step size restrictions and that the original set of partial differential equations are recovered in the limit as  $\Delta t$  and  $\Delta x$  approach zero. What level swell calculations were performed to verify this major change to the code? Please provide results of the model calculations verifying the new model (Please see RAI 440.515 below for candidate level swell tests).

Response:

Following is the requested description. This description is in the form of a revision to Section 4.9 of LTCT-GSR-001 and PXS-GSR-002 which will be included in the NOTRUMP Final V&V Report. The NOTRUMP implicit method is discussed in Section 2-2 of Reference 440.474-1. The method is a direct generalization to more state variables of the implicit method used in the FLASH series of codes (FLASH-4, WFLASH, etc.) and described in Reference 440.474-2. Convergence and stability properties possessed by this implicit method are discussed in this reference. Work is currently underway to respond to the request for verification calculations. The schedule and scope of this work will be provided on or before December 31, 1995.

#### 4.9 Bubble Rise

The NOTRUMP code uses its bubble rise model to calculate the flow of vapor from a stratified fluid node's mixture region to its vapor region. Appendix H of Reference 1 describes the existing model. The model was modified in five ways for application to the AP600. First, the bubble rise mass flow rate was incorporated into the code's numerical scheme implicitly rather than explicitly. Second, the model was modified [ ]<sup>a, c</sup> Third, the model was modified to prevent the bubble rise mass flow rate from going negative. Fourth, an optional, user-specified override of the internally-calculated interfacial area was implemented. Fifth, an option was implemented allowing the bubble rise to be based on the volume flow into a node rather than the mass flow into a node.

NOTRUMP's existing bubble rise model was implemented into the code's numerics explicitly. At the beginning of each time step, the code calculated each node's bubble rise mass flow rate from the known properties of the node, and then the code held this mass flow rate constant throughout the time step. This implementation of the bubble rise model made it unstable if the model convected more liquid out of a region during a time step than existed in that region at the beginning of the time step, i.e., when it violated the material Courant limit.

The material Courant limit on bubble rise becomes prohibitively restrictive as mixture levels approach and cross node boundaries. For example, as a mixture level drops out of one node into the node below it, the mixture region in the upper node becomes infinitesimally small just before the mixture level leaves the node. If this infinitesimally small mixture region is voided, the material Courant limit on the region's bubble rise restricts the time-step size to similarly





infinitesimal values. As a result, the code would have to expend an enormous number of time steps to simulate each level crossing.

To circumvent this problem, the bubble rise model was implicitly implemented into the code's numerics. This implicit treatment does not affect the computation of the bubble rise mass flow rate from the properties of the fluid node. The implicit treatment simply estimates the change in the bubble rise mass flow rate corresponding to the change in the fluid node's state variables during each time step.

In the implicit treatment of bubble rise, the bubble-rise mass-flow rate in a node is given by:

$$W_{BR}(t + \Delta t) = W_{BR}(t) + \frac{\partial W_{BR}}{\partial U_M} \cdot \Delta U_M + \frac{\partial W_{BR}}{\partial M_M} \cdot \Delta M_M + \frac{\partial W_{BR}}{\partial U_V} \cdot \Delta U_V + \frac{\partial W_{BR}}{\partial M_V} \cdot \Delta M_V \tag{4.9-1}$$

A new input variable activates the implicit treatment of bubble rise. This input variable is fluid node specific, and it is IMPBRFN(n) (IMPLICIT Bubble Rise for Fluid Node n). If IMPBRFN(n) equals zero, the bubble rise in fluid node n is handled explicitly. If IMPBRFN(n) does not equal zero, the bubble rise in fluid node n is handled implicitly. The default value of IMPBRFN(n) is zero for all fluid nodes.

Although the implicit treatment of bubble rise allows NOTRUMP to violate the material Courant limit on bubble rise, the bubble rise mass flow rate still approaches zero as the void fraction in a mixture region approaches unity. Equation H-8 of Reference 1 gives the functional dependence of the bubble rise mass flow rate on the mixture region's properties. In this equation,  $\langle\langle V_d \rangle\rangle$  is the drift velocity in the mixture region as determined by the user-selected drift flux correlation. [

[

[

] a, c

] a, c

] a, c

] s

void fraction limit was introduced as a single input variable, VFBRLIM, which affects all nodes.

Although the above two modifications enhanced the robustness of the bubble rise model considerably, the bubble rise mass flow rate still became negative under some circumstances. To prevent this, the bubble rise mass flow rate is simply reset to zero whenever it is negative.

In concert with the enhancements described above for the bubble rise model, two improvements to the drop fall model were also made. First, the drop fall mass flow rate was modified to allow the use of the full range of drift flux correlations used by the bubble rise model. Previously, a very simple mist fall calculation was used in all



instances of drop fall. The drop fall calculation was also made implicit to the numerics as was the bubble rise model.

The derivations and the expressions for the partial derivatives comprising the implicit bubble rise model formulation of equation (4.9-1) are now described. The current equation for the bubble rise mass flow rate with the modifications described above is

$$\left[ \text{Equation (4.9-2)} \right]^{a,c} \tag{4.9-2}$$

When bubble rise is treated explicitly, the derivatives  $\partial W_{BR}/\partial U_M$ ,  $\partial W_{BR}/\partial M_M$ ,  $\partial W_{BR}/\partial U_V$ , and  $\partial W_{BR}/\partial M_V$  in equation (4.9-1) are assumed to be zero.

When bubble rise is treated implicitly, the derivatives  $\partial W_{BR}/\partial U_M$ ,  $\partial W_{BR}/\partial M_M$ ,  $\partial W_{BR}/\partial U_V$ , and  $\partial W_{BR}/\partial M_V$  are needed. There are special cases that must be treated when calculating derivatives. They are now presented as they are coded in subroutine BEFORE. Equation (4.9-2) can be expressed as

$$W_{BR} = \max \left[ \frac{\text{TOP}}{\text{BOT}}, 0 \right] \tag{4.9-3}$$

where

$$\left[ \text{Equation (4.9-4)} \right]^{a,c} \tag{4.9-4}$$

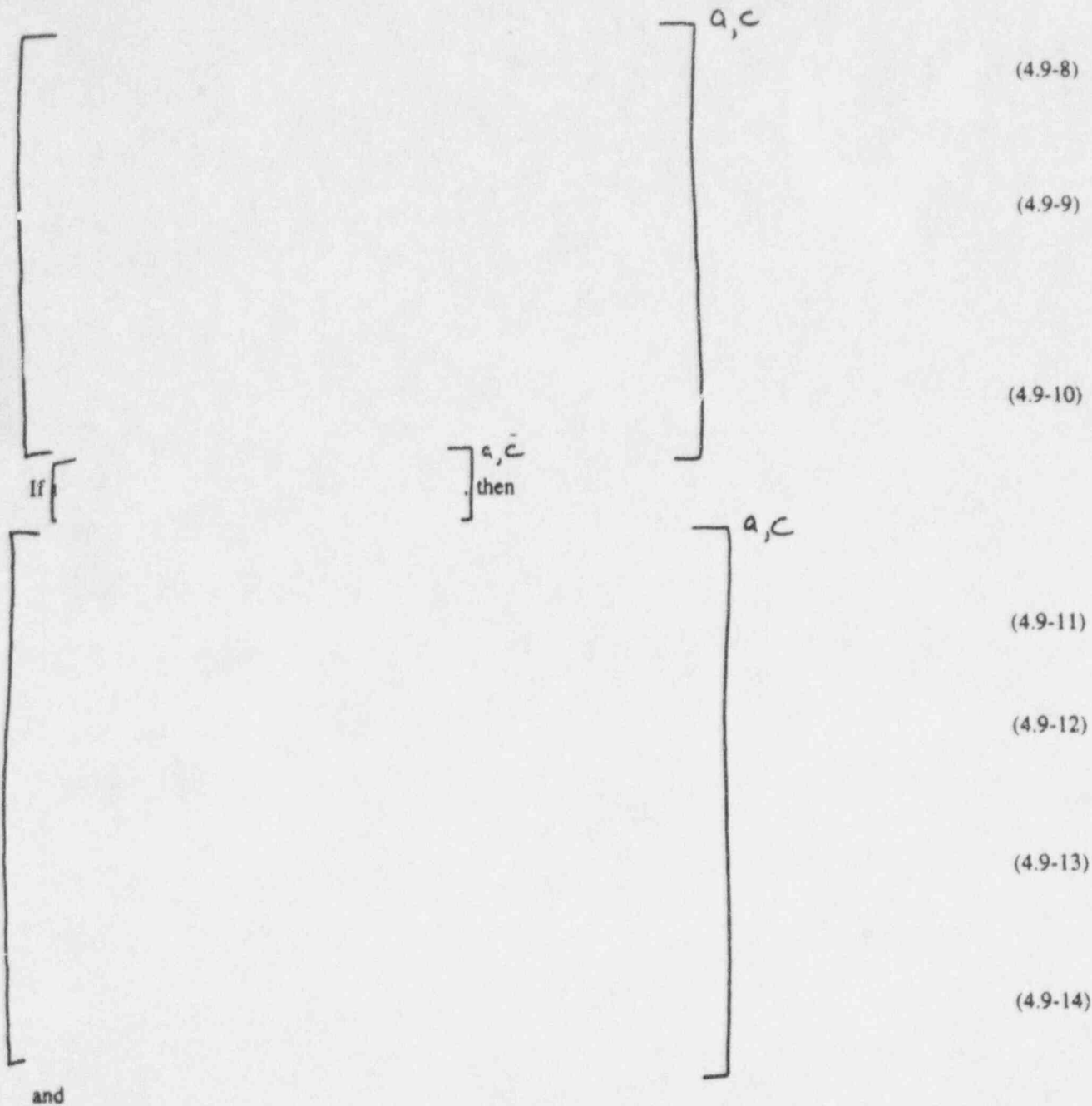
and

$$\left[ \text{Equation (4.9-5)} \right]^{a,c} \tag{4.9-5}$$

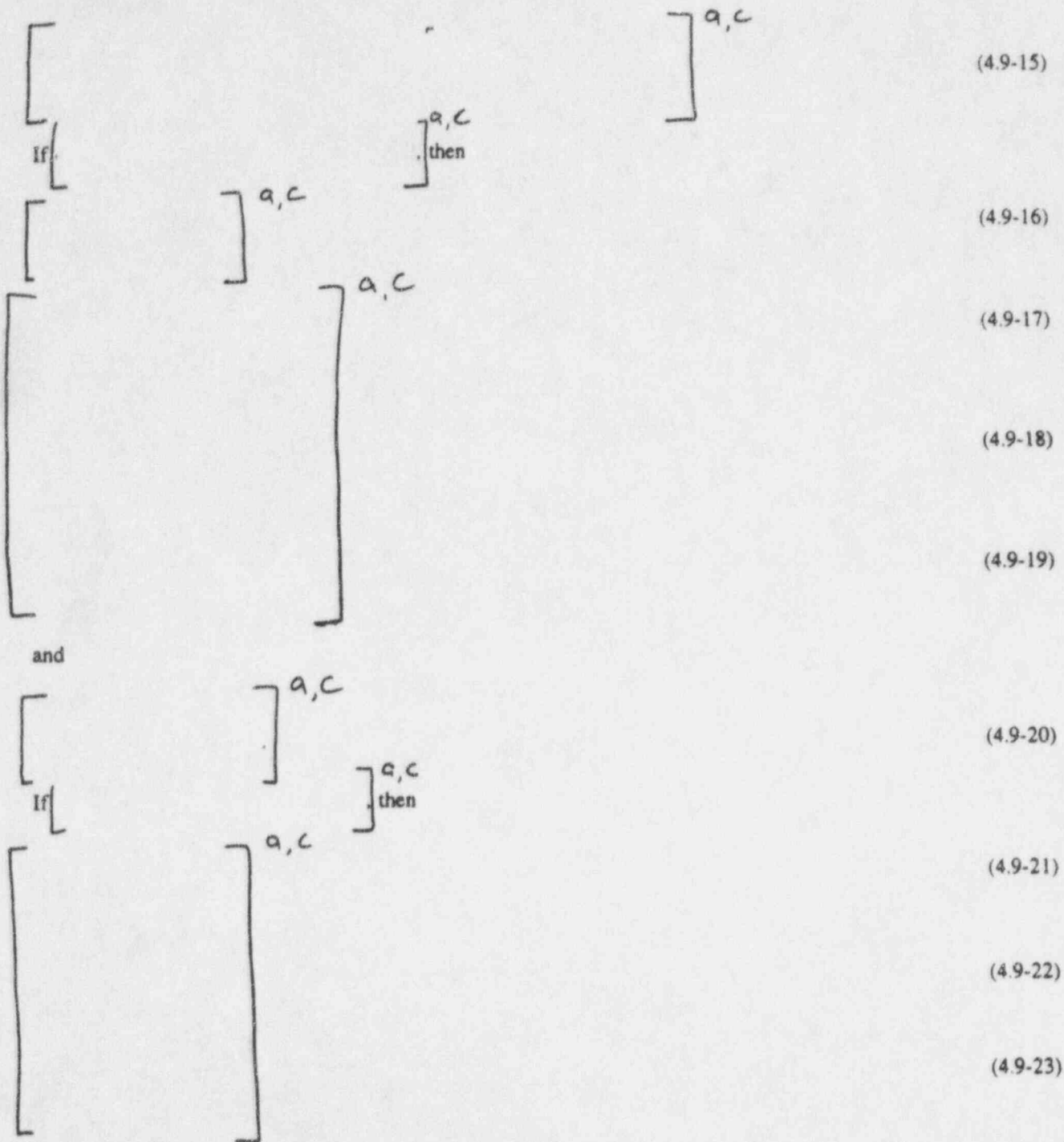
If  $\left[ \text{Equation (4.9-6)} \right]^{a,c}$  then

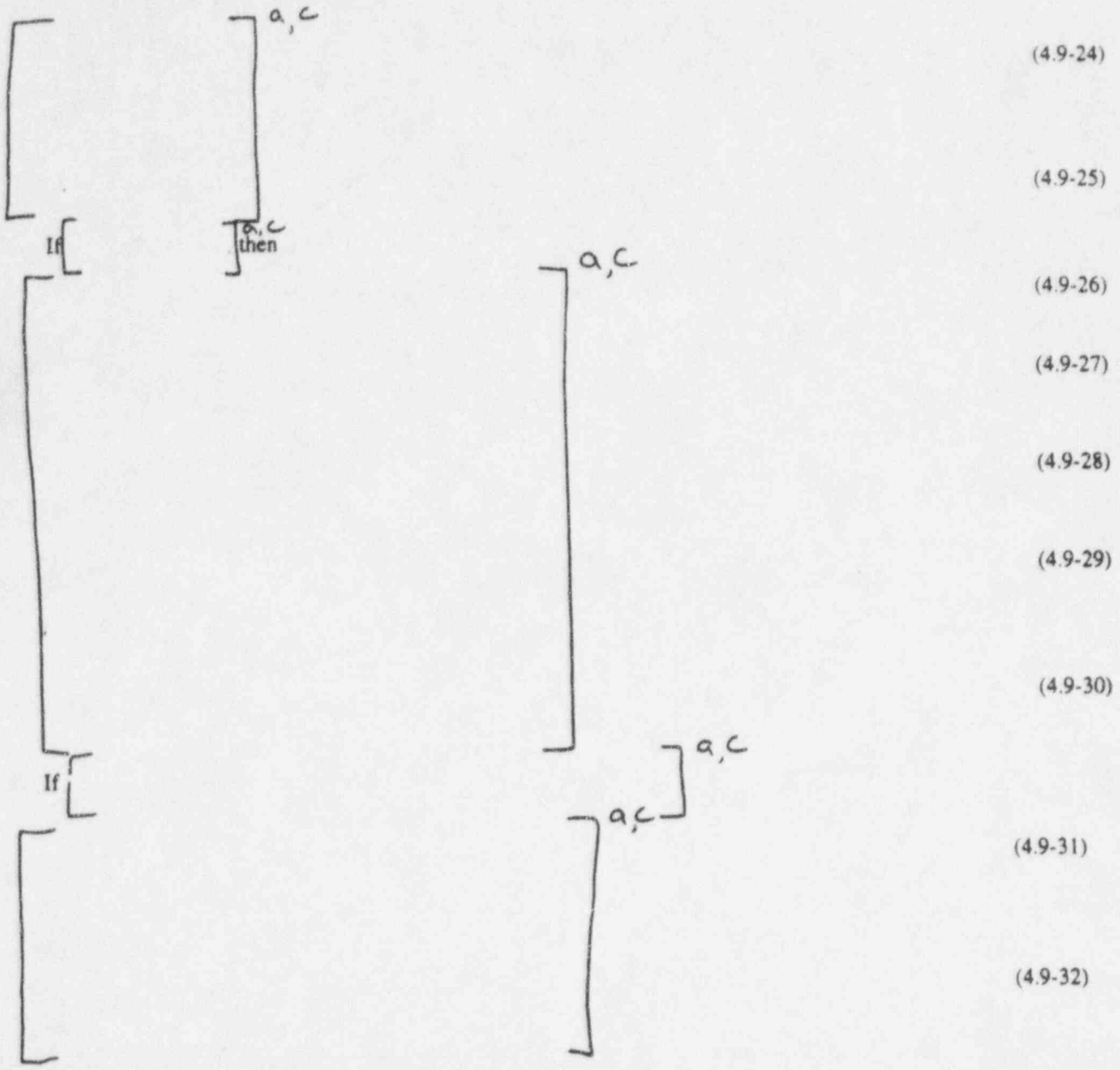
$$\left[ \text{Equation (4.9-7)} \right]^{a,c} \tag{4.9-6}$$

$$\left[ \text{Equation (4.9-7)} \right]^{a,c} \tag{4.9-7}$$

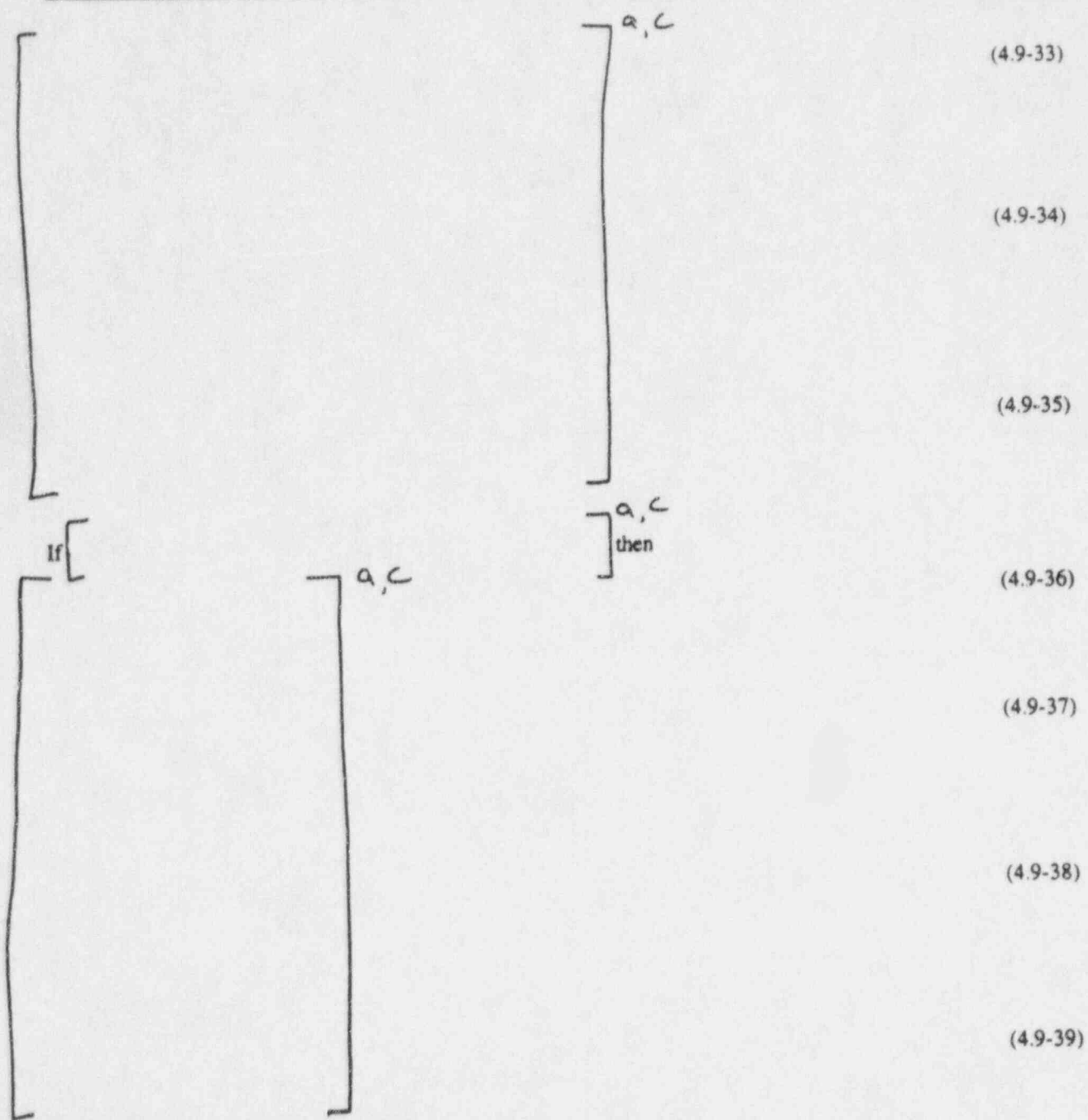


NRC REQUEST FOR ADDITIONAL INFORMATION





NRC REQUEST FOR ADDITIONAL INFORMATION



and



[ ]<sup>a,c</sup> (4.9-40)

If [ ]<sup>a,c</sup> then [ ]<sup>a,c</sup> (4.9-41)

[ ] (4.9-42)

[ ] (4.9-43)

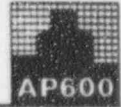
[ ] (4.9-44)

[ ] (4.9-45)

Finally, if  $W_{BR} > 0$ , the quotient rule for differentiation

$$d\left(\frac{TOP}{BOT}\right) = \frac{1}{BOT^2} \cdot [BOT \cdot dTOP - TOP \cdot dBOT] \quad (4.9-46)$$

or



$$d\left(\frac{\text{TOP}}{\text{BOT}}\right) = \frac{1}{\text{BOT}} \cdot [d\text{TOP} - \left(\frac{\text{TOP}}{\text{BOT}}\right) \cdot d\text{BOT}] \quad (4.9-47)$$

gives

[

] a, c

(4.9-48)

(4.9-49)

(4.9-50)

and

[

] a, c

(4.9-51)

and if  $W_{BR} = 0$ , then

$$\frac{\partial W_{BR}}{\partial u_M} = 0.$$

(4.9-52)







$$\frac{\partial W_{BR}}{\partial M_M} = 0 . \quad (4.9-53)$$

$$\frac{\partial W_{BR}}{\partial U_V} = 0 . \quad (4.9-54)$$

and

$$\frac{\partial W_{BR}}{\partial M_V} = 0 . \quad (4.9-55)$$

The mixture region void fraction is calculated in subroutine FLUID as follows:

$$\alpha_M = \min \left[ \max \left[ \frac{X_M \cdot v_g}{X_M \cdot v_g + (1 - X_M) \cdot v_f} , 0 \right] , 1 \right] \quad (4.9-56)$$

The partial derivatives of the mixture region void fraction  $\alpha_M$  with respect to the nodal state variables  $U_M$ ,  $M_M$ ,  $U_V$ , and  $M_V$  are now derived.

For  $0 < \alpha_M < 1$ ,  $\alpha_M$  can be written as

$$\alpha_M = \frac{X_M \cdot v_g}{X_M \cdot v_g + (1 - X_M) \cdot v_f} \quad (4.9-57)$$

where



$$X_M = \frac{v_M - v_f}{v_g - v_f} \tag{4.9-58}$$

Using Equation (4.9-58) in Equation (4.9-57) gives

$$\alpha_M = \frac{v_g \cdot (v_M - v_f)}{v_M \cdot (v_g - v_f)} \tag{4.9-59}$$

Therefore, using the quotient rule for differentiation (See Equation (4.9-47)),

$$\frac{\partial \alpha_M}{\partial U_M} = \frac{v_g \cdot \left( \frac{\partial v_M}{\partial U_M} - \frac{\partial v_f}{\partial U_M} \right) + \frac{\partial v_g}{\partial U_M} \cdot (v_M - v_f) - \alpha_M \cdot \left[ v_M \cdot \left( \frac{\partial v_g}{\partial U_M} - \frac{\partial v_f}{\partial U_M} \right) + \frac{\partial v_M}{\partial U_M} \cdot (v_g - v_f) \right]}{v_M \cdot (v_g - v_f)} \tag{4.9-60}$$

$$\frac{\partial \alpha_M}{\partial M_M} = \frac{v_g \cdot \left( \frac{\partial v_M}{\partial M_M} - \frac{\partial v_f}{\partial M_M} \right) + \frac{\partial v_g}{\partial M_M} \cdot (v_M - v_f) - \alpha_M \cdot \left[ v_M \cdot \left( \frac{\partial v_g}{\partial M_M} - \frac{\partial v_f}{\partial M_M} \right) + \frac{\partial v_M}{\partial M_M} \cdot (v_g - v_f) \right]}{v_M \cdot (v_g - v_f)} \tag{4.9-61}$$

$$\frac{\partial \alpha_M}{\partial U_v} = \frac{v_g \cdot \left( \frac{\partial v_M}{\partial U_v} - \frac{\partial v_f}{\partial U_v} \right) + \frac{\partial v_g}{\partial U_v} \cdot (v_M - v_f) - \alpha_M \cdot \left[ v_M \cdot \left( \frac{\partial v_g}{\partial U_v} - \frac{\partial v_f}{\partial U_v} \right) + \frac{\partial v_M}{\partial U_v} \cdot (v_g - v_f) \right]}{v_M \cdot (v_g - v_f)} \tag{4.9-62}$$

and

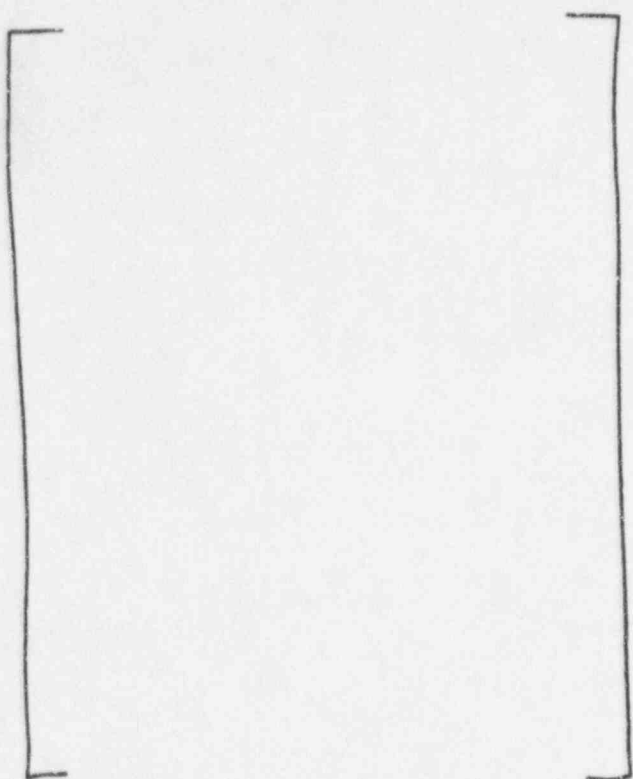


$$\frac{\partial \alpha_M}{\partial M_V} = \frac{v_s \cdot \left( \frac{\partial v_M}{\partial M_V} - \frac{\partial v_f}{\partial M_V} \right) + \frac{\partial v_s}{\partial M_V} \cdot (v_M - v_f) - \alpha_M \cdot \left[ v_M \left( \frac{\partial v_s}{\partial M_V} - \frac{\partial v_f}{\partial M_V} \right) + \frac{\partial v_M}{\partial M_V} \cdot (v_s - v_f) \right]}{v_M \cdot (v_s - v_f)}$$

(4.9-63)

These partial derivatives are calculated in subroutine FLUID.

The partial derivatives of the mixture region specific volume  $v_M$  with respect to the nodal state variables  $U_M$ ,  $M_M$ ,  $U_V$ , and  $M_V$  are calculated in subroutine FLUID using:



a, c

(4.9-64)

(4.9-65)

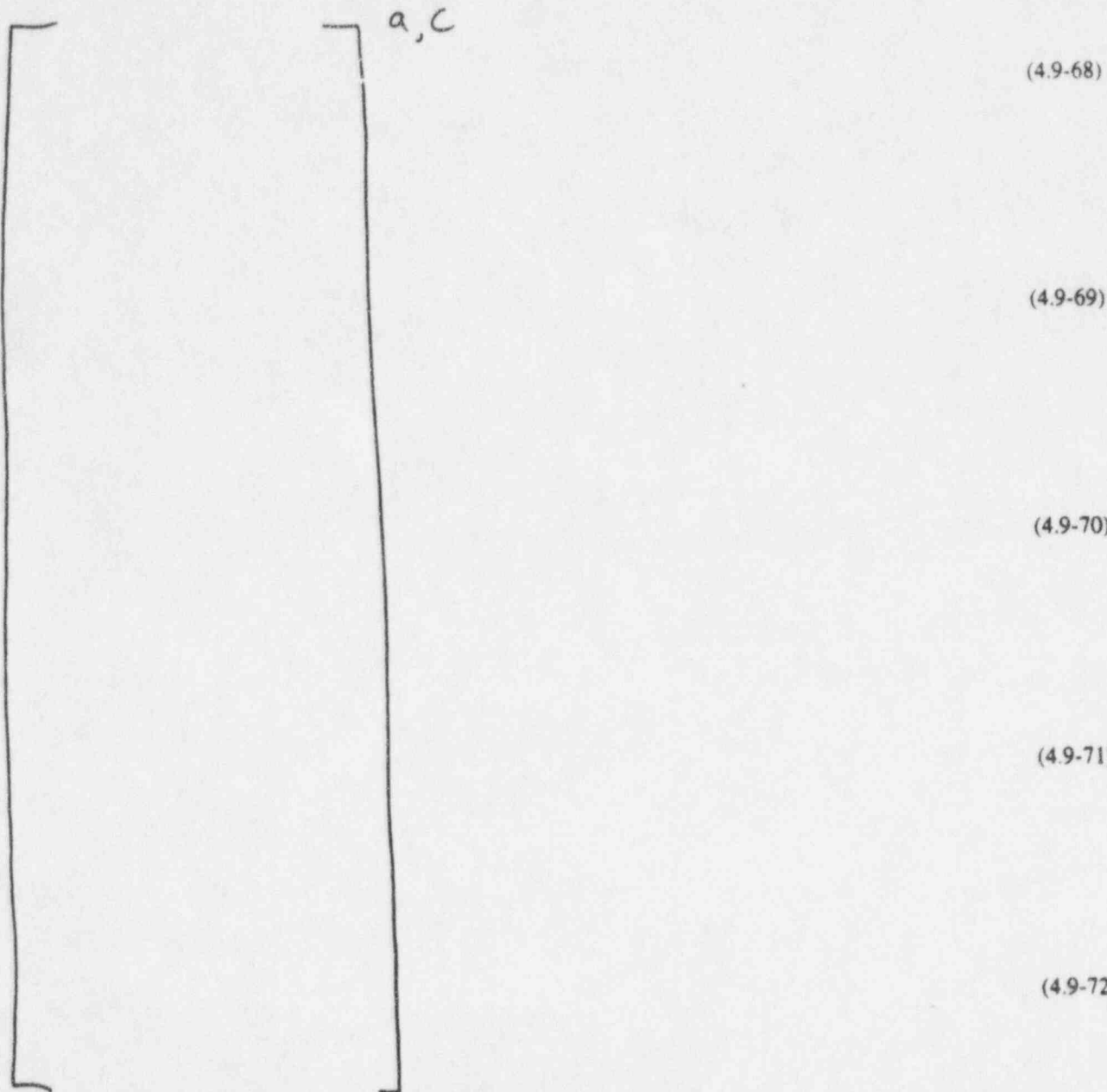
(4.9-66)

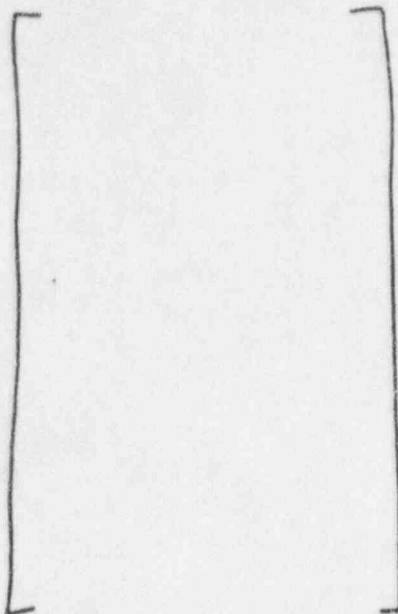
(4.9-67)

# NRC REQUEST FOR ADDITIONAL INFORMATION



The partial derivatives of the saturation specific volumes with respect to nodal state variables  $U_M$ ,  $M_M$ ,  $U_V$ , and  $M_V$  are calculated in subroutine FLUID using:





a, c

(4.9-73)

(4.9-74)

(4.9-75)

The derivatives  $dv/dP$  and  $dv/dP$  are calculated in subroutine SPEEDY using Equations (L-7) and (L-8) of Reference 1, respectively.

The partial derivatives  $(\partial v/\partial P)_{h_m}$  and  $(\partial v/\partial h_m)_p$  are calculated in subroutine SPEEDY using Equations (L-14) and L-15), Equations (L-35) and (L-36), and equations (L-38) and (L-39) for subcooled, saturated, and superheated fluid states, respectively. The partial derivatives  $\partial P/\partial U_m$ ,  $\partial P/\partial M_m$ ,  $\partial P/\partial U_v$ ,  $\partial P/\partial M_v$ , are calculated in subroutine DCALCY using Equations (L-96), (L-98), (L-100), and (L-102), respectively.

For  $\alpha_m = 0$  or  $\alpha_m = 1$ , the partial derivatives of the mixture region void fraction  $\alpha_m$  with respect to the nodal state variables  $U_m$ ,  $M_m$ ,  $U_v$ , and  $M_v$  are set to 0 in subroutine FLUID.

This concludes the description of the derivations and the expressions for the partial derivatives comprising the implicit bubble rise model. The addition of the model into the central numerics is now described.

The NOTRUMP energy and mass conservation equations are given by Equations (2-1) -(2-4) of Reference 1.  $W_i^{MV}$  and  $(Wh)_i^{MV}$  in these equations are the net mass and energy exchange rates between the mixture and vapor regions. The sign convention for these two quantities is that positive means exchange from the mixture region to the vapor region. Currently, these exchange rates are comprised of three parts, interfacial mass and energy transfer, bubble rise, and droplet fall, i.e.,

NRC REQUEST FOR ADDITIONAL INFORMATION



$$W^{MV} = W^{MIV} + W_{BR} - W_{DF} \quad (4.9-76)$$

$$(Wh)^{MV} = (Wh)^{MIV} + W_{br} \cdot h_g - W_{DF} \cdot h_f \quad (4.9-77)$$

The exchange rates and their partial derivatives with respect to the nodal state variables are calculated in subroutine BEFORE using Equations (4.9-76) and (4.9-77) and

$$\frac{\partial W^{MV}}{\partial U_M} = \frac{\partial W^{MIV}}{\partial U_M} + \frac{\partial W_{BR}}{\partial U_M} - \frac{\partial W_{DF}}{\partial U_M} \quad (4.9-78)$$

$$\frac{\partial W^{MV}}{\partial M_M} = \frac{\partial W^{MIV}}{\partial M_M} + \frac{\partial W_{BR}}{\partial M_M} - \frac{\partial W_{DF}}{\partial M_M} \quad (4.9-79)$$

$$\frac{\partial W^{MV}}{\partial U_V} = \frac{\partial W^{MIV}}{\partial U_V} + \frac{\partial W_{BR}}{\partial U_V} - \frac{\partial W_{DF}}{\partial U_V} \quad (4.9-80)$$

$$\frac{\partial W^{MV}}{\partial M_V} = \frac{\partial W^{MIV}}{\partial M_V} + \frac{\partial W_{BR}}{\partial M_V} - \frac{\partial W_{DF}}{\partial M_V} \quad (4.9-81)$$

$$\frac{\partial (Wh)^{MV}}{\partial U_M} = \frac{\partial (Wh)^{MIV}}{\partial U_M} + W_{BR} \cdot \frac{\partial h_g}{\partial U_M} + \frac{\partial (Wh)_{BR}}{\partial U_M} \cdot h_g - W_{DF} \cdot \frac{\partial h_f}{\partial U_M} - \frac{\partial (Wh)_{DF}}{\partial U_M} \cdot h_f \quad (4.9-82)$$



$$\frac{\partial(\text{Wh})^{\text{MV}}}{\partial M_M} = \frac{\partial(\text{Wh})^{\text{MIV}}}{\partial M_M} + W_{\text{BR}} \cdot \frac{\partial h_g}{\partial M_M} + \frac{\partial(\text{Wh})_{\text{BR}}}{\partial M_M} \cdot h_g - W_{\text{DF}} \cdot \frac{\partial h_f}{\partial M_M} - \frac{\partial(W)_{\text{DF}}}{\partial M_M} \cdot h_f, \quad (4.9-83)$$

$$\frac{\partial(\text{Wh})^{\text{MV}}}{\partial U_V} = \frac{\partial(\text{Wh})^{\text{MIV}}}{\partial U_V} + W_{\text{BR}} \cdot \frac{\partial h_g}{\partial U_V} + \frac{\partial(\text{Wh})_{\text{BR}}}{\partial U_V} \cdot h_g - W_{\text{DF}} \cdot \frac{\partial h_f}{\partial U_V} - \frac{\partial(W)_{\text{DF}}}{\partial U_V} \cdot h_f, \quad (4.9-84)$$

and

$$\frac{\partial(\text{Wh})^{\text{MV}}}{\partial M_V} = \frac{\partial(\text{Wh})^{\text{MIV}}}{\partial M_V} + W_{\text{BR}} \cdot \frac{\partial h_g}{\partial M_V} + \frac{\partial(\text{Wh})_{\text{BR}}}{\partial M_V} \cdot h_g - W_{\text{DF}} \cdot \frac{\partial h_f}{\partial M_V} - \frac{\partial(W)_{\text{DF}}}{\partial M_V} \cdot h_f, \quad (4.9-85)$$

$W^{\text{MIV}}$  and  $(\text{Wh})^{\text{MIV}}$  and their partial derivatives with respect to the nodal state variables  $U_M$ ,  $M_M$ ,  $U_V$ , and  $M_V$  are discussed in Appendix V (Interfacial Mass and Energy Transfer Model) of Reference 1.  $W_{\text{BR}}$  and its partial derivatives with respect to  $U_M$ ,  $M_M$ ,  $U_V$ , and  $M_V$  have been described above.  $W_{\text{DF}}$  and its partial derivatives are done analogously to  $W_{\text{BR}}$ .

The partial derivatives of  $h_f$  and  $h_g$  with respect to  $U_M$ ,  $M_M$ ,  $U_V$ , and  $M_V$  are given by Equations (L-110) - (L-117) of Reference 1.

The eight partial derivatives calculated according to Equations (4.9-78) - (4.9-85) are finally used in the central numerics in Equations (E-92), (E-94), (E-96), (E-98), (E-100)-(E-104), (E-106), (E-108), (E-110) and (E-112)-(E-115) of Reference 1. This concludes the description of the addition of the implicit bubble rise (and droplet fall) model into the central numerics.

## NRC REQUEST FOR ADDITIONAL INFORMATION



The final NOTRUMP V&V report will contain a list of variable nomenclature. The following nomenclature will be included in the list.

$W_{BR}$	=	Bubble rise mass flow rate [lbm/sec]
$t$	=	Time at beginning of time step [sec]
$\Delta t$	=	Time step size [sec]
$U_M$	=	Mixture region total internal energy [Btu]
$\Delta U_M$	=	Change in mixture region total internal energy during time step [Btu]
$M_M$	=	Mixture region mass [lbm]
$\Delta M_M$	=	Change in mixture region mass during time step [lbm]
$U_V$	=	Vapor region total internal energy [Btu]
$\Delta U_V$	=	Change in vapor region total internal energy during time step [Btu]
$M_V$	=	Vapor region mass [lbm]
$\Delta M_V$	=	Change in vapor region mass during time step [lbm]
$\alpha_M$	=	void fraction in mixture region [-]
$\langle\langle V_d \rangle\rangle$	=	drift velocity [ft/sec]
$C_o$	=	distribution parameter [-]
$v_g$	=	saturated vapor specific volume [ft <sup>3</sup> /lbm]
$v_l$	=	saturated liquid specific volume [ft <sup>3</sup> /lbm]
$v_M$	=	mixture region specific volume [ft <sup>3</sup> /lbm]
$X_M$	=	mixture region quality
$P$	=	pressure [psia]
$h_M$	=	mixture region enthalpy [Btu/lbm]

### Reference

- 440.474-1 P. E. Meyer, et. al., "NOTRUMP - A Nodal Transient Small Break and General Network Code," WCAP-10079-P-A (Proprietary), WCAP-10080-A (Non-proprietary), August 1985
- 440.474-2 Porsching, T. A., et. al., "Stable Numerical Integration of Conservation Equations for Hydraulic Networks," Nuclear Science and Engineering 43 pp 218-225, (1971)

SSAR Revision: NONE





Question 440.476

Re: NOTRUMP PVR FOR OSU TESTS, LTCT-GSR-001, JULY 1995

Please describe mathematically the implicit treatment of the gravitational head term in the momentum formulation described in Section 4.11 and the formulation of the momentum equation including all of the independent variables appearing on the left hand side of the solution matrix. Also, provide the results of a stability and consistency analysis for this change. Please provide the results of the verification analyses for these modeling changes.

Response:

Following is the requested description. This description is in the form of a revision to Section 4.11 of LTCT-GSR-001 and PXS-GSR-002 which will be included in the NOTRUMP Final V&V Report. The NOTRUMP implicit method is discussed in Section 2-2 of Reference 440.476-1. The method is a direct generalization to more state variables of the implicit method used in the FLASH series of codes (FLASH-4, WFLASH, etc.) and described in Reference 440.476-2. Convergence and stability properties possessed by this implicit method are discussed in this reference. Work is currently underway to respond to the request for verification analyses. The schedule and scope of this work will be provided on or before December 31, 1995.

#### 4.11 Implicit Treatment of Gravitational Head

In NOTRUMP, gravitational head is accounted for within both fluid nodes and flow links as described in Reference 1. Within fluid nodes, the pressure calculated from the known state variables is assumed to apply to the very top of the node. Using this convention, the code sets the pressure at the end of any flow link connected to a fluid node equal to the sum of the pressure at the top of the fluid node and the gravitational head from the top of the fluid node to the flow link-fluid node connection. Within flow links, the code calculates a gravitational head term from the elevation difference between the upstream and downstream ends of the flow link, using the density of the fluid within the flow link. However, the flow link gravitational head model can lead to flow instabilities when the density of the fluid within the flow link changes rapidly.

NOTRUMP's existing fluid node gravitational head model is incorporated into the code's numerics explicitly. At the beginning of each time step, the code calculates the gravitational head between the top of a fluid node and the connecting end of adjoining flow links. The code then holds this gravitational head constant throughout the time step. This implementation of the fluid-node gravitational-head model could also lead to flow instabilities when the fluid node density changes rapidly.

The fluid node gravitational head model was incorporated into the code's numerics implicitly to preclude flow instabilities resulting from the rapid density changes experienced by fluid nodes at low pressures. This implicit treatment does not affect the computation of the fluid-node gravitational head from the properties of the fluid node. The implicit treatment simply estimates the change in the gravitational head corresponding to the change in the fluid node's state variables during each time step.



This implicit treatment of gravitational head through fluid nodes is activated by the flow-link-specific input variable IMPGHFL. The gravitational heads through a flow link's upstream and downstream fluid nodes are treated implicitly when IMPGHFL does not equal zero for that flow link. The gravitational heads through a link's upstream and downstream nodes are treated explicitly when IMPGHFL equals zero for that link. The default value of IMPGHFL is zero.

Following is a mathematical description of the implicit treatment of gravitational head and its addition into the central numerics.

The flow link upstream and downstream pressures are calculated in subroutine FLOW. If flow link k has an IMPGHFL value not equal zero, then the upstream and downstream pressures for the link are calculated using equations (5-3) and (5-4) of Reference 1, i.e.,

$$(P_u)_k = [P(R)]_i \tag{4.11-1}$$

and

$$(P_d)_k = [P(R)]_j \tag{4.11-2}$$

$(P_u)_k$  and  $(P_d)_k$  are then used in subroutine BEFORE to calculate the bracketed part of the right hand side of equation (2-33) of Reference 1. Then  $\dot{W}_k$  is calculated using equation (2-33). Finally if ITYPEFL(K) = 11 or ITYPEFL(K) = 21, then  $\dot{W}_k$  is modified according to equation (4.4-3).

The addition of the implicit treatment of gravitational head is implemented in subroutine SETUP. The details are now presented. In appendix E (Detailed Numerical Equations and Solution Technique) of Reference 1, additional terms representing the linearizations of the gravitational head for flow link k with respect to the nodal state variables  $U_M$ ,  $M_M$ ,  $U_V$ , and  $M_V$  for node i are added to equations (E-61)-(E-64) if flow link k has an IMPGHFL value not equal to zero.

If node i is an interior fluid node, is the upstream node of flow link k, and the elevation of the upstream end of flow link k is below the top of node i, then the gravitational head through the node can change with respect to the nodal state variables as follows:

If  $(E_{mix})_i > (E_u)_k + R$  or  $(E_{mix})_i = (E_u)_k + R$  and  $(\dot{V}_M)_i > 0$  where

$$\dot{V}_M = \frac{\partial V_M}{\partial U_M} \cdot \dot{U}_M + \frac{\partial V_M}{\partial M_M} \cdot \dot{M}_M + \frac{\partial V_M}{\partial U_V} \cdot \dot{U}_V + \frac{\partial V_M}{\partial M_V} \cdot \dot{M}_V \tag{4.11-3}$$



where  $\dot{U}_M, \dot{M}_M, \dot{U}_V$  and  $\dot{M}_V$  are the time rates of change of the nodal state variables and the partial derivatives are given by equations (L-97), (L-99), (L-122), and (L-123) of Reference 1. Then the gravitational head through the vapor region and mixture region is given by

$$GHV = \frac{g}{144g_c} \cdot \left[ \frac{(E_{top})_i - (E_{mix})_i}{(v_v)_i} \right] \quad (4.11-4)$$

and

$$GHM = \frac{g}{144g_c} \cdot \left[ \frac{(E_{mix})_i - ((E_w)_i + R)}{(v_M)_i} \right] \quad (4.11-5)$$

The partial derivatives of GHV and GHM with respect to the state variables, obtained using the quotient rule for differentiation (see equation 4.9-47), are then

$$\frac{\partial GHV}{\partial U_M} = \frac{1}{(v_v)_i} \cdot \left[ \frac{-g}{144g_c} \cdot \frac{\partial(E_{mix})_i}{\partial V_M} \cdot \frac{\partial V_M}{\partial U_M} - GHV \cdot \frac{\partial v_v}{\partial U_M} \right] \quad (4.11-6)$$

$$\frac{\partial GHV}{\partial M_M} = \frac{1}{(v_v)_i} \cdot \left[ \frac{-g}{144g_c} \cdot \frac{\partial(E_{mix})_i}{\partial V_M} \cdot \frac{\partial V_M}{\partial M_M} - GHV \cdot \frac{\partial v_v}{\partial M_M} \right] \quad (4.11-7)$$

$$\frac{\partial GHV}{\partial U_V} = \frac{1}{(v_v)_i} \cdot \left[ \frac{-g}{144g_c} \cdot \frac{\partial(E_{mix})_i}{\partial V_M} \cdot \frac{\partial V_M}{\partial U_V} - GHV \cdot \frac{\partial v_v}{\partial U_V} \right] \quad (4.11-8)$$

$$\frac{\partial GHV}{\partial M_V} = \frac{1}{(v_v)_i} \cdot \left[ \frac{-g}{144g_c} \cdot \frac{\partial(E_{mix})_i}{\partial V_M} \cdot \frac{\partial V_M}{\partial M_V} - GHV \cdot \frac{\partial v_v}{\partial M_V} \right] \quad (4.11-9)$$

$$\frac{\partial GHM}{\partial U_M} = \frac{1}{(v_M)_i} \cdot \left[ \frac{g}{144g_c} \cdot \frac{\partial(E_{mix})_i}{\partial V_M} \cdot \frac{\partial V_M}{\partial U_M} - GHM \cdot \frac{\partial v_M}{\partial U_M} \right] \quad (4.11-10)$$

$$\frac{\partial GHM}{\partial M_M} = \frac{1}{(v_M)_i} \cdot \left[ \frac{g}{144g_c} \cdot \frac{\partial(E_{mix})_i}{\partial V_M} \cdot \frac{\partial V_M}{\partial M_M} - GHM \cdot \frac{\partial v_M}{\partial M_M} \right] \quad (4.11-11)$$



$$\frac{\partial \text{GHM}}{\partial U_V} = \frac{1}{(v_M)_i} \cdot \left[ \frac{g}{144g_c} \cdot \frac{\partial (E_{\text{mix}})_i}{\partial V_M} \cdot \frac{\partial V_M}{\partial U_M} - \text{GHM} \cdot \frac{\partial v_M}{\partial U_V} \right] \quad (4.11-12)$$

$$\frac{\partial \text{GHM}}{\partial M_M} = \frac{1}{(v_M)_i} \cdot \left[ \frac{g}{144g_c} \cdot \frac{\partial (E_{\text{mix}})_i}{\partial V_M} \cdot \frac{\partial V_M}{\partial M_V} - \text{GHM} \cdot \frac{\partial v_M}{\partial M_V} \right] \quad (4.11-13)$$

If  $(E_{\text{mix}})_i < (E_v)_k + R$  or  $(E_{\text{mix}})_i = (E_v)_k + R$  and  $\dot{V}_M \leq 0$ , then

$$\text{GHV} = \frac{g}{144g_c} \cdot \left[ \frac{(E_{\text{top}})_i - ((E_v)_k + R)}{(v_v)_i} \right] \quad (4.11-14)$$

and

$$\text{GHM} = 0$$

so that

$$\frac{\partial \text{GHV}}{\partial U_M} = \frac{1}{(v_v)_i} \cdot \left[ -\text{GHV} \cdot \frac{\partial v_v}{\partial U_M} \right] \quad (4.11-15)$$

$$\frac{\partial \text{GHV}}{\partial M_M} = \frac{1}{(v_v)_i} \cdot \left[ -\text{GHV} \cdot \frac{\partial v_v}{\partial M_M} \right] \quad (4.11-16)$$

$$\frac{\partial \text{GHV}}{\partial U_V} = \frac{1}{(v_v)_i} \cdot \left[ -\text{GHV} \cdot \frac{\partial v_v}{\partial U_M} \right] \quad (4.11-17)$$

$$\frac{\partial \text{GHV}}{\partial M_V} = \frac{1}{(v_v)_i} \cdot \left[ -\text{GHV} \cdot \frac{\partial v_v}{\partial M_V} \right] \quad (4.11-18)$$

$$\frac{\partial \text{GHM}}{\partial U_M} = 0 \quad (4.11-19)$$



$$\frac{\partial \text{GHM}}{\partial M_M} = 0 \quad (4.11-20)$$

$$\frac{\partial \text{GHM}}{\partial U_V} = 0 \quad (4.11-21)$$

and

$$\frac{\partial \text{GHM}}{\partial M_V} = 0 \quad (4.11-22)$$

In the above equations (starting with (4.11-3)),  $\dot{U}_M$ ,  $\dot{M}_M$ ,  $\dot{U}_V$ , and  $\dot{M}_V$  are given by equations (2-1) - (2-4) of Reference 1.  $\partial V_M / \partial U_M$ ,  $\partial V_M / \partial M_M$ ,  $\partial V_M / \partial U_V$ , and  $\partial V_M / \partial M_V$  are given by equations (L-97), (L-99), (L-122), and (L-123), respectively.  $\partial v_M / \partial U_M$ ,  $\partial v_M / \partial M_M$ ,  $\partial v_M / \partial U_V$ , and  $\partial v_M / \partial M_V$  are calculated using equations (4.9-64) - (4.9-67), respectively.  $\partial v_V / \partial U_M$ ,  $\partial v_V / \partial M_M$ ,  $\partial v_V / \partial U_V$ , and  $\partial v_V / \partial M_V$  are calculated in an analogous manner.  $\partial_{(mix)} / \partial V_M$  is calculated in subroutine DIST. This concludes the description of the calculation of GHV and GHM and their derivatives for node i where it is an upstream interior node for flow link k. The derivatives are added to equations (E-61) - (E-64) as follows:

$$(A_{WU_M})_{ki} = (A_{WU_M})_{ki} - \frac{\Delta t \cdot 144g}{\Sigma(L/A)_k} \left( \frac{\partial \text{GHV}}{\partial U_M} + \frac{\partial \text{GHM}}{\partial U_M} \right) \quad (4.11-23)$$

$$(A_{WM_M})_{ki} = (A_{WM_M})_{ki} - \frac{\Delta t \cdot 144g}{\Sigma(L/A)_k} \left( \frac{\partial \text{GHV}}{\partial M_M} + \frac{\partial \text{GHM}}{\partial M_M} \right) \quad (4.11-24)$$

$$(A_{WU_V})_{ki} = (A_{WU_V})_{ki} - \frac{\Delta t \cdot 144g}{\Sigma(L/A)_k} \left( \frac{\partial \text{GHV}}{\partial U_V} + \frac{\partial \text{GHM}}{\partial U_V} \right) \quad (4.11-25)$$

and

$$(A_{WM_V})_{ki} = (A_{WM_V})_{ki} - \frac{\Delta t \cdot 144g}{\Sigma(L/A)_k} \left( \frac{\partial \text{GHV}}{\partial M_V} + \frac{\partial \text{GHM}}{\partial M_V} \right) \quad (4.11-26)$$

If node i is an interior node and it is the downstream node for a flow-link k having an IMPGHFL value not equal to zero, then GHV and GHM and their derivatives are calculated in the same way as for an upstream node, i.e., using equations (4.11-3) - (4.11-26). The only difference is that in equations (4.11-23) - (4.11-26), the terms are added



rather than subtracted. This concludes the mathematical description of the implicit treatment of gravitational head and its addition into the central numerics.

Note: The final NOTRUMP V&V report will contain a list of variable nomenclature. The following nomenclature will be included in the list.

A = flow area (ft<sup>2</sup>)  
 E = elevation (ft)  
 g = acceleration of gravity (ft / sec<sup>2</sup>)  
 g<sub>c</sub> = 32.174 lbm ft / lbf / sec<sup>2</sup>  
 L = length (ft)  
 M = mass (lbm)  
 P = pressure (psia)  
 R = radius of continuous flow link  
 U = internal energy (Btu)  
 V = volume (ft<sup>3</sup>)  
 v = specific volume (ft<sup>3</sup> / lbm)  
 W = mass flow rate (lbm / sec)

Subscripts:

d = downstream  
 k = flow link k  
 M = mixture region  
 mix = mixture  
 u = upstream  
 V = vapor region

Reference

- 440.476-1 P. E. Meyer, et. al., "NOTRUMP - A Nodal Transient Small Break and General Network Code," WCAP-10079-P-A (Proprietary), WCAP-10080-A (Non-proprietary), August 1985
- 440.476-2 Porsching, T. A., et. al., "Stable Numerical Integration of Conservation Equations for Hydraulic Networks," Nuclear Science and Engineering 43 pp 218-225, (1971)

SSAR Revision: NONE

## NRC REQUEST FOR ADDITIONAL INFORMATION



Question 440.481

Re: NOTRUMP PVR FOR OSU TESTS, LTCT-GSR-001, JULY 1995

Provide comparisons of the new NOTRUMP two-phase friction multiplier to separate effects and/or integral test data below 250 psia to justify the new models extrapolation formulation.

Response:

The extrapolation formulation described in Section 4.16 of LTCT-GSR and PXS-GSR-002 has been replaced by an actual extension of the two-phase friction multiplier table in subroutine F44. The table was extended from 250 psia to 14.7 psia by using the Martinelli-Nelson two-phase friction multipliers from Reference 440.481-1. (Recall from Section 4.16 that at and above 250 psia NOTRUMP uses the Martinelli-Nelson two-phase friction multipliers as modified by Thom.) The replacement of the extrapolation formulation by an extended table obviates the need to justify this formulation by comparison to test data. The extended table is already based on test data both above and below 250 psia. To complete the response to this RAI, Section 4.16 of LTCT-GSR-001 and PXS-GSR-002 will be replaced in the final NOTRUMP V&V Report with the following Section 4.16.

### 4.16 Two Phase Friction Multiplier

NOTRUMP uses Martinelli-Nelson two-phase friction multipliers as modified by Thom (see Table 2.3 of Reference 440.481-1) to model two-phase friction, as described in Chapter 5 of Reference 440.481-2. NOTRUMP's use of these friction multipliers was modified in three ways. The first modification affects the quality used to evaluate the friction multiplier. The second modification affects the use of these multipliers below a pressure of 250 psia. The third modification affects the transition from two-phase friction to single phase steam friction.

The Martinelli-Nelson methodology requires knowledge of the flow quality, which is defined as vapor mass flow divided by total mass flow. However, the flow quality becomes undefined in counter-current flow, so the NOTRUMP code has always used the flow link thermodynamic quality in the evaluation of two-phase friction multipliers for flow links in counter-current flow. This abrupt transition from the use of flow quality to thermodynamic quality, as a flow link transitions from cocurrent to countercurrent flow, leads to unrealistic flow oscillations in the AP600 plant and test simulations. To allow the user to eliminate this discontinuity from an analysis, an option was introduced to always use the flow link thermodynamic quality for the computation of the two-phase friction multiplier. This option is invoked for a flow link when the values of FLDPFL or FLDAFL are negative.

The second change to the two-phase friction model extends NOTRUMP's existing model to pressures below 250 psia. NOTRUMP's existing two-phase friction model is only applicable to pressures greater than 250 psia. When pressures drop below 250 psia, the existing model uses friction multipliers evaluated at 250 psia. At pressures above 250 psia, NOTRUMP uses the Martinelli-Nelson two-phase friction multipliers as modified by Thom.

The model was extended below 250 psia by using the Martinelli-Nelson two-phase friction multipliers published in Table 2.2 of Reference 440.481-1 to extend the two-phase friction multiplier table below 250 psia. The independent variables in this table are pressure and quality. Before the modifications described here, the lowest pressure in this



table was 250 psia. Two pressures below 250 psia were added to this table, one at 14.7 psia and the other at 100 psia. The two phase friction multipliers for 14.7 psia and 100 psia were then taken directly from Table 2.2 of Reference 440.481-1. The code's extended two-phase friction model applies the Martinelli-Nelson multipliers as modified by Thom to pressures above 250 psia, it applies the straight Martinelli-Nelson multipliers to pressures below 100 psia, and it uses the pressure range from 100 to 250 psia as a transition region, interpolating the friction multiplier from the straight Martinelli-Nelson multiplier at 100 psia and the Martinelli-Nelson multiplier as modified by Thom at 250 psia. Since this modification is not optional, no input is required to invoke it.

The third modification to NOTRUMP's two-phase friction model smooths the transition from two-phase to single phase steam flow. Before this modification, there was a discontinuity in the friction model as high-quality, two-phase flow transitioned into single-phase steam flow. The frictional pressure drop in very high-quality, two-phase flow was based on the properties of liquid water and the Martinelli-Nelson multipliers, but the pressure drop in pure steam flow was based entirely on the properties of steam. Theoretically, the two should agree at the saturation line. But in practice, discontinuities at the saturation line arise from inconsistencies between the properties built into the Martinelli-Nelson multipliers and the properties used for pure steam, and discontinuities can also arise from different dependencies of the friction multiplier on Reynolds number.

In order to smooth the friction model's transition from two-phase flow to pure steam flow, the value of CKFL for qualities between 0.9 and 1.0 is determined through a linear interpolation between the values of CKFL for 90% quality and pure saturated steam flow.

#### Reference

- 440.481-1 Convective Boiling and Condensation, Third Edition, J. G. Collier and J. R. Thome, Oxford University Press Inc., New York, NY, 1994, pp. 54-59.
- 440.481-2 P. E. Meyer, et. al., "NOTRUMP - A Nodal Transient Small Break and General Network Code," WCAP-10079-P-A (Proprietary), WCAP-10080-A (Non-proprietary), August 1985.

SSAR Revision: NONE





## Question 440.486

Re: NOTRUMP PVR FOR OSU TESTS, LTCT-GSR-001, JULY 1995

Fig. 5.1-11 shows that the NOTRUMP calculated upper head fluid drains early in the event when the data show that fluid remains trapped in this region. This suggests that the NOTRUMP code incorrectly drains liquid from this region which results in minimizing the potential for uncovering of the core. Please explain why the NOTRUMP code upper head liquid drains prematurely in this test, and justify that the code will not incorrectly minimize the potential for core uncovering in the AP600 analyses.

## Response:

The RAI notes that the NOTRUMP simulation of SB01 completes the draining of upper head liquid before it occurred in the test. Figures 5.1-11 and the upper head level comparison plots of the other tests are inconsistent in their treatment of initial level. Figures 440.486-1 through 5 provide more accurate upper head mixture level comparisons than are presented in LTCT-GSR-001. They indicate that the NOTRUMP code does well at predicting the initial draining of the upper head in the OSU test simulations. The difference in behavior, which is judged to be insignificant in the prediction of mixture level above the core, between the predictions and test data occurs in the disposition of the final six or so inches of liquid at the bottom of the upper head. Each NOTRUMP test simulation of the upper head mixture level is discussed below in support of this conclusion.

For the smaller size small break LOCA events, the minimum primary system mass inventory occurs late in the transient, approximately at the inception of IRWST injection. In both of the two-inch break NOTRUMP simulations, as shown in Figures 440.486-1 and 440.486-2, and the test data of OSU tests SB01 and SB09 (Reference 440.486-1, Sections 5.1 and 5.4), the upper head drains completely hundreds of seconds before the reactor vessel minimum mass inventory occurs. Therefore, there is no core inventory misprediction resulting from the prediction of upper head drain at the time of importance, the time at which the minimum inventory occurs. The NOTRUMP SB01 simulation predicts a draining of upper head liquid into the upper plenum after the upper head mixture level has fallen below the downcomer bypass hole elevation at 110 seconds (Figure 440.486-1), which apparently does not occur until later in Test SB01 itself. This premature timing for the completion of upper head draining has no effect on the prediction of potential core uncovering for the two-inch break tests.

The largest break size in the OSU matrix is SB10, the double-ended rupture of the CMT balance line. The NOTRUMP prediction of upper head mixture level (Figure 440.486-3) for SB10 is quite good during the entire draining sequence, over the first two hundred seconds. It is during this time interval that the minimum mass inventory in the reactor vessel occurs (Reference 440.486-1, Figure 5.5.2-40). Liquid draining from the upper head in the NOTRUMP SB10 simulation contributes appropriately to the prediction of upper plenum mixture level and any potential core uncovering.

Figure 440.486-4 indicates that draining of the upper head in the SB12 NOTRUMP simulation agrees well with the test through the first ninety seconds of the transient, at which time NOTRUMP predicts draining which did not occur until later in the test. ADS stage 1 actuates at 86 seconds in the NOTRUMP simulation. A review of the NOTRUMP SB12 simulation reveals that during this second period of upper head drain, between 90 and 150 seconds, ADS operation causes flow to be directed from the upper plenum out the hot leg and into the pressurizer.



The liquid delivered from the upper head into the upper plenum at this time becomes a part of the flow entering the pressurizer, so it does not produce any overprediction of the core mixture level. The predicted core cooling in the SB12 simulation is not affected by the early completion of the upper head draining because the liquid involved does not contribute to the upper plenum mass inventory at the time of minimum reactor vessel mass inventory 150 - 200 seconds into the transient (Reference 440.486-1, Figure 5.6.2-40).

The results of the NOTRUMP simulation of SB14 are similar. After initially predicting upper head draining well, NOTRUMP prematurely completes the draining process (Figure 440.486-5). However, mass draining prematurely from the upper head in the NOTRUMP simulation of SB14 does not contribute to any overprediction of upper plenum mixture level because the mass involved is drawn out the hot leg to the pressurizer as a consequence of ADS operation. Therefore, at the time the minimum reactor vessel mass inventory occurs in SB14 at about 150 seconds (Reference 440.486-1, Figure 5.9.2-40), any liquid delivered prematurely from the upper head does not contribute to the upper plenum mass inventory.

Overall, the degree of inaccuracy in the NOTRUMP simulations of upper head draining in the OSU tests analyzed is not important to the overall system behavior and does not produce nonconservative predictions of upper plenum mixture level. Therefore, NOTRUMP will not underestimate the potential for core uncover in AP600 small break LOCA analyses.

#### Reference

440.486-1      WCAP-14292, Revision 1, OSU Test Analysis Report, September 1995

SSAR Revision: NONE





# Upper Head Level

—	MTH00030	1	0	0 Test Data (SB01)
---	MTH00028	8	0	0 NOTRUMP Simulation

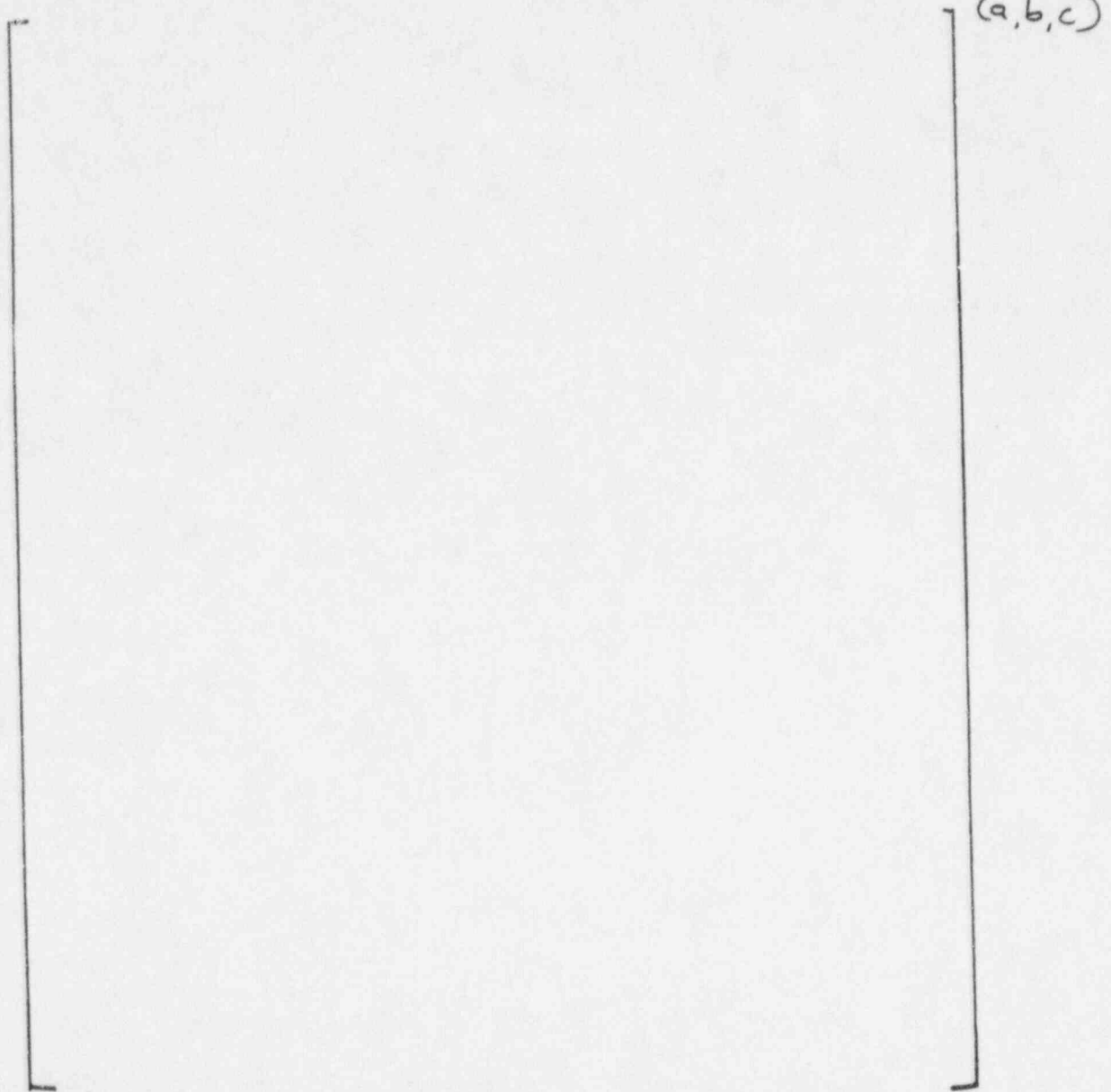


Figure 440.486-1 Upper Head Liquid Level, OSU Test SB01





# Upper Head Level

—— MTH00030 1 0 0 Test Data (SB09)  
---- MTH00028 8 0 0 NOTRUMP Simulation

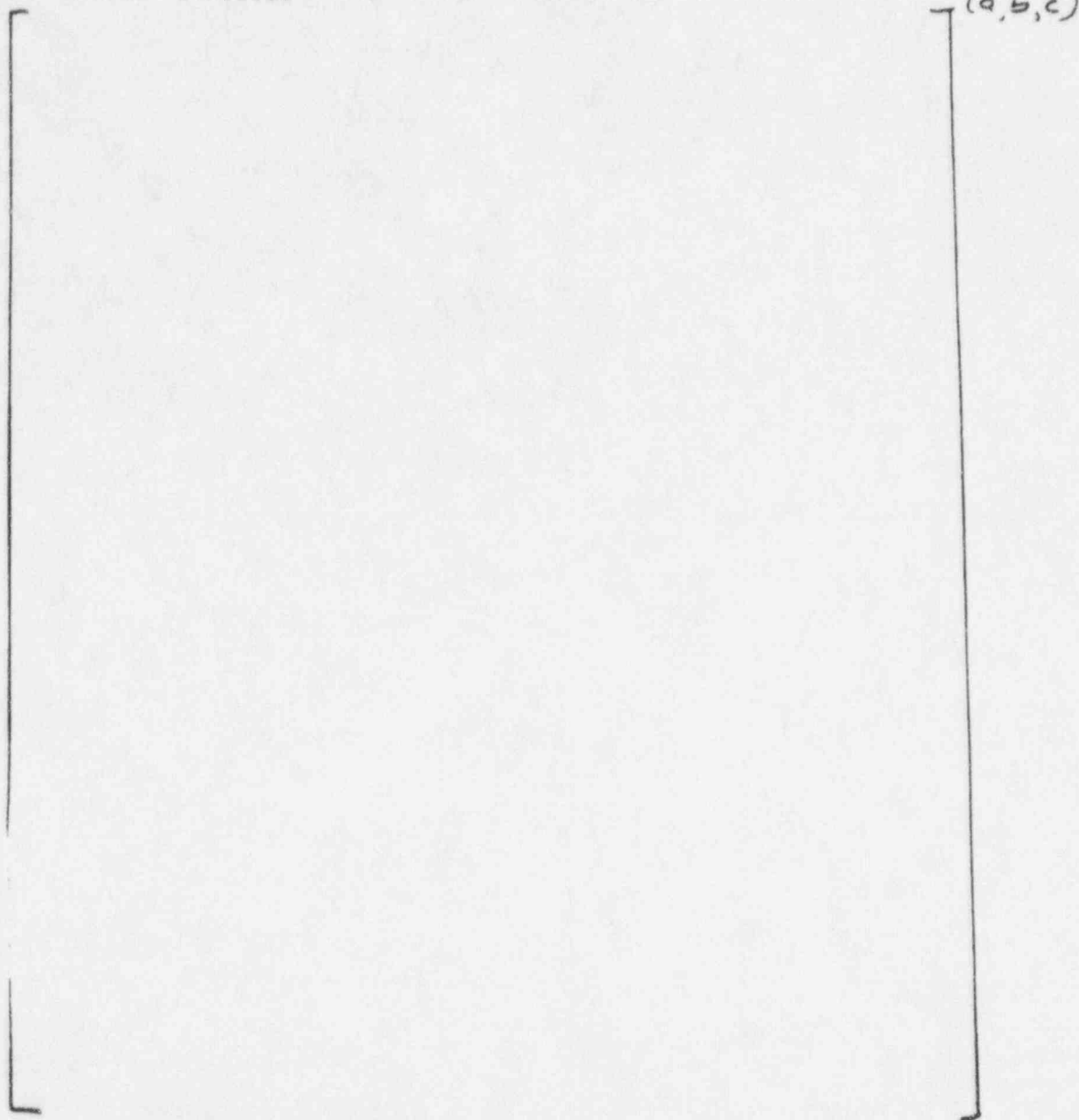


Figure 440.486-2 Upper Head Liquid Level, OSU Test SB09



# Upper Head Level

—— MTH00030 1 0 0 Test Data (SB10)  
---- MTH00028 8 0 0 NOTRUMP Simulation

(a,b,c)

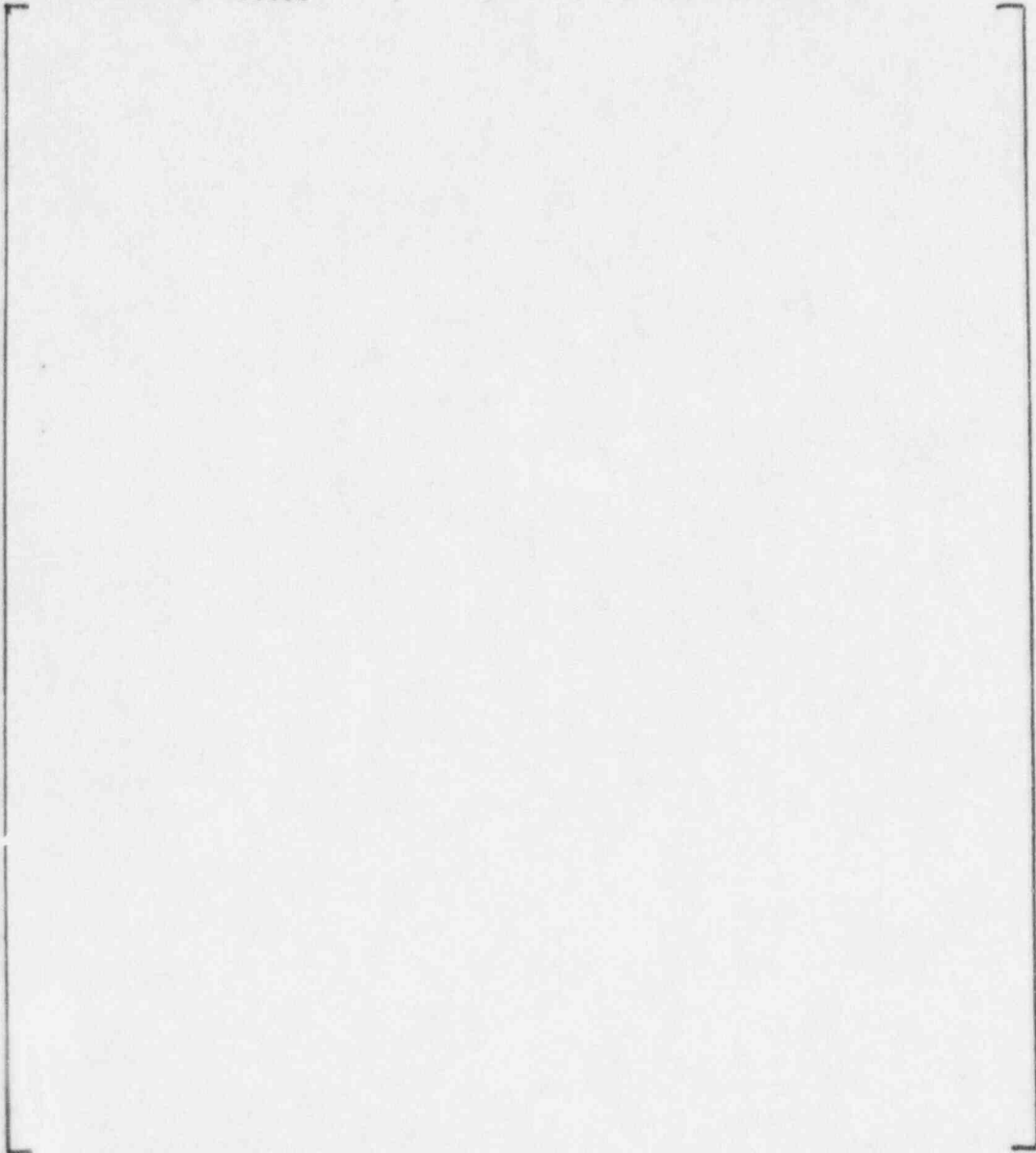


Figure 440.486-3 Upper Head Liquid Level, OSU Test SB10



# Upper Head Level

—	MTH00030	1	0	0 Test Data (SB12)
- - -	MTH00028	8	0	0 NOTRUMP Simulation

(a,b,c)

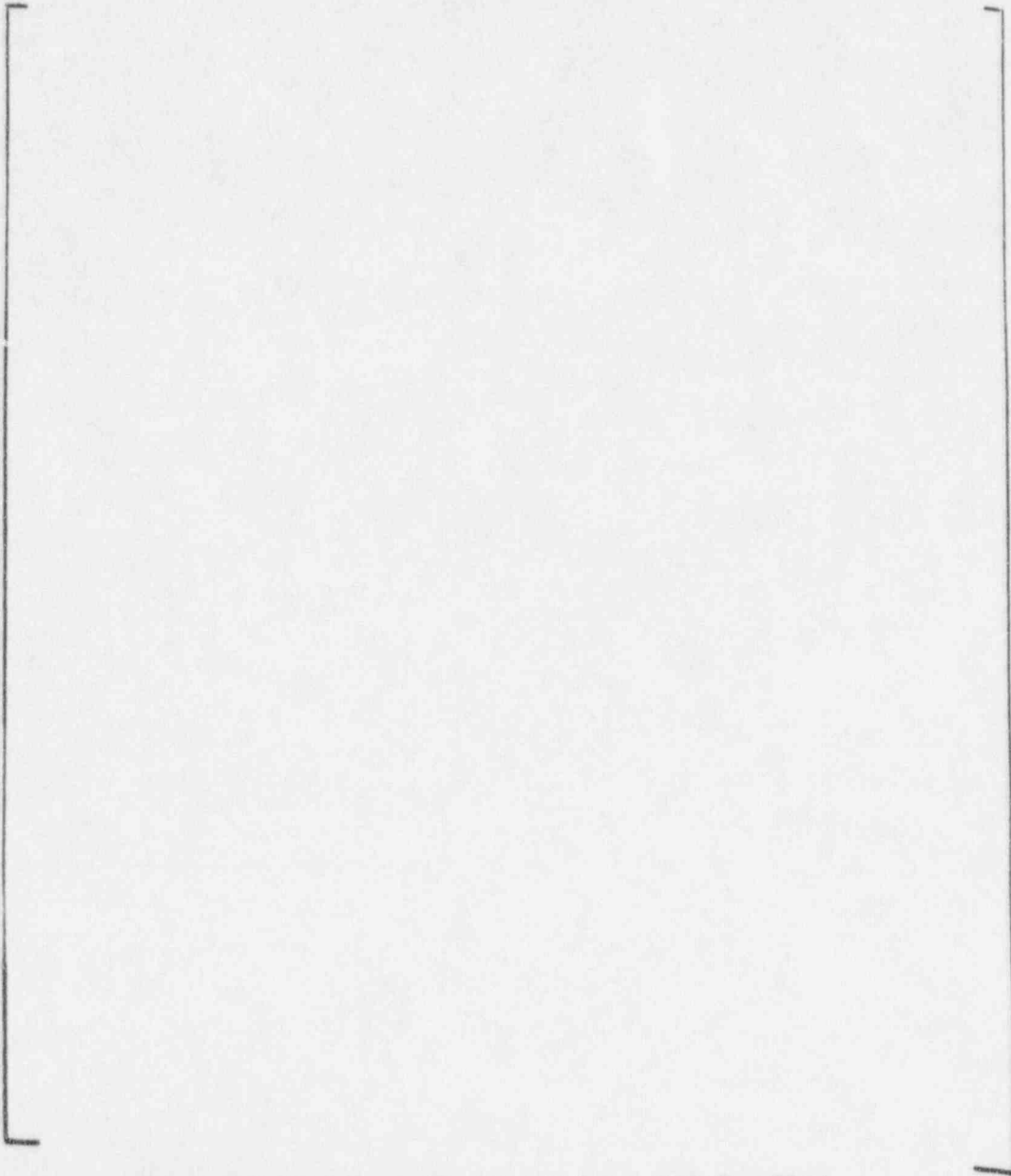


Figure 440.486-4 Upper Head Liquid Level, OSU Test SB12



# Upper Head Level

— MTH00030 1 0 0 Test Data (SB14)  
- - - MTH00028 8 0 0 NOTRUMP Simulation

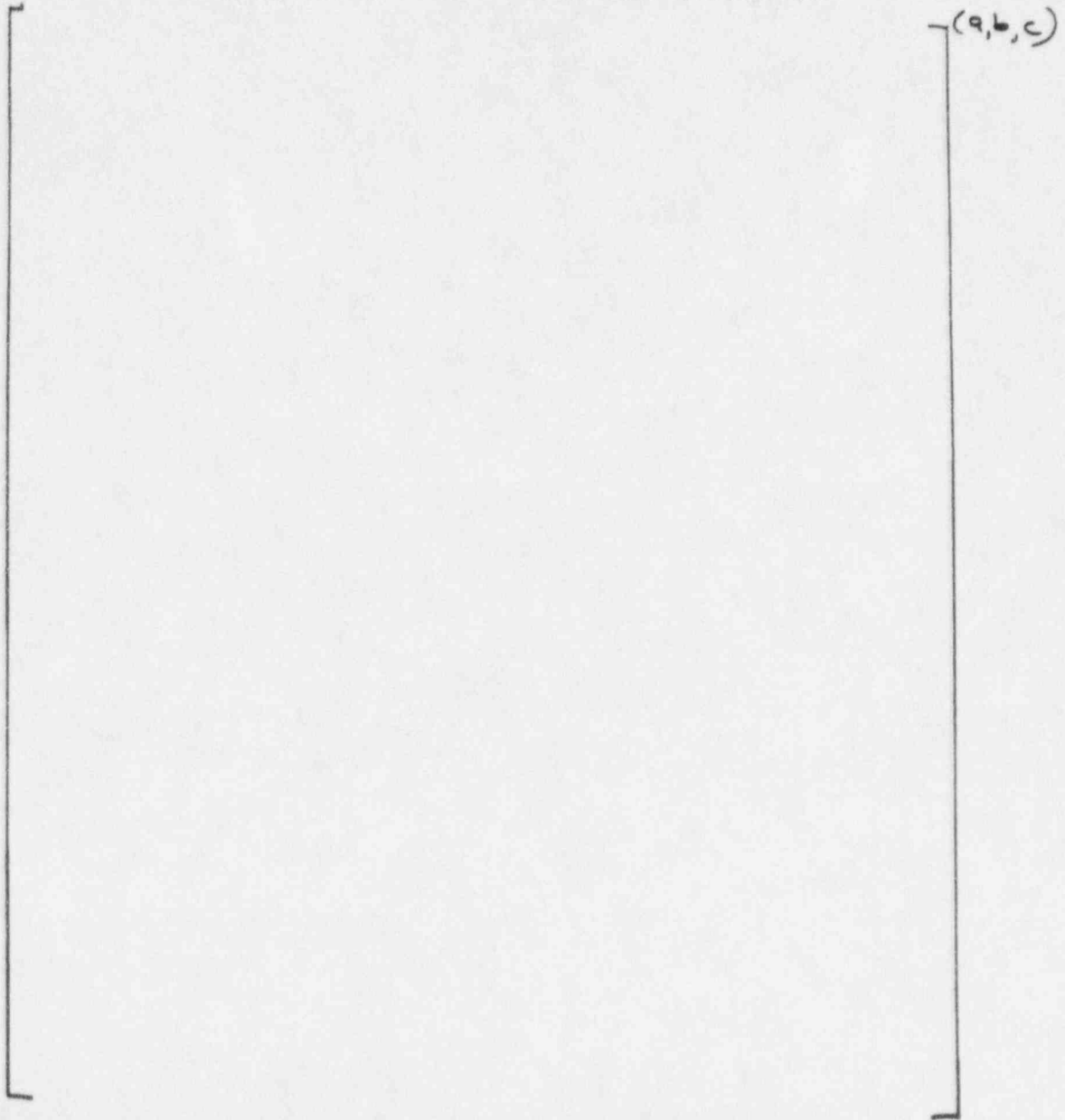


Figure 440.486-5 Upper Head Liquid Level, OSU Test SB14

**NI - REQUEST FOR ADDITIONAL INFORMATION**



Question 440.491

Re: NOTRUMP PVR FOR OSU TESTS, LTCT-GSR-001, JULY 1995

Please provide the core inlet and core bypass mass flow rate predictions for the NOTRUMP code.

Response:

The requested NOTRUMP core inlet and core bypass mass flow rate predictions are provided in Figures 440.491-1 through 440.491-11. For completeness, all the tests analyzed by NOTRUMP are included. The only core bypass flow which is modeled in NOTRUMP is the downcomer to upper head bypass flow which is included in the figures. Pressure spikes produced by boiling in the core can cause the mass flow into the bottom of the core to reverse, but the core flow is predominantly upwards. The predominant upward flow is illustrated in Figure 440.491-2 by a 6th order polynomial fit to the core inlet flow of Test SB01.

SSAR Revision: NONE





# OSU NOTRUMP Simulation (SB01)

WFFL 2 0 0 CORE INLET FLOW

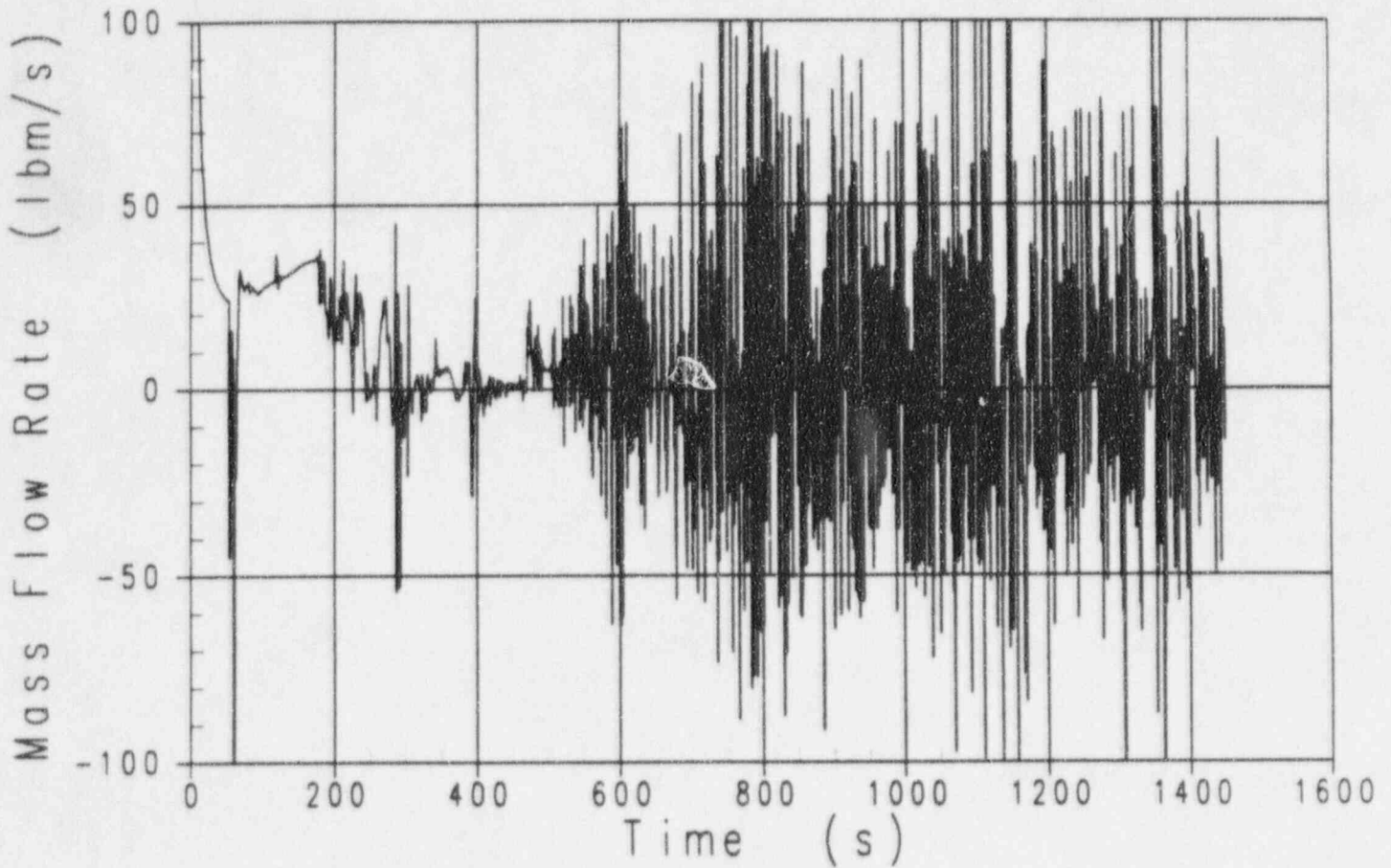


Figure 440.491-1 Core Inlet Flow for Test SB01



# OSU NOTRUMP Simulation (SB01)

— MTH00006 2 0 0 6th 0 fit inlet flow

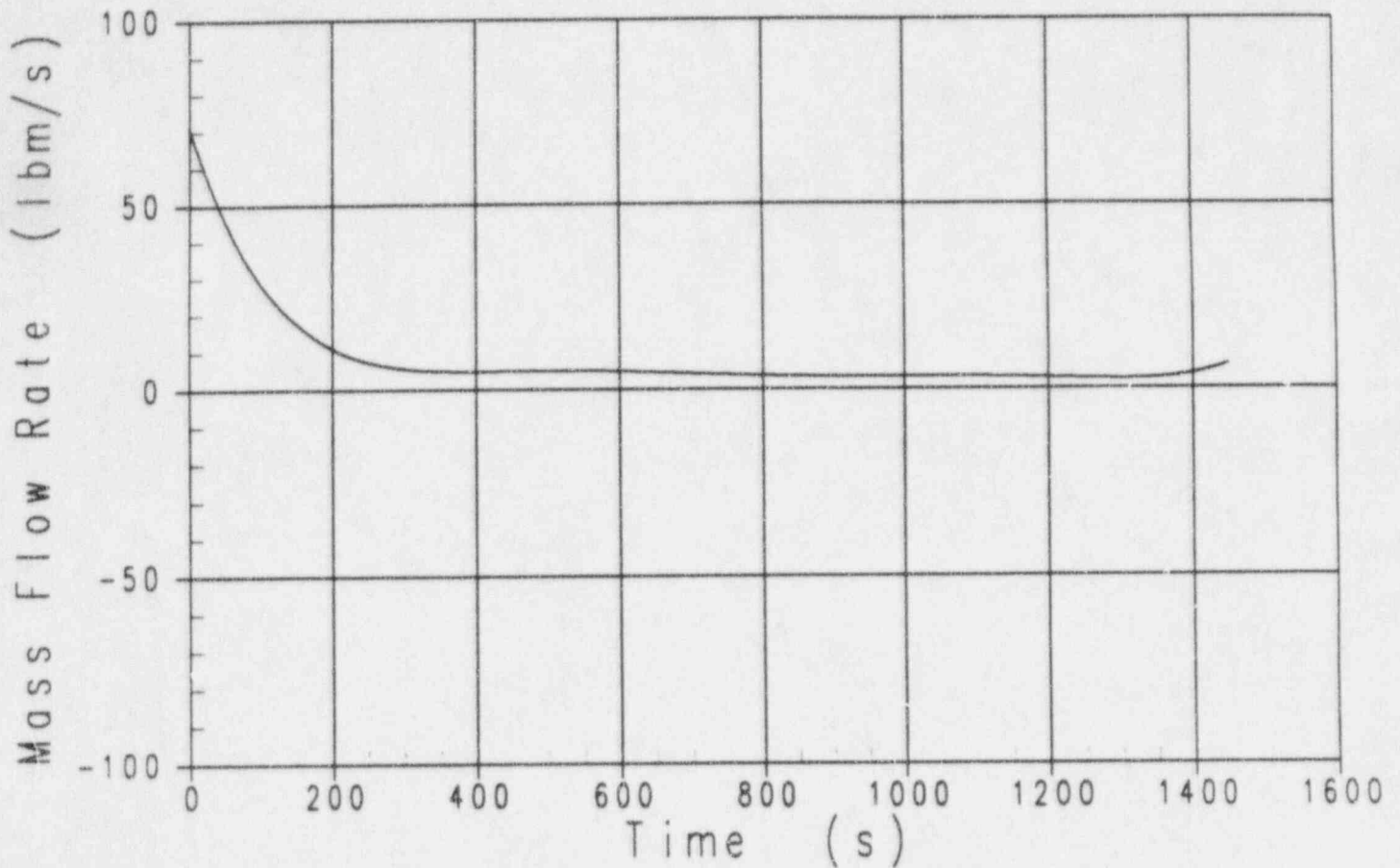


Figure 440.491-2 Fitted Plot of Core Inlet Flow for Test SB01



# OSU NOTRUMP Simulation (SB01)

WFL 8 0 0 UPPER HEAD BYPASS F

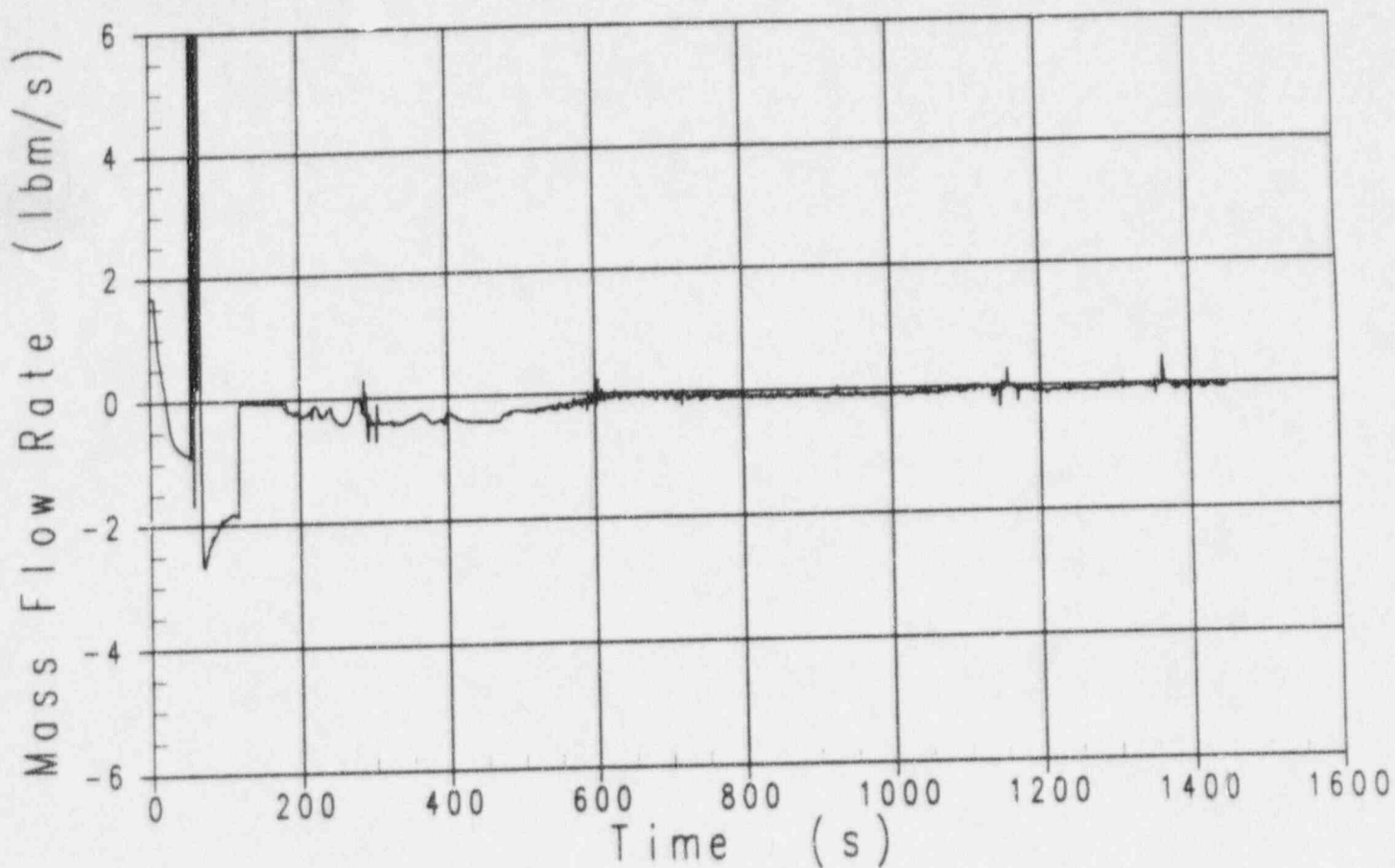


Figure 440.491-3 Upper Head Bypass Flow for Test SB01



# OSU NOTRUMP Simulation (SB09)

WFFL 2 0 0 CORE INLET FLOW

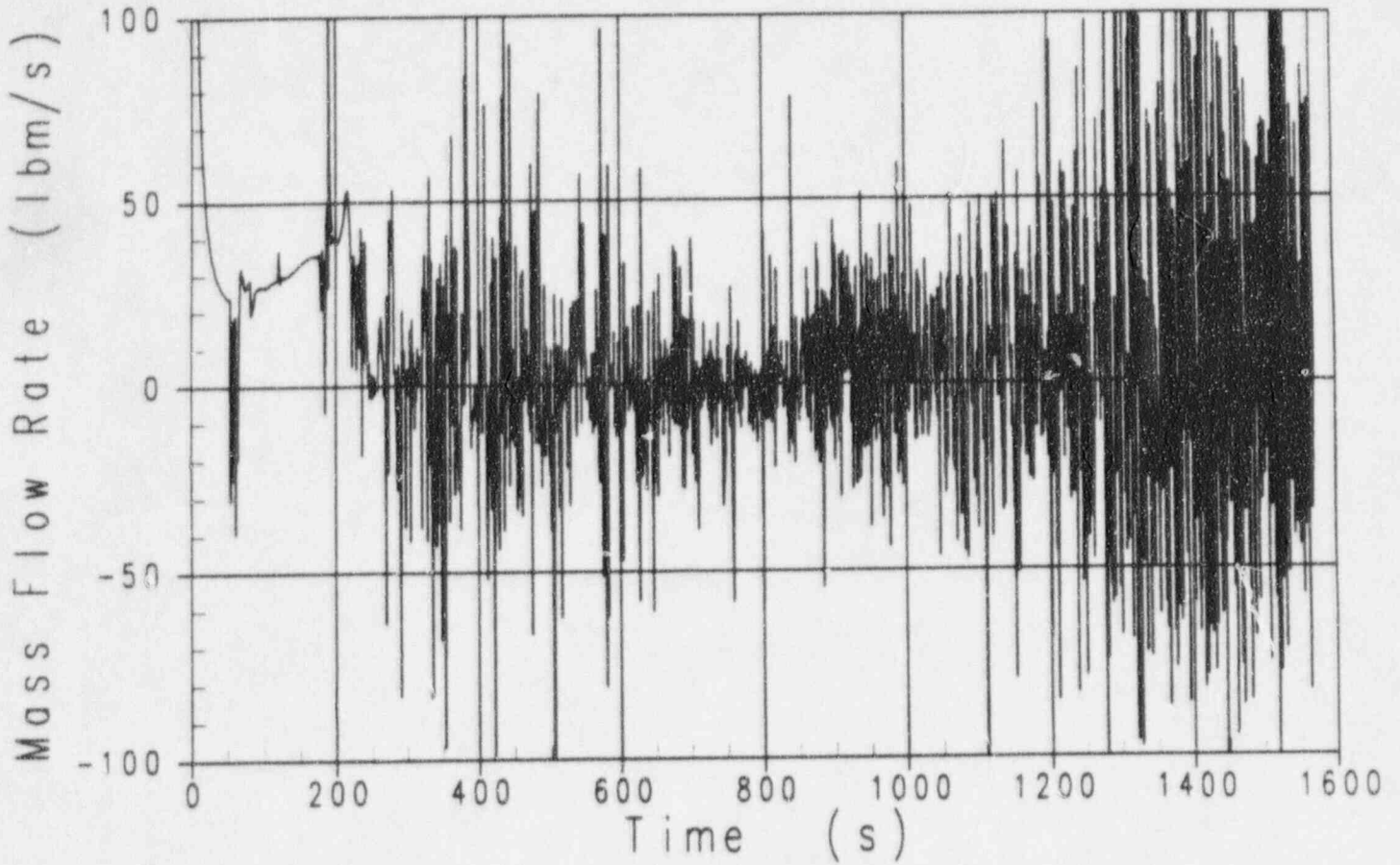


Figure 440.491-4 Core Inlet Flow for Test SB09



# OSU NOTRUMP Simulation (SB09)

WFL 8 0 0 UPPER HEAD BYPASS F

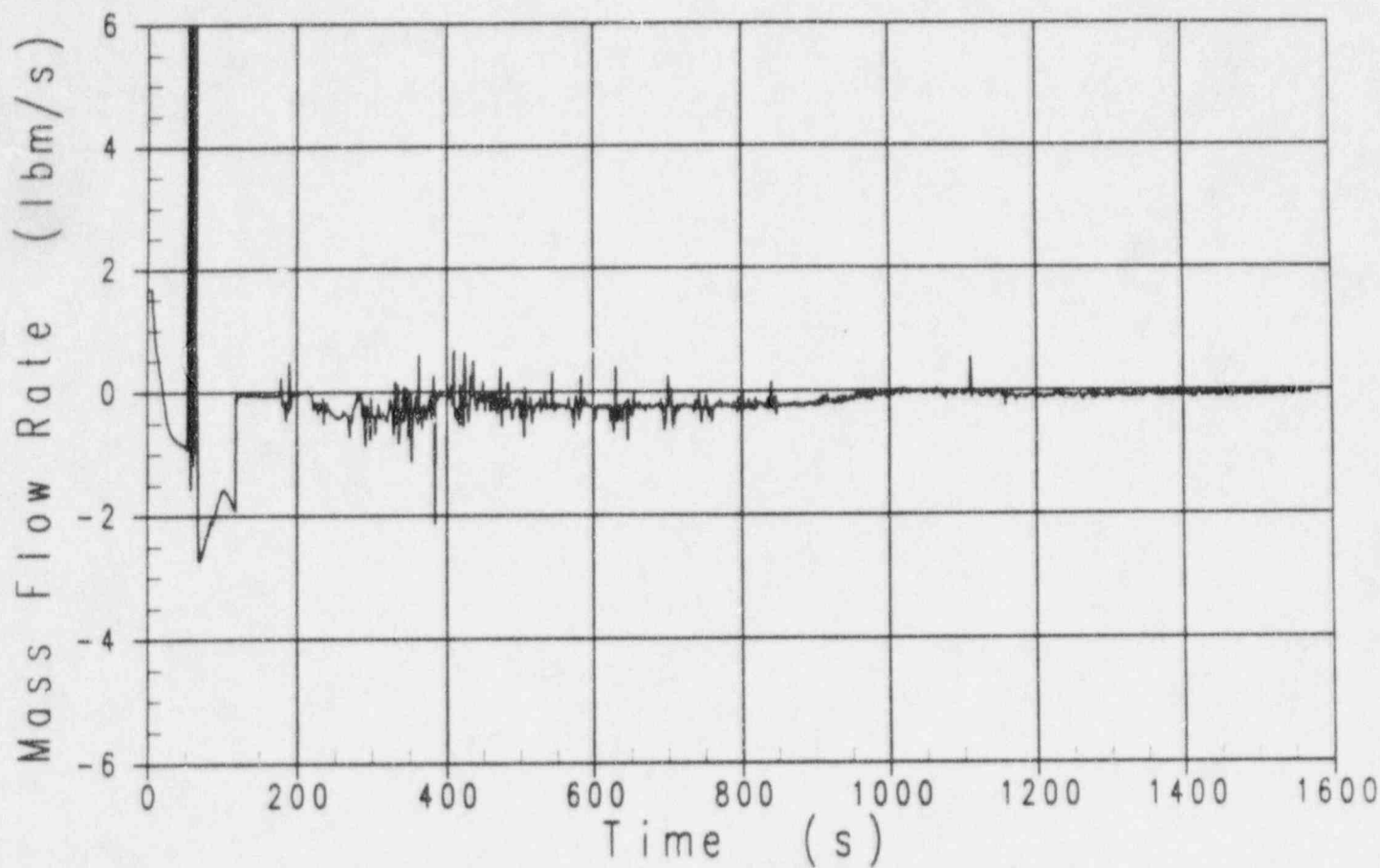


Figure 440.491-5 Upper Head Bypass Flow Rate for Test SB09



# OSU NOTRUMP Simulation (SB10)

WFFL 2 0 0 CORE INLET FLOW

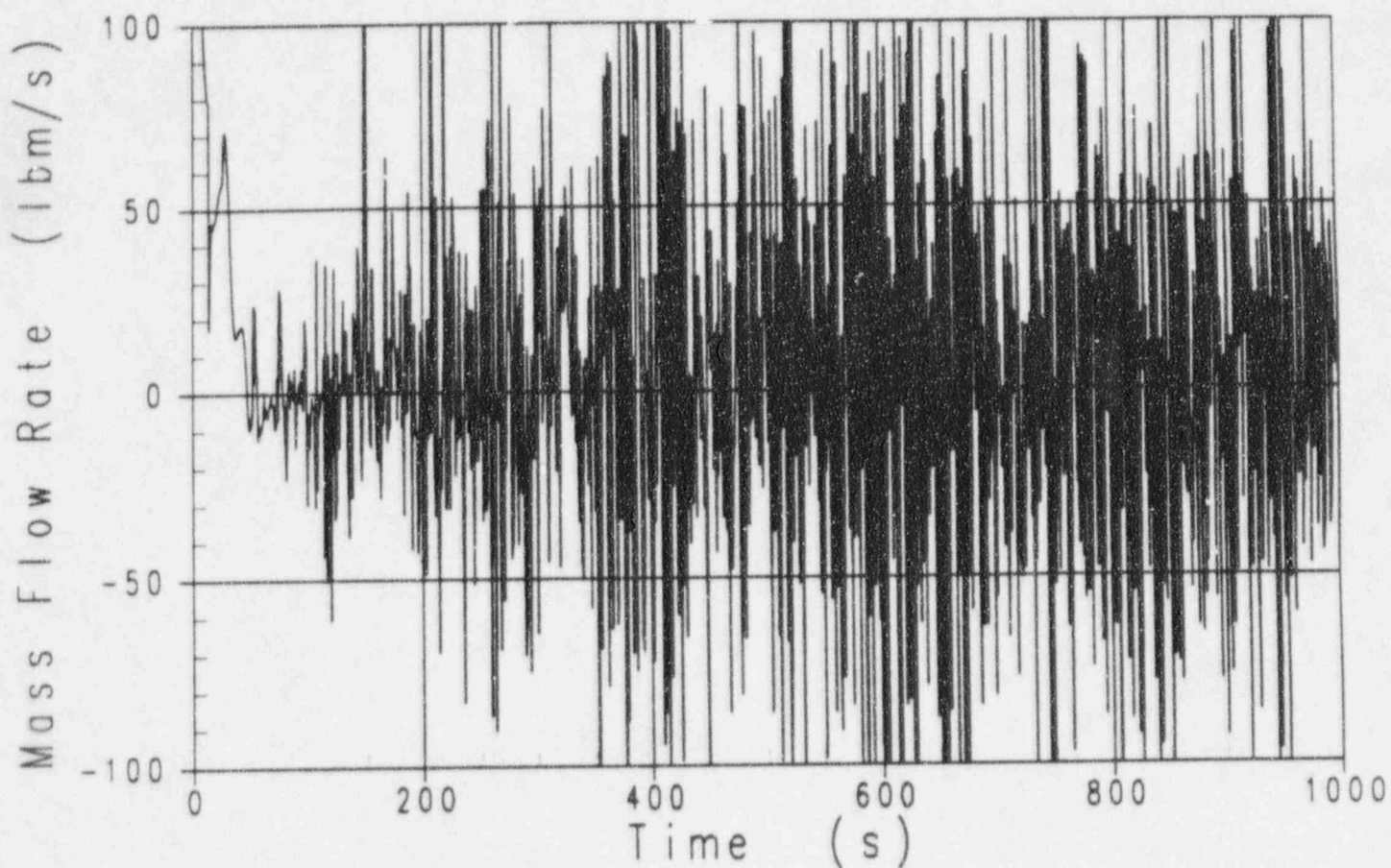


Figure 440.491-6 Core Inlet Flow Rate for Test SB10



# OSU NOTRUMP Simulation (SB10)

WFL 8 0 0 UPPER HEAD BYPASS F

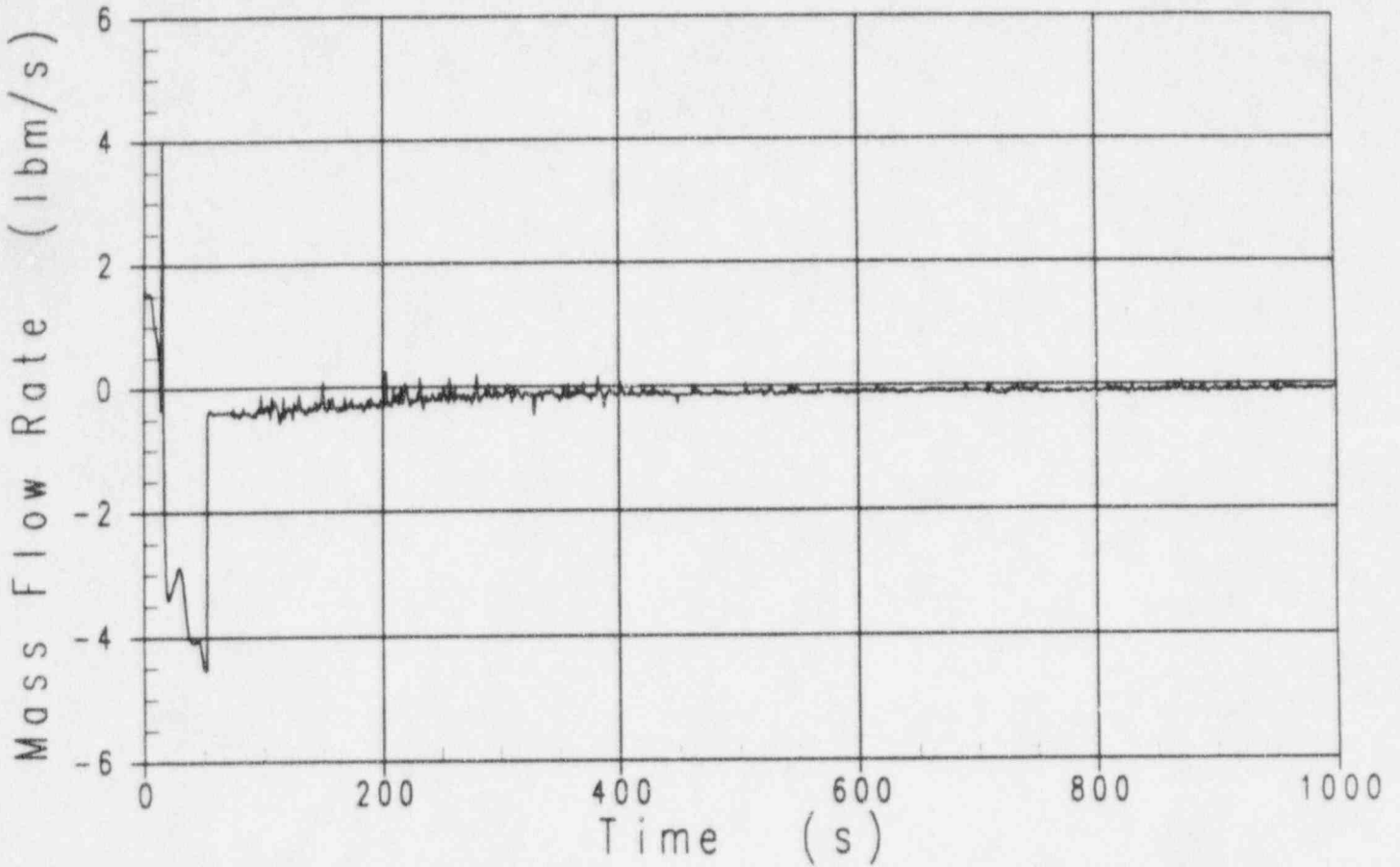


Figure 440.491-7 Upper Head Bypass Flow Rate for Test SB10



# OSU NOTRUMP Simulation (SB12)

WFFL 2 0 0 CORE INLET FLOW

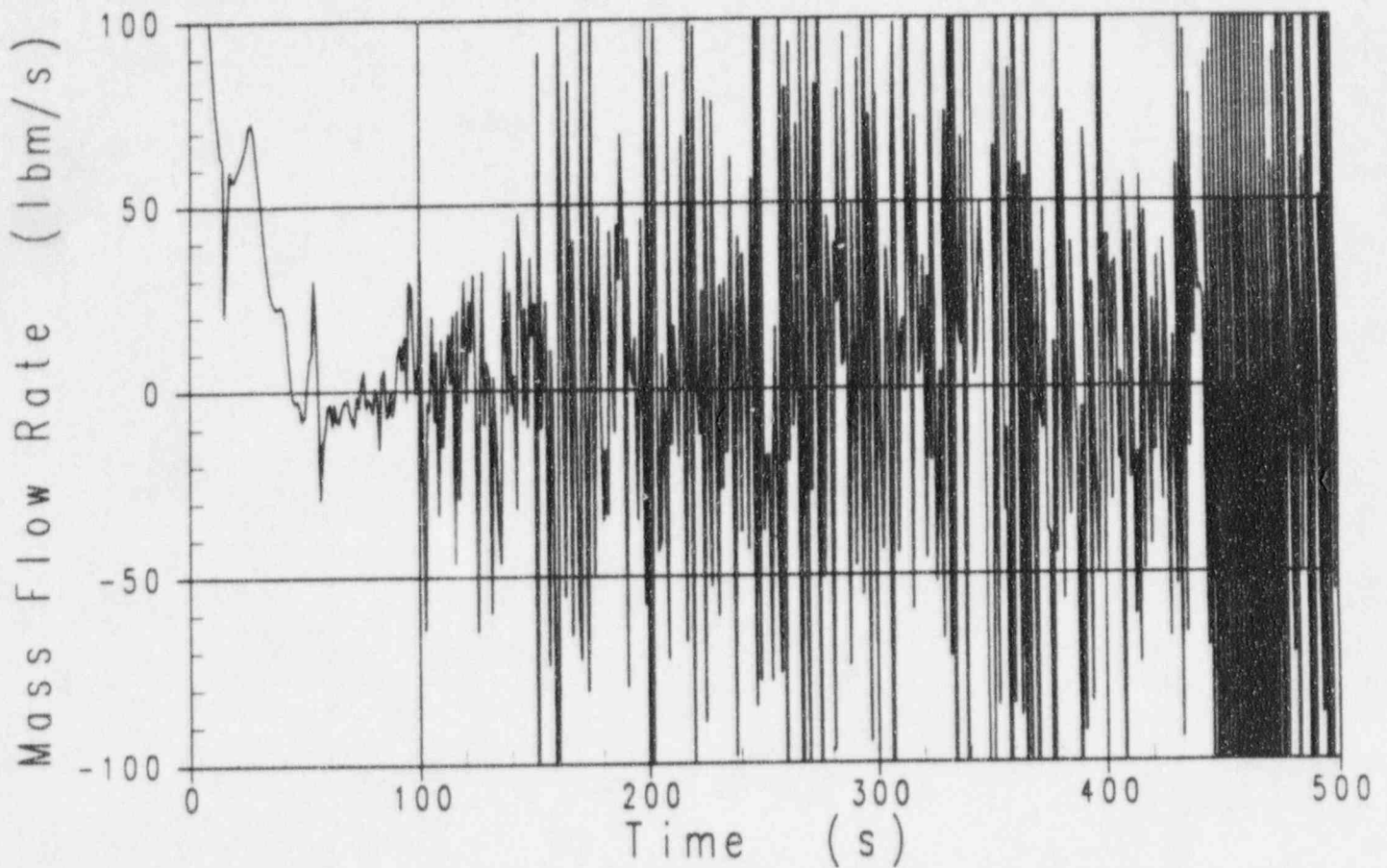


Figure 440.491-8 Core Inlet Flow for Test SB12





# OSU NOTRUMP Simulation (SB12)

WFL 8 0 0 UPPER HEAD BYPASS F

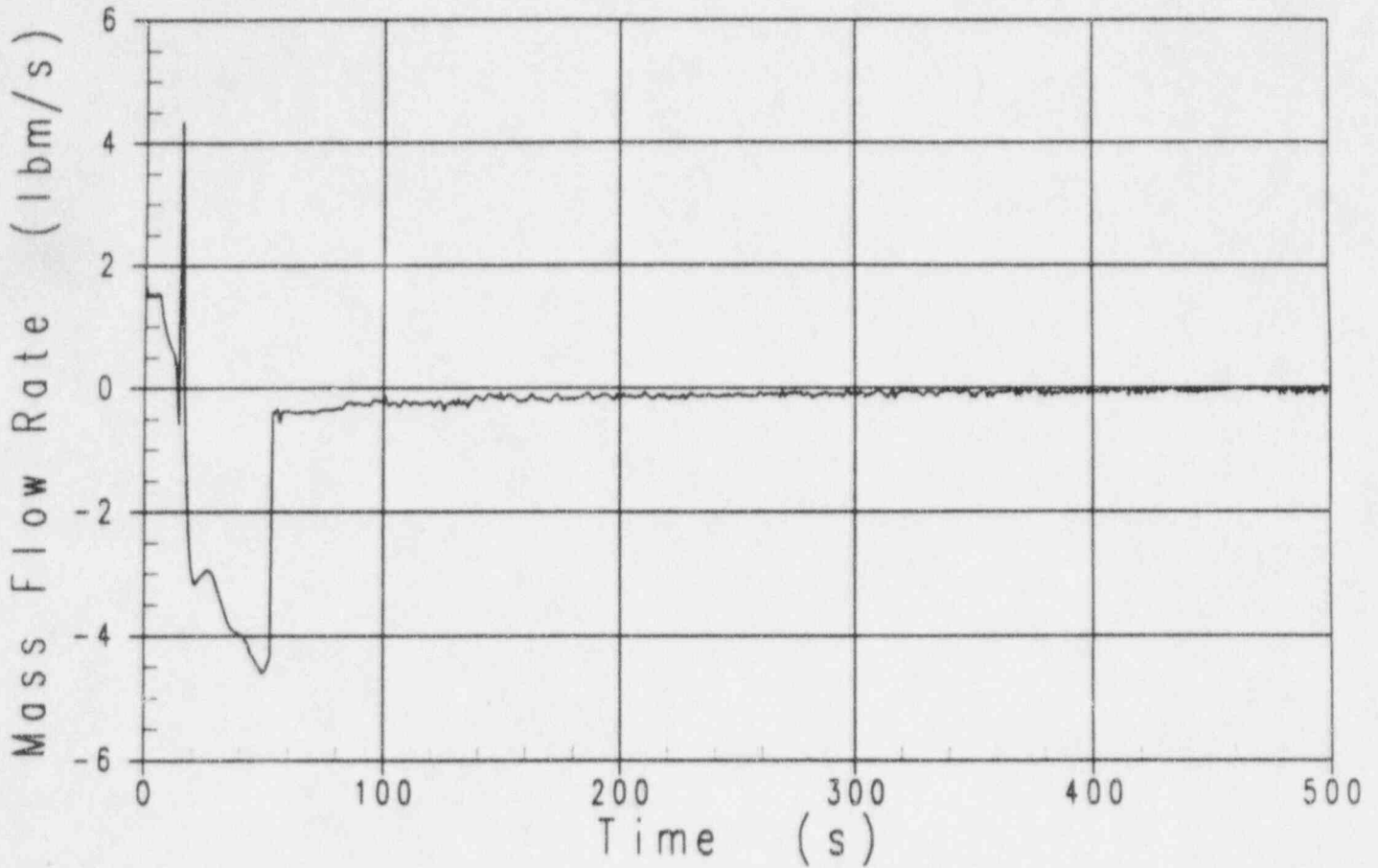


Figure 440.491-9 Upper Head Bypass Flow for Test SB12



# OSU NOTRUMP Simulation (SB14)

WFFL 2 0 0 CORE INLET FLOW

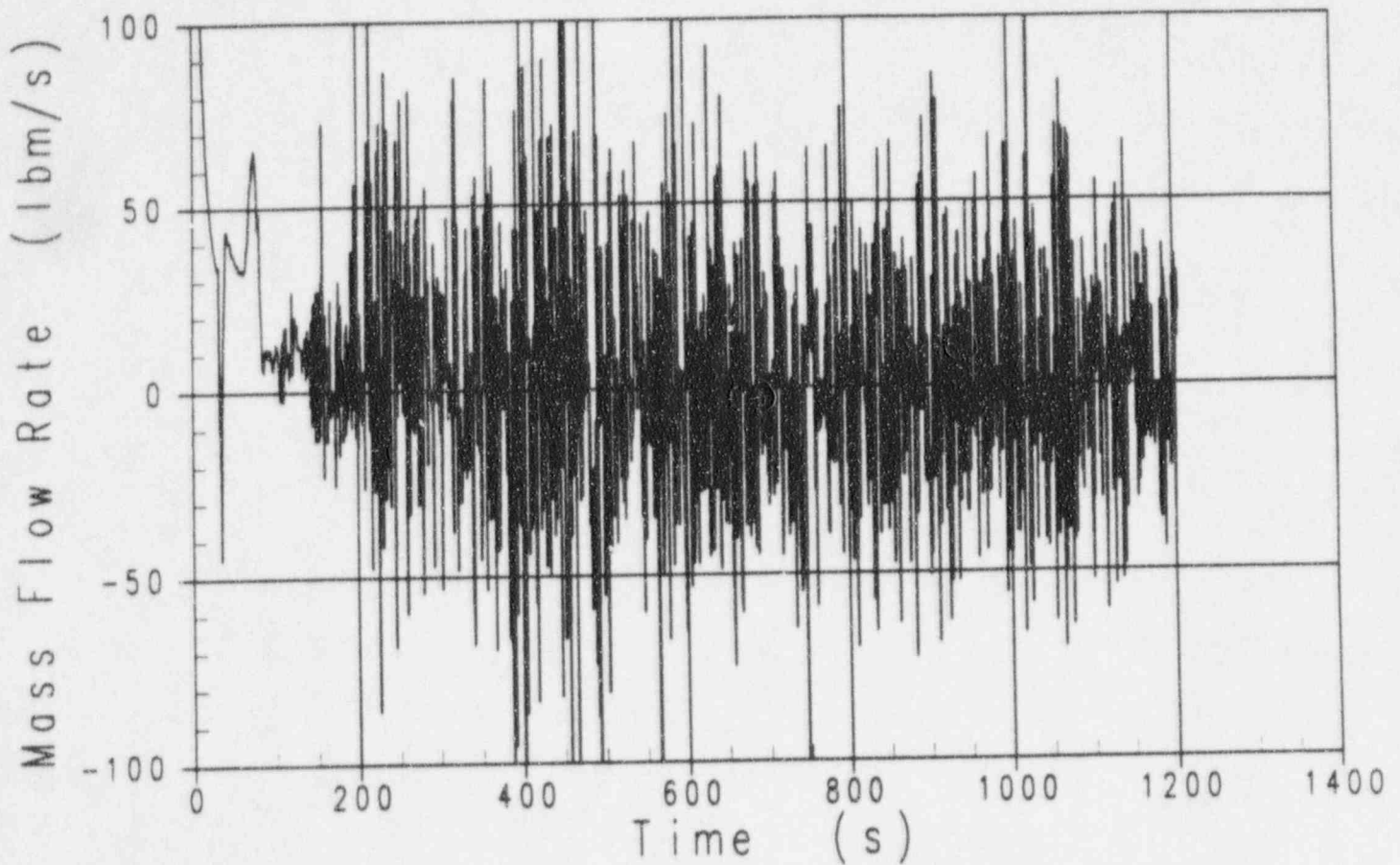


Figure 440.491-10 Core Inlet Flow for Test SB14



# OSU NOTRUMP Simulation (SB14)

WFL 8 0 0 UPPER HEAD BYPASS F

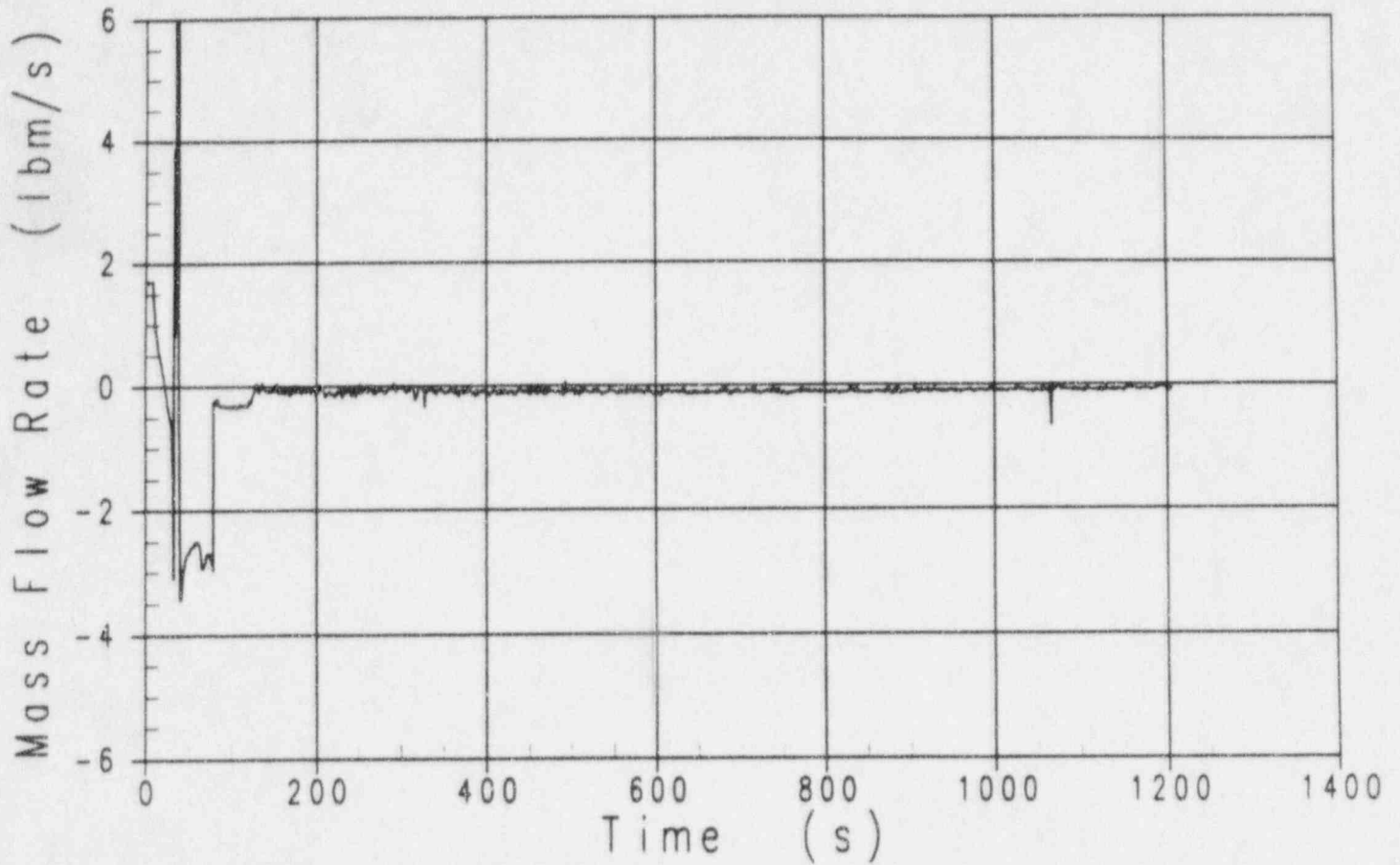


Figure 440.491-11 Upper Head Bypass Flow Rate for Test SB14

## NRC REQUEST FOR ADDITIONAL INFORMATION



Question 440.512

Re: NOTRUMP PVR FOR OSU TESTS, LTCT-GSR-001, JULY 1995

The secondary pressures, levels, and temperatures were not provided for each of the tests. Please provide comparisons of the secondary pressure, level, and temperature test data responses with the NOTRUMP code predictions.

Response:

The requested comparisons of the secondary pressure, level and temperature for all tests analyzed by NOTRUMP are provided in Figures 440.512-1 through 440.512-30. Note that the level in the test data is the collapsed liquid level and the level from NOTRUMP is the mixture level which is different than the collapsed level early in the transients but is the same as the collapsed level on the plots after the level falls and stabilizes (i.e., approximately 375 seconds in Figure 440.512-2).

There are two differences to note when comparing the test data and the NOTRUMP predictions. First, the initial NOTRUMP SG level and mass specifications were taken from early references which do not reflect the actual initial conditions of the tests as specified in the final Test Data Report, Ref 440.512-1. The SG secondary fluid mass was approximately 35% too low in the NOTRUMP calculations. Secondly, the SG relief valve set pressure was reduced from 350 psia to 310 psia (See response to RAI 440.511). The significant discrepancy in the initial SG secondary side mass is not only observed in the level comparison but also affects the NOTRUMP predictions of secondary pressure and temperature. The initial SG levels will be set to 25.5 inches, narrow range, as specified in the Test Data Report for the runs to be included in the final V & V report. Since the secondary pressure exceeds the relief valve set pressure in the NOTRUMP calculations the secondary mass decreases and the level falls. As noted in the response to RAI 440.511, the modeling of the PRHR heat transfer will be improved and checked against the OSU data as part of an IRWST nodalization study. The improved PRHR heat transfer is expected to eliminate the need to lower the SG relief valve set pressure. The final V&V report will include revised versions of Figures 440.512-1 through 440.512-30.

Reference:

440.511-1 WCAP-14252, "AP600 Low Pressure Integral System Test at Oregon State University: Final Data Report," Proprietary [LTCT-T2R-100]

SSAR Revision: NONE



Steam Generator 1 Secondary Pressure (SB01)  
----- MTH00012 34 1 0 Test Data  
----- PFN 40 0 0 NOTRUMP Simulation

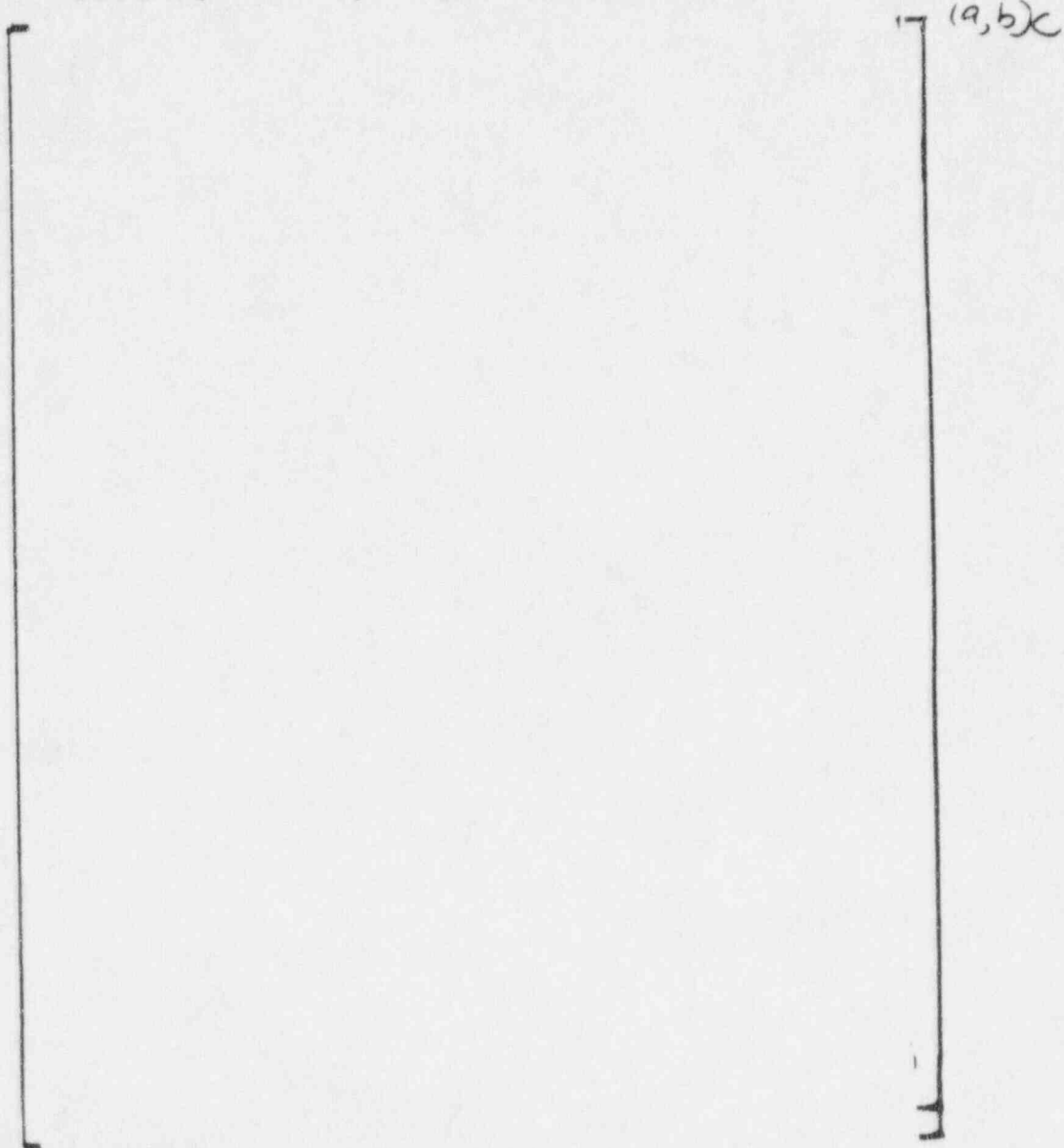


Figure 440.512-1



Steam Generator 1 Secondary Level (SB01)

-----	M*H00008	1	0	0	Test Data
-----	M*H00006	40	0	0	NOTRUMP Simulation

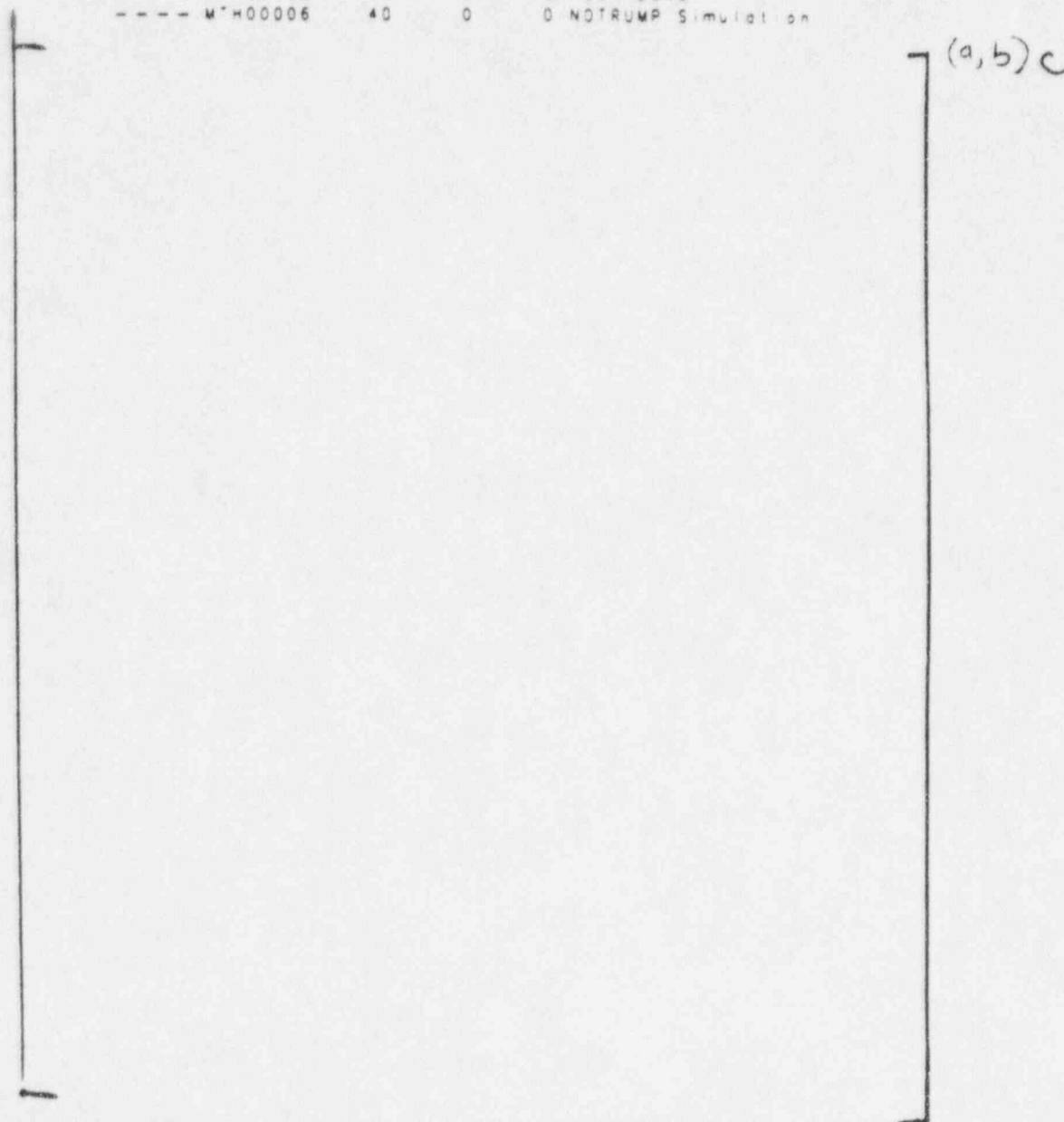


Figure 440.512-2



1995/09/15 18:14:45.79 7310283162017  
Facility Name: OSU Test Number: U0001 Date: 08/01/94 Time: 01:34 PM  
----- TF-307 114 3 0 SG-1 Dwncmr CL Side  
----- TF-305 112 3 0 SG-1 Dwncmr HL Side

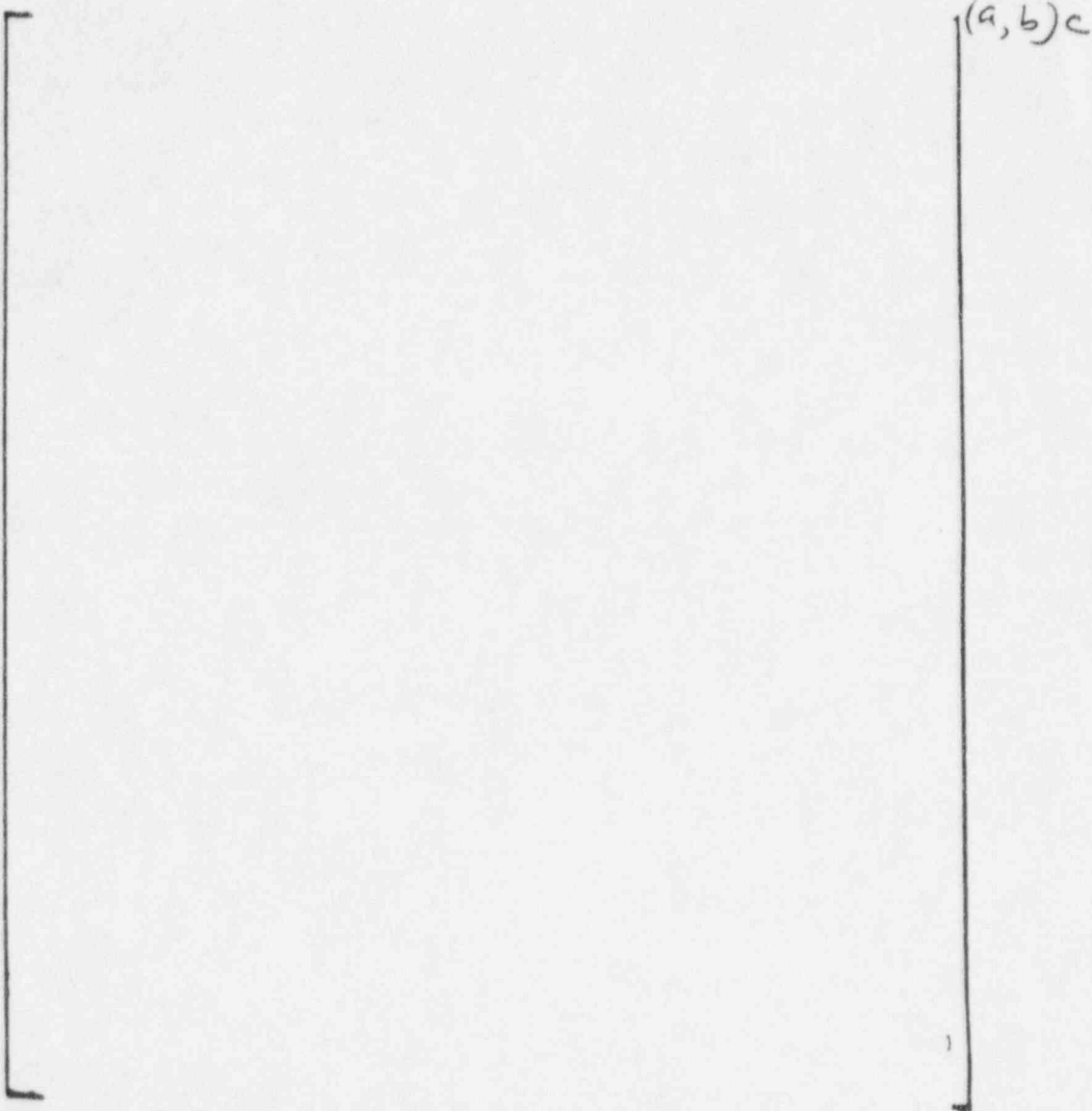


Figure 440.512-3



Steam Generator 2 Secondary Pressure (SB01)  
----- M\*H00013 16 1 0 Test Data  
----- PFN 30 0 0 NOTRUMP Simulation

-(a,b)c

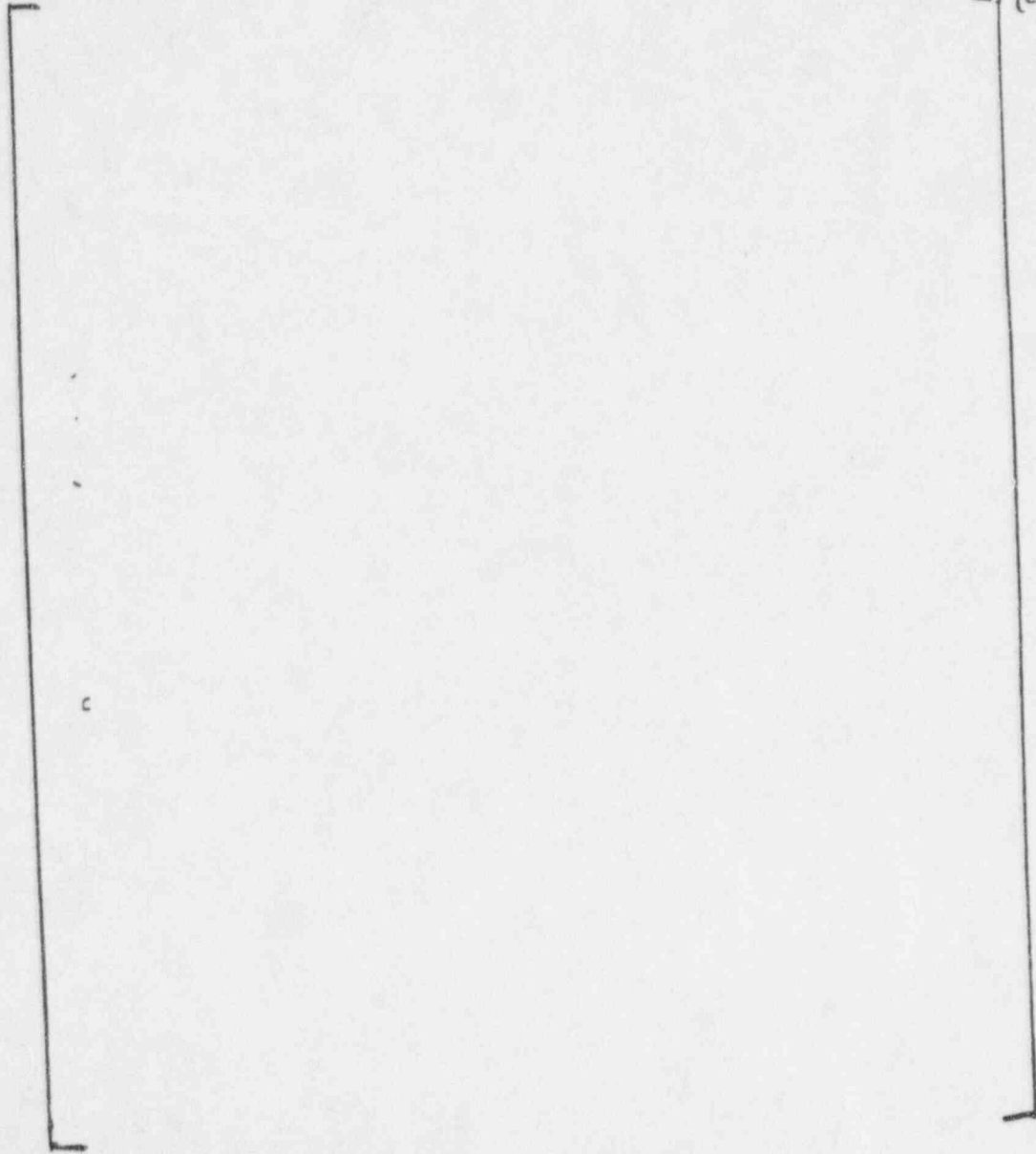


Figure 440.512-4





Steam Generator 2 Secondary Level (SB01)

-----	M*H00009	1	0	0	Test Data
----	M*H00007	30	0	0	NOTRUMP Simulation

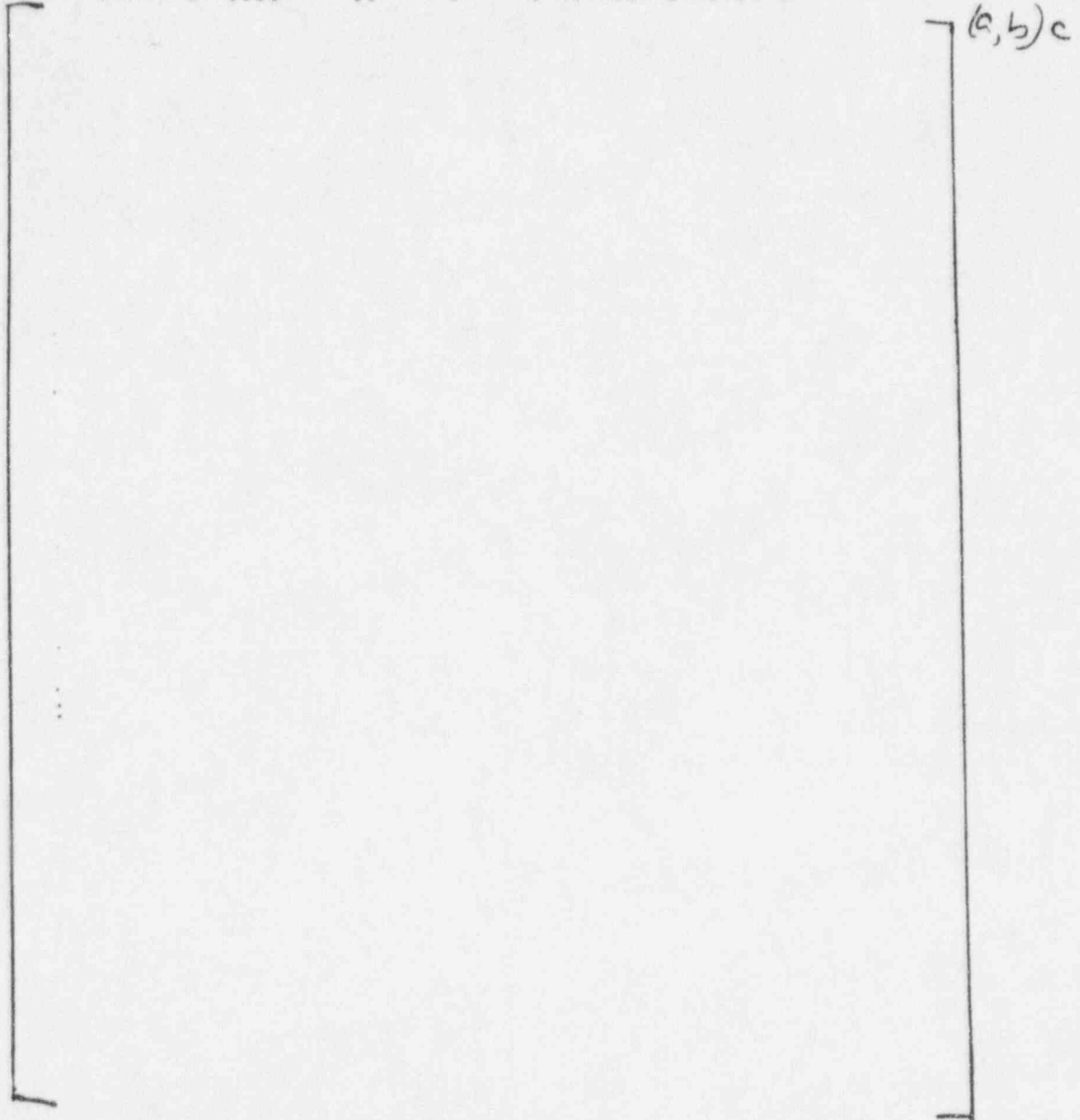


Figure 440.512-5

NRC REQUEST FOR ADDITIONAL INFORMATION



1995/09/15 18:14:45.79 7310283162017  
Facility Name: OSU Test Number: U0001 Date: 06/01/84 Time: 01:34 PM  
----- TF-308 115 3 0 SG-2 Dwnchr CL Side  
----- TF-306 113 3 0 SG-2 Dwnchr HL Side

(a,b)c

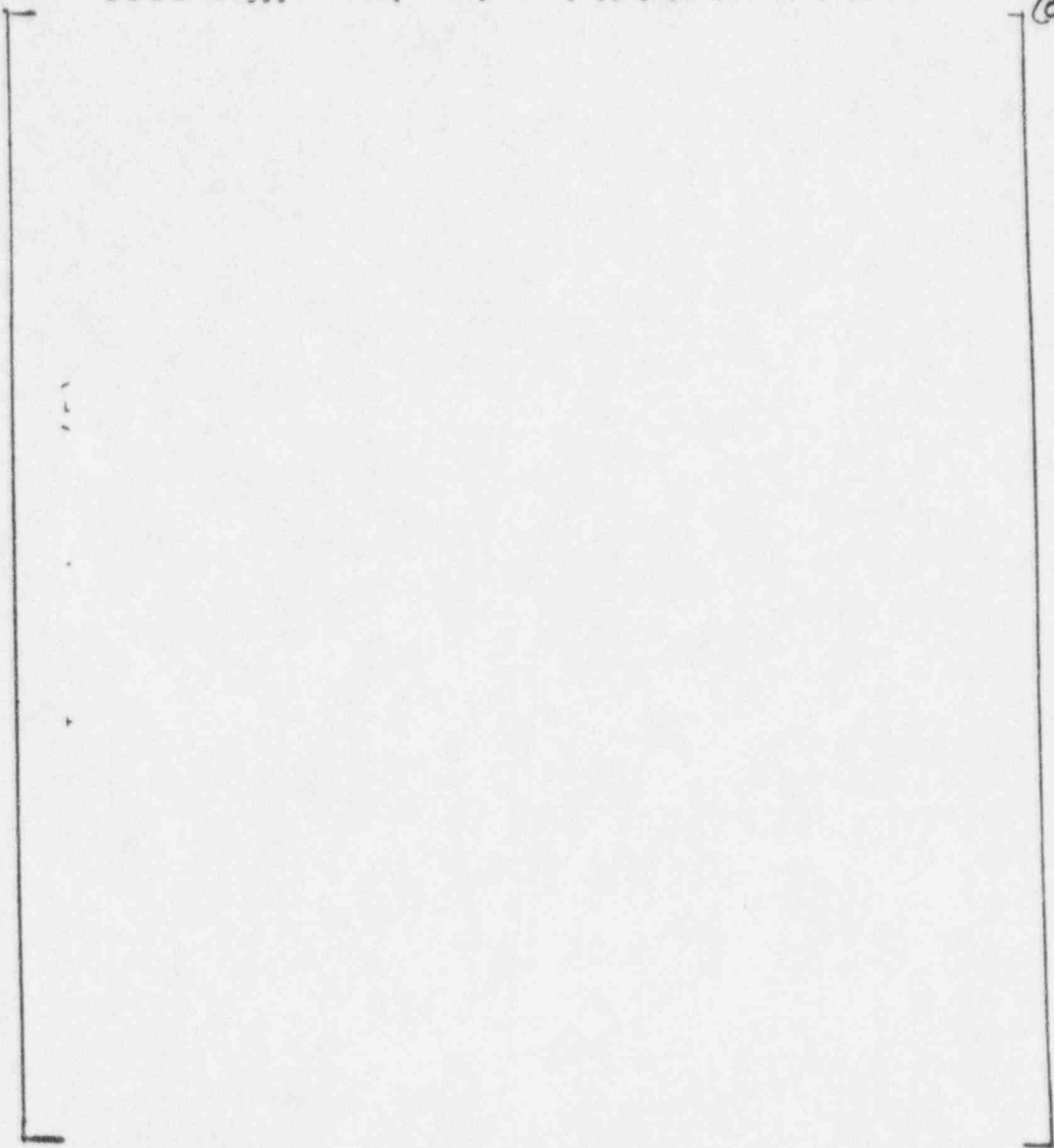


Figure 440.512-6



Steam Generator 1 Secondary Pressure (SB09)

---	MTH00012	30	1	0	Test Data
---	PFN	40	0	0	NOTRUMP Simulation

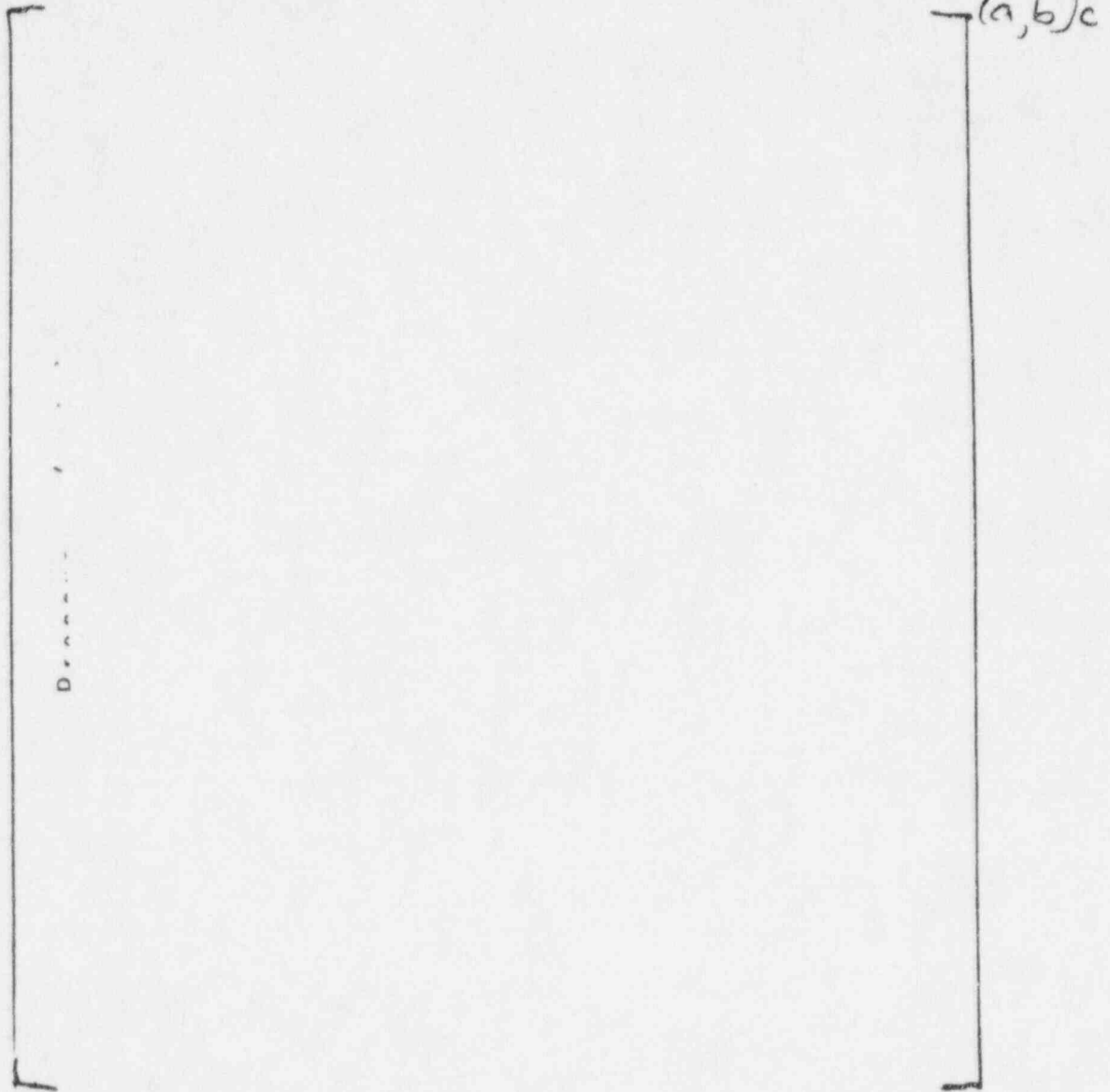
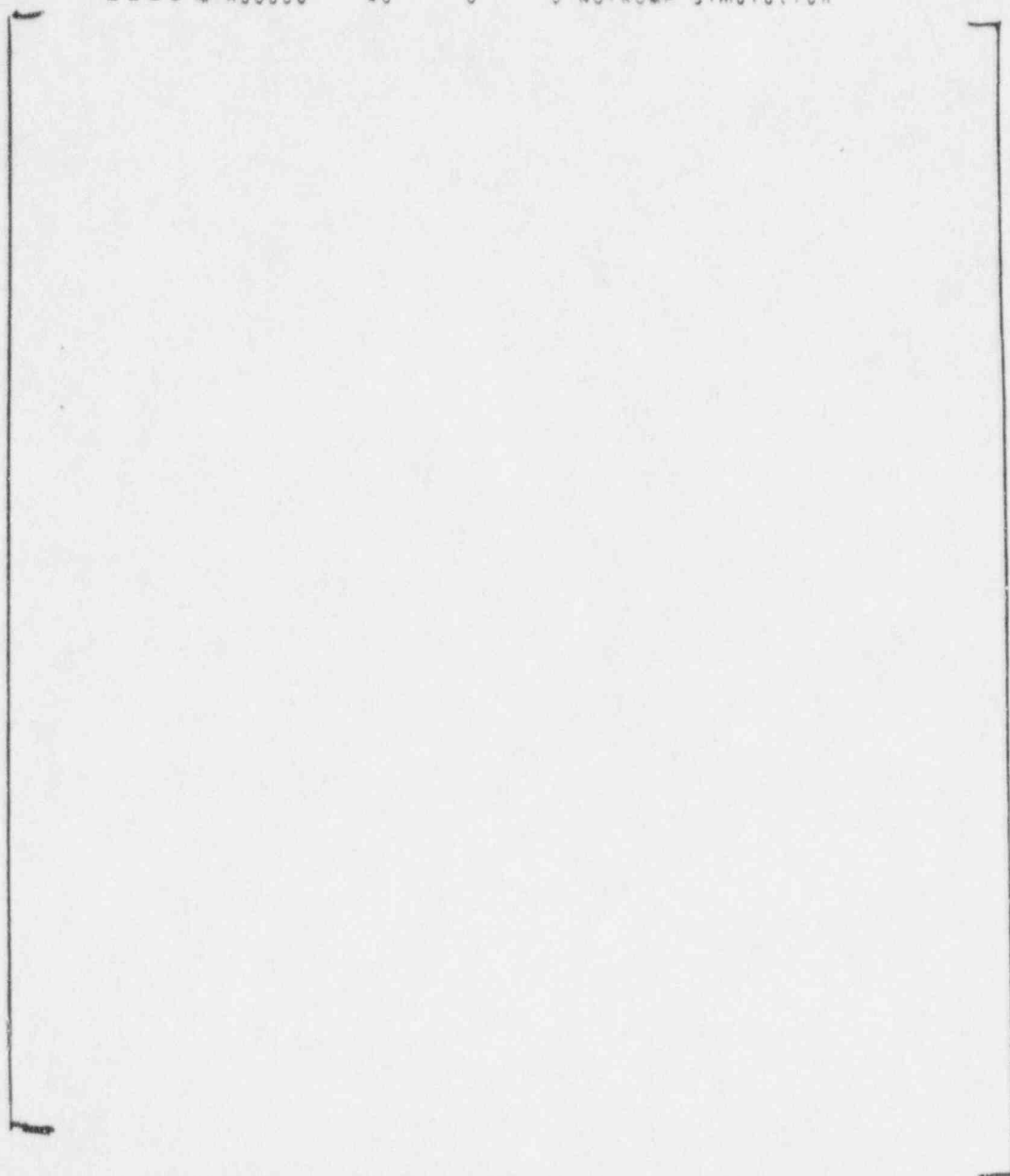


Figure 440.512-7



Steam Generator 1 Secondary Level (SB09)

-----	MTH00008	1	0	0	Test Data
----	MTH00006	40	0	0	NOTRUMP Simulation



(a,b)c

Figure 440.512-8



1995/09/15 18:58:36.17 7310493762017  
Facility Name: OSU Test Number: UG008 Date: 08/28/94 Time: 09:45 PM  
----- TF-307 114 3 0 SG-1 Denchr CL Side  
----- TF-305 112 3 0 SG-1

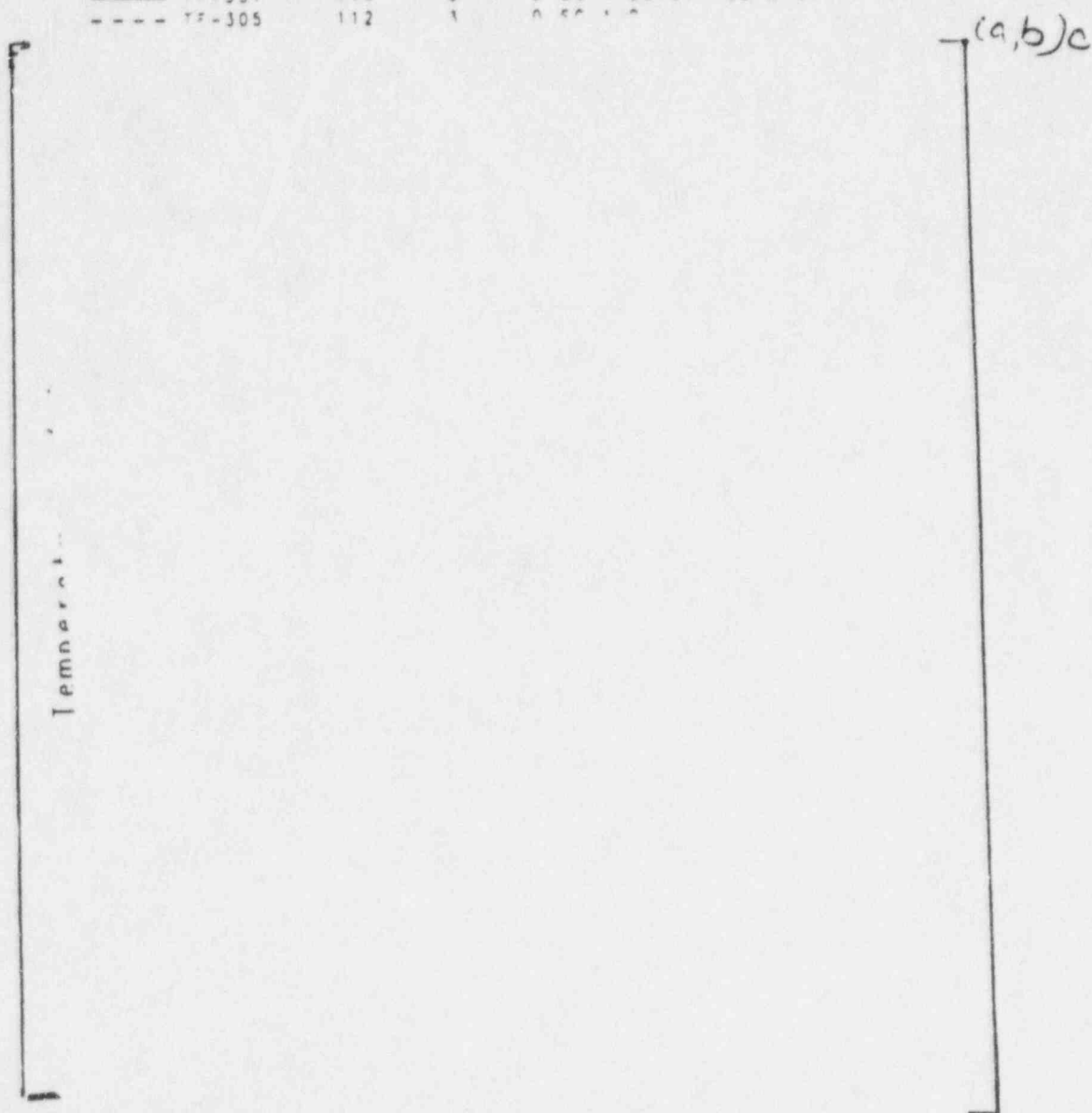


Figure 440.512-9





Steam Generator 2 Secondary Pressure (SB09)

-----	MTH00013	14	1	0	Test Data
-----	PFN	30	0	0	NOTRUMP Simulation

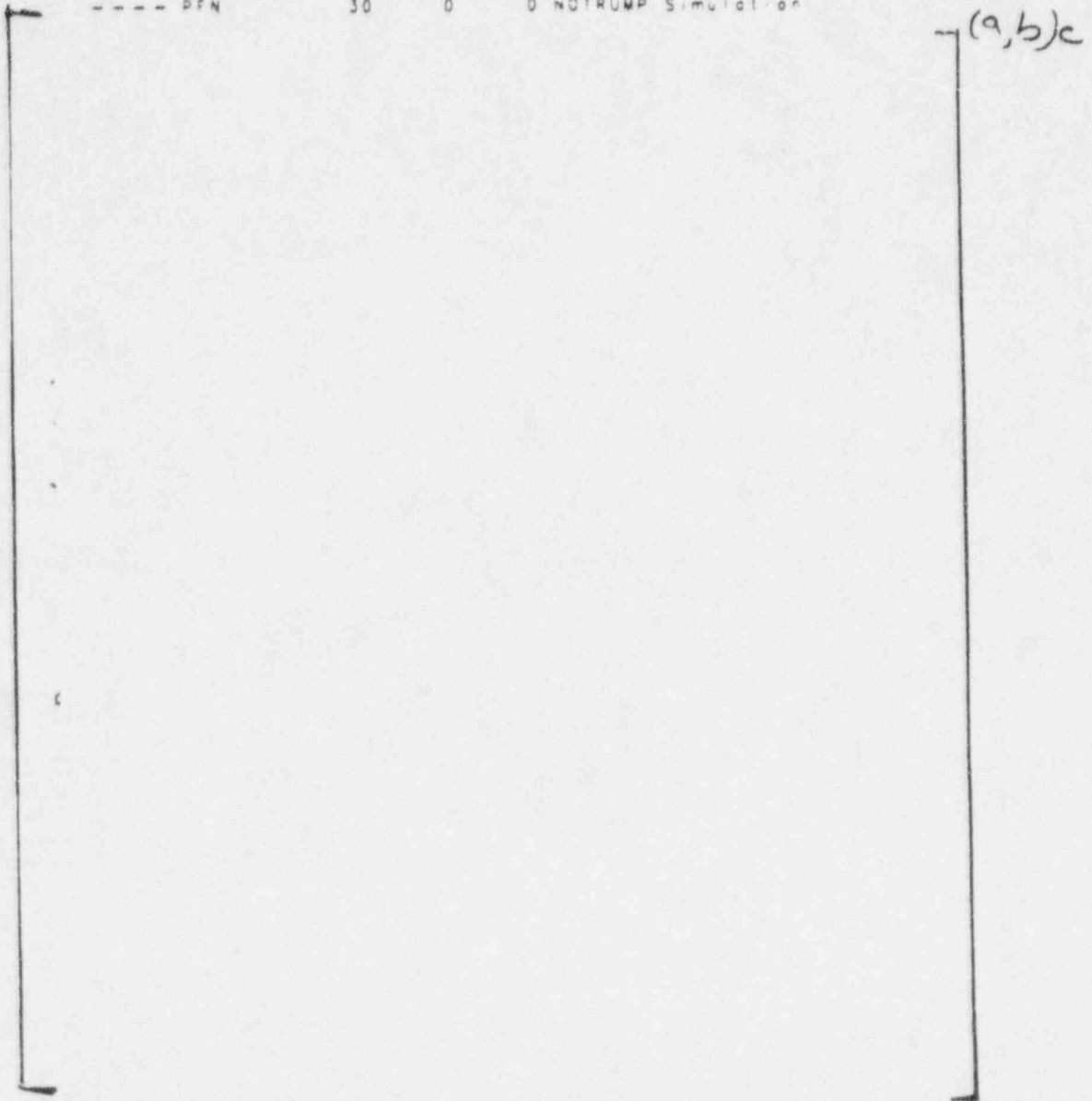


Figure 440.512-10



Steam Generator 2 Secondary Level (SB09)

———	MTH00009	1	0	0 Test Data
----	MTH00007	30	0	0 NOTRUMP Simulation

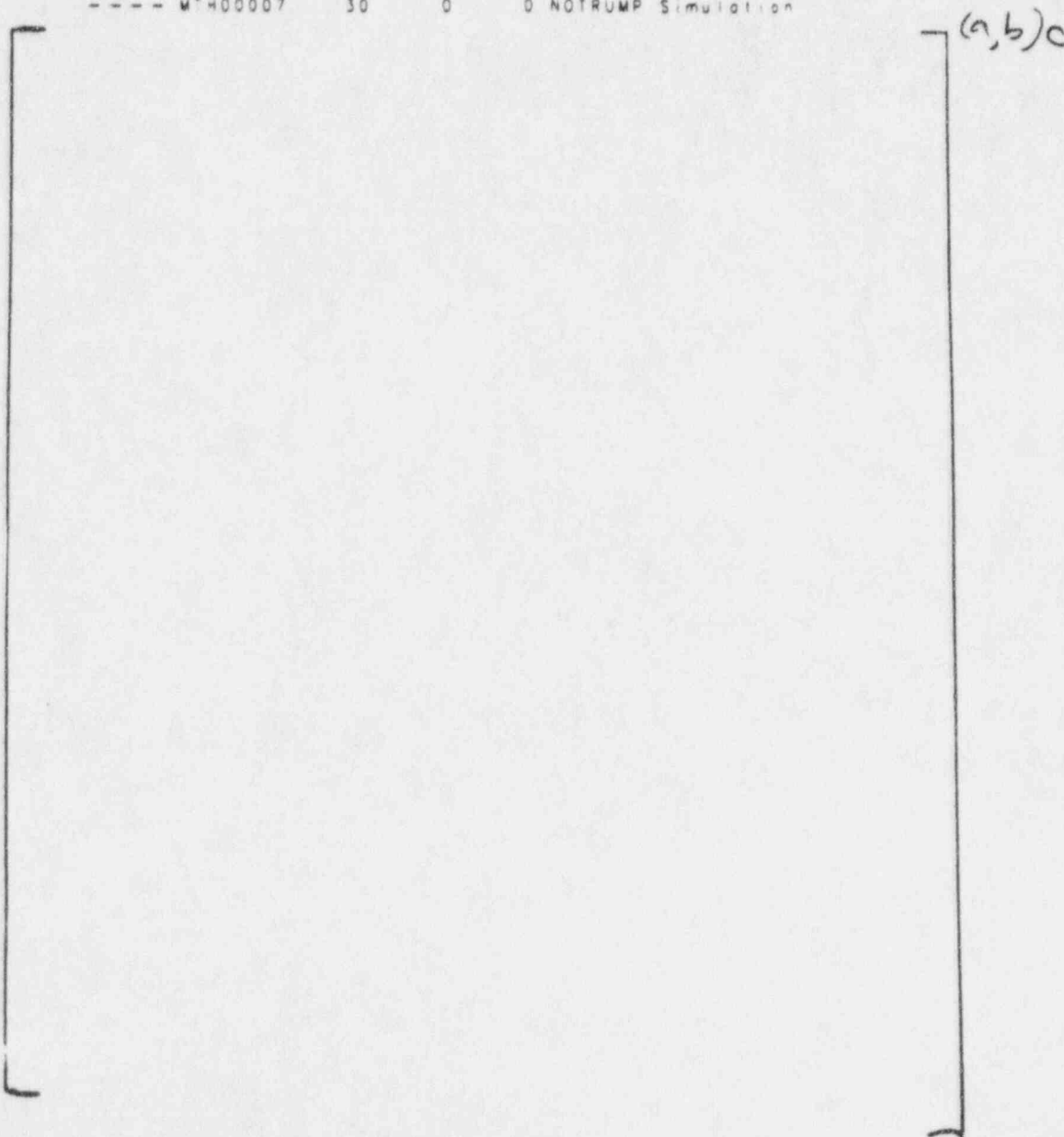


Figure 440.512-11

NRC REQUEST FOR ADDITIONAL INFORMATION



1995/09/15 18:58:36.17 7310493762017  
Facility Name: OSU Test Number: U0009 Date: 09/28/94 Time: 05:45 PM  
----- TF-308 115 3 0 SG-2 Dwnchr CL Side  
----- TF-306 113 3 0 SG-2 Dwnchr HL Side

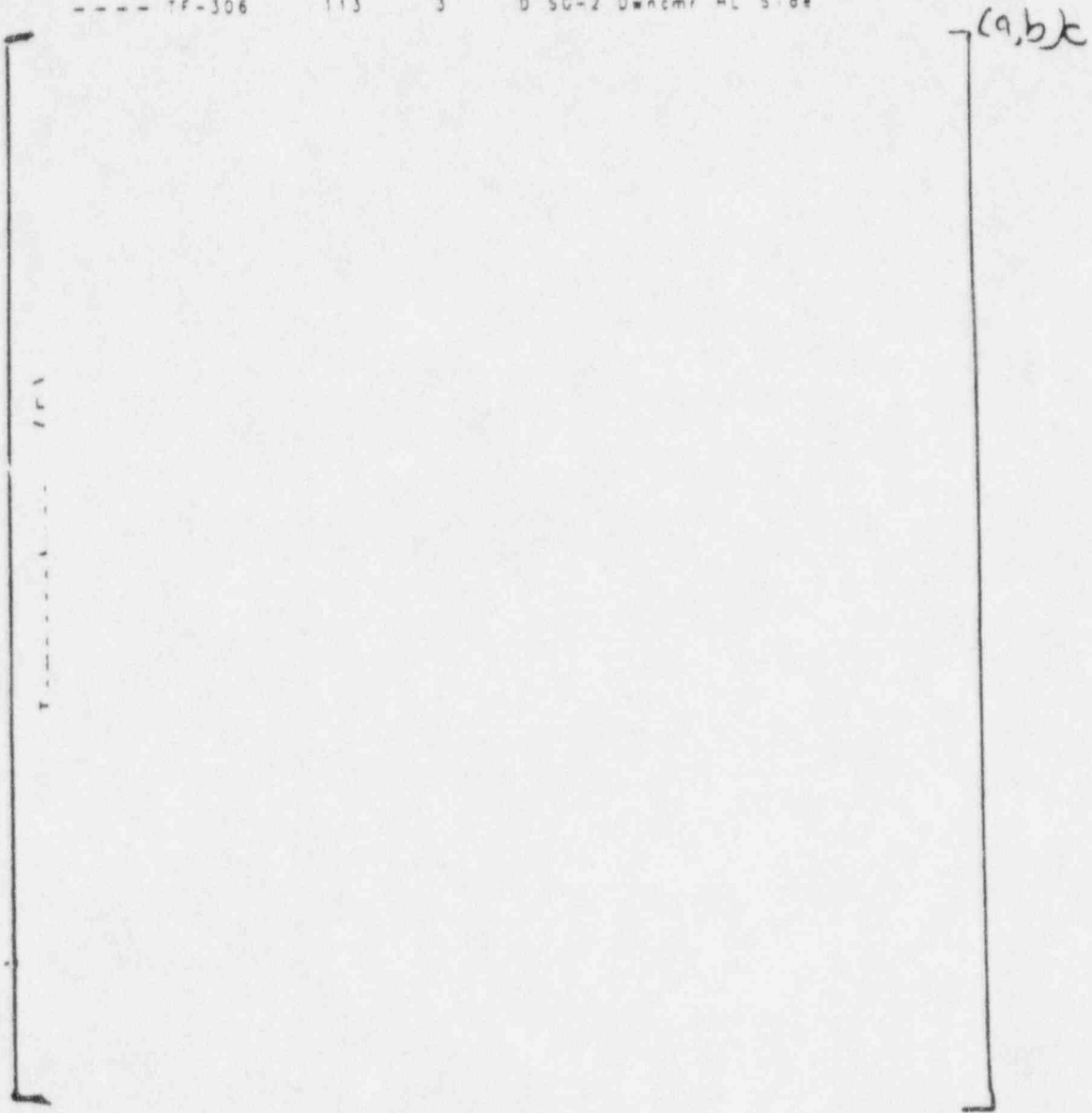


Figure 440.512-12





Steam Generator 1 Secondary Pressure (SB10)  
——— WTH00012 30 1 0 Test Data  
---- PFN 40 0 0 NOTRUMP Simulation

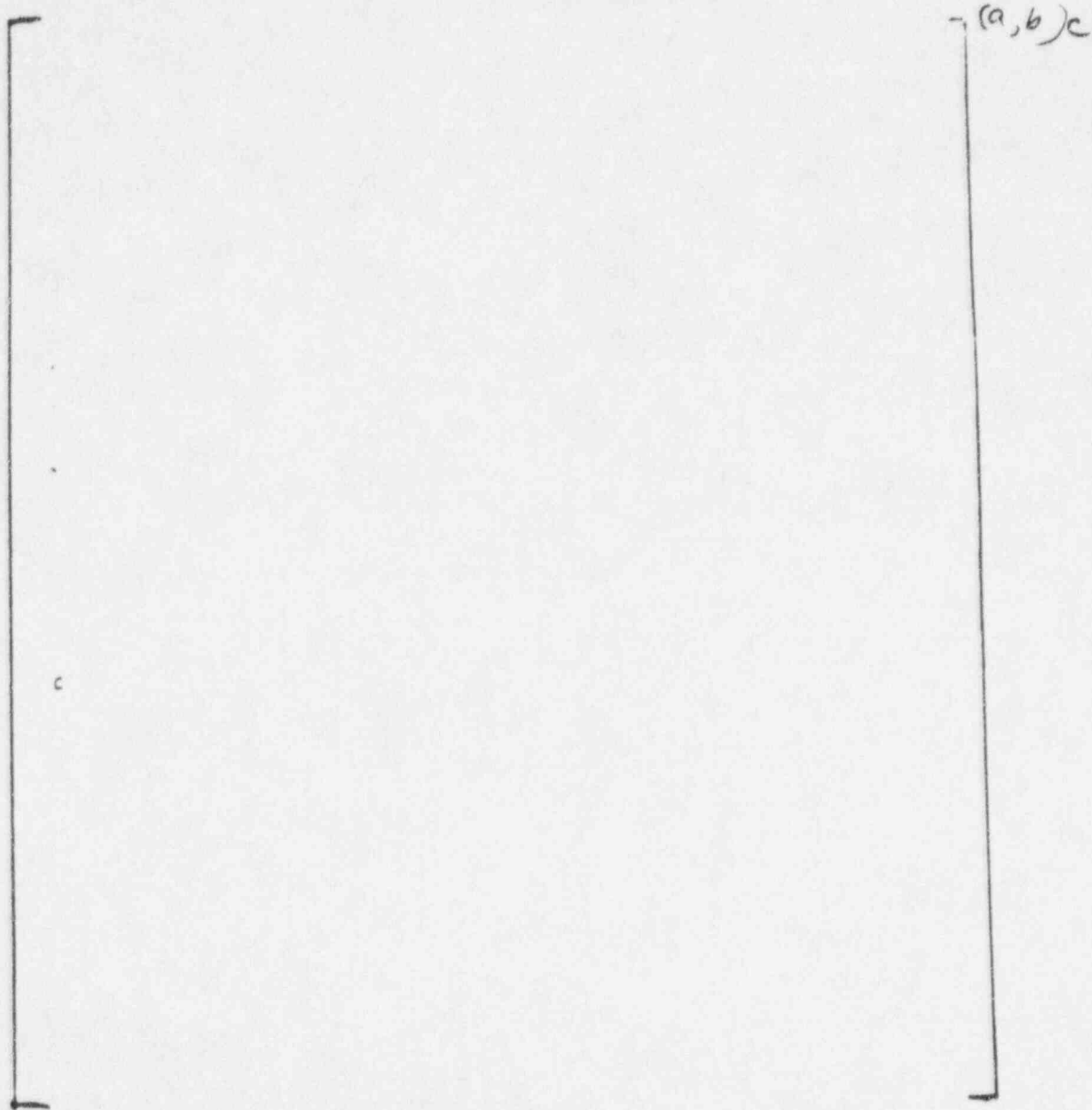


Figure 440.512-13



Steam Generator 1 Secondary Level (SB10)

-----	MTH00008	1	0	0	Test Data
----	MTH00006	40	0	0	NOTRUMP Simulation

(a,b)c

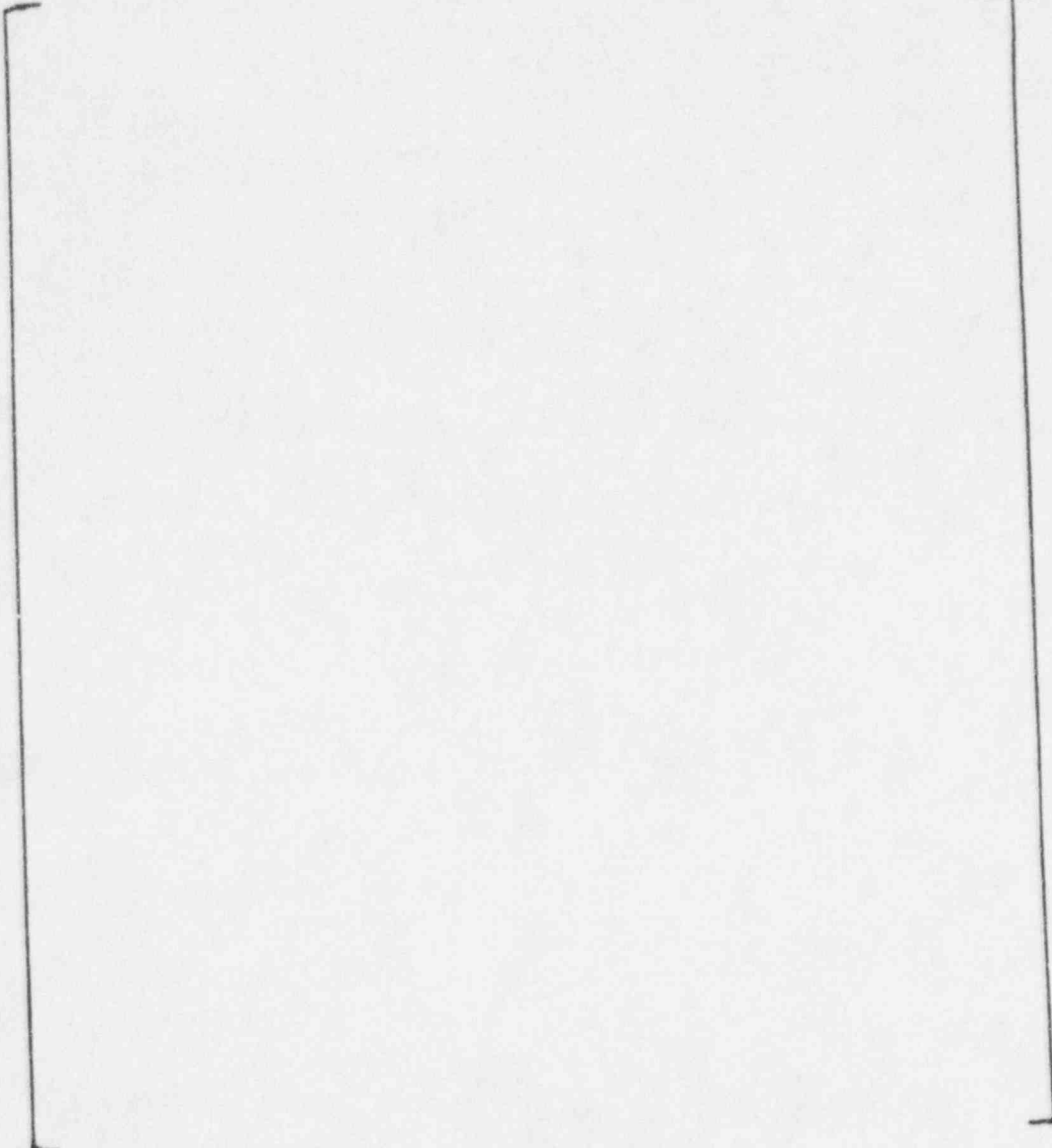


Figure 440.512-14





1995/09/15 19:00:48.26 1192586201773  
Facility Name: OSU Test Number: UO110 Date: 08/24/94 Time: 08:55 PM  
----- TF-307 114 3 0 SG-1 Dwnchr CL Side  
----- TF-305 112 3 0 SG-1 Dwnchr HL Side  
© Westinghouse

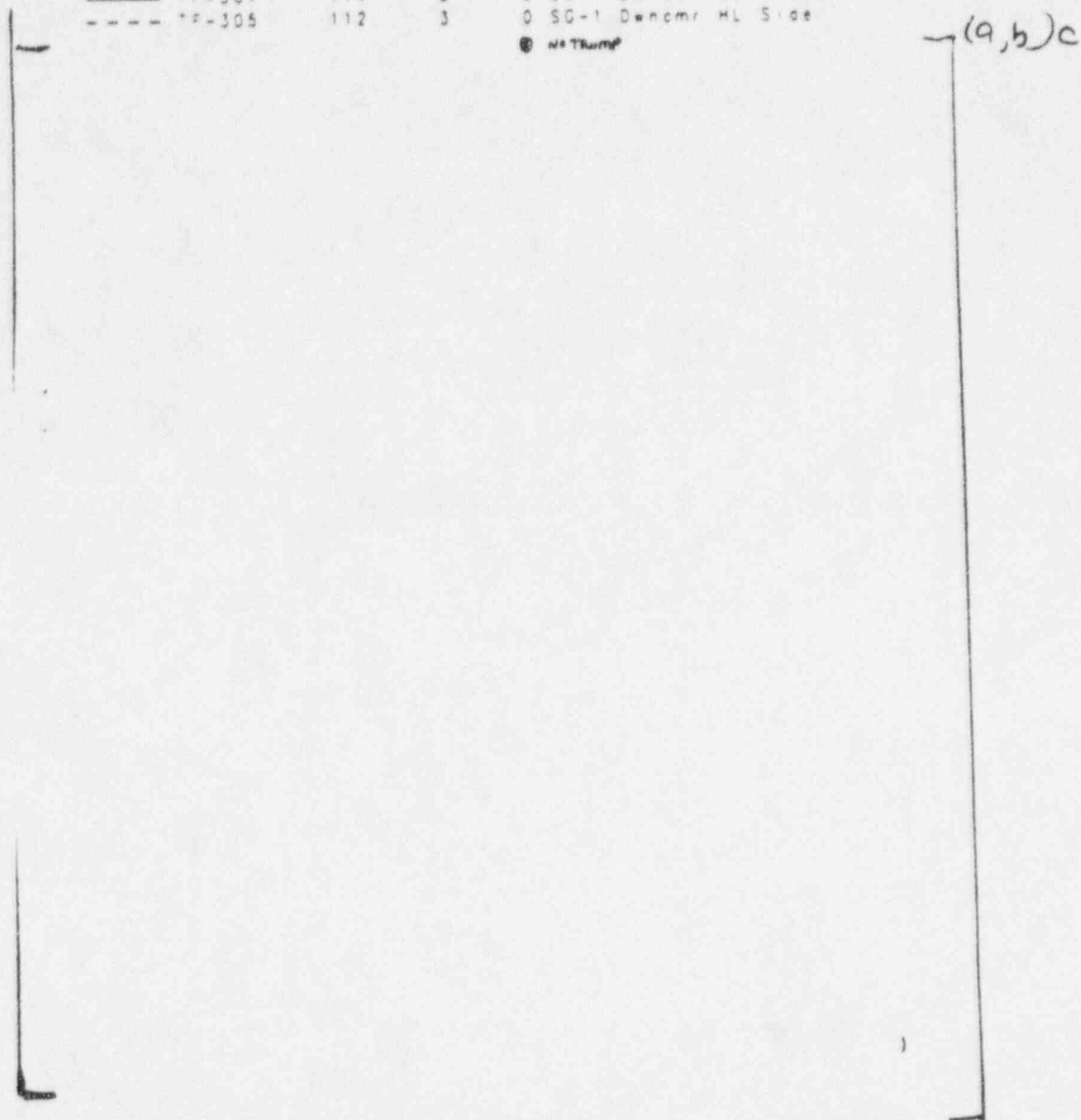


Figure 440.512-15



Steam Generator 2 Secondary Pressure (SB10)

—	MTH00013	14	1	0	Test Data
- - -	PFN	30	0	0	NOTRUMP Simulation

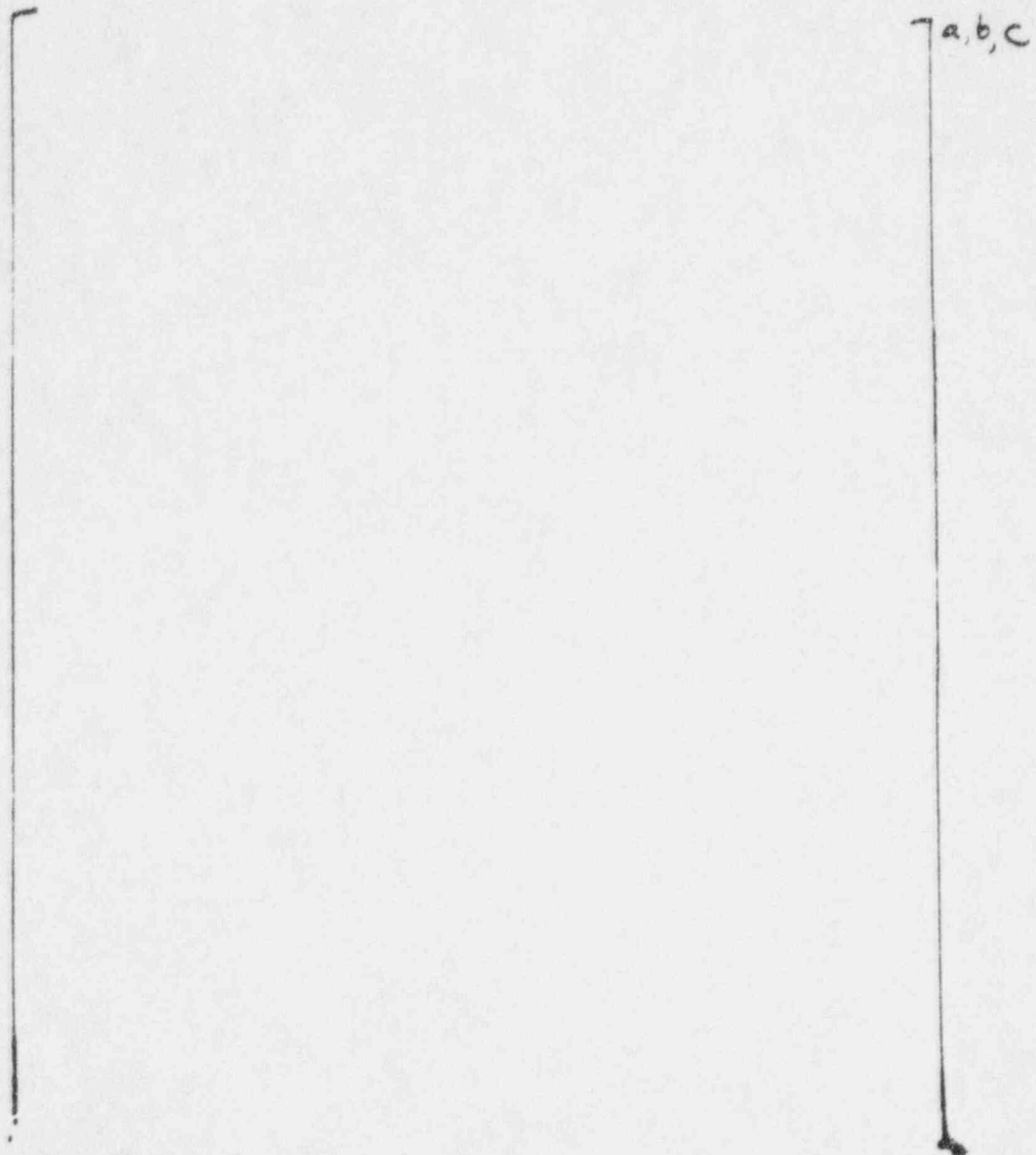


Figure 440.512-16



Steam Generator 2 Secondary Level (SB10)

—	MTH00009	1	0	0	Test Data
- - -	MTH00007	30	0	0	NOTRUMP Simulation

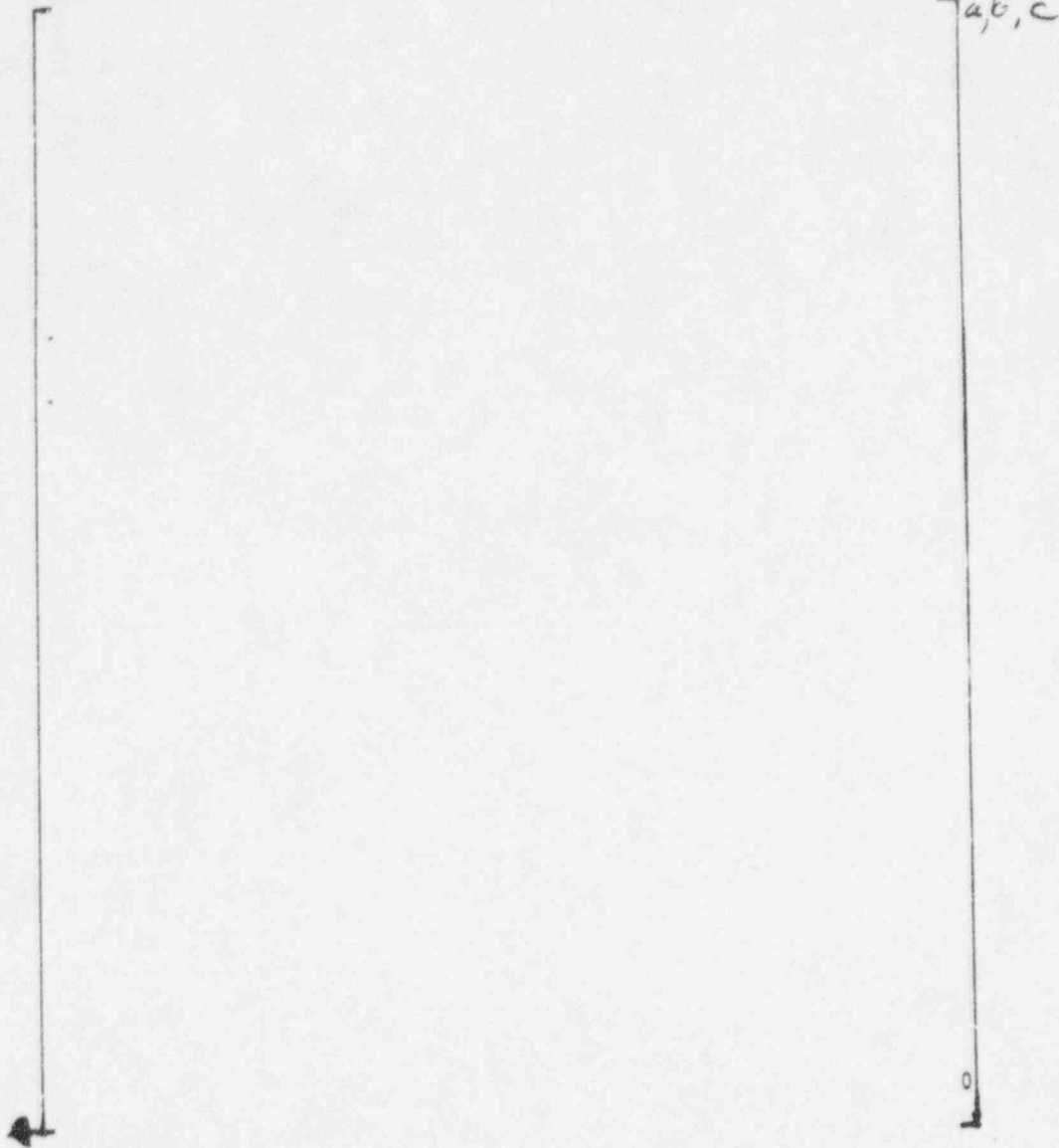


Figure 440.512-17

NRC REQUEST FOR ADDITIONAL INFORMATION



1995/09/15 19:00:48.26 1192586201773  
Facility Name: OSU Test Number: UO110 Date: 08/24/94 Time: 08:55 PM  
---- TF-308 115 3 0 SG-2 Dencmr CL Side  
---- TF-306 113 3 0 SG-2 Dencmr HL Side

Ⓢ NOTRUMP

*da, b, c*

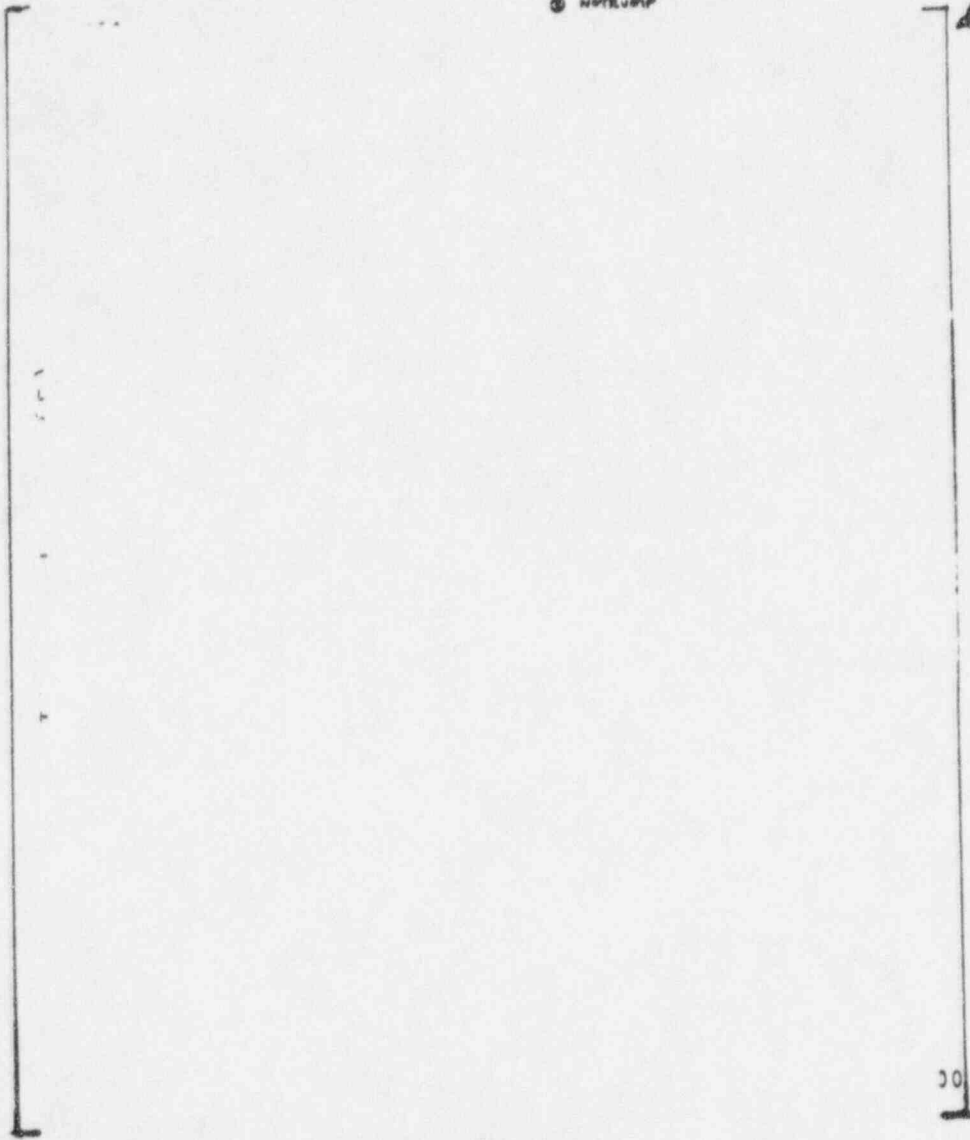


Figure 440.512-18



Steam Generator 1 Secondary Pressure (SB12)

———	WTH00012	34	1	0	Test Data
----	PFN	40	0	0	NOTRUMP Simulation

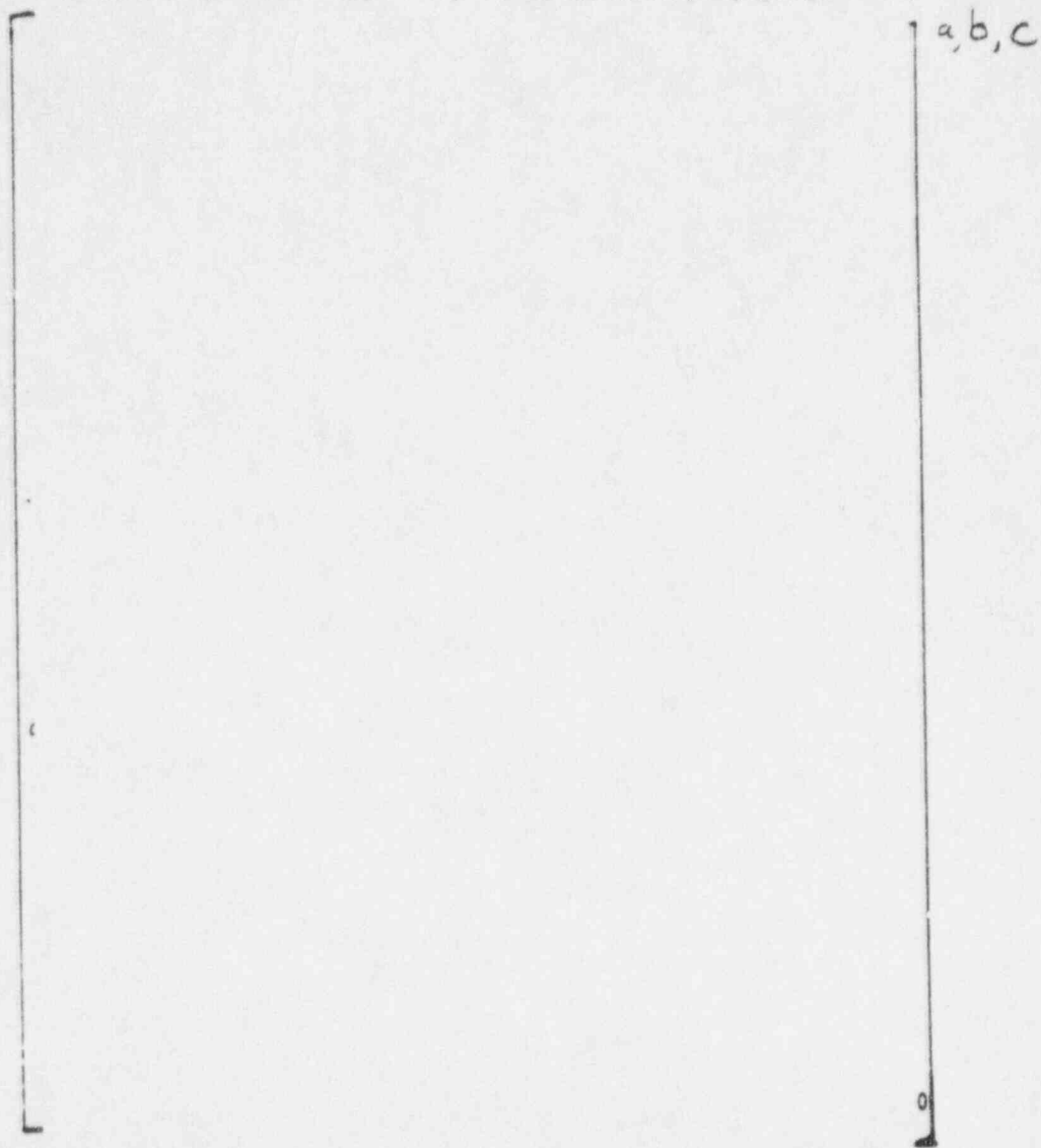


Figure 440.512-19



Steam Generator 1 Secondary Level (SB12)

-----	MTH00008	1	0	0	Test Data
-----	MTH00006	40	0	0	NOTRUMP Simulation

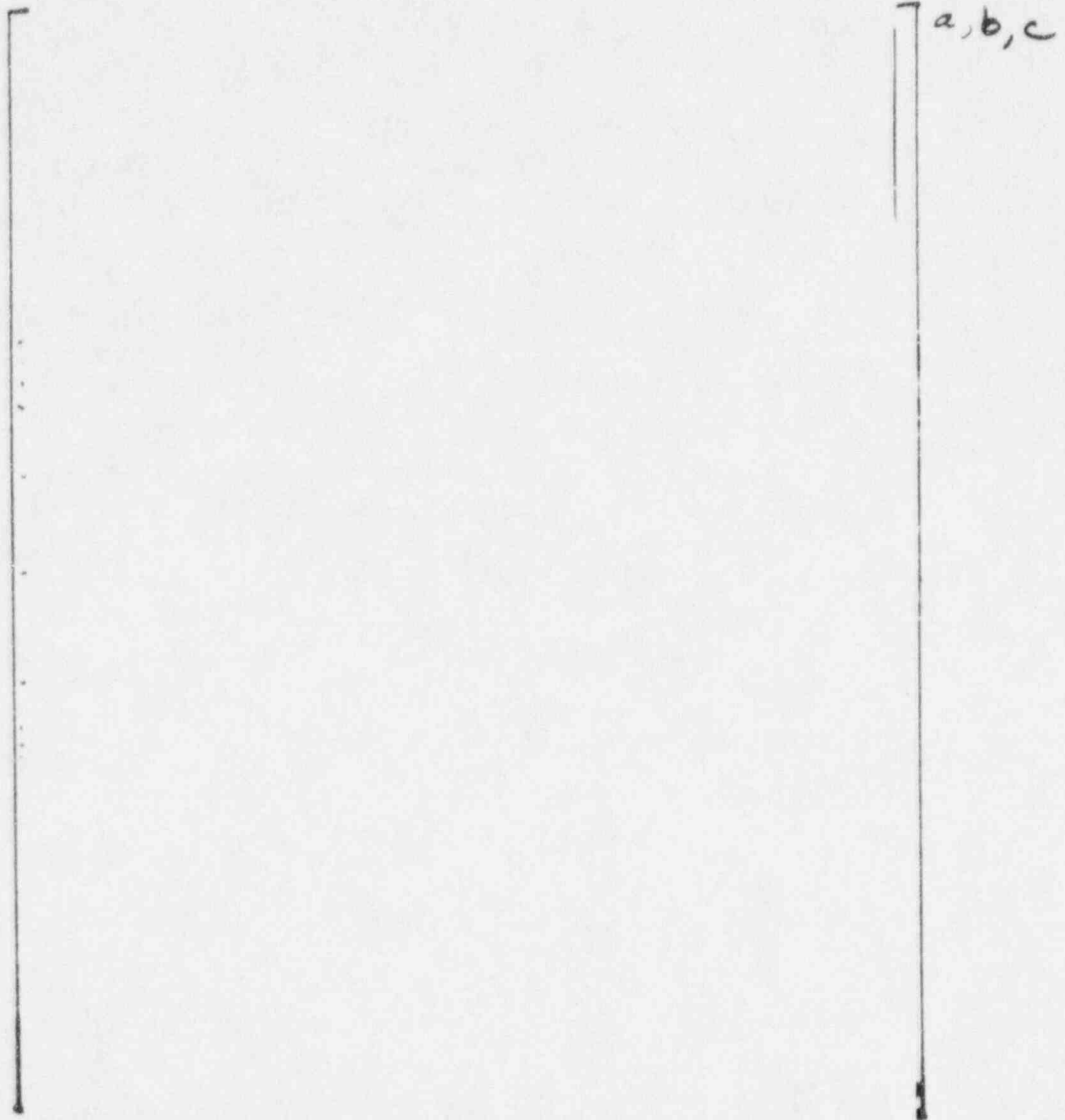


Figure 440.512-20







1995/09/15 19:04:21.81 1196866201773  
Facility Name: OSU Test Number: UD112 Date: 07/21/94 Time: 08:31 AM  
---- TF-307 114 J 0 SG-1 Dwnctr CL Side  
---- TF-305 112 J 0 SG-1 Dwnctr HL Side  
Ⓢ NOTRUMP

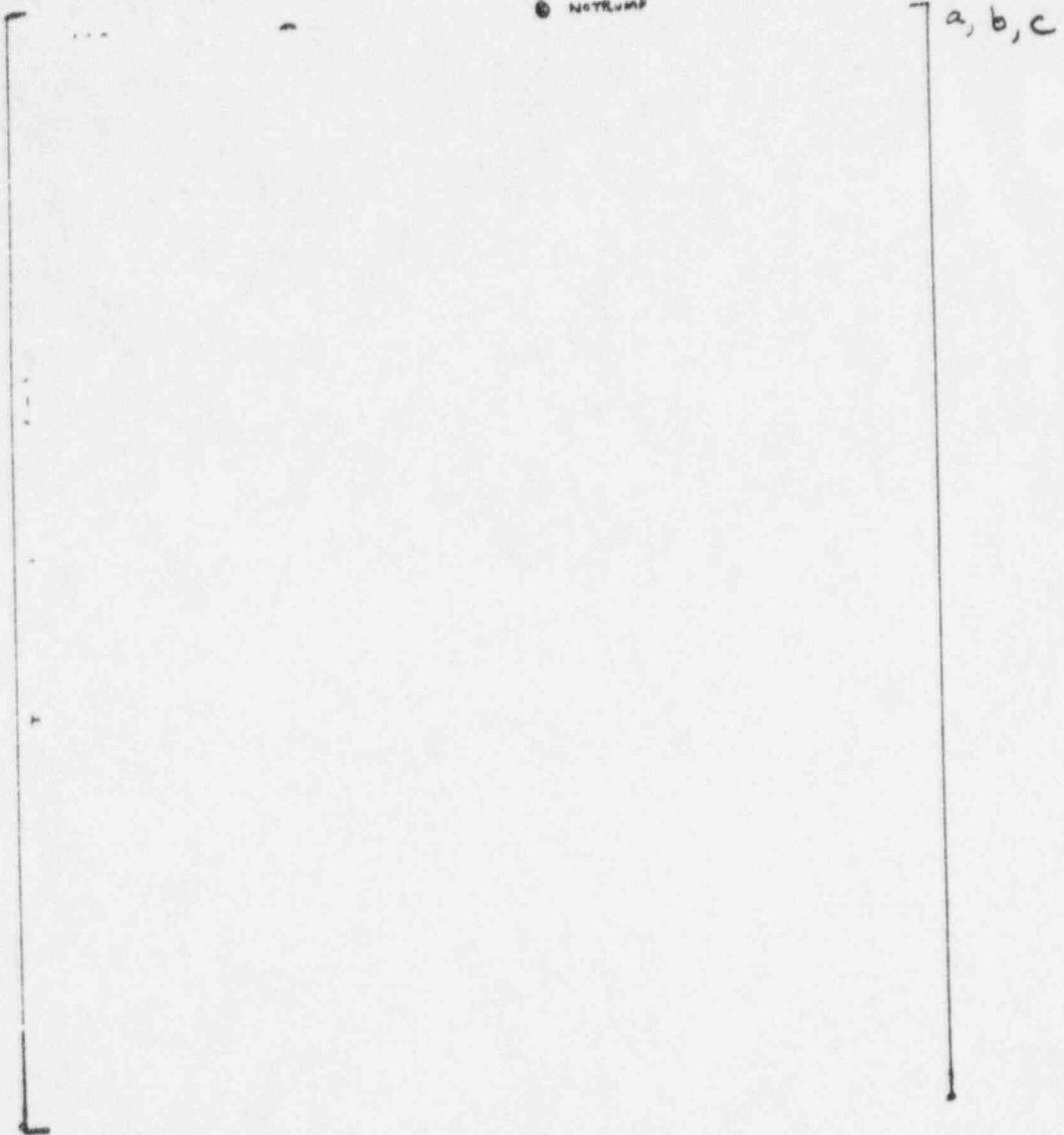
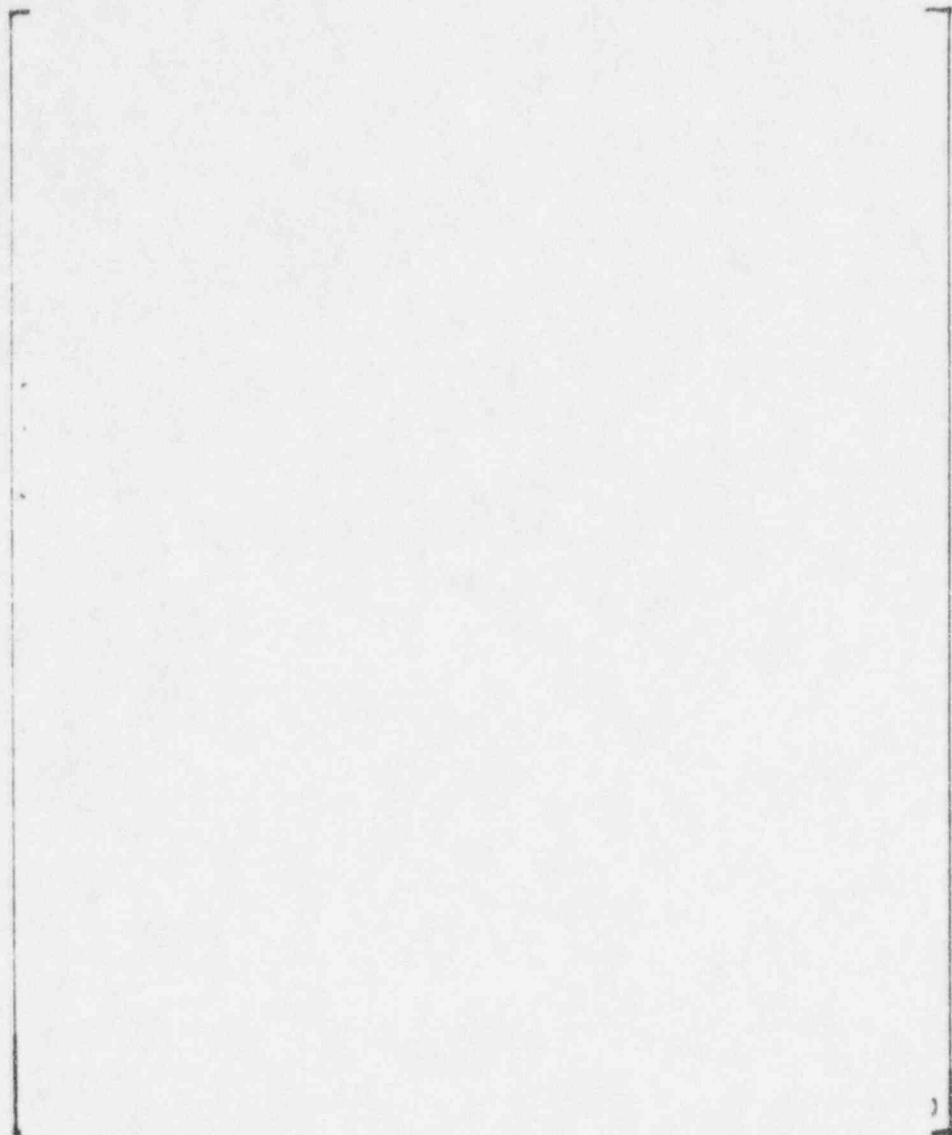


Figure 440.512-21



Steam Generator 2 Secondary Pressure (SB12)  
----- MTH00013 16 1 0 Test Data  
----- PFN 30 0 0 NOTRUMP Simulation



a,b,c

Figure 440.512-22



Steam Generator 2 Secondary Level (SB12)

-----	MTH00009	1	0	0	Test Data
----	MTH00007	30	0	0	NOTRUMP Simulation

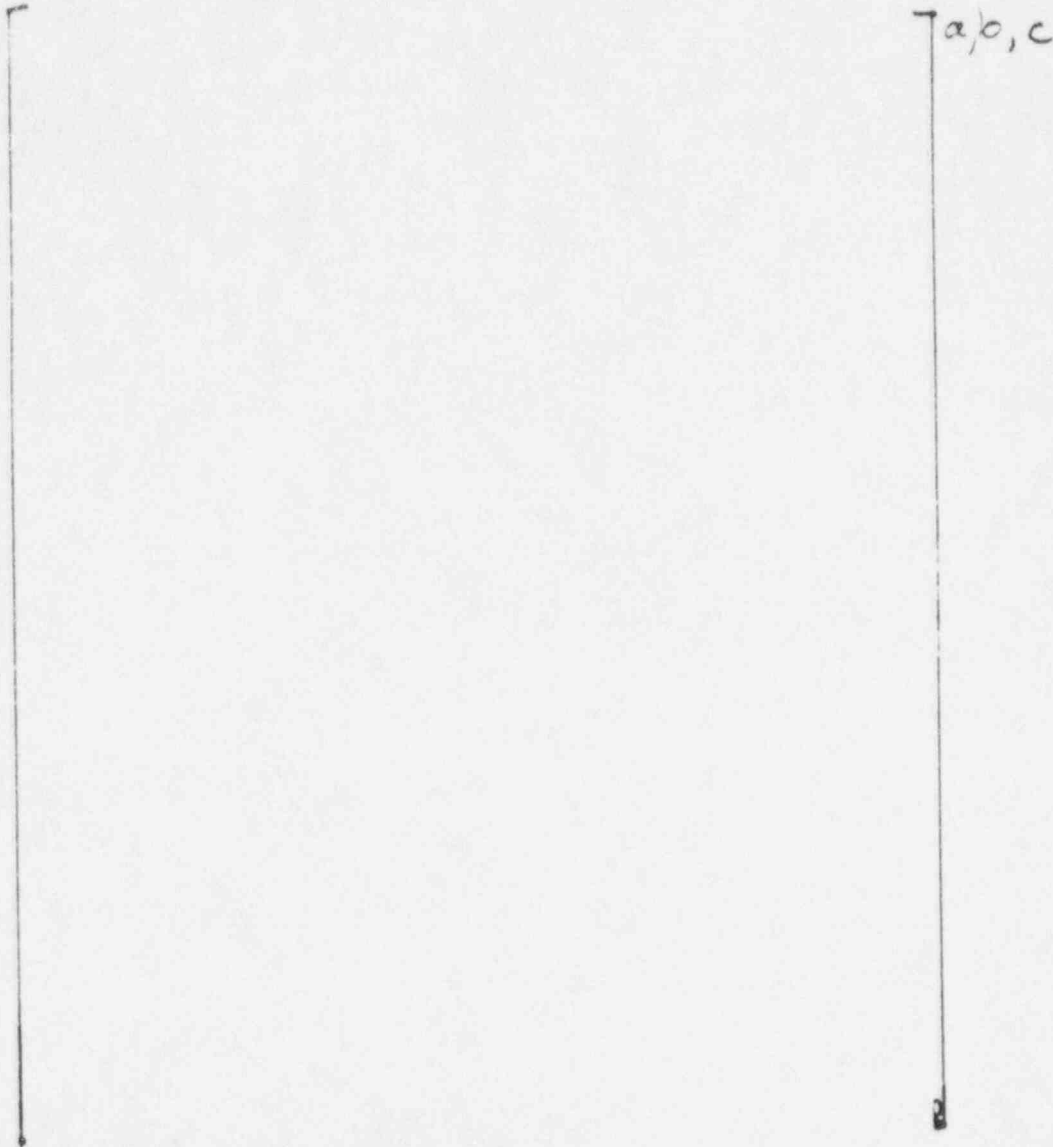


Figure 440.512-23

NRC REQUEST FOR ADDITIONAL INFORMATION



1995/09/15 19:04:21.81 1196866201773  
Facility Name: OSU Test Number: U0112 Date: 07/21/94 Time: 08:31 AM  
----- TF-308 115 3 0 SG-2 Dencmr CL Side  
----- TF-306 113 3 0 SG-2 Dencmr HL Side  
© WRRump

(a, b), c

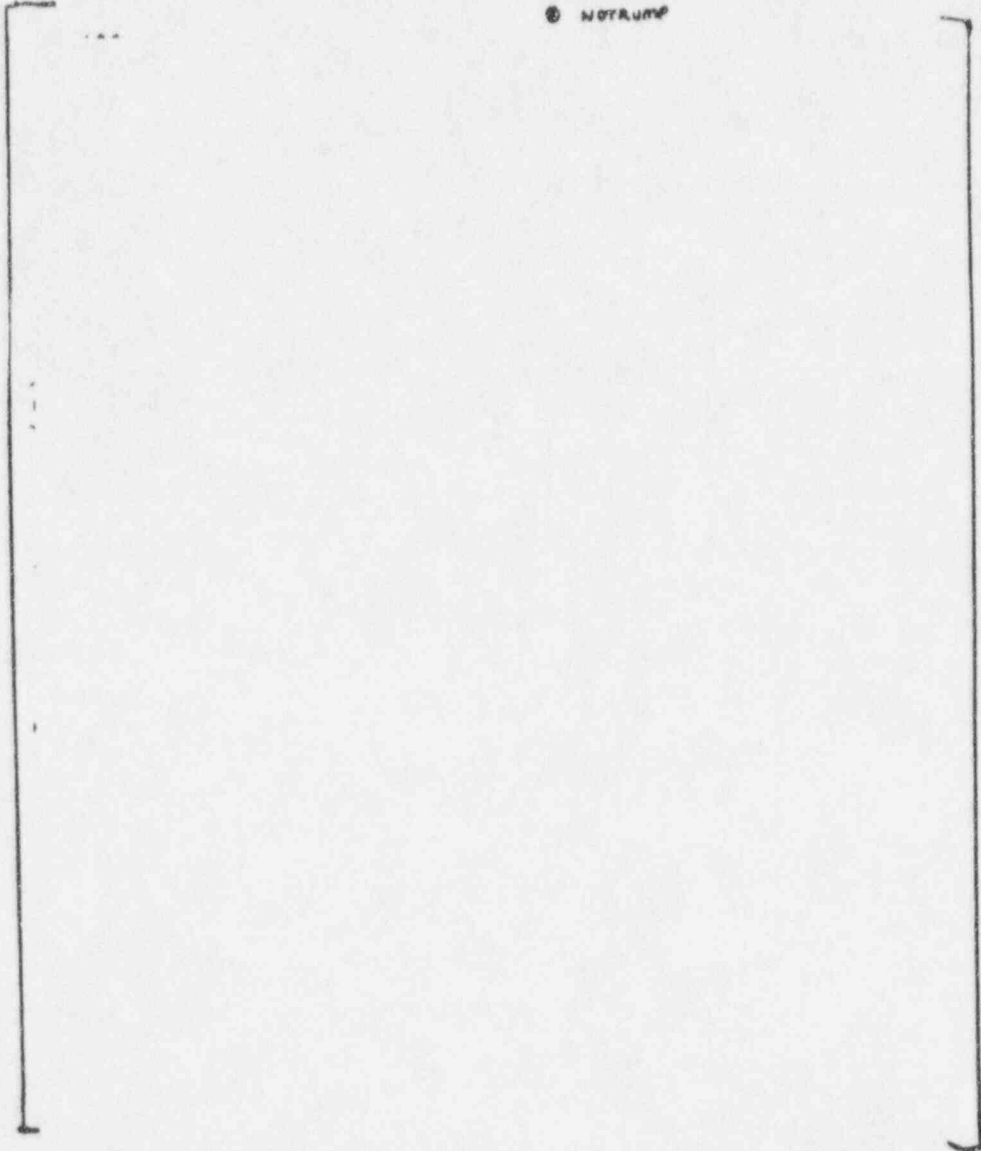


Figure 440.512-24

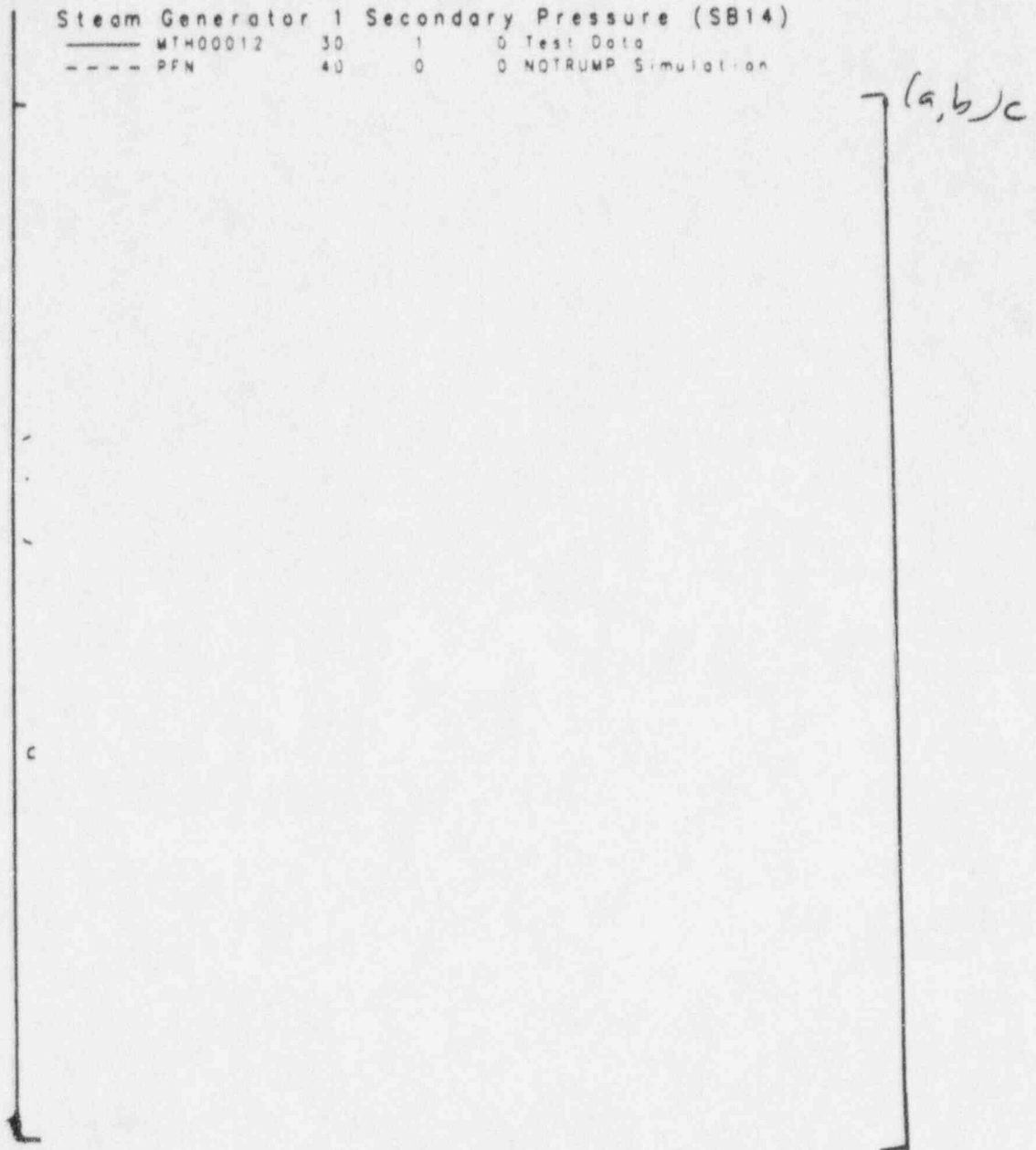


Figure 440.512-25



Steam Generator 1 Secondary Level (SB14)

-----	MTH00008	1	0	0	Test Data
-----	MTH00006	40	0	0	NOTRUMP Simulation

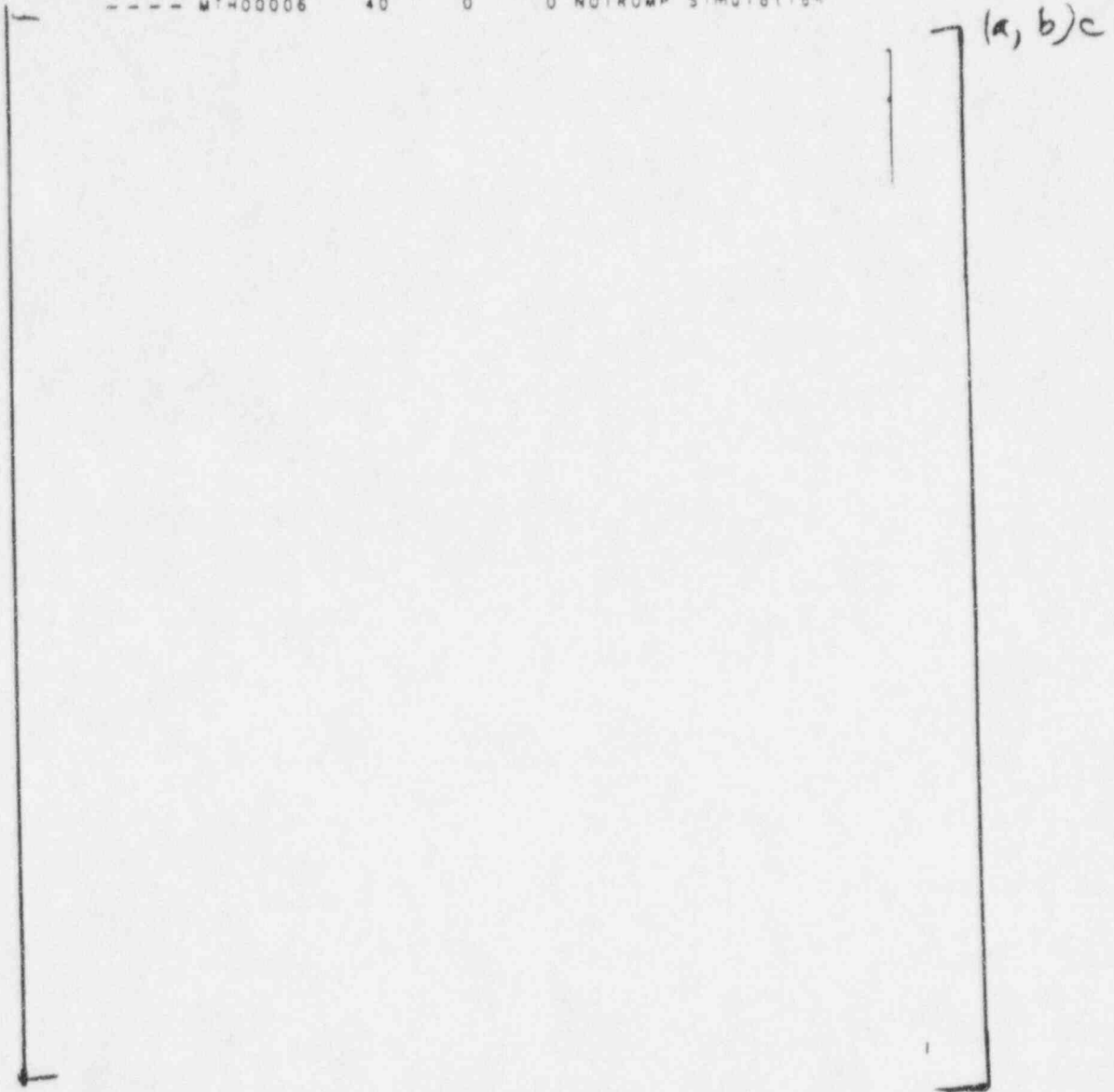


Figure 440.512-26



1995/09/15 19:09:33.87 1124276201773  
Facility Name: OSU Test Number: UO014 Date: 07/07/84 Time: 05:01 PM  
----- TF-307 114 3 0 SC-1 Dwnchr CL Side  
----- TF-305 112 3 0 SC-1 Dwnchr HL Side  
Ⓢ NETBURP

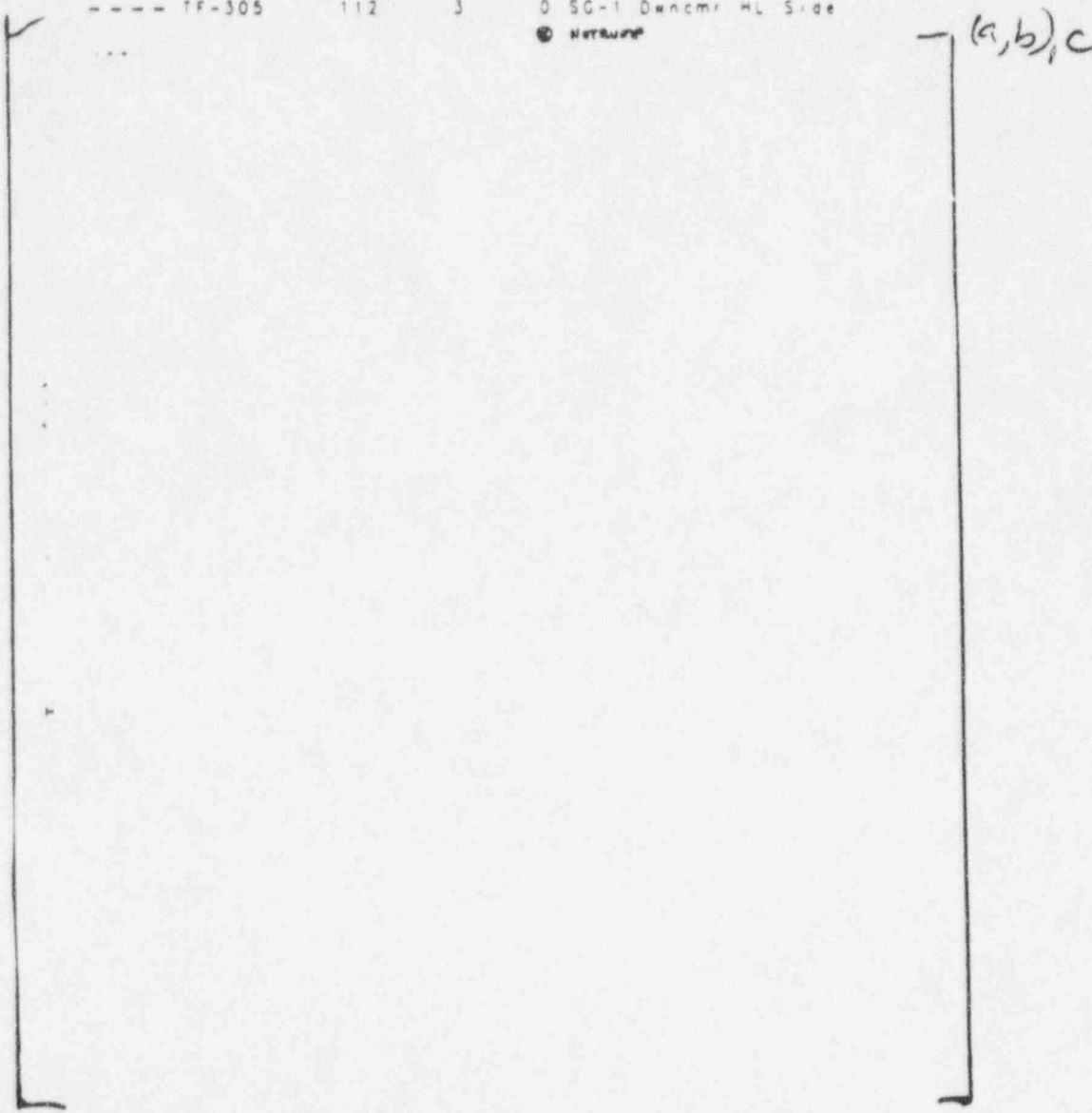
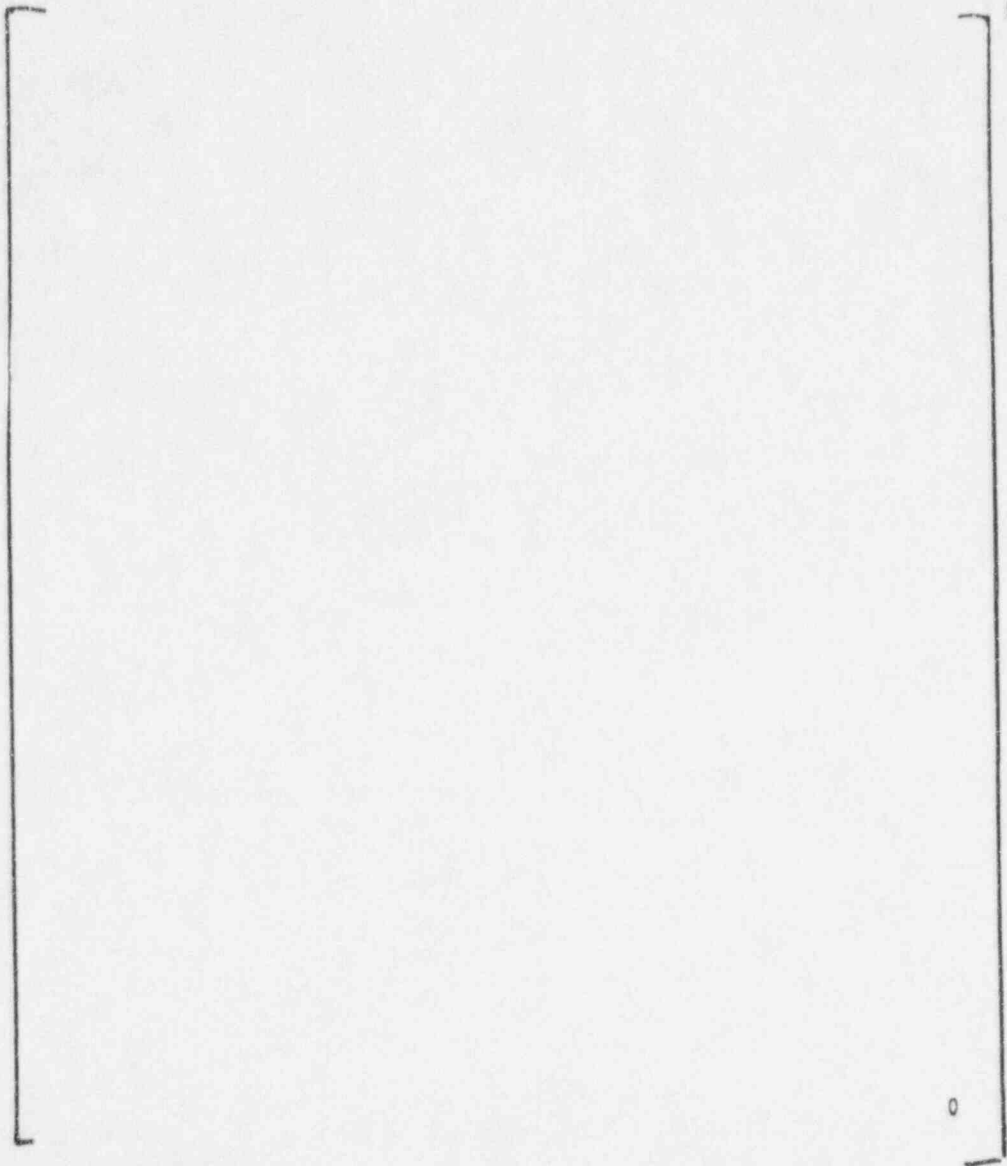


Figure 440.512-27



Steam Generator 2 Secondary Pressure (SB14)  
----- MTH00013 14 1 0 Test Data  
----- PFN 30 0 0 NOTRUMP Simulation



(a,b),c

Figure 440.512-28

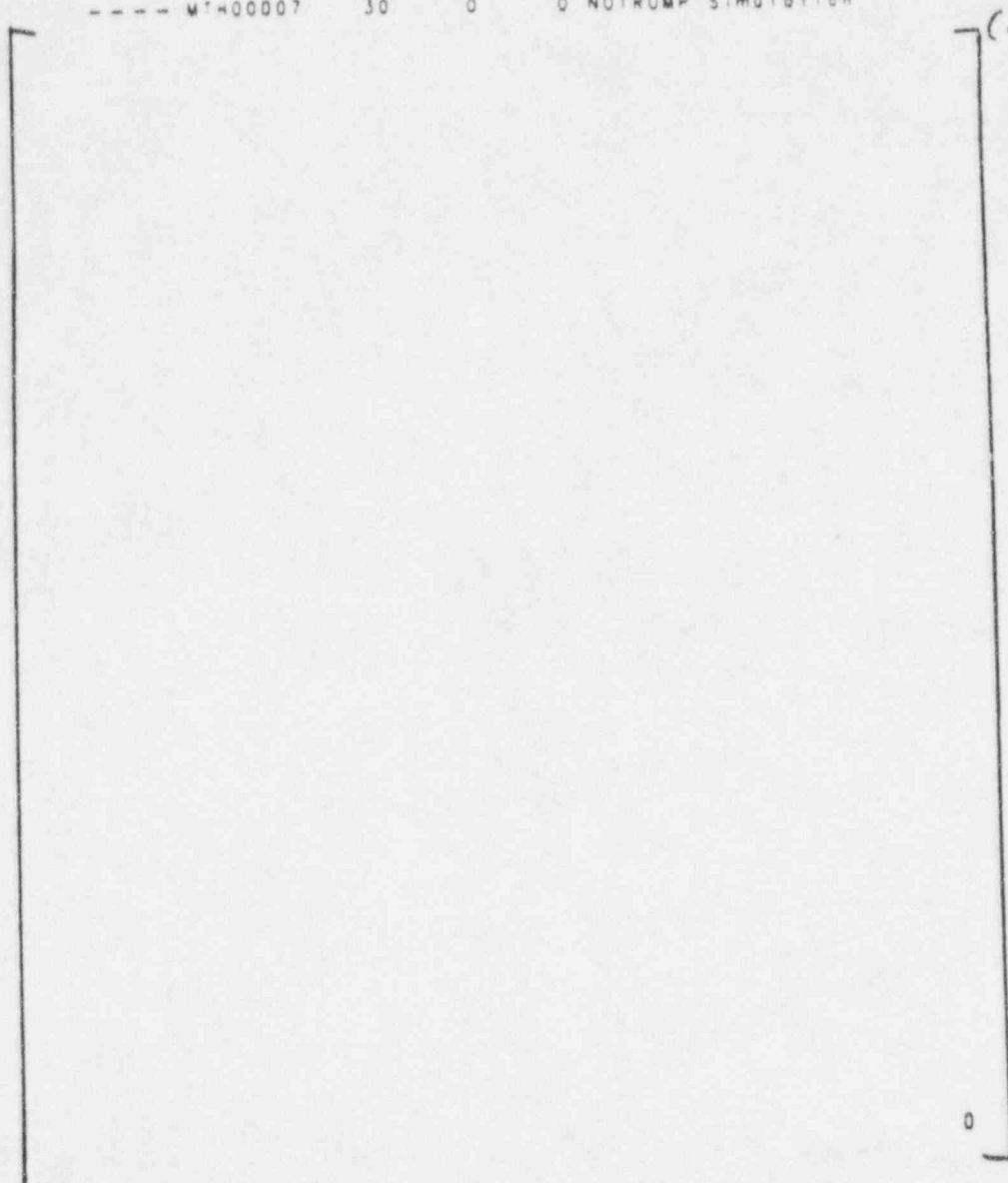






Steam Generator 2 Secondary Level (SB14)

-----	MTH00009	1	0	0	Test Data
-----	MTH00007	30	0	0	NOTRUMP Simulation



(a, b), c

0

Figure 440.512-29



1995/09/15 19:09:33.87 1124276201773  
Facility Name: OSU Test Number: U0014 Date: 07/07/84 Time: 05:01 PM  
----- TF-308 115 3 0 SC-2 Dencmr CL Side  
----- TF-306 113 3 0 SC-2 Dencmr HL Side  
Ⓢ NotRump

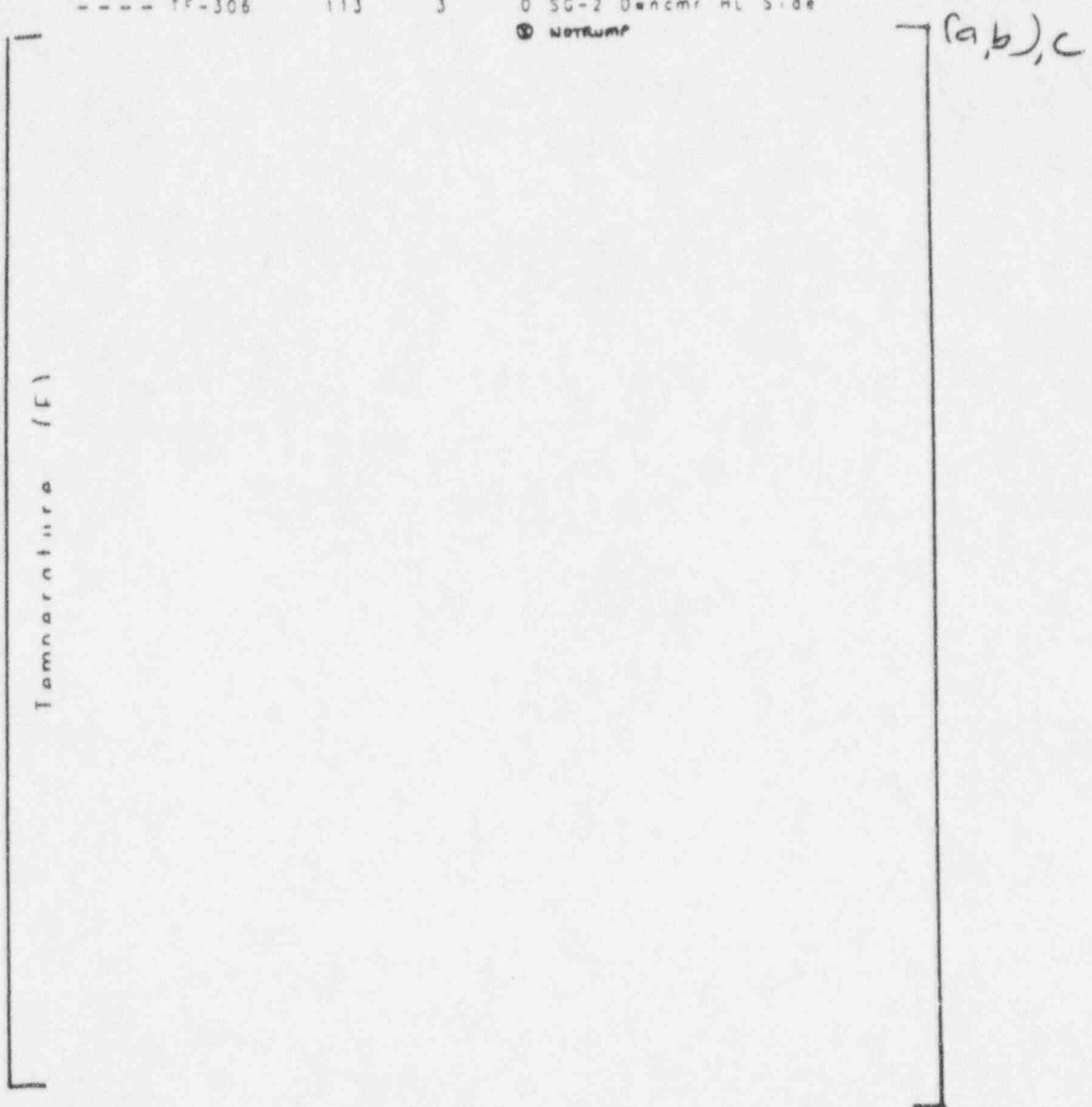


Figure 440.512-30



## NRC REQUEST FOR ADDITIONAL INFORMATION



Question 440.514

Re NOTRUMP PVR FOR OSU TESTS, LTCT-GSR-001, JULY 1995

In general, NOTRUMP overpredicted the flow rates from the IRWST. In particular, for the two inch cold leg break, NOTRUMP predicted a much earlier injection initiation as well as over-predicted the flow rates. Given the non-conservatism associated with the NOTRUMP IRWST injection, the code predictive capability is questionable for assessing the potential for core uncover during the long term for small break LOCAs in AP600. Please justify that this NOTRUMP code deficiency will not restrict the code from assessing the potential for long term core uncover.

Response:

Figures 5.1-21 and 22 of Reference 440.514-1 indicate that NOTRUMP predicts earlier IRWST injection than occurred during Test SB01. However, the same is not true for any of the other NOTRUMP OSU test simulations therein. The SB14 NOTRUMP simulation predicts the initiation time of IRWST injection to be very close to the test data for one DVI line and later than the test for the other. For Test SB09, the NOTRUMP prediction of initiation of IRWST injection (Reference 440.514-2) is the same as the test data for one DVI line and after the test time for the other. Moreover, the NOTRUMP prediction of IRWST injection initiation occurs well after the test data in both the SB10 and the SB12 simulations. Accuracy in predicting the initiation of IRWST injection is a consequence of predicting the system depressurization accurately. No non-conservative bias exists which causes NOTRUMP to predict initiation of IRWST flow too early.

As regards long term core uncover, NOTRUMP is not used for the post-LOCA long-term cooling calculations of AP600; the WCOBRA/TRAC computer code is being validated against the OSU test data for this purpose (Reference 440.514-3). NOTRUMP is applied in the AP600 small break LOCA analyses (Reference 440.514-4) only until stable, sustained IRWST injection is computed. Predicted IRWST injection rates after initiation at the end of the depressurization phase of the small break LOCA transients exceed the initial test flowrates but later agree well with the data (Reference 440.514-5).

References:

- 440.514-1 M.G. Willis et.al., "LTCT-GSR-001:NOTRUMP Preliminary Validation Report for OSU Tests," Westinghouse Electric Corporation, July 1995.
- 440.514-2 M.G. Willis et.al., "LTCT-GSR-004: Addendum to NOTRUMP Preliminary Validation Report for OSU Tests," Westinghouse Electric Corporation, September 1995.
- 440.514-3 S.K. Chow et.al., "LTCT-GSR-003: WCOBRA/TRAC OSU Long-Term Cooling Preliminary Validation Report," Westinghouse Electric Corporation, August 1995.
- 440.514-4 Letter NTD-NRC-95-4503, "Preliminary Marked Up Sections of SSAR Chapter 15, Revision 5", July 10, 1995.
- 440.514-5 Response to RAI 440.510, November, 1995, Attachment A to Westinghouse Letter NTD-NRC-95-4587, November 3, 1995

SSAR Revision: NONE

## NRC REQUEST FOR ADDITIONAL INFORMATION



Question 480.223

Re: Questions on OSU Data:

In addition to the specific issue of CMT refill, the staff requests that Westinghouse evaluate the potential for other large pockets of saturated or superheated steam that might exist in the AP600 primary system to undergo rapid refill due to cold water contact with the steam. Examples of such volumes of steam include: pressurizer, steam generator channel heads, and the PRHR heat exchangers. The evaluation should conform to the same general guidelines as those stated in the previous question.

Response:

As noted, pockets of saturated or superheater steam may exist in the pressurizer, steam generator channel heads, and PRHR heat exchangers. However, no evidence of rapid condensation of steam in these components was detected at the OSU facility.

Although the pressurizer could often be filled with saturated steam, there are no readily apparent mechanisms for transporting the cold water to the pressurizer and mixing the cold water with the steam to produce rapid condensation. A slow depressurization due to condensation would not occur in the pressurizer due to the vacuum breaker on the ADS discharge line. Therefore, water in the surge line would not rise to the bottom of the pressurizer.

The SG channel heads could also be filled with either saturated or superheated steam. However the SG channel heads at the OSU facility did not experience any rapid condensation, even during system wide oscillations which caused channel head level to rise and fall. This indicates that a hot layer of water must have quickly formed on any water which rose into the channel head and/or sufficient mixing did not take place to allow rapid condensation.

Steam could also exist for periods of time at the top of the PRHR heat exchanger, however for most small break LOCAs at the OSU facility, steam flow to the PRHR stopped and the inlet temperature decreased slowly over the long term. For large break LOCAs, the steam flow to the PRHR heat exchanger was continuously condensed and returned to the cold legs. In addition, for rapid condensation to occur, sufficient mixing of the hot steam with the cold water must occur. The source of the cold water could not be from the PRHR inlet line due to arrangement of the piping at the top of the heat exchanger. Water from the bottom of the heat exchanger would contact the steam inside the heat exchanger tubes, providing limited surface area and mixing for rapid condensation.

The scaling of the OSU test facility (Reference 480.223-1) assured that the system response was appropriate. Any distortion would likely result in increased occurrence of condensation events because of 1/4 length piping, as occurred in the Core Makeup Tanks. Because no rapid condensation events occurred in the pressurizer, PRHR or steam generators at the OSU facility, no evidence exists which would indicate that rapid condensation would occur in these components in the AP600 plant.

NRC REQUEST FOR ADDITIONAL INFORMATION



---

Reference

480.223-1 WCAP-14270, Revision 0, "Westinghouse AP600 Long Term Cooling Test Facility Scaling Report,"  
January 1995

SSAR Revision: NONE

## NRC REQUEST FOR ADDITIONAL INFORMATION



Question 480.243

Re: OSU/APEX Pre-Operational Tests, Tests OSU-V-01 through -V-08:

The information in the report on CMT volume does not correspond to the characterization information needed due to the change in ADS logic. The necessary information must be interpolated from that given in the report.

Response:

Section 4.1.2 of Reference 480.243-1 describes the test performed to determine the volume of the core makeup tanks at the OSU facility. Tables 4.1-5 and 4.1-6 provide the test data obtained for CMT-1 and CMT-2 respectively. The setpoint used for ADS-1 operation was 41 inches in either of the CMTs. The setpoint used for ADS-4 operation was 17.1 inches in either CMT. The volume of the CMT at 41 inches is approximately 75% and the volume at 17.1 inches is approximately 26%. These setpoints/volumes were used in evaluating the test data from the OSU facility.

Reference

480.243-1 WCAP-14252, "AP600 Low Pressure Integral System Test at Oregon State University: Final Data Report," Proprietary [LTCT-T2R-100], May 1995.

SSAR Revision: NONE

**NRC REQUEST FOR ADDITIONAL INFORMATION**



Question 480.246

Re: Test OSU-HS-02:

The explanation of the test procedure is not entirely clear. For test U-2001, the procedure says (p. 5-1) that the "cold leg break [was] isolated," and that the "new break was ADS stage 1 valve opening." This would seem to indicate that there was no break in the cold leg, and the system was allowed to blow down through the ADS valve. Similar statements are made for tests U-2002 and U-2003. However, from the table on the following page, it appears that the break valve was open in addition to the ADS valves indicated for these three tests. Westinghouse should clarify this part of the report.

Response:

Test U-2001 simulated an inadvertent opening of the ADS-1 valve at low pressure. Tests U-2002 and U-2003 were low pressure tests of each of the ADS-4 valves. The break valve was not opened for any of these tests.

SSAR Revision: NONE

## NRC REQUEST FOR ADDITIONAL INFORMATION



Question 480.247

Re: Test OSU-HS-02:

The "dip" on LDP-140 is explained as possibly a bubble in the upper head collapsing. This behavior is observed in all of the tests. Considering the consistency of the behavior from test to test (only the timing of the dip seems to change), further discussion and characterization of this behavior is appropriate. This discussion should address the entire sequence of events, which appears (using LDP-140 as a benchmark) to include a step increase in indicated level at the initiation of the test, a period of constant or slowly increasing level, and a sharp drop thereafter. Westinghouse should address this behavior in more detail.

Response:

Section 7.1 of Reference 480.247-1 provides a discussion of the condensation events which occurred at the test facility. In addition, a description of the entire sequence of events is provided for the matrix tests discussed in section 5 of Reference 480.247-1.

Reference

480.247-1 WCAP-14252, "AP600 Low Pressure Integral System Test at Oregon State University: Final Data Report," Proprietary [LTCT-T2R-100], May 1995.

SSAR Revision: NONE



## NRC REQUEST FOR ADDITIONAL INFORMATION



Question 480.249

Re: Test OSU-HS-03:

Instrument LDP-140 in Test HS-02 is denoted as vessel level from bottom to the upper head bypass. In this test, LDP-140 is denoted as the downcomer level. Were instruments changed between the two tests? If so, this should be noted in the report. If instruments were not changed, please explain the apparent discrepancy in these instrument descriptions.

Response:

LDP-140 provides downcomer level from approximately 2-inches from the bottom of the vessel to the top of the downcomer at the upper head bypass flow holes. No instrument changes were made. Appendix C of Reference 480.249-1 provides an instrumentation data base applicable to the tests. Deviations from the data base are noted in the individual test descriptions.

Reference

480.249-1 WCAP-14252, "AP600 Low Pressure Integral System Test at Oregon State University: Final Data Report," Proprietary [LTCT-T2R-100], May 1995.

SSAR Revision: NONE



Westinghouse

480.249-1

**NRC REQUEST FOR ADDITIONAL INFORMATION**



Question 480.250

Re: Test OSU-HS-03:

The report indicates that the failure to shut off the pressurizer heaters should have no material effect on the test results. This conclusion should be justified.

Response:

The primary purpose of the HS-02 test was to assess the performance of the Break and Measurement System during various types of loss of coolant accidents. The failure of the pressurizer heaters to shut off did not affect the performance of the BAMS.

SSAR Revision: NONE

## NRC REQUEST FOR ADDITIONAL INFORMATION



Question 480.251

Re: Test OSU-HS-03:

The extreme compression in time on the data plots makes it difficult to differentiate specific phenomena. However, some features are relatively clear. For interest, the pressurizer level (Plot 12) shows an almost linear increase over a period of about 2000 seconds, followed by an almost instantaneous emptying at about 6000 seconds. The drop in level also seems to be correlated with features on other plots, such as a sharp increase in flow to the ADS-4 separators (Plots 57, 58); however, there is no indicated change in vessel level. Could this be due to backflow through the ADS 1-3 discharge lines? The staff expects to see these types of interactions described and discussed from the phenomenological standpoint in the Test Analysis Report or in other documentation produced in conjunction with this test program.

Response:

The increase in level in the pressurizer followed by an almost instantaneous emptying at about 6000 seconds was due to a lack of a vacuum breaker on the sparger line inside the IRWST. As the piping and components cooled between the pressurizer and the sparger, the steam condensed inside and the pressure fell, resulting in a slight vacuum in this line. This caused the level to slowly rise in the pressurizer. When the level in the IRWST decreased to the point where the sparger arms uncovered, the vacuum was broken and the level in the pressurizer fell rapidly. Section 5 of Reference 480.251-1 provides a description of events for the matrix tests included in the report.

Reference

480.251-1 WCAP-14252, "AP600 Low Pressure Integral System Test at Oregon State University: Final Data Report," Proprietary [LTCT-T2R-100], May 1995.

SSAR Revision: NONE

## NRC REQUEST FOR ADDITIONAL INFORMATION



Question 480.260

Re: Test OSU SB3:

The BAMS discharge line thermocouples (Plots 75, 76) show considerably different behavior. TF-916 shows that the discharge is largely saturated during the long term portion of the test. However, TF-917 (signal conditioned output) shows significant subcooling in the exhaust flow. Explain this apparent discrepancy.

Response:

Hot leg temperatures (plots 13, 14, 15, 16) indicate that the hot legs are subcooled from about 3800 seconds to about 8000 seconds. This would indicate that no steam is leaving the vessel and exiting the BAMS during this time. Thermocouple TF-917 was on the line used for steam flow during this test. Thermocouple TF-916 was on a closed line. When steam flow dropped, TF-917 experienced a gradual cooldown. When steam flow began again at about 8000 seconds, the cooldown ended and the temperature again began to rise to saturation. Also, it should be noted that the two thermocouples are in two different heat traced zones which are operated by independent controllers. The differences in temperatures are due to a combination of the heat tracing, the open vs. closed pipe, and the steam flow.

SSAR Revision: NONE

## NRC REQUEST FOR ADDITIONAL INFORMATION



Question 480.261

Re: Test OSU SB5:

PT-107 (Plot 1) appears to have a (negative) zero offset, which is not noted in the plot table. If the zero is not offset, explain why this pressure is at a slight vacuum. Other pressure instruments also appear to have offsets that are not explained (e.g., PT 401, 402).

Response:

Many of the pressure indicators at the OSU facility were ranged for indications from 0 to 600 psig. When set for this range, an error analysis of these instruments shows the possibility of approximately 3 psi error in the DAS pressure reading or 0.5% of span. Therefore, these instruments may indicate below zero when in fact the pressure is just above 0 psig, as is the case for PT-107 during the long term transient. Care should be taken when using wide range indications for low pressure measurements.

SSAR Revision: NONE

## NRC REQUEST FOR ADDITIONAL INFORMATION



Question 480.262

Re: Test OSU SB7:

The behavior of the vessel level (e.g., LDP-127, Plot 2) is consistent with that observed in other SBLOCA tests. The large fluctuations in level early in the test (reduction to <50", recovery, rapid reduction again to <50", and rapid refill between about 5000 and 6000 seconds) should be the subject of detailed analysis in a future report.

Response:

As noted, the behavior of the vessel level is consistent with that observed in other small break LOCA tests. Although SB7 is not specifically addressed, discussions of this type of phenomena for other small break LOCA tests are included in section 5 of Reference 480.262-1 and section 5 of Reference 480.262-2.

### References

- 480.262-1 WCAP-14252, "AP600 Low Pressure Integral System Test at Oregon State University: Final Data Report," Proprietary [LTCT-T2R-100], May 1995.
- 480.262-2 WCAP-14292, Revision 1, "AP600 Low-Pressure Integral Systems Test at Oregon State University Test Analysis Report," Proprietary [LTCT-T2R-600], September 1995.

SSAR Revision: NONE

## NRC REQUEST FOR ADDITIONAL INFORMATION



Question 480.267

Re: Test OSU SB13:

The description of the behavior of LDP-115 on p. 6-2 does not appear to conform very well to the data (Plot 82); timings are off and several features of the data are not described at all.

Response:

The Quick Look Report was used as a mechanism to provide data to reviewers in a timely manner. Therefore, an evaluation of all test phenomena was not provided. The Quick Look Reports have been superseded by References 480.267-1 and 480.267-2. For discussions of SB14, an inadvertant ADS actuation, see section 5.5.1 of Reference 480.267-1 and section 5.8 of Reference 480.267-2.

### References

- 480.267-1 WCAP-14252, "AP600 Low Pressure Integral System Test at Oregon State University: Final Data Report," Proprietary [LTCT-T2R-100], May 1995.
- 480.267-2 WCAP-14292, Revision 1, "AP600 Low-Pressure Integral Systems Test at Oregon State University Test Analysis Report," Proprietary [LTCT-T2R-600], September 1995.

SSAR Revision: NONE

## NRC REQUEST FOR ADDITIONAL INFORMATION



Question 480.268

Re: Test OSU SB13:

The data from this test appear to conform, for the most part, to trends noted in the data from many of the other SB tests.

Response:

The Quick Look Report was used as a mechanism to provide data to reviewers in a timely manner. Therefore, an evaluation of all test phenomena was not provided. The Quick Look Reports have been superseded by References 480.268-1 and 480.268-2. For discussions of matrix tests, see section 5 of these references.

### References

- 480.268-1 WCAP-14252, "AP600 Low Pressure Integral System Test at Oregon State University: Final Data Report," Proprietary [LTCT-T2R-100], May 1995.
- 480.268-2 WCAP-14292, Revision 1, "AP600 Low-Pressure Integral Systems Test at Oregon State University Test Analysis Report," Proprietary [LTCT-T2R-600], September 1995.

SSAR Revision: NONE



## NRC REQUEST FOR ADDITIONAL INFORMATION



Question 480.269

Re: Test OSU SB14:

There are very many failed instruments for this test, some of which are flagged as "critical," yet Westinghouse considers the test acceptable, apparently on the basis that none of failed instruments are crucial for conducting a mass/energy balance on the system. While it is true that the capability to calculate such a balance is essential, it is not the only purpose of these tests, and Westinghouse must justify the acceptance of the test on the basis on acquisition of sufficient data to permit analysis of loop behavior and code assessment.

Response:

Section 5.5.1.2 of Reference 480.269-1 addresses instruments on the Critical Instrument List which are considered inoperable or invalid during all or portions of SB14. The discussion contains details of when the instrument is failed and if necessary, what alternate indications will be used to evaluate facility performance. Sufficient data has been obtained to permit analysis of loop behavior and code assessment.

Reference

480.269-1 WCAP-14252, "AP600 Low Pressure Integral System Test at Oregon State University: Final Data Report," Proprietary [LTCT-T2R-100], May 1995.

SSAR Revision: NONE

## NRC REQUEST FOR ADDITIONAL INFORMATION



Question 480.270

Re: Test OSU SB14:

As well as overall trends, the dynamic behavior of the loop both early and late in the transient should be addressed. Examples include: the sharp down-spike and almost immediate subsequent up-spike in upper plenum level (LDP-139, Plot 83) within the first 1000 seconds of the test; oscillations and fluctuations seen after about 12000 (aside from those suspected to be related to interactions between the RCS and the BAMS); and hot leg level, which shows a sharp up-spike shortly before 1000 seconds, possibly as a result of ADS-4 actuation.

Response:

The Quick Look Report was used as a mechanism to provide data to reviewers in a timely manner. Therefore, an evaluation of all test phenomena was not provided. The Quick Look Reports have been superseded by Reference 480.270-1 and Reference 480.270-2. For discussions of SB14, see section 5.5.1 of Reference 480.270-1 and section 5.8 of Reference 480.270-2.

### Reference

- 480.270-1 WCAP-14252, "AP600 Low Pressure Integral System Test at Oregon State University: Final Data Report," Proprietary [LTCT-T2R-100], May 1995.
- 480.270-2 WCAP-14292, Revision 1, "AP600 Low-Pressure Integral Systems Test at Oregon State University Test Analysis Report," Proprietary [LTCT-T2R-600], September 1995.

SSAR Revision: NONE

**NRC REQUEST FOR ADDITIONAL INFORMATION**



---

Question 480.272

Re: Test OSU SB14:

The pressurizer refill noted and questioned above for Test HS-03 is not seen in this test. The staff notes that the pressurizer refilled in Test SB1 due to the failure to install a vacuum breaker on the ADS discharge line. Was this also the case for HS-03, accounting for the difference in behavior?

Response:

The vacuum breaker was installed on June 10, 1994, after the performance of SB1 and the shakedown tests. The lack of a vacuum breaker caused the difference in the pressurizer behavior noted between HS-03 and SB14.

SSAR Revision: NONE